

GRAPHITISATION CHARACTERISTICS AND MECHANICAL PROPERTIES OF MALLEABLE IRONS ALLOYED WITH COPPER

A THESIS

*submitted in fulfilment of
the requirements for the degree*

of

DOCTOR OF PHILOSOPHY

in

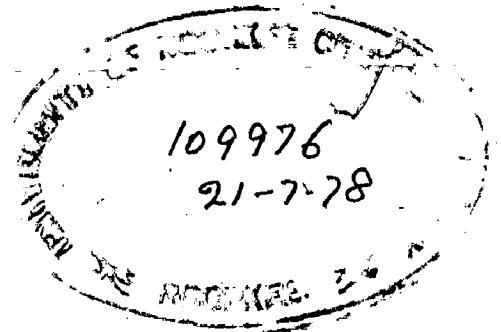
METALLURGICAL ENGINEERING

of the

UNIVERSITY OF ROORKEE



By
S. K. GOEL



DEPARTMENT OF METALLURGICAL ENGINEERING
UNIVERSITY OF ROORKEE

ROORKEE (INDIA)


August, 1977

C E R T I F I C A T E

Certified that the dissertation entitled 'Graphitisation Characteristics and Mechanical Properties of Malleable Irons Alloyed with Copper', which is being submitted by Sri S.K. Goel for the award of Degree of Doctor of Philosophy in Metallurgical Engineering of University of Roorkee is a record of candidate's own work carried out by him under my supervision and guidance. The matter embodied in this dissertation has not been submitted for the award of any other degree.

This is further to certify that he has worked part-time for a total period of four years and seven months from January 1973 to July 1977 for completing the dissertation for Doctor of Philosophy Degree at this University.

Dated August 15, 1977


(M.N. Saxena)
Professor and Head,
Department of Metallurgical Engineering,
University of Roorkee
Roorkee. U.P.

SYNOPSIS

Continued interest exists in shortening the malleabilisation cycle as well as in obtaining high duty pearlitic malleable irons in the UTS range of nearly 80-90 kgs/mm² with corresponding 5/6 percent elongation to suit special engineering requirements. These property combinations will excell 120-90-02 variety of S.G. Iron (270-350 BHN) designated by Gray and Ductile Iron Founder's Society of America. Development of such a high duty pearlitic malleable iron would, not only make a superior grade available to the design engineer, but would also solve certain regional problems, where the manufacture of S.G. Iron is considered relatively more difficult for one reason or the other. This is especially true of Indian situation.

The present investigation, therefore, had two distinct aims. The first, was to develop high strength pearlitic malleable iron with adequate ductility, and the second was to shorten the malleabilisation cycle, normally used for obtaining such a product. Apart from these aims, it was also thought to examine the controversies pertaining to the cast white iron structure, and the mechanism through which, pre-treatments help in shortening the malleabilisation cycle.

After careful considerations, copper was selected as an alloying element for achieving these objectives.

In addition to using the influence of copper on graphitisation characteristics as well as on the mechanical properties, other factors like composition adjustment pre-treatments, cooling rate etc. were employed to achieve the aims, set in this work.

It was found that tiny graphite particles of varying sizes, ranging from nearly 5-10 Å to approximately 5-6 microns, are an integral part of a cast white iron structure. Sizes of these graphite particles were found to vary depending on the cooling rate during freezing. The definition of 'mottling', therefore, needs revision. In fact 'mottling' must be defined in terms of the sub-microscopic sizes of graphite particles present in the cast white iron structure. On getting thermally activated during pre-treatments, these tiny graphite particles diffuse and coagulate. Thus, a large number of tiny graphite particles, appear in the structure on pre-baking or quench-baking, since these tiny graphite particles grow from sub-microscopic levels to the microscopic level. Considerable shortening in FSG period was obtained in individual cases due to various pre-treatments. Shortening in FSG period was also found to be a function of mainly Si and Cu content of base alloys. Maximum percent shortening in FSG period was found to correspond to ~1.4 wt % Si (unalloyed series) and to ~1.2 wt % Cu (alloyed series) content of base alloy. Also, maximum number of nodules were found in the pre-treated specimens corresponding to these compositions only. It was thought

that the formation of tiny graphite nuclei is initiated during liquid to solid transformation, which on further cooling grow to different sizes due to partial decomposition of eutectic cementite in the temperature range of 1145°C to nearly 920°C .

Also, it was found that the microhardness of eutectic cementite in thin and thick sections is not appreciably changed by varying copper and silicon contents in the base-melt. A maximum of nearly 0.9% copper was found to partition to eutectic cementite at nearly 1.2 wt % average copper content of base-melt, while the amount of copper partitioning to the austenite phase increases in proportion to the average copper content of base alloy. These results were significant with respect to the maximum percentage shortening obtained in FSG period at about 1.2 wt % copper content of base-alloy.

Significantly again, the best mechanical properties were found in oil and air-quenched and tempered condition at about 1.4 wt% Si and 1.2 wt % copper contents of base alloy. "Interrupted Annealing" technique was found most suitable for the purpose. Precipitation hardening characteristics of Fe-Cu system were used in the present study for strengthening the base-matrix. Copper would precipitate from the super saturated solid solution, as tempering proceeds and therefore, hardness is virtually held constant between 2 and 6 hours of tempering at 600°C draw temperature.

This phenomenon resulted in superior mechanical properties in copper bearing irons compared to unalloyed ones. Optimum mechanical properties were found at 1.2 wt % copper content of base alloy, as stated above. Copper was found to influence mainly the yield strength and percentage elongation, both of which, have higher values in copper bearing irons compared to the unalloyed compositions.

The present study shows that copper has a great potential with respect to its influence on not only the graphitisation characteristics of white irons but also on the mechanical properties of high strength pearlitic malleable irons.

Use of copper in the manufacture of air-quenched variety of high strength pearlitic malleable iron can thus be recommended. Such high strength pearlitic malleable irons shall excell or at least be equal to the 120-90-02 variety of S.G. Irons upto 20 mm section thicknesses. The problem of importing the inoculant for the manufacture of S.G. Irons can thus be avoided, particularly with regard to India. Further, no such strict composition controls, as are required for the production of S.G. Irons like extremely low sulphur contents etc, would have to be exercised in the manufacture of pearlitic malleable irons, since any excess sulphur can be easily balanced by appropriate Mn content.

ACKNOWLEDGEMENT

I wish to express my deep sence of gratitude to Dr. M.N. Saxena, Professor and Head, Department of Metallurgical Engineering, University of Roorkee, for his invaluable guidance and inspiration. But for his deep interest in the problem and encouragement at every stage of work this dissertation could not have been completed.

I am also thankful to Professor P.R. Dhar and Professor P. Banerjee of Indian Institute of Technology, Kharagpur for providing necessary facilities at their institute for carrying out Electron. probe micro-analysis and the Electron microscopy work. My best thanks are also due to Professor T.R. Anantharaman for providing INSTRON Universal Testing Machine and Electron Microscope facilities at the Department of Metallurgical Engineering, Banaras Hindu University, Varansi.

Thank are also due to my colleagues and the laboratory staff of the Heat-treatment, Metallography and Foundry laboratories for their kind and helpful attitude throughout the entire period of experimental work.



(S.K. GOEL)

C O N T E N T S

	<u>Page</u>
<u>CHAPTER-1</u> : INTRODUCTION	... 1
<u>CHAPTER-2</u> : GRAPHITISATION CHARACTERISTICS OF MALLEABLE IRONS	... 5
2.1 Preliminary	... 5
2.2 Essential features, FSG and SSG	... 6
2.3 Kinetics of FSG and SSG	... 9
2.3.1 General approach	... 9
2.3.2 Influence of Alloying and trace elements	... 13
2.3.3 Influence of initial microstructure	... 32
2.3.4 Influence of Nodule counts	... 33
2.3.5 Influence of pre-treatment and other processing variables	... 37
2.4 Mechanism of graphitisation	... 40
<u>CHAPTER-3</u> : HIGH STRENGTH MALLEABLE IRONS	... 48
3.1 Existing grades and varieties	... 48
3.2 Effect of alloying and trace additions.	... 60
3.3 Influence of Heat-treatments	... 64
3.3.1 Mn alloyed pearlitic malleable and hardened Ferritic Malleable	... 65
3.3.2 Air-quenched Pearlitic Malleable	... 66
3.3.3 Liquid quenched Pearlitic Malleable	... 67
3.4 Related Microstructures and Mechanical Properties.	... 71
3.5 User requirements	... 72
3.6 Transformation Mechanisms	... 75

<u>CHAPTER-4</u> : SPHEROIDAL GRAPHITE CAST IRONS	...	78
4.1 Introduction	...	78
4.2 Types and Applications	...	79
4.3 Composition limits	...	82
4.4 Heat-treatment	...	84
4.4.1 Stress relief	...	85
4.4.2 Ferritisation	...	85
4.4.3 Normalising and Tempering	...	88
4.4.4 Quenching and Tempering	...	91
4.4.5 Other heat treatments	...	92
4.5 Mechanical Properties	...	92
4.6 Manufacturing Techniques and problems	...	100
4.7 S.G. Iron Vs. Malleable Iron	...	107
 <u>CHAPTER-5</u> : DEVELOPMENT OF HIGH-STRENGTH SHORT CYCLE PEARLITIC MALLEABLE IRON	...	109
5.1 Introduction	...	109
5.2 The approach	...	112
5.3 Basic considerations in the selection of composition	...	113
5.3.1 Base Metal Composition	...	113
5.3.2 Alloying Elements	...	115
5.3.2.1 Mottling considerations	...	115
5.3.2.2 Shortening of FSG and SSG	...	117
5.3.2.3 Response to pre-treatment	...	117
5.3.2.4 Nodule Number, shape and size	...	118
5.3.2.5 Partitioning in different phases	...	119
5.3.2.6 Hardenability considerations	...	120
5.3.2.7 Strengthening due to Precipitation-hardening	...	121
5.3.2.8 Ductility and toughness	...	122

5.3.3	As Cast Structures	...124
5.3.3.1	Basic requirements	...124
5.3.3.2	Influence of Cooling Rate	...124
5.3.3.3	Influence of graphitisers	...124
5.3.3.4	Concept of Mottling	...125
5.3.3.5	Response of As-cast Structures to pre-treatments	...127
5.4	The Heat-treatment	...127
5.4.1	FSG completion	...127
5.4.2	Further Heat-treatment	...128
<u>CHAPTER-6:</u>	<u>EXPERIMENTAL PROCEDURE</u>	...132
6.1	Alloy Preparation132
6.2	As cast structures	...134
6.3	The Heat-treatment	...135
6.3.1	Pre-treatments	...135
6.3.2	FSG and SSG Estimations	...138
6.3.3	FSG with pre-treatments	...142
6.3.4	Quenching after FSG completion and tempering	...143
6.4	Metallography	...145
6.4.1	Optical Microscopy	...145
6.4.2	Electron Microscopy	...147
6.4.2.1	Introduction	...147
6.4.2.2	Replica preparation	...148
6.4.2.3	Examination of Replicas	...149
6.5	Fracture studies	...149
6.6	Partitioning of Alloying Elements	...150
6.6.1	Electron Probe Micro-Analysis	...150
6.6.2	Error Analysis	...153
6.7	Mechanical Testing	...157
6.7.1	Hardness and Microhardness tests	...157
6.7.2	Tensile Testing	...158
6.7.3	Impact Testing	...159

<u>CHAPTER-7</u> : RESULTS AND DISCUSSION	...160
7.1 As Cast Structure	...160
7.1.1 Optical Microstructures	...160
7.1.2 Fracture studies	...162
7.1.3 Carbon Replica studies	...163
7.1.4 Microhardness of Eutectic Cementite and Base Matrix	...164
7.1.5 Discussion of Results	...166
7.1.6 Conclusions	...177
7.2 Pre-treatment and Shortening of FSG period	...180
7.2.1 Introduction	...180
7.2.2 Results	...181
7.2.2.1 Influence of pre-treat- ments on N_V and average size of largest nodules	...181
7.2.2.2 FSG period shortening due to various pre- treatments	...188
7.2.2.3 Influence of graphiti- sers on the effective- ness of pre-treatments	...191
7.2.3 Discussion of Results	...193
7.2.4 Conclusions	...199
7.3 Partitioning of copper in different phases	...202
7.3.1 Introduction	...202
7.3.2 Results	...202
7.3.2.1 Electron Probe partition data	...202
7.3.2.2 Probe Scan data	...207
7.3.3 Discussion of Results	...207
7.3.4 Conclusions	...213
7.4 Unalloyed and copper alloyed pearlitic malleable iron	...214
7.4.1 Introductory	...214

7.4.2 Results	...215
7.4.2.1 Tempering Characteristics	...215
7.4.2.2 Mechanical properties	...222
7.4.2.3 Optical Microstructure	...227
7.4.2.4 Replica Studies	...228
7.4.3 Discussion of Results	...229
7.4.4 Conclusions	...235
<u>CHAPTER-8</u> : SUMMARY OF RESULTS	...236
<u>CHAPTER-9</u> : SUGGESTIONS FOR FURTHER STUDIES	...240
REFERENCES	...241
APPENDIX	...253

CHAPTER - 1

I N T R O D U C T I O N

The main object of present investigation was to shorten the malleabilisation process in general and to obtain high strength malleable iron with reasonable toughness. Also, attempts were made to study the fundamental mechanism, through which, large number of temper carbon nodules are formed either during pretreatments at sub-critical temperatures, or during very early stage of heating from ambient to the austenitic temperatures.

A large number of variables have to be suitably controlled to achieve effective shortening of the malleabilisation period. Only few factors viz. alloying elements, pre-treatments and the heat treatment cycles have been varied in the present work keeping other factors constant. The objective has been to shorten the malleabilisation period and also to obtain strong and tough malleable irons simultaneously by properly adjusting these variables. This has formed the first part of present work.

Conflicting views exist regarding the origin of temper carbon nucleii obtained in large number during pre-treatments of white irons at sub-critical temperatures or during early part of heating from ambient to austenitic temperatures. It is known that maximum nucleation of tempered carbon nodules occurs between 350 - 400°C. Large number of temper carbon nodules formed during

sub-critical pre-treatments have helped in shortening the FSG. These facts have been used in the present work for achieving considerable shortening of FSG. Different views on this fundamental aspect have been scrutinised and the hypothesis of 'Partial decomposition of Cementite during freezing' projected from present studies. These studies formed the second part of present work.

A particular strategy was followed for realising simultaneously the shortening of FSG period as well as the superior mechanical properties in malleable irons. Among various known methods of base-matrix strengthening like solid solution hardening, precipitation hardening, dispersion hardening, strain hardening, order hardening, phase transformation hardening etc., it was decided to use phase - transformation - precipitation hardening combination in the present work. The basic idea was to retain higher hardness of base matrix during tempering by virtue of precipitation hardening, so that superior mechanical properties are obtained. Copper as an alloying element was selected for the purpose. It is known that copper shortens the FSG period, which is further accentuated by the help of pre-treatments. At the same time, iron copper system exhibits precipitation hardening. Already this phenomenon has been used with some advantage in case of Ferritic Malleables. But the strategy adopted in the present study was to use precipitation hardening during tempering of martensitic base matrix. Strengthening

of base-matrix due to copper precipitation could thus be achieved in higher hardness ranges with consequent superior mechanical properties. This formed the third part of investigation.

Besides having specific interest in the problems discussed above, it was decided to study the partitioning of copper in different phases of white-irons in as-cast stage as well as during the progress of FSG reaction. This study could reveal such factors like the extent of segregation in the cast structure and the influence of copper on thermodynamic stability of cementite. Although some data is available on this aspect but it could not be regarded as complete especially with respect to the partitioning behaviour of copper during the progress of FSG reaction. It was, therefore, decided to obtain further data on this aspect.

The methodology adopted for experimental work was based on well established theoretical principles. However, emphasis in the present work was more on simulating the actual plant conditions and specifications so that the findings could also be of significance to the industries. This philosophy is reflected in the choice of alloy compositions, melting, founding, thermal cycling set-up and procedure, and the methods adopted for measurements of mechanical properties.

In addition to studying the normal first stage graphitisation characteristics of plain and cu-alloyed

compositions with and without pre-treatments, their tempering characteristics too were examined in detail. Standard procedure for determining N_a , N_v and FSG completion periods was followed. Hardness variations after 2 and 6 hrs. of tempering at subcritical temperatures, subsequent to FSG completion and quenching in various media viz. air, oil and water were found in all cases. These hardness variations in case of plain and alloyed pearlitic malleables would quantify the influence of copper-precipitation on the base matrix of alloyed pearlitic malleable. A study of their mechanical properties was then undertaken, after these variables were optimised.

CHAPTER - 2

GRAPHITISATION CHARACTERISTICS OF MALLEABLE IRONS:

2.1. PRELIMINARY:

Very extensive research work has already been carried out on various aspects of malleable iron metallurgy and technology. This is evidenced by a vast amount of technical literature available in this field.

The basic aim of all these investigations have been to reveal the fundamental mechanisms involved in solid state graphitisation, and to study the liquid to solid and solid to solid transformations as influenced by scores of trace and alloy additions. Technological advantage of these fundamental investigations has been taken in shortening the malleabilisation cycle on the whole and in obtaining high duty malleable irons with excellent combinations of strength, toughness and machinability. There has been much interest currently in this area of research.

The investigations so far have shown that the factors of fundamental importance for solid state graphitisation are the thermodynamic stability of eutectic cementite as influenced by trace and alloy additions to simple Fe-C system, graphitisation temperature and the nucleation and growth of temper carbon modules during FSG reaction. Also, SSG is basically a function of T.T.T. characteristics of a particular alloy. In addition to these fundamental factors,

however, several technological factors influence these reactions, which are discussed in subsequent paragraphs.

2.2. ESSENTIAL FEATURES, FSG AND SSG.

As cast white iron is a highly complex alloy with considerable microscopic heterogeneity.⁽¹⁵⁾ It is basically because rapid solidification rates are normally necessary to obtain a white structure. Microscopic studies have shown that the coring of primary dendrites would occur in a normal white iron during solidification dependent on the period of time during which the alloy exists between liquidus and solidus.⁽¹⁵⁻²⁴⁾ This may not be serious as regards carbon due to its high diffusivity, but significant segregation of substitutional alloying elements may occur.⁽¹⁵⁾ This discrepancy will increase as non-equilibrium cooling rates increase with respect to the diameter of section cast. Also, this situation may result in the formation of more eutectic iron than indicated by the metastable equilibrium diagram. The austenite-carbide eutectic may occur in two forms under these conditions, viz. as ledeburite and in platelike form. The platelike eutectic is further removed from metastable equilibrium than the former type and will thus show non-equilibrium effects in a more striking manner. These microscopic heterogeneities of a white iron structure can not be removed prior to graphitisation.

On raising this alloy to austenitic temperatures

through eutectoid range, the pearlite transforms into austenite by a process of rapid diffusion of carbon atoms from cementite into the iron to form a solid-solution of carbon in gamma-iron. But the massive eutectic carbide is virtually unaffected during the process of heating to austenitic temperatures. Hence, the resultant austenite would be unsaturated with respect to carbon. If the eutectic-carbide began to breakdown immediately at this stage, the initial carbon so liberated would dissolve in the austenite to make up for its carbon deficiency. The precipitation of graphite would only commence when the austenite becomes supersaturated with carbon. (15,24,29) This stage could occur at the austenite/carbide interface when the carbon concentration gradient in the austenite became shallow and the rate of diffusion of carbon into the austenite less than the rate of production by carbides. (24) Thus, the growth of graphite and the solution of carbon by austenite would occur simultaneously. The term "Gamma-range Graphitisation" has been employed by some workers to denote these reactions. (8)

The investigations so far have established that the entire process of malleabilization involves graphitisation of white iron, which represents a transition from the metastable Iron-Iron Carbide system to the stable Iron-graphite system. Three individual reaction take place that are necessary for malleabilisation:-

1. Nucleation of graphite

2. First stage graphitisation(FSG).

- a) Cementite \rightarrow dissolves into \rightarrow Austenite.
- b) Extra carbon diffuses to \rightarrow existing Nuclei and precipitates as temper carbon.

Nuclei - are preferably present at cementite/austenite interfaces.

3. Second stage graphitisation:-(SSG).

- a) Austenite \rightarrow Ferrite + graphite (Direct Reaction)
- b) Austenite \rightarrow Pearlite \rightarrow Ferrite + graphite (Indirect Reaction).

Thus, the basic function of malleabilization annealing process is to decompose the massive eutectic cementite during FSG and lower the carbon content dissolved in the base matrix to make it ferritic (0.006% carbon) during SSG. By the decomposition of massive carbides and diffusion of carbon atoms, the nodules grow around the centres of nucleation, which are usually termed as temper-carbon Nodules. During the second stage of graphitisation (SSG) in the temperature range of eutectoid transformation, there occurs a considerable decrease in the solubility of carbon, during which, new graphitisation occurs with migration of carbon atoms and the growth of temper carbon nodules. If iron is cooled very slowly through the critical temperature range, austenite will transform directly into ferrite and graphite (Direct SSG reaction). If, however, the cooling rates are faster, direct-reaction may not get completed and a part of austenite may get transformed into an intermediate phase i.e. pearlite. Pearlite later may

decompose into ferrite + graphite (indirect-reaction). The direct second stage reaction corresponds to the fastest transformation rates and is, therefore, preferred to the indirect SSG reaction, which is much slower. (4,27)

2.3 KINETICS OF FSG AND SSG

2.3.1. General Approach:

Basically, quantitative metallography and dilatometric techniques have been employed by various workers to study the kinetics of FSG and SSG reactions. Very wide range of pure as well as commercial compositions have been subjected to this study so far. Work of fundamental nature in this area of study has been carried-out notably by Swartz (7,50), Brown and Hawkes (8), Burke (5,6,10,15,20,22,33,35) Pearce (23,24), and Sandoz (4,27,28,51).

"Point counting method" (quantitative metalloraphy), has been most extensively employed in such studies to determine the percentage completion of FSG or SSG reaction at the end of selected graphitisation periods. Metallographic techniques are always employed to determine the number of Nodules/mm³ (Nv) and the average diameter of largest size tempered carbon nodules, in order to determine their growth rates. Dilatometric measurements coupled with microscopic examinations

have also been extensively used by some workers to obtain basic data on the kinetics of graphitisation. The growth measurements made by dilatometric techniques are essentially macroscopic in nature giving net effects, whereas morphological changes during graphitisation are basically microscopic. The result is that only average growth rates are detected by dilatometric technique. This technique has mostly been employed in case of isothermal graphitisation studies. Quantitative metallographic technique has an edge over dilatometric technique particularly with regard to the study of graphitisation in early stages. A large incubation period prior to the commencement of FSG reaction was reported by different workers using dilatometric technique, while it has recently been confirmed using metallographic techniques that the incubation period for FSG reaction is virtually negligible. (29)

Earlier work on the kinetics of graphitisation was concerned mainly with a study of nucleation frequency of graphite nodules, their growth and percentage transformation occurred at austenitising temperatures during isothermal or conventional graphitisation. Influence of reaction temperature, composition and alloying elements was studied on these aspects by different workers. Notable among them is the basic work of S.A.

Saltykov⁽¹⁾, H.A.Schwartz^(7,50) and B.F.Brown and M.F.Hawkes⁽⁸⁾. Quench method and quantitative metallographic techniques were employed by these investigators for their studies.

Burke and Coworkers^(5,6,10,15,20,22,33,35), for the first time, correlated the experimental nucleation and growth rates with isothermal graphitisation rates by the following expression:-

$$y = 1 - \exp [-(Kt)]^n \quad \dots (1)$$

or,

$$\log \log \frac{1}{1-y} = n \log t + n(\log K - \log 2.3) \quad \dots (2)$$

where,

y = Fractional graphitisation at reaction time t .

$n = (3a + b)$

K = Rate constant

a and B = constants (usually $b=1$).

Thus the plot of $\log \log \frac{1}{1-y}$ against $\log t$ is linear upto $y = 1/2$, the slope being n . Most of the data relating to first stage graphitisation behaves in this way. Evaluation of gradient gives n , and thus a , using $n = (3a+1)$. n is usually in the range of 1.5 to 4.0⁽³³⁾. It was, however, pointed out that a difference existed between the growth kinetics of pure alloys and commercial alloys⁽¹⁵⁾, which was attributed mainly to the microstructural variations. Equations (1) and (2) are

now generally employed by most investigators for such studies of graphitisation kinetics of white irons. Similarly, isothermal graphitisation rate curves, when plotted between percentage fraction transformed (y) and $\log t$ at a particular reaction temperature, are sigmoidal. (8,15) Such rate curves always show an incubation period, which depends on composition, temperature and thermal history of specimens. (8,15) These sigmoidal curves will shift to the left or right along the $\log t$ axis, as composition, initial microstructure, thermal history and FSG reaction temperatures are varied. The rate of growth of temper carbon nodules is the gradient of the graph of nodule radius against time. These curves are reported to be parabolic by different workers, at least in case of commercial black-heart irons. (33) Rate of growth of temper carbon nodules as well as the nucleation rate are influenced by temperature and composition variations. (8,33)

Direct SSG reaction rate is measured by finding (also by quantitative metallography) the proportions of pearlite and ferrite remaining in the matrix of the irons as a function of the linear cooling rate from 899°C to 649°C (eutectoid transformation temperature range) subsequent to FSG completion. The irons are quenched from 649°C in order to minimise the graphitisation of any pearlite. (4,27,28) This plot produces a series of

straight lines with definite slope. Any variation in N_v brought about by some pre-treatment like pre_baking, quench-baking or slow rate of heating upto 850°C , shall produce a series of parallel lines on this plot, referred to above, with a definite slope, characteristic of untreated iron. These parallel lines, associated with individual N_v values, shift to the right on log linear cooling rate axis, as N_v value increases progressively. The presence of alloying or trace elements and the Mn/S ratio of the base composition shall cause a shift of these parallel straight lines along x-axis, depending on whether the direct SSG reaction is accelerated or retarded. (27,28) Similar curves were drawn earlier by Brown and Hawkes⁽⁸⁾ to represent ferrite graphite eutectoid isothermal reaction as against log reaction time with similar conclusions that such curves are influenced not only by composition but also by nodule size distribution and thermal history.

2.3.2 Influence of Alloying and Trace Elements.

Table-2.1 summarises the influence of more common alloying and trace elements on the kinetics of FSG and SSG reactions, which in turn represents their carbide stabilising or graphitising characteristics. Chemical interaction between various elements is vital in few cases e.g. Mn and S. Also, elements sometime exert one effect in trace amounts and quite the opposite when present in larger quantities for example Mg and Al. The trace elements are, in general, found to exert considerable influence on

INFLUENCE OF COMMON ALLOYING AND TRACE ELEMENTS ON THE GRAPHITISATION CHARACTERISTICS OF WHITE-IRONS

Sl. No.	Element	Added pct. by Wt.	Influence on Primary graphitisation "Mottling"	Influence on secondary graphitisation		Influence on nodules counts.	References
				FSG	SSG		
1	2	3	4	5	6	7	8
1.	Silicon (Si)	0.5/2.3	St.Pro.	St.Pro.	Pro.	St.Inc.	8, 10, 26, 38(a and b), 39, 51, 52, 55, 59, 70, 95, 124, 161.
2.	Manganese (Mn)	0.06/0.8	Neg.	Pro. upto 5.35 ratio	Pro. at Mn/S ratio of 3/3.5	St.ret.	3, 8, 27, 28, 35, 51, 156, 160, 161, 164.
3.	Sulphur (S)	0.03/0.2 ratio of 0.43/7.0			Ret. beyond this ratio.	when Mn/S ratio > 3.0	
4.	Phosphorus (P)	0.05/0.18	Pro.	Ret.	Ret.	Inc.	8, 51, 59.
5.	Nickel (Ni)	0.06/3.0	Pro.	Pro.	Pro.	W.Inc.	8, 28, 51, 65, 73.
6.	Copper (Cu)	0.1/2.0	Mil. Pro.	Mil.Pro.	Mil.Pro.	Inc.	8, 28, 51, 65, 67, 68, 69, 72, 73, 74, 75, 86, 87, 88, 89, 90, 101, 126, 159, 162.
7.	Aluminium (Al)	0.01/0.18	Pro.if >0.1%	Pro. upto 0.1%	Pro.upto 0.05%	St.Inc.	8, 38, 52, 54, 51, 55, 57, 66, 85, 154, 163.
8.	Chromium (Cr)	0.02/1.4	Ret.	St.Ret. if >0.05%	St.Ret.if >0.05%	Decr.	8, 28, 51, 57, 62, 155.
9.	Molybdenum (Mo)	0.2/0.7	Ret.	Ret. if >0.1%	Ret. if >0.1%	Decr.	8, 51, 96, 115, 15.

Table contd.

Table 2-1 continued

1	2	3	4	5	6	7	8
10.	Titanium (Ti)	0.01/0.18	St.Pro.	Pro. upto 0.15%.	Pro. upto 0.01%.	Inc.	8, 38, 52, 71, 154.
11.	Tin (Sn)	0.01/0.16	Neg.	Ret.	Ret. > 0.015%.	Decr. > 0.05%	8, 27, 38, 52, 78, 79, 86, 87, 88, 89, 97, 102.
12.	Antimony (Sb)	0.01/0.10	-	Neg.	Pro. upto 0.003%, then reduces.	Neg.	8, 27, 38, 52, 97.
13.	Zinc (Zn)	0.05	N.D.	Neg.	Neg.	St.Inc.	8, 27, 38, 52, 39, 61, 77.
14.	Lead (Pb)	0.006/ 0.03	-	Neg.	Neg. upto 0.029%.	Neg.	27, 38, 52, 97, 154.
15.	Cobalt (Co)	0.2/0.8	Mildly Pro.	Mildly Pro.	Mildly Pro.	St.Inc.	6, 55, 51, 64, 15, 13, 33, 141.
16.	Magnesium (Mg)	< 0.04	Ret.	Ret. if > 0.1%.	Ret. if > 0.1%.	W. Decr.	38, 39, 52, 47, 122, 123, 154.
17.	Bismuth (Bi)	0.005/ 0.09	Ret.	Controver- sial. Gener- ally Ret.	W. Ret.	Sl. Decr.	8, 27, 38, 52, 53, 54, 60, 64, 66, 82, 91, 93, 99, 100, 154, 95, 164.
18.	Tellurium (Te)	0.002/0.1	St. Ret.	Ret.	Neg. if adequ- ate nodules present.	Decr.	38, 39, 52, 53, 60, 64, 82, 93, 98, 124, 154.
19.	Arsenic (As)	0.01	Neg. at 0.8 Si	Neg. upto 0.4%.	Neg. upto 0.4%.	-	3 8, 52, 84.
20.	Boron (B)	0.002/ 0.003	Pro. in small amounts	St. Pro. upto 0.003% Ret. beyond 0.02%.	St. Pro. upto 0.003% Ret. beyond 0.02%.	Inc.	54, 57, 58, 66, 104, 154
21.	Calcium (Ca)	0.01	No eff- ect.	St. Ret.	Ret.	No effect	38, 52.

Table 2-1 continued

1	2	3	4	5	6	7	8
22.	Vanadium (V)	0.02/0.3	Ret.	Ret.	Ret.	Decr. 0.2%.	28, 51, 92.
23.	Cerium (Ce)	0.35/0.4	Ret in irons with S < 0.015 or 0.025%.	Ret.	Ret.	Decr.	38, 39, 76, 81, 52, 93.
24.	Selenium (Se)	0.01/0.05	No effect	St. Ret.	Ret.	Decr.	38, 52, 39, 98.
25.	Barium (Ba)*	0.02	No effect	St. Ret.	Ret.	St. Decr.	39, 38(a), 52.
26.	Cadmium (Cd)	0.003	Neg.	Ret. St.	Pro. with low Mn/S ratio.	Inc.	27.
27.	Thallium (Tl)	0.0025/0.05	Ret. St.	Neg.	Ret. with high Mn/S ratio	No effect	38, 52.
28.	Indium (In)	0.0025/0.01	No effect	Neg.	Pro. St.	No effect	38, 52.
29.	Hydrogen (H)						8, 98, 167, 14.
30.	Oxygen (O)						8.
31.	Nitrogen (N)						8, 56.
32.	Iridium (Ir) □						80
33.	Platinum (Pt) □						80
34.	Palladium (Pd) □						8

Notes: --

*-Barium added as BaCl₂. Present as residual element from galvanised castings charged with the scrap.

St. Pro. - Slightly promotes. Decr. - Decreases.

Pro. - Promotes. Neg. - Negligible.

St. Inc. - Slightly increases. W.D. - Not determined.

St. Ret. - Slightly retards. St. - Slightly increases.

Ret. - Retards. Inc. - Increases.

W - Weekly.

Mil - Mildly.

□ Pt, Pd and Ir. - shown as "probably graphitizers" in reference (18). No further data found in subsequent literature.

primary as well as secondary graphitisation reactions, which is of vital significance in practice. These trace elements may be present as tramp elements in the starting raw-material or they may be present as residual elements in the return scrap. Behaviour of these alloying and trace elements during the primary and secondary graphitisation, as well as their influence on the mechanical properties of standard and pearlitic grades of malleable irons has been ascertained through systematic research mainly during the last thirty years. Table 2.1 presents consolidated information only with regard to the behaviour of alloying and trace elements during primary and secondary graphitisation reactions. The influence of these elements on the mechanical properties of standard and pearlitic grades of malleable irons is discussed in subsequent chapters.

It should be appropriate here, at this stage, to include a discussion of the influence of rather commonly employed trace and alloying elements on the kinetics of FSG and SSG reactions.

Silicon is known to be the strongest graphitising element, promoting both primary as well as secondary graphitisation reactions. Silicon upto 2.3% has been used in 3.86 C.E. irons along with 0.01% Te plus hydrogen or with 0.02% Te alone for mottle control in 3" dia bars. (124) Generally, however, Si is employed in the range from 1.40 to 1.70% along with 0.01 to 0.02% Bi or 0.005% Te for mottle control. (26) Such high Si contents resulted in

shorter FSG periods, faster critical cooling rates for SSG completion and a higher nodule number. (26,33,52,161) It was reported by Sandoz⁽⁵¹⁾ that comparatively small quantity of silicon partitions to the cementite phase. The silicon % going to the cementite phase was found to be less than 0.25% in an iron containing 0.78 to 1.15% Si. Also, the change in partitioning of Si, as influenced by the presence of other alloying elements or as a result of partial FSG at 900°C., was reported to be negligible.⁽⁵¹⁾ It was suggested from these studies that small amounts of alloying elements entering the cementite phase may be affecting its thermodynamic stability. This change in thermodynamic stability of cementite phase was thought to be responsible for experimental observations that FSG and SSG is enhanced by Si additions.⁽⁵¹⁾ Further, it was shown by Burke⁽³³⁾ that the effect of Si was greater on the nucleation than on the growth. It is because of this reason that N_v is greatly increased by higher Si additions.

Cu, Ni, Co and Al were reported to have similar partitioning behaviour as that of Si.^(51,28,73) It would, therefore, be expected that their behaviour during FSG and SSG would be similar to that of Si, although of varying degree. Further, it was reported by Sandoz⁽⁵¹⁾ that the partitioning of these elements between austenite and eutectic cementite is not influenced by the presence of other alloying elements in the base-melt, and also no

significant change in partition ratio was observed in all these cases with the progress of FSG at 900°C. Small amounts of these elements entering the cementite phase would thus affect its thermodynamic stability, and cause their behaviour to be similar to that of Si during FSG and SSG.

The influence of Cu on FSG, SSG and Nv has been studied in detail by Heine et al⁽⁸⁹⁾, Sandoz⁽²⁸⁾ and Albert de Sy⁽⁷³⁾. It was shown by the first two workers that FSG and direct SSG reactions are enhanced and that Nv is increased by copper additions. Copper is reported to be a mild graphitiser during solidification stage and is estimated to be 1/3rd to 1/5th powerful compared to Si.⁽⁷³⁾ Copper being an austenite stabiliser, exhibits anti-ferritising effect during cooling through critical transformation range, and consequently promotes pearlite formation during SSG.⁽⁷³⁾ This anti-ferritising behaviour of Cu has been reported in case of cast irons and SG Irons.⁽⁷³⁾ It is believed that copper, contrary to nickel (which is also a powerful austenite stabiliser), diffuses slowly in austenite, thus accumulating in austenite at the austenite/ferrite interface creating a diffusion barrier⁽⁷³⁾. Thus copper functions as a strong pearlite former in case of cast irons and S.G. Irons. On the contrary, as stated earlier, Sandoz and Heine et al have shown that Cu functions as a graphitising element both during FSG as well as during SSG reactions of malleable irons. The suggestion has been that an increase in nodule number due to Cu addition opposes and overcomes an intrinsic

retarding effect. (28,89,162)* Cu employed in these investigations varied from 0.10 wt % to almost 2.0 wt %:

The influence of Ni on FSG and SSG reactions is well reviewed by Sandoz. (28) Several workers have confirmed that small amounts of Ni partitioning to the cementite phase (28) decrease its stability and therefore accelerate FSG reaction. Ni also accelerates direct SSG reaction in malleable irons (28) while Albert de Sy (73) has shown that Ni acts as a mild anti-ferritizer in case of grey irons and S.G.Irons, although it is much less effective than Cu. Also, it was found in case of malleable irons too, that Ni is far less effective than Cu in accelerating either FSG or SSG reaction. (28) Nickel employed in these investigations varied from 0.06 to 3.00 wt % approximately.

Appleton (13), Burke (6,15,33) and Surendra et al (64) have shown that Co behaves in the same manner as Si, Ni and Cu during FSG and SSG reactions. Also, Co was shown to partition in the same fashion as Cu and Ni. (51) Co has been employed in trace amounts mainly to accelerate the FSG reaction. The percentage of Co employed in these studies has varied between 0.2 to 0.8 wt %..

Al and Ti have been employed alone or in conjunction with each other for the purpose of deoxidation of melts. Heine (163), Loper and Heine (38-a,52), Amrhein and Heine (85) and E.I.Bader (154) have investigated in detail the influence

of these elements on graphitisation characteristics and mechanical properties of malleable irons. It was reported by Heine⁽¹⁶³⁾ that small additions, 0.01-0.03% Al, caused a marked decrease in the number of graphite nodules in the treated iron compared with the untreated iron. Aluminium additions larger than these resulted in a marked increase in the number of graphite nodules. At 0.05% Al addition, as many or more nodules as occurred in untreated iron, were found. As the deoxidising addition is made still larger, 0.07 to 0.11%, or 0.12 - 0.18%, inclusions appear, the nodules become sprawly ~~sprawly~~, flakes of graphite and mottling appears in the structure. These observations, however, depend on the degree of oxidation of melt at tapping stage, for this will determine the residual aluminium in the melt. For example, the metal as it came from the air-furnace, required from 0.02 to 0.12% Al for complete deoxidation, which is equivalent to about 0.02 to 0.12% oxygen in the melt. In a later investigation, Loper and Heine^(38-a) have shown that 0.013% Al addition yielded fully white fracture in 4" x 4" x 8" casting with T.C. 2.0% and Si 0.79%. By 0.137% Al addition to nearly the same base composition, a mottled fracture resulted. Further, 0.151% Al addition

resulted in heavily mottled fracture in 4" x 4" x 8" casting. Thus, small percentage of Al and Ti added to white cast irons function initially as deoxidisers, while amounts sufficient to leave a residual alloying percentage form complex carbides in the malleabilised iron. The former behaviour promotes graphitisation and ultimately mottling. (38-a, 52, 163) These observations are in line with the partition data reported by Sandoz⁽⁵¹⁾ that Al concentrates in the austenite phase in the range investigated between 0.2 to 1.1% addition. Al, therefore, should function similarly as Si, Cu, Ni and Co in this regard. Trace amounts of Al are generally employed in practice to take care of dissolved oxygen in the melt, which is known to be a strong carbide former.⁽¹¹²⁾ Such additions result in rapid graphitisation periods.⁽¹¹²⁾ Again it has recently been confirmed by E.I. Bader⁽¹⁵⁴⁾ that Al, B, Ti and Zr act as graphite formers and that trace amounts of Al, Bi, Al + B + Bi or Ti increase the specific pearlite/carbide interface area, representing faster cooling conditions during freezing. Brown and Hawkes⁽⁸⁾, on the contrary, have included Al in the category of carbide stabilisers.

Trace amounts of B have been shown to promote

FSG and SSG reactions of white cast irons and that excessive amounts of B retard these reactions. (58) Small amounts (0.002-0.003%) of B have been used commercially to neutralise the retarding effect of Bi, (43,112,164) and it has been often reported that B is effective in neutralising Cr as well. (155) B in trace amounts (0.003%) has also been employed to increase the nodule number. (93) Increasing amounts of B shift the FSG sigmoidal curves to the left along log time axis, showing that FSG reaction is enhanced. But as the graphitisation is 90-95% complete, a reversal of FSG reaction takes place. It may be because the B content of cementite increases as graphitisation proceeds and the last traces of cementite get enriched in B to the extent that graphitisation proceeds either very slowly or not at all. It is now known that B may be substituted for C in cementite. Also, B is known to diffuse in austenite at about the same rate as C. Carbon may be released as B substitutes in the cementite and this finely distributed released C could serve as nuclei. (58) Nodule number is increased by B addition probably through this mechanism. R.D. Shellag (104) has shown that the borocarbides (formed from Fe_3C after diffusion of B) are very stable. Microprobe analysis of these borocarbides revealed that only Mn, V and Cr were present in them in addition to iron.

Among the common graphitisation retarders may be

included elements like Cr, V, Mo Mn, S, Bi, Te, N, O and Ce.

Cr is known to be a strong carbide former and hence it retards both first and second stage graphitisation reactions severely. Also decreasing nodule numbers were reported with increasing Cr content. (8,28,62,155) It is because Cr dissolves in and stabilizes cementite. (28,51) Also, it is known that Cr partitions preferentially in cementite phase of Cr-bearing white cast irons. (28,51) Further, it has been shown that the Cr content of cementite of white iron increases during the course of first-stage graphitisation. (51) This increase in Cr occurs because of the partial solution of cementite as FSG progresses. But only the highest Cr bearing irons (0.4% Cr) displayed this enrichment tendency clearly. (51) The presence of other alloying elements were found to affect this enrichment tendency in Cr bearing irons (0.34 to 0.57% Cr). In lower Cr irons, which graphitise too rapidly for complete retention of the Cr in cementite the addition of elements that give a net decrease in graphitisation rate may cause an increased tendency for Cr enrichment. Cr employed in these investigations varied between 0.02 to 1.4%. It was confirmed by Sandoz⁽²⁸⁾ that, if present in sufficient amount, Cr not only retards the FSG, but reverses it.

White Irons containing 0.02 to 0.30% V were investigated by Sandoz⁽²⁸⁾ to ascertain the influence of V on FSG and SSG reactions. The investigations revealed that the presence of V retards the first stage reaction and

the direct second stage reaction. In another work Sandoz⁽⁹²⁾ has shown that nearly 1.02% Cu neutralizes approximately 0.10% V during FSG. However, V still retards the graphitisation of the last traces of eutectic cementite even though copper is present. Similarly, 1.0% Cu more than counteracts the retarding action of 0.1% V in direct SSG reaction. White irons containing highest V content in the series (0.23 and 0.3%) did not show the completion of FSG reaction even after an exposure of 200 hrs., suggesting that cementite was gradually becoming more thermodynamically stable with the progress of FSG reaction.⁽⁹²⁾ It was earlier shown by Sandoz⁽⁵¹⁾ that V partitions mainly to the cementite phase, in a ratio of 14:1 between cementite and Austenite phases regardless of the average V content of white iron. During annealing again at 900°C, the V content of remaining cementite increases with time at this temperature. Electron-probe microanalysis studies have shown that no concentration gradients existed with respect to Vanadium contents in the cementite grains of the base matrix.^(28,92)

Mo is known to retard graphitisation as it is a carbide former.^(8,15,96,115) The partitioning behaviour of Mo in white irons was found to be similar to that of Cr and V.⁽⁵¹⁾ But Mo enriched only slightly in the cementite phase either with time at 900°C or with the progress of FSG reaction. Mo, therefore, showed less ability to diffuse into the receding cementite phase than either Cr or V.⁽⁵¹⁾

Mo employed in these investigation varied between 0.2 to 0.7%.

It is known that Mn or S, functioning individually are carbide stabilisers and, therefore if either of the two is present in excess of the amounts required to form the compound MnS , shall retard both the first stage and direct second stage reactions. And it is also known, that the retarding effect is more severe on direct SSG reaction than on FSG reaction if this Mn/S ratio is unbalanced. Also, the optimum Mn/S ratios for both these reactions are not identical, (3,8,27,28,33,156,160,161,164) One of these investigators⁽³³⁾ have shown that when excess S is present, the graphite becomes spheroidal, while the nodules are of flake type when some excess Mn is present in the white iron. In contrast, when graphite is formed during solidification, the presence of free sulphur gives rise to flakes and the addition of Mg to scavage the S produces spherulites.⁽³³⁾ It was shown by many workers (28,156,160,161) that FSG sigmoidal curves are shifted to the left along log time axis (showing that the reaction is accelerated) as the Mn/S ratio increases from 0.43 to a maximum of 5.35. This FSG acceleration would be reversed with further addition of Mn. The maximum SSG rates were found to correspond to a Mn/S ratio of about 3. In practice, however, special attention is paid to this factor particularly with regard to the SSG reaction, because unbalanced or higher Mn/S ratios will inhibit this reaction

severly. (112,164,156) Partitioning studies by Sandoz (28,51) have shown that excess Mn or S partitions to cementite at the beginning of FSG reaction of white cast iron. The concentration of Mn in the cementite of irons with excess Mn increase slightly during FSG reaction. R.A.Sidorenko et al (3) have further reported that Mn retards the graphitisation of cementite particles isolated from white cast iron containing excess Mn i.e. with higher Mn/S ratios. It was reported by Sandoz (28) that irons with lowest Mn/S ratio developed no ferrite surrounding the graphite, thereby indicating that excess S seems to stop the nucleation of ferrite at the graphite particles.

Bi, Te and Ce are used in trace amounts primarily for mottle control at higher Si limits in the base composition or in thick sections. These additions are generally employed and are accompanied by low nodule numbers inspite of their different chemical nature.

Bi has been used in amounts from 0.005% to 0.09% for mottle control. (8,27,38,52,53,54,60,64,66,82,91,93,95,99,100,154,164,165) It is, therefore, termed a strong carbide stabiliser or a strong retardant of primary graphitisation. Presumably, Bi inhibits graphitisation by suppressing the growth of stable graphite embryos during freezing, thereby permitting the unstable carbide embryos to grow. Since Bi is a strong carbide former, it might be inferred that it would retard graphitisation during annealing, as other carbide formers do. However,

Boegehold⁽¹⁶⁴⁾ has shown that 0.005% Bi added to a high Si (about 1.65-1.6%) iron not only prevents mottling, but actually accelerates the annealing cycle. On the contrary, it was reported by Sandoz.⁽²⁷⁾ that Bi (upto 0.09%) retards both FSG and SSG reactions intrinsically, regardless of the Mn/S ratios (varying from 1.0 to 7.0). Work of AFS Malleable Div (6D) Committee, Heine et al^(38-a,52,91,93,95), Moore⁽⁶⁰⁾ and T.D.Hutchinson⁽⁸²⁾ is in general agreement with the results stated above. Heine et al^(38-a,52,93,95) have further stressed that processing variables such as Si content, section thickness, nodule- counts, pre-treatments etc. are more vital for FSG and SSG reactions than Bi addition. In line with the results of Boegehold⁽¹⁶⁴⁾, Kannan et al⁽⁶⁶⁾ have reported that 0.03% Bi addition slightly reduces the FSG period (with < 5% Fe₃C in the matrix) and that the rate constant is slightly decreased signifying that Bi exhibits a slight accelerating effect on FSG rate. They have also reported that Bi slightly reduces the critical cooling rate in SSG. Their results may be supported by the findings of E.I. Bader⁽¹⁵⁴⁾. He reported that Bi (0.001-0.1%) increases the specific austenite/cementite interface area to the maximum possible extent compared with other trace additions like Al, B, Ti or Al+B+Bi. The effect is similar to that of faster cooling rates during solidification. Majority of temper-C nodules develop on this interface area during heat-treatment. Therefore, this increased specific surface area will

result in the formation of a larger number of nodules and hence results in faster rates of FSG reaction.

Cerium has been revealed as another element capable of producing white fractures at C and Si percentages, where mottle or grey fractures would normally occur. The effectiveness of cerium in raising C and Si limits for mottling is similar to that of Tellurium, but the percentage addition required is larger. (38,39,52,76,93). Ce was found to be ineffective in the range of 0.01 to 0.11% addition. This was attributed to a side reaction of Ce with S resulting in the formation of cerium-sulphide. (76) S content of melt was lowered in one of the experiments (76) from 0.05/0.09 to 0.015/0.025%. and cerium additions were tried in amounts of 0.11 to 0.70% by plunging at 1510°C. White fractures resulted when the added cerium exceeded 0.35 to 0.40% in desulphurised melts. Even 0.2 to 0.3% Ce will prevent eutectic flake graphite solidification in desulphurised iron. (39) Also cerium in amounts of 0.35-0.40% produced a white fracture in 1-7/8" dia bar without prior desulphurisation of iron. The metal composition in these investigations was T.C = 2.5% and Si = 1.5-2.5%. (76). The number of compact graphite nodules which are permitted to nucleate when sufficient cerium or mischmetal is used to prevent flake graphite is greater than in case of tellurium additions being upto 900/mm³. Higher Si percentage in the iron does not increase compact graphite nucleation (39). It was further reported by these workers that the influence

of metallic cerium or cerium as mischmetal was not different in this regard. ⁽³⁹⁾ It was shown by the same workers in a similar investigation that Bi, Te and Ce additions for mottle control are accompanied by low nodule numbers, at least in thick section during annealing. ⁽⁹³⁾ Thus increasing mass appears to be an anti-nucleating factor. Heine and Co-workers ^(38-a, 52, 76, 93) therefore, resorted to all known means of increasing the nodule counts, in an effort to improve the nodule counts in thick section casting so that FSG and SSG rates could be enhanced. Their conclusions are that only increasing the Si% produces a significant increase in nodule number, among all other factors known to cause large increase in nodule numbers in lighter sections. In a recent study, W. Westerholt et.al ⁽⁸¹⁾ have found that 0.1% cerium-mischmetal addition to the blackheart malleable iron considerably promotes cementite disintegration during FSG and accelerates pearlite disintegration during SSG reaction.

It was shown by Heine and Co-workers ^(38-a, 39, 52, 93) that Te suppresses nucleation of flake graphite eutectic. Te additions greater than 0.015% prevent the formation of flake or film graphite in eutectic area, but permit compact graphite to be nucleated adjacent to the carbide interfaces or within the primary austenite in a base iron of 2.82% TC, 2.23% Si and 0.07% S. ⁽³⁹⁾ The percent of Te required to prevent flake graphite depends on the S content of the iron, C and Si contents, and section size of the castings. At a sulphur level of 0.07-0.08% only, 0.02% Te is required to eliminate flake and film

graphite, while at 0.2% S, the % Te required is 0.08%. These results apply to a base composition of 2.6-2.8% C, 2.3% Si, 0.32% Mn and 0.13% P. (39) It was demonstrated by these workers, that the base curve representing maximum C and Si contents, that will produce a fully white fracture due to Te additions, is shifted upwards, and this shift in the base curve is greater for 0.01% Te addition than for any other additions. As with the Bi and water-vapour additions, the effect of Te additions is greater at low Si contents. (38-a) It was further reported by these workers that Te additions greater than 0.01% were not effective in altering the base line obtained from a 0.01% Te addition. (38-a, 93) Te, therefore, functions as strong carbide stabiliser. J.V. Dawson (98, 124) has quoted his results of Te addition to high C.E. iron for mottle control. The three base compositions, he selected for study, varied in C.E. from 3.66% to 3.86% , and the diameter of bars varied from 3" to 6" . His studies revealed that the addition of hydrogen in conjunction with 0.02% Te produced fully white structures in the 6" dia bars from irons of 3.66% and 3.76% C.E. but not from 3.86% C.E. iron. 3" diameter bars were found to be white in all the three irons. Hydrogen addition was thus shown to enhance the influence of Te on mottle control. (98, 124) 0.02% Te addition without H₂ was found to be adequate to yield fully white fracture in 3" dia bars, while only 0.01% Te addition with H₂ served the same purpose.

Influence of Si content on the period of FSG completion at 900°C with and without 0.01% Te addition was investigated by Heine and co-workers^(52,93) and these factors were correlated. It was found that Te additions in the range of 0.002% to 0.10% do not change the base line established for 0.01% Te addition. This base line for 0.01% Te addition, therefore, represented the maximum FSG time required at 900°C as related to % Si. FSG is seen to be retarded considerably from these observations and so also the nodule number. Nodule number, however, could be increased in such cases by pre-treatments which is discussed in subsequent chapters, and hence FSG could also be shortened accordingly. The influence of Nodule counts is all the more felt in thicker sections, because of the adverse "mass effect" on nodule numbers.^(52,93) E.I. Bader⁽¹⁵⁴⁾ studied the possibility of replacing Bi by Te due to rapid burn-off of the former, and found that Te slightly increases the interface area. He reported that Te did not speed up FSG until Si was raised to 1.5% or more when annealing time was 20% shorter.

2.3.3. Influence of initial microstructure.

As stated in section 2.2 non equilibrium cooling rates are required to obtain a fully white structure in as cast stage, which causes coring of primary dendrites and gives an increase in eutectic cementite/austenite interface area. Such non-equilibrium cooling rates give

rise to platelike austenite/carbide eutectic, which is different in morphology than normal ledeburite. The platelike morphology of this eutectic is associated with larger interface area between eutectic cementite and austenite, compared to a normal morphology of ledeburite formation. Larger interface area will provide more nucleation sites for C atoms during initial stages of FSG reaction. Varying degrees of non equilibrium cooling rates would thus cause varying as-cast micro-structures, which will influence the nucleation of temper-carbon nodules, and will ultimately influence the kinetics of FSG reaction. The work of Brown and Hawkes⁽⁸⁾, K. Pearce⁽²⁴⁾ and Burke^(15,33) confirms the facts stated above. Any treatment that refines the eutectic structure increases the nodule number by increasing the interfacial area available for nucleation. Superheating the melt or increasing the rate of cooling from the liquid stage act in this way.⁽³³⁾ E.I Bader⁽¹⁵⁴⁾ has reported that trace additions of Al, Bi, Ti alone or in combination like (Al +Bi) increase the specific austenite carbide interface area. This result is similar to that of faster cooling during freezing with identical effects on nucleation sites for temper carbon nodules.

2.3.4. Influence of Nodule Counts:

It is now generally agreed that nodule-count is by far, the most important single factor that has profound effect on the kinetics of FSG and SSG reactions. Investigation by numerous workers have shown that higher is the nodule

number, shorter is the FSG and SSG periods. The following factors have been found effective in increasing the number of nodules:

- (i) Superheating of melt
- (ii) decrease in section-size
- (iii) faster rate of freezing. (stripping the mould after 2-3 minutes of pouring).
- (iv) pre-queenching from austenitic temperatures followed by sub-critical annealing.
- (v) Sub-critical annealing at 400-600°C
- (vi) Proper composition control. Graphitising elements increase nucleation, for example Si, whilst carbide formers like Mo, Cr and Mn decrease it.
- (vii) Use of trace elements like Al, Bi, Ti and B or combinations like Al+B+Bi as ladle additions.
- (viii) Graphite bearing materials in the melting furnace charge.
- (ix) Higher annealing temperatures.

In practice, however, factors (iii), (v), (vi), (vii) and (ix) are extensively employed to increase the nodule number with the aim of achieving faster rates of FSG and SSG reactions. The necessity of increasing the nodule counts in thicker sections is rather more vital because their FSG and SSG periods are comparatively prolonged.

George Sandoz in his studies⁽⁴⁾ confirmed that the FSG and direct SSG reactions are sensitive to nodule

number and the latter especially so. He developed certain normalisation curves and formulae, that predict the influence of nodule number variations on these graphitisation reactions. These developments were based on the observation that the plots of log of time to reach a given level of first or direct second stage graphitisation against the log of nodule number are linear. Moderate changes in composition were found to displace these lines from each other, but the slopes did not change greatly. But when large amounts of Cr were added to the base-melt, the first stage slopes were found considerably changed. He found that the influence of nodule number on the indirect SSG reaction was small and hence normalisation curves were not constructed in this case. In his later work, G. Sandoz^(27,28,58,62,92) has utilised this concept of nodule number normalisation and the log log plots, stated above, to separate the intrinsic effect of alloying elements from their influence on nodule-number. It is because any departure from the parallel line relationship of log log plots would indicate the intrinsic effect of alloying element. Substantial quantities of alloying elements can alter the graphitisation mechanisms so drastically that these slopes would change. For example, it was shown by Sandoz⁽⁴⁾, that 0.40% Cr addition to the base-melt renders the slopes essentially zero, indicating that there is no effect of nodule number on the rate of FSG. He, therefore, concluded that the slopes of these parallel lines in an individual log log plot are dependent on composition. For

example, it was shown in the same investigation that Cr influences the value of exponent such that it is -0.29 at 0.0% Cr in iron and -0.0 at 0.4% Cr in iron as stated earlier too. The expressions developed by Sandoz for normalising Nodule number differences between base and alloy iron heats made from the same split heat are as under:

First stage-graphitisation (FSG)

$$TFN(\text{alloy}) = TF(\text{alloy}) - TF(\text{base}) \left[\left(\frac{Nv(\text{base})}{Nv(\text{alloy})} \right)^{0.29} - 1 \right] \dots (3)$$

where,

TF= time to graphitise to a given level, say 50%.

TFN= time to graphitise the alloyed iron to the 50% level had no nodule number change resulted from the addition of alloying element.

Direct second state graphitisation (SSG)

$$RCN(\text{alloy}) = Rc(\text{alloy}) - Rc(\text{base}) \left[\left(\frac{Nv(\text{alloy})}{Nv(\text{base})} \right)^{0.45} - 1 \right] \dots (4)$$

where,

Rc(base) = Linear cooling rate observed to give a selected amount of pearlite in a base iron.

Rc(alloy)= The linear cooling rate observed to give the same amount of pearlite after the alloying element addition.

RCN(alloy)= The cooling rate that would have given the same amount of pearlite in the alloy iron had no nodule number change resulted from the addition.

Electron-microprobe studies by Sandoz^(28,51) have

shown that various alloying elements partition themselves differently between eutectic cementite and austenite phases according to their graphitising or carbide stabilising characteristics, thereby influencing the thermodynamic stability of cementite phase. These studies have also shown that most of the alloying elements partition to the cementite phase at least to some extent. Sandoz concludes from these studies that the net observed influence of alloying elements on FSG kinetics is partly caused due to a change in nodule number and partly due to the intrinsic effect of these alloying elements.

2.3.5. Influence of pre-treatments and other processing variables.

Pre-treatments have been found extremely effective in increasing the number of nodules, and hence, this factor has been used in practice to enhance FSG and SSG rates in thin as well as thick sections. This factor was, therefore, listed in section 2.3.4 among other known variables that would increase the nodule counts. J. Burke^(15,35), P.B. Burgess and R.G. Trimberger⁽⁴⁴⁾, M.C. Mittal et al⁽⁵⁴⁾, R.W. Heine and T.W. Mueller⁽⁹³⁾ and Floyd Brown⁽¹¹⁷⁾ have shown that the thermal history of white cast iron has profound effect on the number of nodules, and hence this treatment can be effectively utilised in practice to accelerate the FSG and SSG reactions. Generally, subcritical annealing (pre-baking) is considered more useful in practice compared to quench-baking, because the castings are liable to

develop quench-cracks during the latter pre-treatment.

Among other factors, that influence the kinetics of FSG and SSG reactions, the following variables may be listed:

- (i) Rate of heating to the austenitic temperature (12).
- (ii) Section thickness of casting (38-a, 52, 93) (casting geometry).
- (iii) Charge materials and melting conditions. (48, 105, 106, 107, 108, 109, 125)
- (iv) Annealing furnace equipment and atmosphere in the furnace. (109, 112, 137, 139, 140, 141, 167)
- (v) Neutron irradiation of unalloyed and alloyed white iron. (118)
- (vi) Variations in annealing cycles. (119)
- (vii) High pressure mould castings. (120)
- (viii) Propane gassing of liquid melt. (121)
- (ix) Modified malleable by Mg addition. (123, 122)
- (x) Deoxidation practice. (163)
- (xi) Annealing under vacuum. (116)
- (xii) High FSG temperature.

The influence of these variables on primary as well as secondary graphitisation and Nodule counts is summarised in Table-2-2.

TABLE-2-2Influence of other processing variables on FSG and SSG kinetics and mottling tendency.

<u>S.No.</u>	<u>Variables</u>	<u>Primary graphitisation (mottling)</u>	<u>Secondary graphitisation</u>	
			<u>FSG</u>	<u>SSG</u>
1.	Slow rate of heating to FSG temperature.	-	Pro.	Pro.
2.a)	Fine grain sizes or decreasing casting thickness (faster rate of solidification)	Ret.	Pro.	Pro.
	b) Thick castings (Slow rate of freezing)	Pro.	Ret.	Ret.
3.a)	Charge materials:			
	i) Graphitic materials in charge.	Pro.	Pro.	-
	ii) Oxidised or rusty materials in charge.	Ret.	Ret.	Ret.
	iii) Steel in charge	Ret.	Ret.	Ret.
b)	Melting conditions:			
	i) Slags high in FeO over 25%.	Ret.	Ret.	-
	ii) Oxidising melting conditions.	Ret.	Pro.	Pro.
	iii) Atmospheres containing-			
	Oxygen	Ret.	Pro.	Pro.
	Nitrogen	Ret.	Pro.	Pro.
	CO	Pro.	Ret.	Ret.
	Water vapour	Ret.	-	-
	iv) high melt superheat	Ret.	-	-
	v) Deoxidation of melt.	Pro.	Pro.	Pro.
4.	Annealing:			
	a) Furnace atmosphere:			
	Hydrogen	-	St.Ret.	St.Ret.
	CO	-	Neg.	Ret.
	Water-vapour	-	Ret.	Ret.
	N ₂	-	Neg.	Neg.

4. b) high FSG temp. c) Under Vacuum	-	Pro.	Ret.
5. Neutron Irradiation.	-	Pro.	Pro.
6. Cast in high pressure moulds.	-	Ret.	-
7. Propane gassing	-	Pro.	Pro.
8. Mg. addition	Ret.	Pro.	Pro.

INDICATIONS: - Ret. - Retards.
 Pro. - Promotes.
 St. - Strongly
 Neg. - Negligible.

2.4 Mechanism of Graphitisation.

Essential features pertaining to the FSG and SSG reaction and their kinetics were discussed in 2.2 & 2.3.1 respectively.

Various mechanisms of nucleation and growth of graphite during first stage graphitisation, as proposed by different workers, have been critically discussed by Burke⁽³³⁾ and Sandoz⁽²⁸⁾. H.A. Schwartz^(7,50) and Richard Schneidewind⁽³²⁾ et al were among the earliest workers, who attempted to form a scientific basis of nucleation and growth phenomenon occurring during graphitisation of white-iron. Schwartz^(7,50) considered that the following steps must occur for the nucleation and growth phenomenon to take place in white-iron:

- a) Solution of cementite.
- b) Decomposition of Cementite.
- c) Migration of C.
- d) Crystallisation of C.

It was stated earlier that faster cooling rates during freezing⁽³²⁾ or the use of some trace elements increase the rate of malleabilisation at a given soaking temperature by one or both of the mechanisms mentioned below. First, it will produce a finer grain-size casting giving finer or platelike eutectic cementite net work. The increased austenite cementite interface will increase the rate of cementite solution (as above), since rate of solution is proportional to the surface area of solute exposed to the solvent. Secondly, a faster cooling rate increases the under cooling of austenite at the lower critical, and the austenite on its transformation will contain more than the theoretical concentration of eutectoid C. Upon reheating above the critical temp., there may either be a tendency to form a supersaturated austenite or excess carbides may be precipitated in fine dispersion which will offer a large amount of surface area to the austenite. Schneidewind, Reese and Tang⁽³²⁾ have shown the correlation between log cooling rate (Log V/A) and log graphitisation period to be linear at various FSG temperatures, the graphitisation period increasing with slower cooling rate of castings and with lower FSG temperatures.

Brown and Hawkes⁽⁸⁾, W.S.Owen⁽¹⁹⁾, Burke and Owen⁽¹⁰⁾, Hulgren and Ostberg⁽¹⁴⁾, Owen and Wilcock⁽¹⁷⁾, A.Taub⁽⁴¹⁾, Gill and Epplesheimer⁽¹¹⁾, Burke^(5,6,15,20,22,33,35), Sandoz^(28,51), Pearce^(23,24), Walker and Kondic⁽¹²⁾, Appleton⁽¹³⁾, Vasil'ev et al⁽³⁴⁾, Ashton⁽²⁰⁴⁾, Bhide and

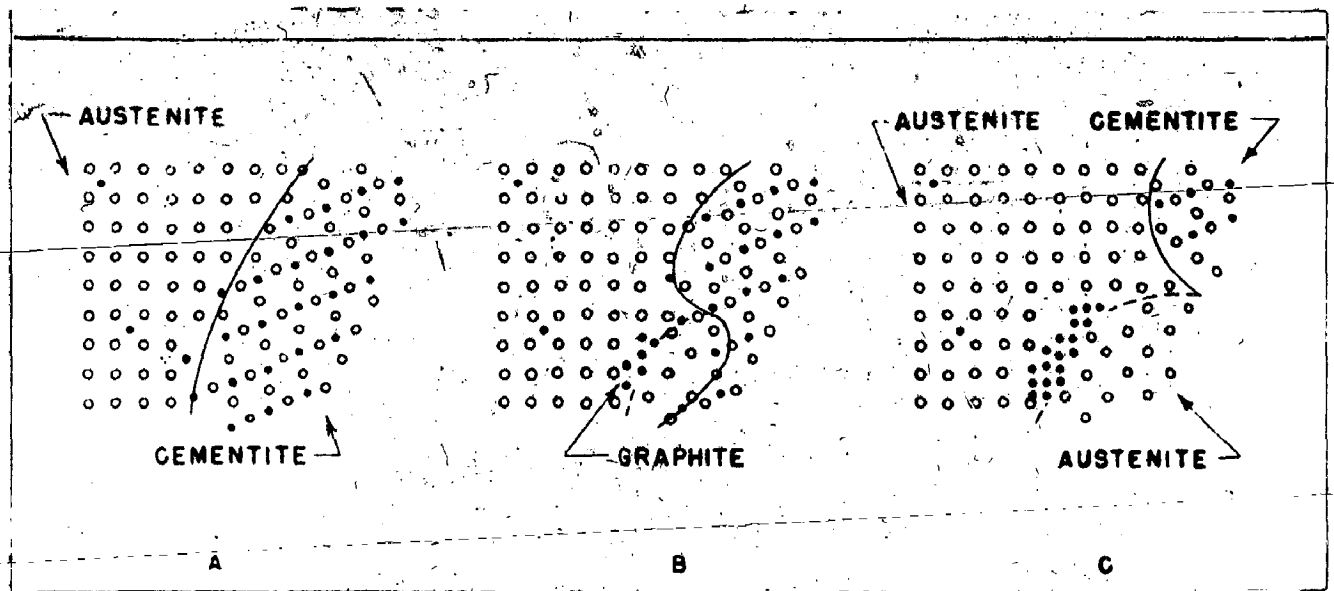


Fig. 2.1 - Mechanism of gamma-range graphitisation (Schematic)
 Solid Circles-carbon
 Hollow Circles - Iron.
 After Brown and Hawkes (8).

Banerjee⁽²⁹⁾ and Paley and Williams⁽¹⁶⁷⁾ have been among the later contributors to this field.

Brown and Hawkes⁽⁸⁾ have classified various graphite forming reactions that occur in cast-irons. The reactions of vital importance for FSG reaction is termed as 'Gamma-range-graphitisation' by these workers and involves the decomposition of massive carbides. Subcritical graphitisation of cementite is shown to be much slower than the eutectoid reaction. It is stated by these workers that the graphite produced by any of these reactions, deposits on the existing graphite nuclei produced earlier. Fig.2-1 shows the schematic representation of gamma-range-graphitisation reaction mechanism, as proposed by Brown and Hawkes⁽⁸⁾. Graphite nuclei thus formed continue to grow, as C atoms from the decomposing cementite diffuse through austenite and precipitate on them. Simultaneously, the iron atoms released by the decomposing cementite, attach themselves to the adjacent austenite lattice. Morphology of graphite thus produced is controlled by the composition of alloy and by the reaction temperature. Growth curves of these nuclei were found to be approximately parabolic. They also observed that the carbide particles nearest to a nodule dissolve faster than those somewhat more remote, but more remote particles too continue to be in the process of dissolution. Fine carbides were found to dissolve more rapidly due to their large interface area, as also noted by most other workers. According to Brown and Hawkes⁽⁸⁾, the elements

which affect the graphitisation rate of white cast iron do so primarily through their effect on the stability of cementite. Hence, any alloying element which increases the overall graphitisation rate increases the rate of nucleation in such proportions that the rate of growth of an individual nodule is slower than that for the unalloyed iron. It is because of this reason that white irons containing elements like Ni, Cu and high Si yield large number of nodules with decreased sizes. It was pointed out by these workers that the graphite lattice is so dissimilar to those of austenite or cementite that it was unlikely that graphite could grow coherently with either of these phases. Cementite/Austenite interface, therefore, functions as the nucleation site for graphite particles. It was found during these studies that the rate of nucleation increases progressively faster as time proceeds. The number of nodules is seen to reach a maximum and then decrease. The explanation offered is that probably the 'solution potential' of carbon at the surface of nodules of smaller diameter is greater than that at the surface of nodules of larger diameter. There would thus always be some tendency for smaller nodules to disappear by giving up carbon atoms to diffuse through the surrounding austenite and deposit on larger nodules. Rate of nucleation was found to increase with increase in reaction temperature and so also was affected the growth rate. This concept of 'Carbon diffusion potential' proposed by Brown and Hawkes is shown schematically

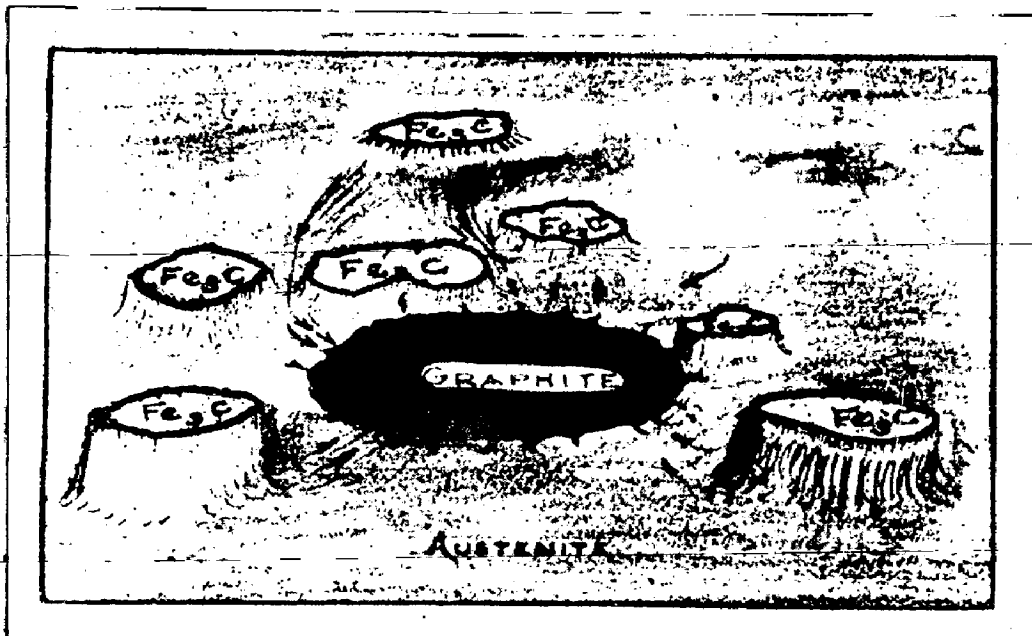


Fig. 2.2 - Carbon diffusion potential terrain in gamma range graphitisation (Schematic)
After Brown and Hawkes (8).

in Fig.2-2.

Burke and Owen⁽¹⁰⁾ and Owen and Wilcock⁽¹⁷⁾ have concluded from metallographic observations on high purity white-cast irons that temper carbon nucleates preferentially at the cementite/Austenite interface in the eutectic or at the surfaces of inclusions during first stage graphitisation. Most of the investigators agree on this point. Burke^(15,33) suggested that interfacial nucleation occurs because the surface energy associated with the interface reduces the energy barrier to the formation of a critical nucleus. Also, the concentration of C atoms is greatest at the grain boundaries, in a similar way as the dislocation atmospheres, and hence the probability of C atoms grouping together is much greater on the grain boundaries than within the body of either cementite or austenite grains.

A.Taub⁽⁴¹⁾ and later Gill and Epplesheimer⁽¹¹⁾ suggested that nucleation sites are located at the interface between austenite and undissolved small carbide particles remaining in the austenite, due to incomplete solution of pearlitic cementite. They suggest that nucleation takes place in three stages:

- a) Precipitation of secondary carbides during the initial parts of the incubation period.
- b) Spheroidisation of these carbide particles.
- c) Nucleation of graphite at the interfaces between austenite and secondary carbides.

Secondary carbides provide the initial C atoms for the formation of the graphite nucleus. Direct metallographic evidence was produced to support the third stage nucleation. Burke⁽³³⁾, and Walker and Kondic⁽¹²⁾ have re-examined this concept and found that with the possible exception of very low graphitisation temperatures, the graphite nuclei are always associated with the massive eutectic cementite. Walker and Knodic⁽¹²⁾ have shown that the rate of solution of eutectic cementite is greater than the rate of solution of spheroidized pearlitic cementite since large number of spheroidized pearlite remain in austenite for some considerable periods of time and at very high annealing temperatures. At the end of the incubation period, graphite nuclei are formed at austenite/eutectic cementite interfaces, which appear to grow initially at the expense of the spheroidal pearlitic cementite. The last traces of spheroidal cementite disappears after approximately 15% of the reaction. Incubation period was reported to be about 8 minutes in this case. Once graphite has nucleated, it will grow with the diffusion of C atoms towards it and the cross diffusion of other elements away from it. So far as the morphology of temper carbon is concerned, it was shown by Hultgren and Ostberg⁽¹⁴⁾ that it is determined not by the nucleation process but by the conditions during subsequent growth, which in turn depend upon temperature, composition and annealing atmosphere.

As stated earlier, the number of nucleation sites, vary with the composition and thermal history. It was shown by

Brown and Hawkes⁽⁸⁾, that graphitising elements increase the number of nodules, while carbide stabilisers reduce it. In fact, the effect of an alloying addition on the overall rate of graphitisation is almost entirely associated with the change in nucleation rate, the variation in growth rates being relatively slight.^(8,15,33) Subcritical annealing prior to FSG has been found to increase the number of nuclei. Walker and Kondic⁽¹²⁾ have reported that maximum number of graphite nodules are formed by pre-annealing at 400°C. According to them, the two factors, diffusion and spheroidization, are best balanced at this temperature, to cause the formation of large number of graphite particles which act as nucleation centres for further graphitisation during subsequent FSG reaction.

As discussed by Burke^(33,15) at length, it appears, therefore, necessary to consider the graphitisation reaction in two independent stages, i.e. (a) nucleation and (b) growth of graphite particles. These principles of solid state graphitisation have now been by and large accepted.

But some controversy has arisen regarding the origin of graphite nuclei and the exact stage, at which these nuclei are formed in the malleabilised structure, due to the work of M.C.Ashton⁽²⁰⁴⁾ and others. Also, it was shown conclusively by Bhide and Banerjee⁽²⁹⁾ that the "incubation period" for the formation and appearance of graphite particles, visible under optical microscopy at about 1800X,

is negligible, as against fairly large incubation periods reported by earlier workers. It was mainly because, the earlier workers had employed the dilatometric technique for graphitisation studies, while Bhide and Banerjee⁽²⁹⁾ employed mainly the optical microscopy technique for such investigations. Paley and Williams⁽¹⁶⁷⁾ in a recent study have again emphasised that the spheroidization of carbide in the pearlite plays a significant role in the kinetics of first stage graphitisation reaction, thus reverting back to the ideas of A. Taub⁽⁴¹⁾ and Gill and Epplesheimer⁽¹¹⁾.

These studies, however, go to show that if the "incubation period" is negligible, graphite particles smaller than the optical sizes might be already existing in the cast white iron structure, which in very early part of isothermal graphitisation or even during sub-critical pre-annealing, could coalesce together and form graphite particles large enough to be visible under optical microscopy. Also, the stage at which, these sub-microscopic graphite particles might be forming in the cast-structure, needs to be ascertained. But, if it is found that such tiny sub-microscopic graphite particles already exist in the cast white-iron structure, then the definition of "Mottling" will have to be suitably changed.

CHAPTER 3.

HIGH STRENGTH MALLEABLE IRONS

3.1 EXISTING GRADES AND VARIETIES

Normally, pearlitic malleable irons are designated as high strength malleable irons. The pearlitic malleable irons again include a variety of micro-structures, obtained due to different heat-treatments, which have resulted into a wide spectrum of mechanical properties in higher strength ranges. The micro-structures covered by this category are martensite, tempered martensite, spheroidised pearlite and lamellar pearlite along with temper carbon nodules. Thus, the malleable iron that contains purposely retained eutectoidal carbides or low temperature (Sub-critical) transformation products is called pearlitic malleable iron or just pearlitic malleable.⁽¹⁶⁶⁾ The nature of the carbides and their abundance, size and distribution directly affect the properties of the material.⁽¹⁶⁶⁾ A proper control and manipulation of variables such as composition and processing of base-melt, use of alloying and trace elements, combined C in the base matrix, type of heat treating equipment and the heat-treatment cycle itself results in a variety of grades of pearlitic malleable with their characteristic mechanical properties. Standard specifications laid down by A.S.T.M, S.A.E. and I.S.S. for various grades are presented in Table 3.1 below:

Table 3.1
ASTM, SAE and ISS specifications of Pearlitic
Malleable Irons

Specifying Agency	Number	Grade	Minimum T.S. psi (kgs/mm ²)	Minimum Y.S. p.s.i (kgs/mm ²)	Minimum Elongation % in 2"G.I	Hardness BHN
ASTM ⁺	A.220. 55T	45010	65,000 (45.82)	45,000 (31.72)	10	163-207
		45007	68,000 (47.94)	45,000 (31.72)	7	163-217
		48004	70,000 (49.35)	48,000 (33.84)	4	163-228
		50007	75,000 (52.87)	50,000 (35.25)	7	179-228
		53004	80,000 (56.40)	53,000 (37.36)	4	197-241
		60003	80,000 (56.40)	60,000 (42.30)	3	197-255
		80002	100,000 (70.5)	80,000 (56.4)	2	241-269
SAE ⁺	-	43010	60,000 (42.3)	43,000 (30.31)	10	163-207
		48005	70,000 (49.35)	48,000 (33.84)	5	179-228
		53004	80,000 (56.40)	53,000 (37.36)	4	197-241
		60003	80,000 (56.40)	60,000 (42.30)	3	197-241
		70002	90,000 (63.45)	70,000 (49.35)	2	241-285
*ISS	2640- 1964	A	99,260 (70)	77,990 (55)	2	241-285
		B	92,170 (65)	60,974 (43)	3	212-248
		C	77,990 (55)	51,048 (36)	4	192-241
		D	70,000 (50)	45,376 (32)	5	170-229
		E	63,810 (45)	36,868 (26)	7	149-201

*ISS: 2640-1964 (covering grades A to E) represent all section-thicknesses. Dia of test bar specified in each case is 15 mm.

+ASTM and SAE specifications drawn from reference (166).

Table-3.2

Base Composition, Alloying, Heat-treatment Cycles, Microstructures and Mechanical Properties of Pearlitic Malleable Irons.

(Abstract of Different - Practices)

N.	Base Composition and Alloying Elements wt %	Heat Treatment Cycles and Remarks	Final Microstructure	Mechanical Properties			Investigator (Reference)	
				UTS x 1000 psi (kgs/mm ²)	YS x 1000 psi (kgs/mm ²)	% Elongation G.L.		
				5	6	7	8	
							9	
	T.C. = 2.43 Si = 1.19 Mn = 0.43 S = 0.14 P = 0.072 Cu = 0.19 Alloying Cu = 0.5-1.5	FSG over, Air cooling, bars machined to 1/2 inch dia. Best results obtained at 1.04% Cu. FSG-14 hrs. at 955°C, Air quenched tempered at 715°C 7 hrs., Air Q. Oil quenched subsequent to tempering, Aged at 450°C for 16 hrs. FSG + Air cool + temper at 705°C + Air cooled. Temper at 665°C, water quenched, Aged at 500°C for 5 hrs. (Mainly AQ process)	At 1.57% Cu At 0.54 Cu At 1.17 Cu At 1.17 Cu At 1.57 Cu	127 (89.53) 77.1 (54.28) 83 (58.51) 84.5 (59.57) 107 (75.43)	104 (73.32) 53.1 (37.36) 63 (44.41) 60.2 (42.44) 96 (67.68)	2.5 9.0 9.0 6.5 3.0	321 174 187 187 269	P.B. Burgess (90)



109976

Table 3.2 Continued

1	2	3	4	5	6	7	8	9
2.	T.C. = 2.7 Si = 0.95 Mn = 0.75- 0.85 S = 0.06 P = 0.10	Pearlitic Malleable as per ASTM: A-220-55T, grade 48004. Malleabilised in Tunnel- furnace.	Pearlite + max. 10% Ferrite	70 (49.35)	46.2 (33.18)	4 Min.	165-180	B. Thyberg (128)
	Alloying-Mn Te= 0.001 Cu= 1.0	Subsequent Heat-treatment: a) 1 hr. at 850°C, oil quenched, tempered for 1 hr. at 675°C. b) 1 hr. at 850°C, salt quenched at 240°C, held 30 mits. 1 hr at 675°C. c) 1 hr. at 850°C, Air quenched to about 600°C, Annealed at 710°C for 3 hrs. d) As (C) above, but annealed at 710°C for 5 hrs.	Lamellar Pearlite +20/40% Ferrite (Starting material) Cementite, Spheroids embedded in Ferritic matrix + temper car- bon Nodules. (Common stru- cture in all the cases). Pearlitic structure.	96.36 (69.2)	74.14 (53.2)	6	224	
		Grade A-5	Pearlitic (50)/(55.1)	69.7/76.7 (50)/(55.1)	35/40.5 (25.1)/(29)	7/10	160/190	
		Grade A-8	Pearlitic (59.2)/(64.12)	82.5/89.3 (59.2)/(64.12)	48.8/54.6 (35)/(39.2)	5/8	190/220	
		Grade A-9	Pearlitic (62)/(67)	86.5/93.3 (62)/(67)	53/58.7 (38)/(42.2)	5/8	195/230	

Table 3.2 continued.

1	2	3	4	5	6	7	8	9
3.	T. C. = 2.5/2.6 Si = 1.3/1.4 Mn = 1.7xS+ S = 0.15 P = 0.12/ 0.14 Cr = 0.04/ 0.05 0.03/ 0.0 5	FSG over, Air quenched, drawn (Air quenched pearlitic grades) Grade - 45007 Grade - 50007 Grade - 53004	Pearlitic Pearlitic Pearlitic	70 (49.35) 75 (52.87) 80 (56.4)	45 (31.72) 50 (35.25) 55 (38.77)	7 7 4	163/217 179/228 197/241	R. F. Marande (130)
	Alloying-Mn.	FSG over, Air quenched, reheated to 871-885° for 1 hr. upto the temp. and soaked for 30 minutes, Oil quenched, drawn for 2 hrs and 15 minutes. (Temperatures varied to obtain the desired hardness) (Oil quenched pearlitic grade)						

4.	Alloying by Cr, Mo and Mn.	Grade - 60003 Grade - 80002	Pearlitic Pearlitic	80 (56.4) 100 (70.5)	60 (42.3) 80 (56.4)	3 2	197/255 241/269	
		Black-heart ferritic malleable converted into a heat-treatable material by carbon resolution from tempering time) and varying hard-						

Table 3.2 continued

1	2	3	4	5	6	7	8	9
	ness obtained depending on the efficiency of quench. Compared with AQ, considerably higher hardness obtained by Oil quench.							
(WQ)	Unalloyed, water quenched and tempered at 450°C for 1 hr. or tempered at 650°C for 1 hr.	Intermediate structures of Martensitic hardening.		17.6 (12.4)		1	375	
(OQ)	Unalloyed, Oil quenched and tempered at 580°C for 6 hrs. or, tempered at 600°C for 2 hrs. or, tempered at 650°C for 1 hr.	- do - - do - - do -		93.5 (67.15) 99.0 (71.1) 101.2 (72.68)		5 3 4.5	246 255 255	
(AQ)	Air quenched, No tempering. or, tempered at 590°C for 4 hrs. or, tempered at 670°C for 4 hrs.	- do - - do - - do -		129.8 (93.22) 101.2 (72.68) 81.4 (58.46)		2.0 4.6 6.0	341 249 205	
	Air Quenched preferred for lower strength Pearlitic Malleable and thin walled castings. Higher yield strength obtained in							

Table 3.2 contd.

	1	2	3	4	5	6	7	8	9
			oil Quenched cases, same UTS obtained at lower B.H.N. by OQ. Compared to steels, UTS, YS stand comparison, while % elongation is lower. Better machinability compared with steel castings and forgings.						
5.			Pearlitic malleable as per ASTM A220:55T (7 grades) made by different plants using different heat-treatment cycles.						AFS Malleable Div. Committee 6E. R.W. Heine Chairman. (132,133)
	<u>Plant-D</u>		Plain, unalloyed		120 (84.6)	88 (62.04)	4		
	T.C-2.2/2.35 Si- 1.3/1.35+ Mn -0.48/1.0 S- 0.125/0.149 Cr-0.020/0.025		Plain, unalloyed		118 (83.19)	86.5 (61.0)	4.5		
			Mn alloyed		88.65 (62.49)	62.4 (43.99)	9.5		
			Mn alloyed		88.25 (62.21)	62.65 (44.16)	10.5		
	+(Mn alloyed)		in case of Mn alloying heated to 960°C, soaked for 18 hrs Air quenched to black temp., reheated to 705°C, held for 6 hrs., dropped to 686°C, held for 18 hrs. (castings used for wear purposes).						
	<u>Plant-E</u>		(High Elongation grades only)						
			For various grades heat-treatment held constant, only alloying varied.						
			FSG at 940°C, 34/36 hrs. for 8 ton load. Air quenched by						
					Ferritic 67.5 (unalloyed)(47.58)	45 (31.72)	19.0	149	

Table contd./-

Table 3.2 contd.

1	2	3	4	5	6	7	8	9
---	---	---	---	---	---	---	---	---

Plant E (Cont.)

Mn-0.8/1.15 forced draft. Then spheroidized in 34/36 hrs. at 705/715°C. (Alloyed) 100 (70.5) 62.5 (44.06) 8.5 241

Cu-0.5/1.0 Alloying. (Alloyed) 100 (70.5) 62.5 (44.06) 8.5 241

Mo added in some cases along with Mn and Cu. Te and Bi used for mottle. control. Intermediate structures of martensitic hardening. 88 (62.04) 62 (43.71) 14 200

Plant F.

T.C.-2.3/2.5 EFG-45 hrs. at 938°C, Air quenched, reheated to 705°C, 10 hrs. for spheroidization. 67.5 (47.58) 45 (31.72) 14/19 149

Si -0.5/1.0 With maximum combined C in the matrix. 100 (70.5) 63 (44.41) 5.5/8.5 241

Mn -0.75/0.85+ 133.5 (94.11) 120 (84.6) 1 332

S -0.07/0.10 97.5 (68.73) 76 (53.58) 7 228

P -0.1/0.14

Cu -0.5(opti-onal)

Cr -0.01/0.03

+Mn alloying
Cu for corrosion Resistance only.

Plant I

T.C.-2.25/2.35 Pearlitic malleable produced by reheating fully ferritic malleable iron, oil quenched and drawn to desired hardness and strength levels. 90/105 (63.5)/(74) 65/80 (46)/(56.4) 3/8 228/241

Si -1.15/1.2 97/120 (68.4)/(84.6) 75/90 (53)/(63.5) 3/6 241/285

Mn -0.33/0.38

S -0.86/0.08

P -0.1/0.15

High strength grades ASTM-60003 and 80002 and sometimes 50007 and 53004 are made by liquid quench rather than Air

quench. Liquid quench gives higher Y.S. at a given hardness. YS/UTS ratio of 0.8 produced by liquid quench and temper.

6. Regular Malleable Mn = 0.40	Regular or standard Malleable correspond to ASTM - 35018	Ferritic								P. W. Green (129)
Pearlitic Malleable Mn = 0.80/ 0.85	Pearlitic Malleable: FSG over, Air quenched, Spheroidizing treatment just below the critical temperature. (Air quenched spheroidized pearlitic grades)	fine pearlitic matrix.	85 (60)	55 (38.78)	8					
		spheroidized pearlitic	75 (52.9)	45 (31.7)	17					

Both the above products can be heat-treated similar to steels.
Further heat treatment:

(a) Both classes of Malleable solution treated at 870°C, soaked for one hour, oil quenched to ambient temp., tempered at various sub-critical temperatures for 2 hours.

Pearlitic Malleable (0.8%Mn)-										
As Quenched										
tempered at 485°C			150 (105.75)	115 (81.07)	1					
tempered at 650°C			110 (77.55)	80 (56.4)	3/3.5					

Continued Table 3-2

	2	3	4	5	6	7	8	9
Regular or Standard Malleable (0.4 Mn):								
As quenched								
tempered at 485°C				130 (91.65)	110 (77.55)	1.5	520	
tempered at 650°C				100 (70.5)	80 (56.4)	4.5	220	
(b) Salt-bath treatment:								
Solution treated at 870°C in salt bath, soaked for 20 minutes, quenched in a constant subcritical temperature bath and held sufficiently long for complete transformation to take place.								
Pearlitic Malleable (0.8 Mn):								
Quench temperature--485°C and held long.				120 (84.6)	92 (64.86)	4		
Quench temperature 650°C held long.				100 (70.5)	75 (52.87)	3		
Standard Malleable (0.4 Mn):								
Quench temperature--485°C and held long				103 (72.61)	78 (54.99)	3.5		
Quench temperature--650°C and held long				85 (59.92)	57 (40.2)	5.5		

Table continued/-

Table 3-2 continued

	1	2	3	4	5	6	7	8	9
7.	Mg inoculated with less than 0.04% Mg.		FSG-2/3 hrs. at 870°C, normal malleable requires 8 hrs. at 930°C for FSG completion.	Pearlitic	137.5 (98.75) max.	107.8 (77.42) max.	2.0		123.
	T.C.=2.5/2.6 Si=1.5/1.6 Cr=0.03/0.05		Reheated ferritic and oil quenched, and tempered. Na = 102.		81.6 (57.52)	64.5 (45.47)	5.5	187	P.B. Burgess (111)
	Alloying: Mn=1.7xS+ 0.1/0.15% B = 0.0025		Interrupted anneal, reheat, oil quenched and tempered. Na = 67.		76.2 (53.72)	59.4 (41.87)	8.0	187	
			* Direct oil quenched " process adopted. Continuous pusher type marten-sitic structure (50% marten-sitic structure site at the centre of 1" round.)						
			Drawn for 2 hrs. at various temperatures for final required hardness.		71 (50.05)	51 (35.95)	8	175	
			Note:-(a) Impact Resistance:- Impact Transition temp. in case of direct OQ process. is definitely lower than other processes. Lancelar pearlite generally considered deleteri-ous for impact resistance. Fully hardened structure (mar-tensitic) obtained by direct OQ process and shows better		100 (70.5)	87 (61.53)	3	250	
					110 (77.55)	100 (70.5)	2	275	

Table 3+2 continued

1	2	3	4	5	6	7	8	9
		impact properties.						
		(b) Machinability:- Slightly superior in case of directly QQ pearlitic malleable compared to the reheated QQ drawn product.						
9	T.C.=2.5/2.6 Si =1.5/1.6 Mn =0.62/0.72 S =0.06/0.07	Pearlitic grade DIN specification GTS -45	Lamellar (45) to spheroidized pearlite + temper carbon	-	-	7	160/200	U.K. Bhatta- charya (141)
	Alloying: Mn. Mn/S ratio 9:1, 12:1. B=0.001/0.0015 Bi=0.01 B = 0.001 found optimum for Mechanical properties.	FSG over, Air quenching, tempering: 23, 18 and 15 hrs. cycles tried. 23 hrs. cycle tried in practice. Total cycle:- (i) heating to FSG temp (950°C) in 4.4 hrs. holding 5 hrs., slow cooling to 870°C in 1 hr., Air-quenching for 10 minutes. (ii) Temper by heating to 720°C in 2 hrs., holding for 4 hrs., slow cooling to 690°C in 2 hrs. (Air quenched pearlitic)	Lamellar to (50)/(60) spheroidized pearlite + temper carbon.	-	-	8/10	190/210	
			Mainly spheroidized pearlite					

Sequence of developments pertaining to pearlitic malleables are summarised in Table 3.2. This summary brings out the influence of composition variation, alloying and a variety of heat-treating cycles employed so far on the resulting microstructures and important mechanical properties.

3.2 Effect of Alloying and Trace Additions

Alloying and trace elements have been extensively employed in the production of pearlitic malleable iron for one or more of the following purposes:

- a) To achieve superior mechanical properties.
- b) To obtain in particular, better abrasion resistance in fully hardened product.
- c) To obtain better hardenability for through hardening of sections upto 25 mm in thickness.
- d) To impart corrosion resistance to the final product.
- e) Trace elements like Bi and Te used for mottle control.
- f) To develop a required microstructure at specific stages of heat-treatment cycle.

Basically, all the elements used in steels could be used in malleables too. But in practice so far, Mn, Cu, Mo, Cr and Ni have been employed as alloying elements, while B, Bi, Mg and Te have been used in trace amounts for different purposes.

The influence of Cu on the mechanical properties of

pearlitic malleable irons has been studied by many workers. P.B. Burgess⁽⁹⁰⁾ found that the mechanical properties of Cu alloyed pearlitic malleables can be improved by the help of age-hardening treatment subsequent to FSG completion and tempering at 715°C for 7 hrs. Maximum improvement in mechanical properties was found at 1.17 percent Cu content. The UTS improved by nearly 13,000 psi (9.165 kgs/mm²), the Y.S. by 12,000 psi (8.460 kgs/mm²), and the hardness increased by 24 BHN, while the percentage elongation decreased slightly (0.5 percent only), through an ageing treatment at 450°C for 16 hrs. This material may be considered excellent for medium strength ranges, the details of their mechanical properties are listed in Table-3.2. It can be noted from the work of Burgess that the mechanical properties of just air-cooled pearlitic malleable subsequent to FSG completion, improved as the Cu content increased from 0.54 to 1.57 percent. In an earlier work, B. Thyberg⁽¹²⁸⁾ had brought-out the advantages of employing Cu as an alloying element, but he did not employ the ageing treatment in his work. He found that Cu alloying yields higher UTS and Y.S. with increasing Cu content, but the percentage elongation deteriorates slightly. The compositions investigated by him were initially alloyed with 0.8/0.85 percent Mn and had Cu alloying upto 1.0 percent. Various heat-treatments resorted to in his work are listed in Table-3.2, and they involved mainly solutionising at

850°C, quenching and tempering subsequent to normal malleabilisation anneal in tunnel-furnace. Best property combinations reported by him were: UTS-67/71 kgs/mm², Y.S.-42/48 Kgs/mm² percent elongation - 5/6 and Hardness-218/230 BHN. The final microstructure of these pearlitic- malleables had cementite spheroids embedded in the ferritic matrix plus temper carbon nodules. Plant "E" in another reference (132,133), has been stated to be following the similar practice as described by Thyberg. Only the cycle details were different at this plant. The spheroidized pearlitic malleable produced at this plant had 70.5 kgs/mm² UTS, 44.0 kgs/mm² Y.S., 8.5% Elong. and 241 B.H.N. Such copper alloyed pearlitic malleables are designated as "high elongation grades" at this plant. In some cases (132,133), copper is employed upto 0.5% only for imparting corrosion resistance to the castings and is considered optional.

Upto about 1.0% Ni, the influence of Ni was found to be of the same order as Cu. (128) Hence, alloying with Ni increased the ratio of Y.S./U.T.S. Schneidewind (157) had reported that the Y.S. increased by 30% due to 2.5% Ni addition. However, the use of Ni has not been preferred in industrial practice due to its prohibitive cost, as it is nearly five times more expensive than Cu.

Molybdenum (0.5%) has been reported to increase the strength with impaired ductility. (128,134). Simult-

aneously, 0.3-0.5%. Mo was found to delay both FSG and SSG reactions. Molybdenum, therefore, has to be used in a controlled manner in pearlitic malleables. Cr similarly, as mentioned earlier, shall retard both FSG and SSG reactions drastically since it is a very strong carbide former.

Manganese is the alloying element, that has been most commonly employed in the manufacture of pearlitic grade malleable iron. Manganese in the range of 0.75/1.25%. (Mn: S ratios of 9:1 to 12:1) would suppress SSG (111,134) without undue interference with FSG. This fact provided one way of producing pearlitic malleable from the same equipment that is normally employed for the production of ferritic malleable iron. The two products can, therefore, be made simultaneously in the same equipment. Mn-alloying and ferritic heat-treatment produces a microstructure with lamellar pearlite and blocky ferrite around tempered carbon nodules. This microstructure results in strength properties of lower order and poor machining characteristics (111). Also the impact-resistance of lamellar pearlitic structure, obtained by this process, is inferior to that of tempered and spheroidised martensitic structure of the same hardness. Mn has generally been employed to improve hardenability of comparatively thicker sections for the production of pearlitic malleable castings. (111,128,129, 130,132,133,134,141). A wide range of mechanical properties can be developed by suitable heat treatment of Mn-alloyed

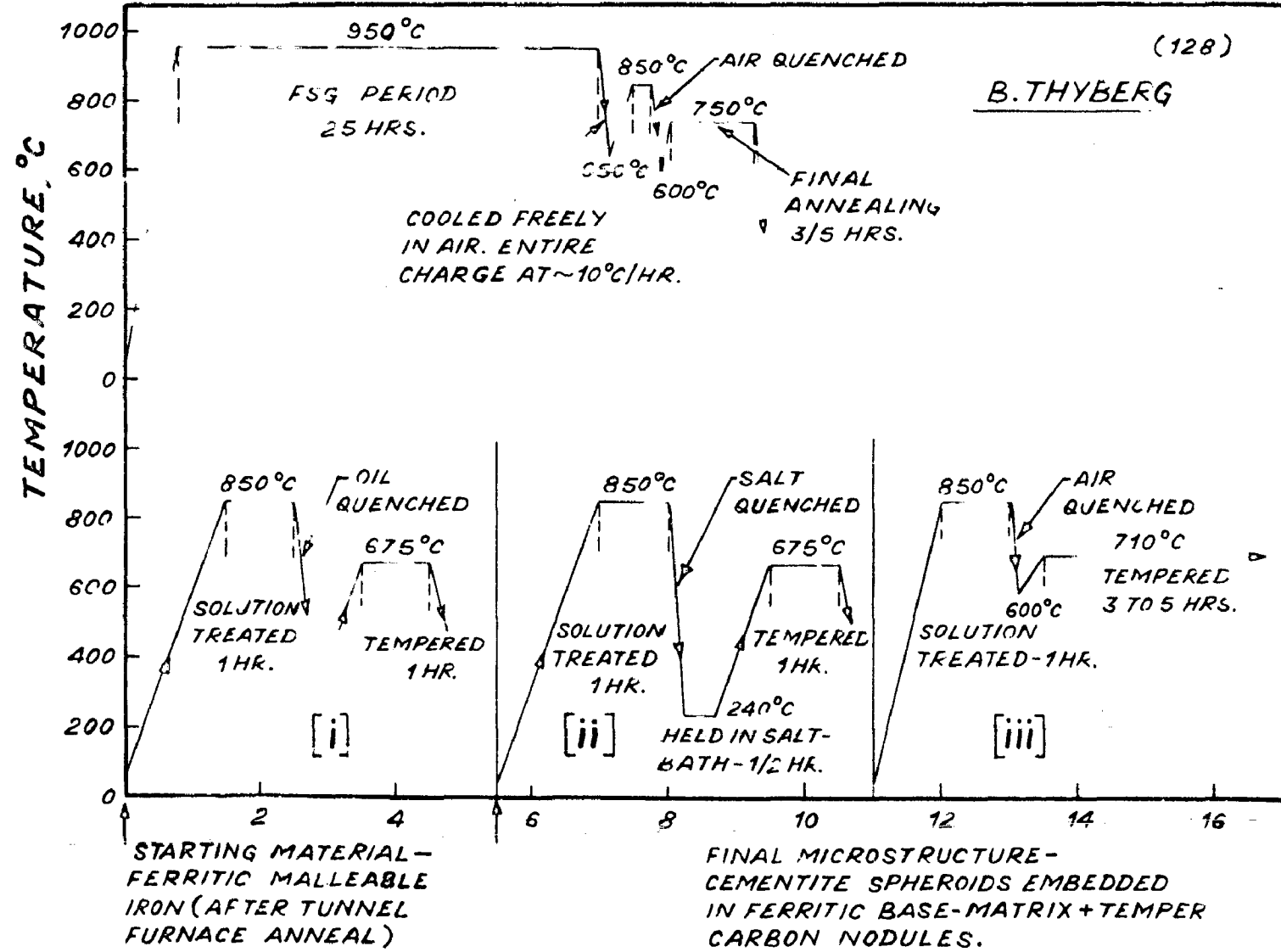
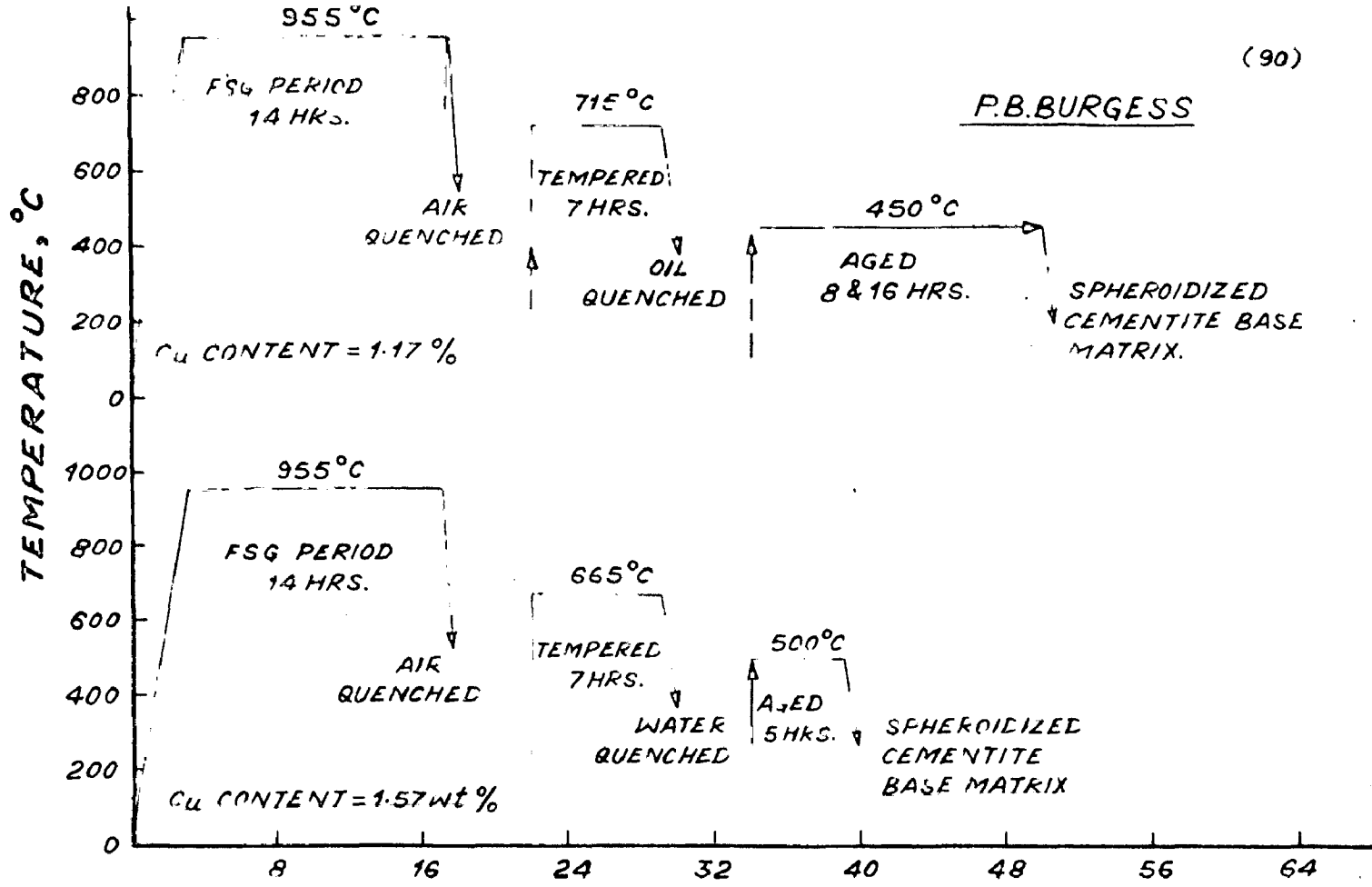


FIG.-3.1. HEAT-TREATMENTS FOLLOWED FOR THE MANUFACTURE OF HIGH DUTY PEARLITIC MALLEABLE IRONS.

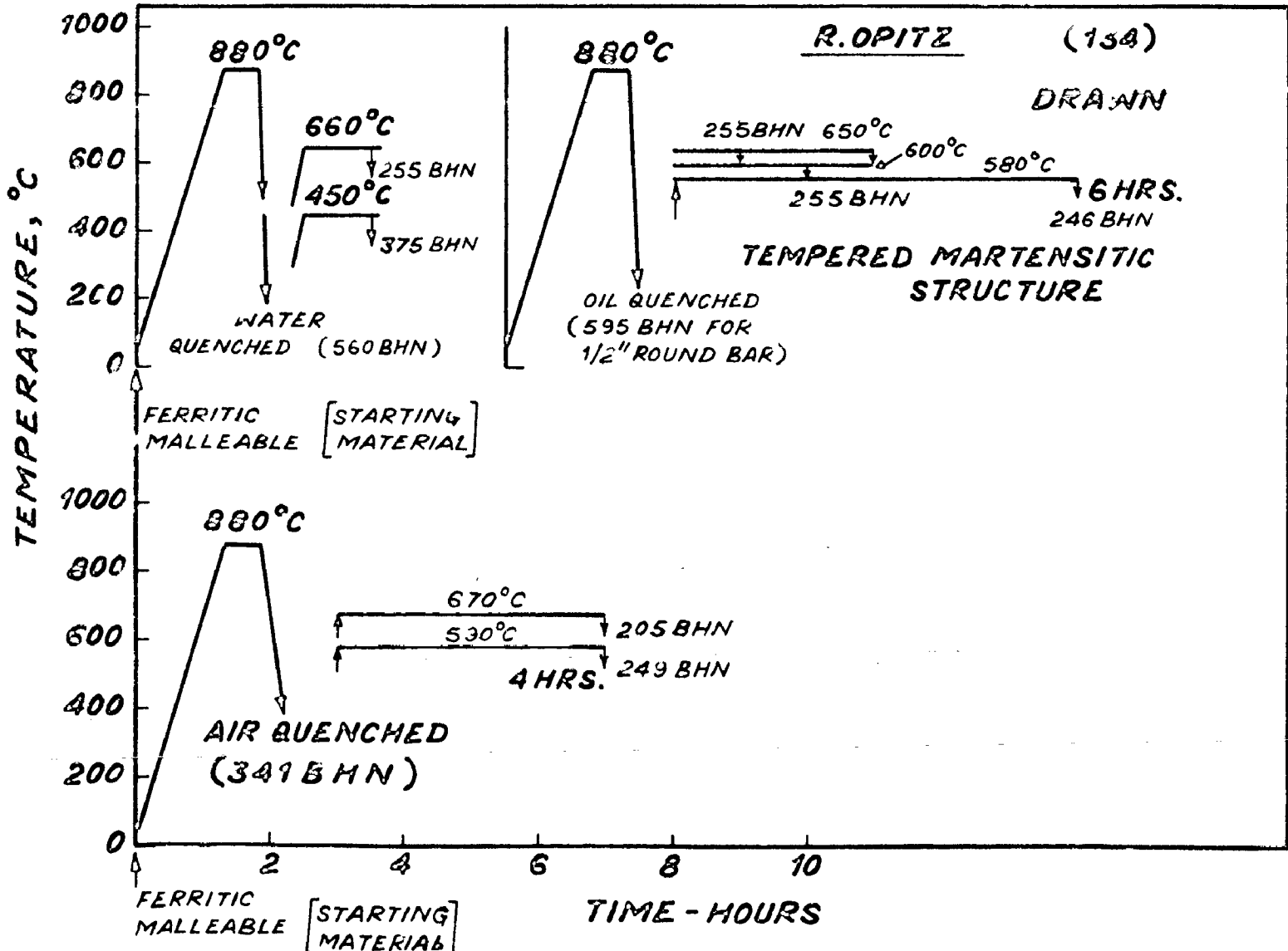
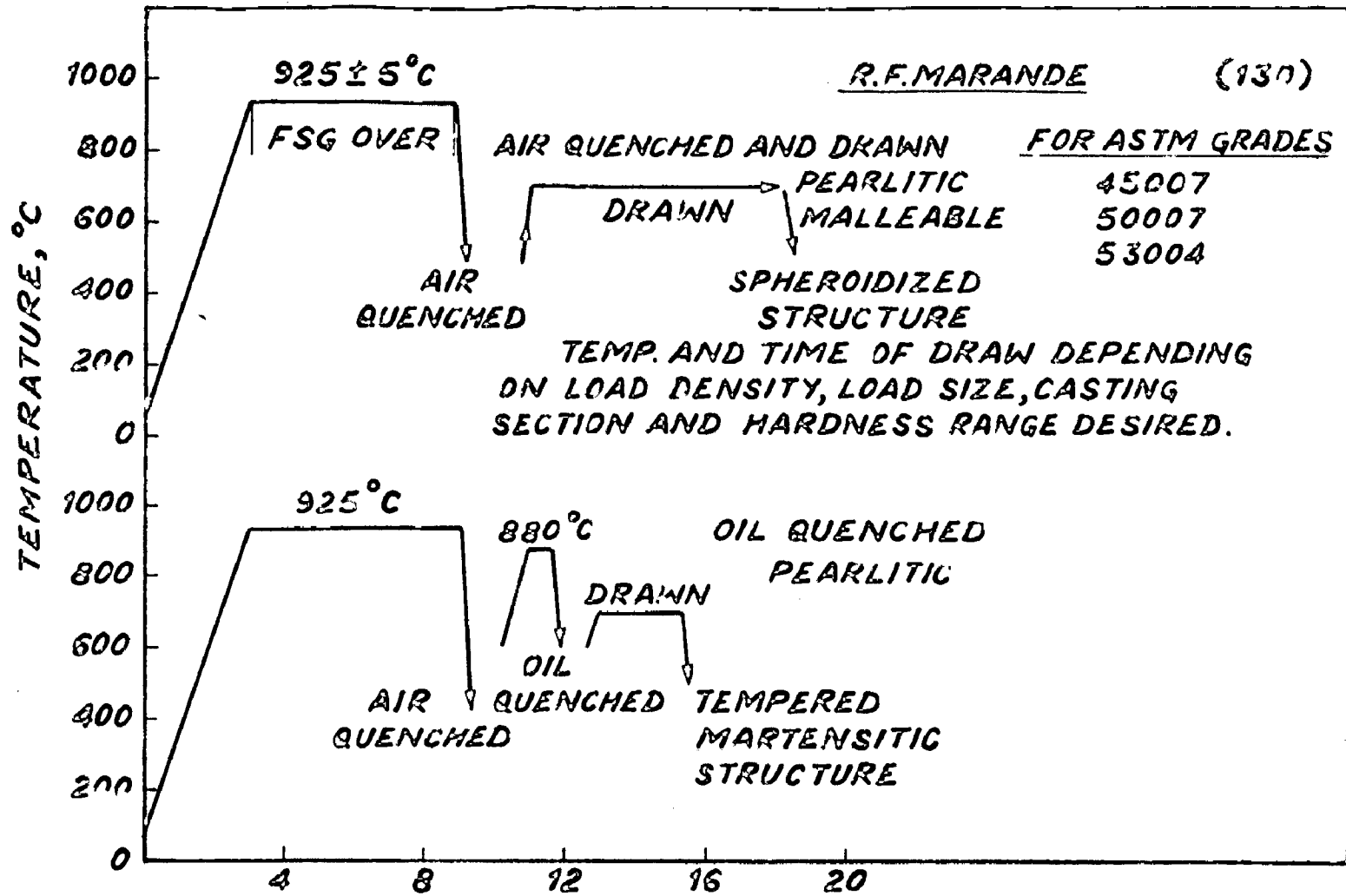


FIG.- 3.1 (ii) CONTINUED.

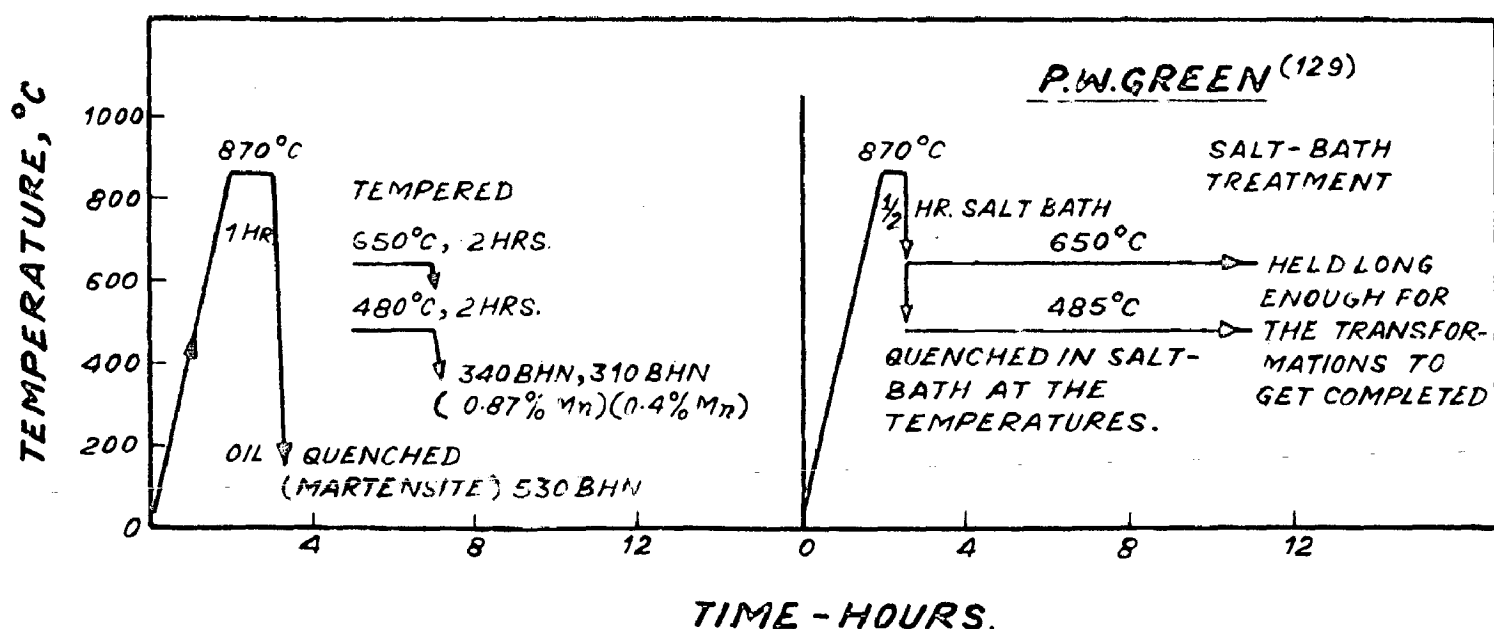
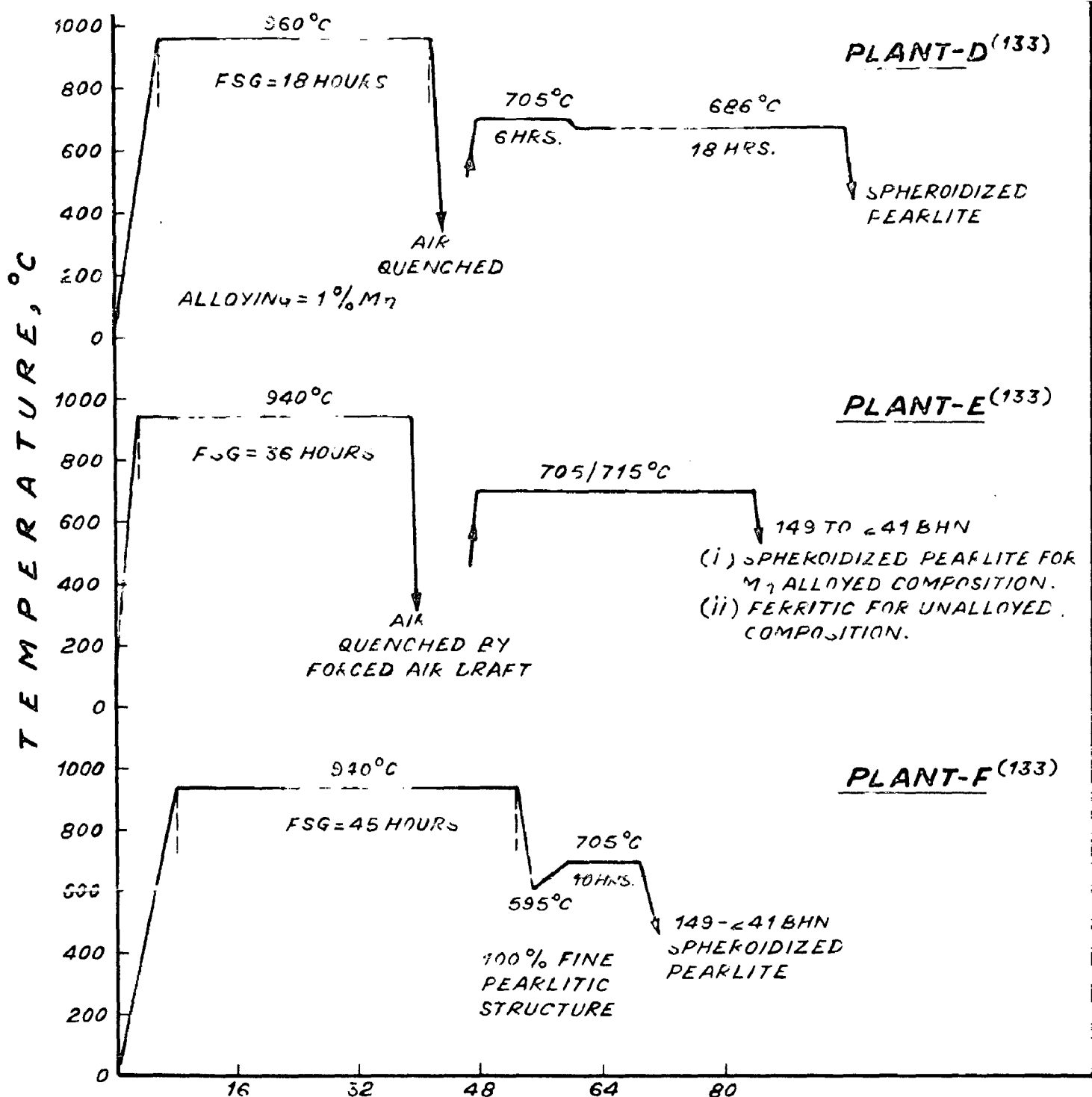


FIG.-3.1(iii) CONTINUED.

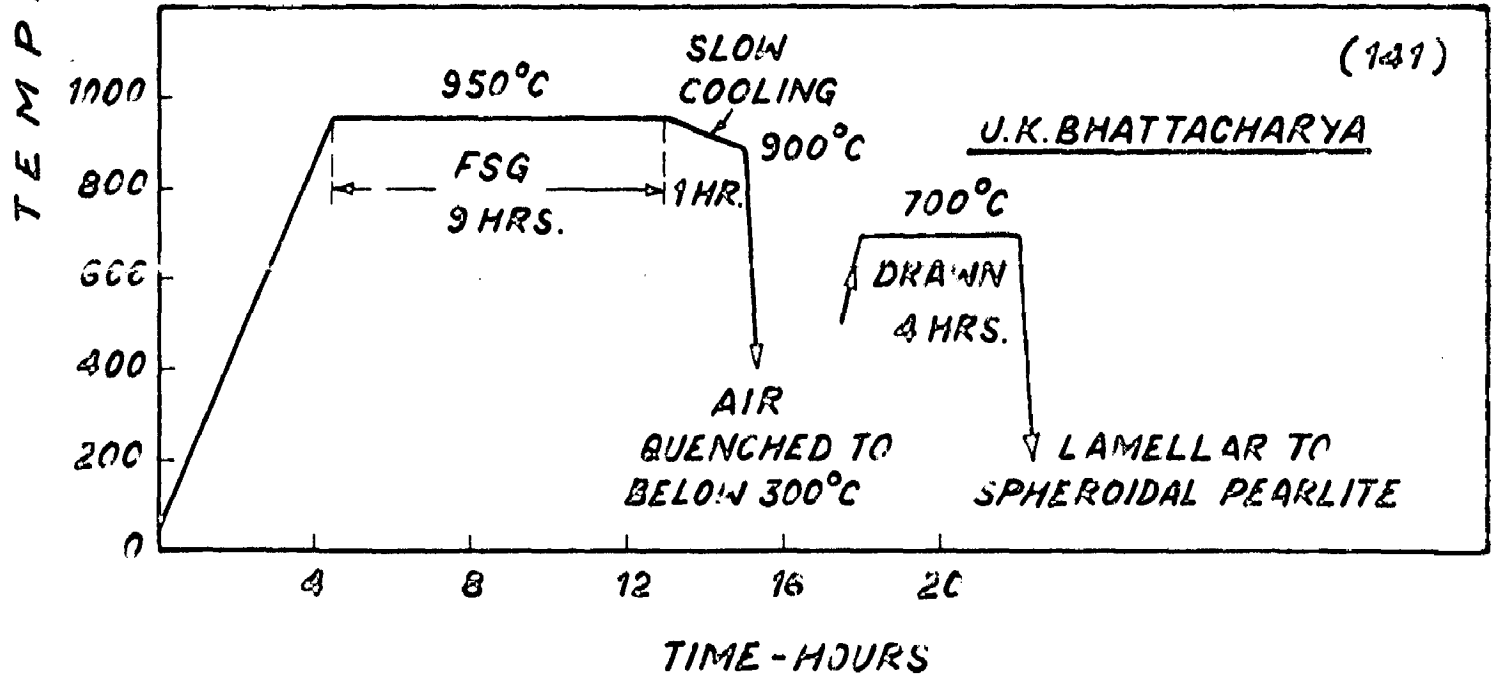
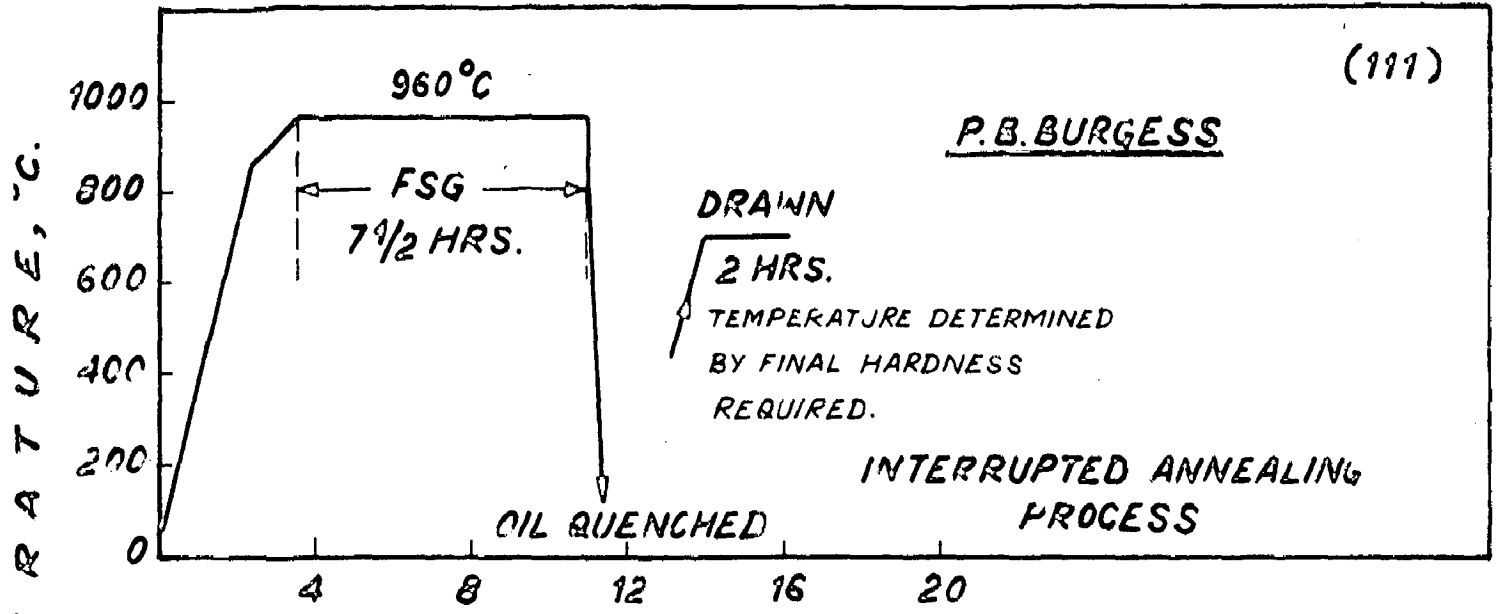


FIG.-3.1 (iv) CONCLUDED.

composition, which are discussed in subsequent sections of this chapter. On the whole, Manganese offers considerable advantages in the production of pearlitic malleable irons and simultaneously it is cheap and is easily available.

Trace elements like Bismuth (0.01 to 0.02%) and Tellurium (0.001%) have been used for mottle control primarily. As shown in Table 2-1, these trace elements do not effect annealability unfavourably, but prevent mottling effectively. Boron has been used in the range from 0.001 to 0.003% in pearlitic malleable iron manufacture in order to counteract the influence of Bi on nodule counts. Satisfactory mechanical properties were found at 0.001% B level, while these properties deteriorated at 0.0015% B level, because of the presence of considerable amount of ferrite in the microstructure of airquenched and tempered pearlitic malleable iron.⁽¹⁴¹⁾ Probably 0.0015% Boron caused SSG reaction during tempering.⁽¹⁴¹⁾ Inoculation by 0.04% Mg caused drastic shortening of FSG period and yielded excellent mechanical properties in pearlitic malleable condition according to one reference.⁽¹²³⁾

3.3 Influence of Heat-Treatments:

Table 3.2 and Fig. 3.1 summarise the details of heat-treatment cycles developed so far for the manufacture of pearlitic malleable irons with wide range of mechanical properties. Systematic evolution of these different processes was mainly governed by the existing equipment

facilities at individual plants and the final mechanical properties desired from the finished product. The main aim of all these heat-treatment processes was, therefore, to produce a desired microstructure and grain size corresponding to a definite range of mechanical properties in the finished product. Basically, all the heat-treatment that can be applied to low and medium carbon steels, can be used in pearlitic malleables too.

3.3.1 Mn-Alloyed Pearlitic-Malleable and Hardened Ferritic Malleable

One of the earliest methods of producing pearlitic malleable was the practice of hardening completely annealed ferritic malleables or the suppression of SSG reaction during normal ferritic anneal by Mn alloying (0.75/1.25% with 10:1 or 12:1 Mn/S ratios). Severity of quench followed by re-austenitising was important in the previous case and the final mechanical properties were adjusted by suitable tempering or spheroidization treatment in both the processes. Lower hardenability and higher N_v (No. of Nodules/mm³) associated with completely ferritic malleables compared to the later process or the processes which employ either manganese alloying or interrupt the process after FSG completion, put a stricter limitation on the maximum section thickness that can be properly hardened. Thus a part of the ferritic-malleable production could be hardened to different pearlitic malleable grades as desired. And both

normal ferritic anneal composition as well as manganese alloyed pearlitic compositions could be treated simultaneously in the same ferritic anneal equipment. These two processes were successfully employed by many foundries after World War II. Details summarised in Table 3.2 and Fig. 3.1 show that wide range of mechanical properties can be developed in standard ferritic or spheroidized malleable irons by suitable hardening and tempering treatment.

3.3.2 Air-Quenched Pearlitic Malleable

" Interrupted annealing process " has inherently more flexibility of operation and can treat smaller bulk of loads, though this process requires a separate furnace equipment. The process involves completion of FSG, lowering of temperature for the adjustment of austenitic carbon content, quenching under air-blast and tempering to the desired final hardness. Air quenching from lowered austenitic temperature shall result in lamellar pearlitic structures even in thinner sections, which on drawing, will yield partial carbide spheroidization. These air-hardened grades require longer tempering periods, or in case of equal periods, higher tempering temperatures than oil-hardened grades. Thus, the same UTS can be obtained by means of higher temperatures and short periods or vice-versa. In practice, longer periods at lower temperatures are preferred, since a higher uniformity over all the charge can be expected. This process is, therefore, suitable only .

for making medium strength pearlitic malleable irons. Also, lamellar pearlitic structure produced due to air-quenching process, results in non-uniform hardness, poor machinability and low impact-resistance. Further, air-quenched pearlitic malleable tend to have lower elongation and yield strength than oil-quenched pearlitic grades of the same hardness. But air-hardening requires less heat-input compared with oil-hardening and this method is to be preferred for lower strength pearlitic malleable irons and especially for castings with thin walls. Investigations conducted by different workers, summarised in Table 3.2 and Fig. 3.1, show that the mechanical properties developed in air-quench-tempered, Mn-alloyed, pearlitic malleables are within the following limits:

UTS-50-70 kgs/mm²
Y.S. 32-44 kgs/mm²
%. Elong - 19-5
B.H.N.-174-249
Y.S/UTS ratio-0.64-0.63

3.3.3 Liquid-Quenched Pearlitic Malleable

Air-quenched castings after FSG completion are re-austenitised, oil-quenched and drawn in this process. Later on, "continuous pearlitic malleable heat-treatment process" was developed because of the problems associated with "AQ, reheat, OQ, drawn" process.

Depending on the factors of hardenability, section-

size and quench-efficiency, fully hardened or martensitic structures are produced by oil-quenching subsequent to re-austenitising in sections upto 1-1/4" dia. Drawing subsequently can produce a wide range of structures varying from highly acicular tempered martensite to well spheroidised cementite particles embedded in a ferritic matrix depending on the final hardness desired. Most pearlitic malleable castings of hardness greater than 200 BHN have been produced by AQ, reheat, OQ process. The principal problem associated with this process is the formation of upto 0.005" thick decarburised layer on the castings, which interferes seriously with the efficiency of oil-quenching.⁽¹¹¹⁾ These thick oxide layers are formed due to lack of atmosphere control in hardening furnaces. Well quenched, fully hardened martensitic structures respond more readily to drawing than the lamellar pearlitic structures. Draw periods are thus reduced from 5 hrs. to 2 hrs. in case of martensitic hardening. Use of proper austenitising and quench temperature, superior quench oils, alloying and the direct oil-quenching method subsequent to FSG completion, ensures that at least 50% martensite is formed at the centre of 1" round compared to the earlier limitation of 5/8" round and that no scale is formed on the castings, which otherwise would lower the efficacy of quench.⁽¹¹¹⁾ As quenched martensitic structures are later tempered to the desired hardness. This "continuous pearlitic malleable heat-treatment process" requires a special pusher type continuous furnace, provided

with protective atmosphere. And tempering is done in a continuous belt furnace in 2 hr total cycle time at temperatures required for final hardness.

Investigations by P.B. Burgess⁽¹¹¹⁾ B. Thyberg⁽¹²⁸⁾, R.F. Marande⁽¹³⁰⁾, R. Opitz⁽¹³⁴⁾ AFS. Committee 6-E⁽¹³³⁾ P.W. Green⁽¹²⁹⁾, and H.H. Johnson and W.K. Bock⁽¹¹⁰⁾ summarised in Table 3-2, have shown that optimum engineering properties in pearlitic malleable castings are developed by drawing fully hardened martensitic structures. Use of "continuous pearlitic malleable heat-treatment process", Mn alloying, quenching from a protective atmosphere in superior oils has been recommended by Burgess.⁽¹¹¹⁾ Impact transition temperature of 3/4" dia pearlitic malleable heat-treated by direct quench process was found to be definitely lower than when heat-treated by other processes.⁽¹¹¹⁾ Burgess⁽¹¹¹⁾ argues that this may be related to better hardening and elimination of lamellar pearlite which is generally considered deleterious for impact resistance. Direct oil quenched pearlitic malleable have also slightly superior machining characteristics compared to the reheated and oil-quenched product.⁽¹¹¹⁾ Mechanical properties obtained by direct oil-quenched pearlitic malleable process are approximately the same as developed by "reheat-oil-quenched process" at hardness upto 241 B.H.N. But the tensile and yield strength at hardness levels beyond 241 B.H.N. are comparatively higher in case of direct oil quenched pearlitic process.⁽¹¹¹⁾ A higher yield strength is developed

in case of reheated oil quenched - tempered product compared to air-quenched cases and the same UTS is obtained by OQ at lower B.H.N. ⁽¹³⁴⁾ These pearlitic malleables have been found to have better machinability compared with steel castings and forgings. ⁽¹³⁴⁾ Investigation data summarised in Table 3-2 shows, that higher strength pearlitic malleable grades are best made by liquid quenching and tempering. ⁽¹³³⁾ Since liquid-quench gives higher yield strength at a given hardness, higher Y.S./T.S. ratio (0.8) is produced by liquid quenching and tempering. ⁽¹³³⁾ Also, it can be seen that alloying is not a factor in the tensile and yield-strength values except that it permits different casting sections to be thoroughly hardened by liquid or air-quenching, but it has been reported that alloying has favourable effect on ductility. ⁽¹³³⁾ Lower carbon and silicon have also been found to yield higher % elongation. ⁽¹³³⁾ Highly acicular structure formed by salt-bath treatment has been found to yield superior mechanical properties (T.S., Y.S., % Elong) than the oil quenched and tempered pearlitic transformation products at comparable hardness levels. ⁽¹²⁹⁾ Impact properties of these highly acicular transformation products are also superior than oil-quenched and tempered pearlitic malleable of the same hardness. ⁽¹²⁹⁾ Optimum mechanical properties developed by these processes are :

UTS-84.0 kgs/mm², % Elong-4

Y.S.-64.00 kgs/mm², B.H.N.-285, Y.S./UTS ratio= 0.76

3.4 RELATED MICRO-STRUCTURES AND MECHANICAL PROPERTIES

Influence of alloying and trace elements and different heat treatment practices on final micro-structures and corresponding mechanical properties of pearlitic malleable irons were discussed in previous sections of this chapter. Investigation results of different workers in this regard are summarised in Table 3.2.

Wide range of micro-structures varying from coarse lamellar pearlite plus some 20% ferrite to highly acicular tempered martensite can be produced in pearlitic malleable irons by suitably adjusting the alloying and heat-treatment practice details. Final mechanical properties developed in different grades of pearlitic malleable irons are thus directly related with their corresponding microstructures. The Microstructures developed at individual stages of heat-treatment are closely controlled by suitable adjustment of operating parameters, commencing from the initial stages of composition adjustment and alloying etc.

It can be seen from the data in table 3.2 that the tensile and yield strength of higher order (84-85 kgs/mm² UTS and 64-65 kgs/mm², Y.S./UTS ratio of 0.8) are associated with highly acicular tempered martensitic structure. This microstructure may be developed in castings by different processes viz. direct oil quenching and tempering air-quenching re-austenitisation-oil quenching and tempering and salt bath treatment etc discussed in details in section 3.3.3.

Essentially, this micro-constituent is strong, hard and tough and therefore these structures possess much higher impact strength compared to lamellar pearlitic structures and show nearly 3/4 percent elongation at 285/290 B.H.N..

Completely or partially spheroidized pearlitic microstructures yield medium strength grades of pearlitic malleables. Strength ranges in this case are UTS-50/70kgs/mm², Y.S.-32/44 kgs/mm², Y.S/UTS ratio-0.6/0.65%. Elongation 5/19 and B.H.N. 174/249. These microstructures may be developed in pearlitic malleables by a variety of heat-treatments, discussed in detail in sections 3.3.1 and 3.3.2. Liquid quenched and drawn completely spheroidized structures yield superior mechanical properties compared to air-quenched and drawn microstructure since some ferrite is usually associated with the later structure. Yet, forced air-draft is employed in practice for quenching large bulks of pearlitic malleable castings for economy reasons. But Mn alloying (0.85/1.25) ensures that less ferrite is present in air-quenched microstructures. On the whole, air-quenched malleable castings correspond to the lower strength grades.

3.5 USER REQUIREMENTS

A wide range of physical mechanical and engineering properties offered by different grades of pearlitic malleable irons, make it a versatile material to meet variety of user requirements. It offers to the designer ultimate tensile strengths upto 85.0kgs/mm² and yield strengths upto 70.5kgs/mm²

with corresponding percentage elongation of 2% minimum in 2" G.L., yield to tensile ratio of 0.65 to 0.9 obtainable in high strength pearlitic malleable irons. Wide range of hardness offered by different grades (163 to 280 B.H.N.) make it suitable for frictional, wear and abrasion resistant applications. In addition, the concerned component may be either surface or through hardened to develop much higher hardness values.

Pearlitic malleable irons have been found to exhibit a good factor of safety against notch fatigue failure.⁽¹⁶⁸⁾ And the fatigue life of pearlitic malleable is extended many fold by adequate shot-peening in critical locations.⁽¹⁶⁶⁾ Shear-Strengths of pearlitic malleable have been reported to lie between 70 and 85% of their UTS values. Charpy V-notched bars of spheroidized pearlitic malleable iron gave maximum values upto 14 feet.pounds (1.932 kgm).^(166,168) Only by a sufficient lowering of the temperature did a brittle-type-fracture develop and this when the Impact values had dropped to about 4 or 5 feet pounds (0.69 kgm). Charpy un-notched tests on both air-cooled and oil-quenched pearlitic malleable specimens gave impact values of 22 to 35 feet-pounds (3.03-4.83 kgm).⁽¹⁶⁶⁻¹⁶⁸⁾ It was stated earlier that tempered martensitic and spheroidized structures offer better impact and machinability properties than lamellar pearlitic structure at comparable hardness levels.⁽¹¹¹⁾ Suitable grades of pearlitic malleables can thus be selected to meet the design requirements of different components.

Several studies on the influence of elevated temperature on the mechanical properties of pearlitic malleable irons have confirmed that high strength combined with considerable ductility is maintained between 0°C and 315°C.⁽¹⁶⁶⁾ Strength declines and ductility increases above 315°C. These results correspond to short exposure periods of 15-20 minutes at the temperatures. During long period exposure tests, upto 1000 hrs at 535°C, 595°C and 650°C, it was revealed that alloying with 0.3% or more molybdenum helped to stabilise and strengthen the pearlitic matrix.^(96,166) These studies indicate that pearlitic malleable irons alloyed with at best 0.3% Mo can be usefully employed upto 350°C. Alloying, similarly, was found to delay the softening reaction and therefore raises the final minimum hardness obtained after elevated temperature exposure. Higher silicon and phosphorus contents, and greater combined carbon in the matrix (corresponding to higher strength, higher hardness pearlitic malleables) tend to raise the transition temperature. Complicated casting geometries can be cast to close dimensional tolerances and with good surface finish due to good fluidity of white iron. And because of prolonged heat-treatment cycle of pearlitic malleable iron manufacture, all the internal stresses of castings are fully removed. Also, the degree of machinability suitable for a particular requirement, can be readily available in case of pearlitic malleable irons, since a wide range of hardness and structure is obtainable in this class of malleable irons. Higher the hardness, better is the final

finish after machining.⁽¹⁶⁶⁾ It was reported that the addition of 1 percent Cu increased the machinability of the pearlitic malleable iron to 85% of that of the standard malleable iron.⁽¹⁶⁶⁾ Pearlitic malleable irons are generally considered unsuitable for welding, which is one undesirable factor from consumer view-point. But a higher degree of structural uniformity is found in pearlitic malleable iron-castings compared to steel forgings of equal hardness and strength, which is entirely due to the prolonged heat-treatment given to these castings, the heat-treatment being an integral part of the process.⁽¹³⁴⁾ It is thus seen that pearlitic malleable irons can meet a wide variety of user requirements upto 300°C.

3.6 TRANSFORMATION MECHANISMS

As mentioned earlier in section 3.2 and 3.3 all the transformations that can be carried out in low and medium carbon steels can be carried out in pearlitic malleable irons too. Also, it was discussed in the preceding sections that the characteristic properties in pearlitic malleable irons were obtained due to the combined carbon (0.3 to 0.9%) in the base matrix. Depending upon the nature of the carbides, their abundance, size and distribution, different properties in pearlitic malleable can be developed. The microstructures can thus vary over a wide-range, from spheroidized cementite to highly acicular tempered merrtensite.

Basically, the transformations from austenitic

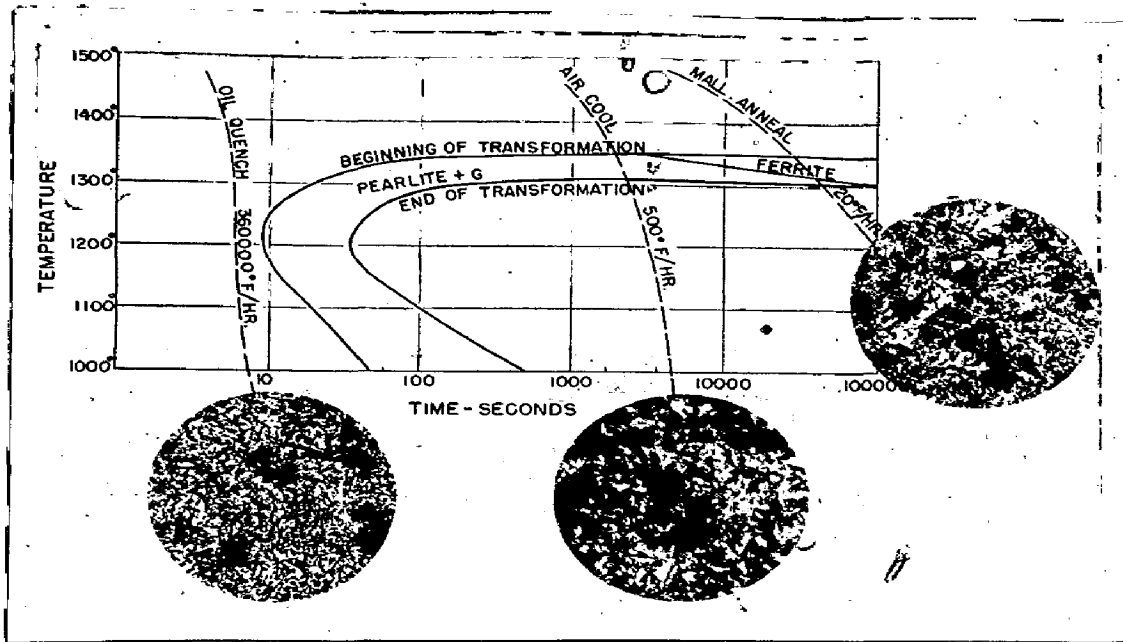


Fig. 3.2 - TTT diagram of unalloyed pearlitic malleable iron (133).

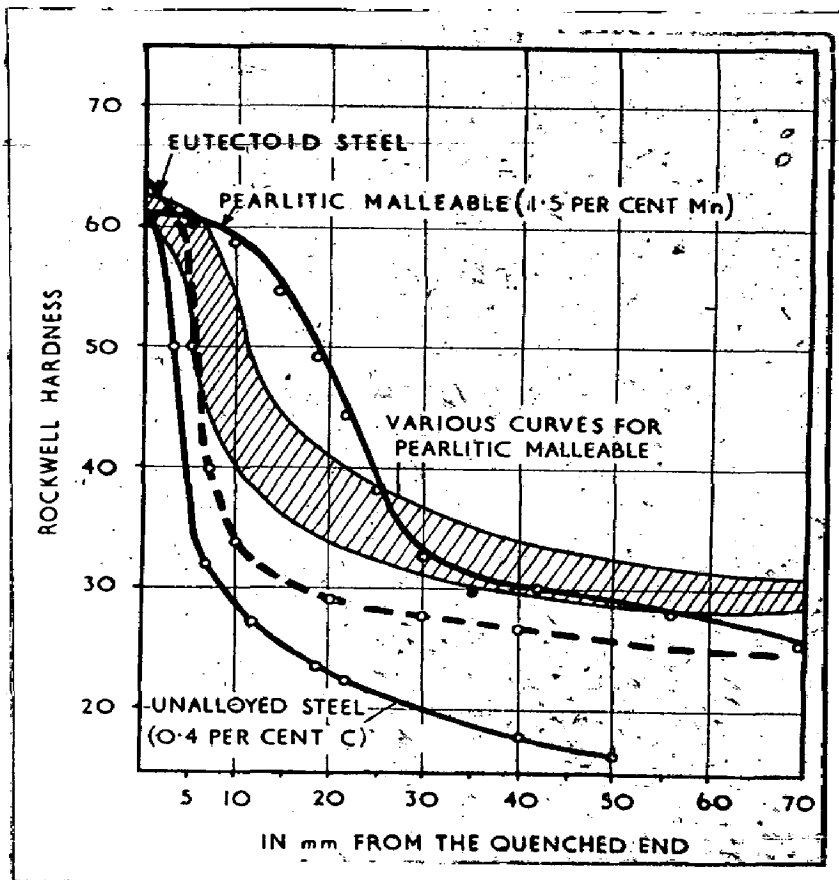


Fig. 3.3 - Hardenability Curves of pearlitic malleable irons in comparison with those of steels. R. Optiz. (134)

temperature range are controlled by typical TTT (time-temp-transformation) diagrams and hardenability curves of individual pearlitic malleable iron compositions. These characteristics are greatly altered by suitable alloying elements viz. Mn, Ni, Cu, Mo etc. One of these typical TTT diagrams for unalloyed pearlitic malleable irons is shown in Fig. 3-2. (133) Elements like Mn will shift this diagram to the right, resulting into fully pearlitic structures in reasonably thick sections on air-cooling. Austenitising temperature and the soaking period may be suitably controlled to retain the desired quantity of carbon in the base-matrix. A faster rate of cooling from the austenitic temperature shall result in fully hardened or martensitic structures since the diffusion of carbon is not permitted in this case. The depth of hardening in a given section shall be determined by its hardenability characteristics, which is again controlled by the base-composition and alloying. One of these typical hardenability curves for unalloyed and Mn-alloyed pearlitic malleable irons is shown in Fig. 3-3, which also compares this material with unalloyed 0.4% steel and eutectoid steel in this regard. (134) Subsequent isothermal treatment at different subcritical temperatures for shorter or longer durations may give rise to a variety of microstructures, corresponding with a wide range of mechanical properties.

Pearlitic malleable irons respond more readily to hardening compared to ferritic malleable irons (128),

because the former has carbon in the form of graphite and cementite evenly distributed throughout the matrix prior to quenching. The austenite quickly dissolves the necessary amount of carbon, since the diffusion paths are short and also because the diffusion rate of carbon is high in austenitic temperature ranges. This is more difficult in wholly ferritic material. Hence, in case of flame and induction hardening, where extremely short heating times are involved, a wholly pearlitic matrix is a prerequisite to a satisfactory final result.⁽¹²⁸⁾ It was reported that hardenability of pearlitic malleable iron varies with quench-temperature and the nodule counts.^(111,127) It is because of high speed of carbon diffusion at elevated temperatures that the carbon content of austenite is reduced during cooling or quenching, which finally yields lower as-quenched hardness values. The effect of lower hardenability with higher nodule counts, is also possibly associated with diffusion during cooling so that the combined carbon of castings with higher nodule number tends to be lower than that with lower nodule counts.⁽¹¹¹⁾

CHAPTER-4

SPHEROIDAL GRAPHITE CAST IRONS.

4.1 INTRODUCTION

Spheroidal Graphite, Nodular or Ductile iron is a family of alloys, which combine the principal advantages of grey iron (-low-melting point, good fluidity and castability, excellent machinability and good wear resistance) with the engineering advantages of steel (high strength, toughness, ductility, hot-workability and hardenability).⁽¹⁷¹⁾ A wide range of mechanical properties can be developed in ductile-irons by suitably controlling their base-matrix. The control of base-matrix can be achieved, through proper adjustment of base-composition, alloying, founding practice and heat-treatment. Thus ultimate tensile-strengths upto about 105 kgs/mm^2 can be developed in S.G. irons along with 1 to 4 percent elongation on 2" gauge length. Ductile-irons have, therefore, proved to be an excellent engineering material for widespread end applications. Major varieties of this material are summarised in Table 4-1 and 4-2.

4.2 TYPES AND APPLICATIONSTable 4-1Principal types of Ductile-iron (171)

(according to Grey and Ductile iron Founders Society)

Type No.	Brinell hardness No.	Characteristics	Applications
80-60-03	200-270	Essentially pearlitic matrix, high-strength as cast. Responds readily to flame or induction hardening	Heavy-duty machinery, gears, dies, rolls for wear resistance and strength
60-45-10	140-200	Essentially ferritic matrix, excellent machinability and good ductility	Pressure castings, valve and pump bodies, shock-resisting parts.
60-40-15	140-190	Fully ferritic matrix, maximum ductility and low transition temperature (has analysis limitations)	Navy shipboard and other uses requiring shock resistance.
100-70-03	240-300	Uniformly fine pearlitic matrix, normalized and tempered or alloyed. Excellent combination of strength, wear resistance, and ductility	Pinions, gears, crank-shafts, cams, guides, track rollers
120-90-02	270-350	Matrix of tempered martensite. May be alloyed to provide hardenability. Maximum strength and wear resistance	

Table 4.2

Indian Standard Specifications of S.G.Irons

IS: 1865-1968(Clause 10.1.1 and 10.3.1)

Property	Units	80/2	70/2	60/2	50/7	42/12	38/17
Tensile Strength Min.	kgf/mm ²	80	70	60	50	42	38
Proof-stress (0.2%) Min.	kgf/mm ²	48	45	40	35	28	24
Elongation Min.	%	2	2	2	7	12	17
Impact-strength min.	kgf.M.	(Charpy V notch beam type)					
a) Average	-	-	-	-	-	0.9 (optional)	1.7
b) Individual	-	-	-	-	-	0.6 (optional)	1.5
Brinell	HB	260	230	210	170	187	171
Hardness		330	300	280	240	max.	max.

Table 4-3

ASTM Specifications of Nodular Iron

Class	Minimum Tensile strength x 1000 psi	Minimum yield strength 0.2% off-set x 1000 psi	Minimum % Elog. in 2"	Composition requirement	Condition
-------	-------------------------------------	--	-----------------------	-------------------------	-----------

ASTM A 339-55

80-60-03	80a	60	3.0	-	As Cast.
	60a	45	10.0	-	Usually Annealed

ASTM A 396-58

120-90-02	120a	90	2.0	-	Heat-treated
	100a	70	3.0	-	Heat-treated

ASTM A 395-56T

60-45-15	60a	45	15.0	e	Ferritized by annealing
----------	-----	----	------	---	-------------------------

MIL I 17166 A

60-40-15	60a	40	15.0	f	Ferritized by Annealing to 190 BHN.
----------	-----	----	------	---	-------------------------------------

a- Test specimen to be machined from 1" keel-block or Y block in 1/2, 1 or 3" size.

e- 3% C Min, 2.75% Si, 0.08% P max.

f- Same as e + 4.5% C.E. max.

4.3 COMPOSITION LIMITS:

C.K. Donoho⁽¹⁵⁰⁾ has shown that a wide range of cast-iron compositions can be rendered ductile by magnesium process, while cerium process requires only hypereutectic analysis of cast-iron. For various reasons, the Magnesium process has now been universally accepted. The range of total carbon is wide, and it can vary from 3.0 to 4.0%. But the carbon equivalent value is limited to about 4.6% for section thicknesses greater than 25 mm, beyond which, graphite flotation may occur and may cause gross carbon segregation in cope surface of the casting. Simultaneously, Nodule counts are directly affected by the carbon content-greater number of spheroids formed at higher carbon contents. Limit of C.E. stated above may, however, be exceeded in case of thin sections which freeze faster.

The normal range of silicon in ductile iron is from 1.80 to 2.80%. The final silicon levels may vary from 2.0 to 3.0%. Magnesium has a greater degree of solubility in irons of higher silicon content. Since silicon affects C.E. value, it also affects the Nodule-number and the phenomenon of flotation. Also silicon promotes the formation of ferrite during eutectoid - transformation reaction and strengthens it. Silicon contents of upto 6.0% are used for increasing temperature-resistance upto 760°C.

Sulphur is held as low as possible, since magnesium and rare-earth metals both react first with sulphur. It is, therefore, desirable that sulphur content of melt prior to Mg or Ce treatment should preferably be less than 0.02% for economy reasons. Sulphur content after treatment is usually 0.015%.

A maximum of 0.1% phosphorus can be permitted, as phosphide constituents begin to appear at 0.11% phosphorus. It also reduces elongation and impact-strength. It is because of this reason that a maximum of 0.05% phosphorus is usually specified.

Manganese can range from 0.15 to 0.9%. It should be on the lower side for maximum ductility and fast ferritisation by heat-treatment. Higher Mn contents are desirable for highest as-cast strength and best response to hardening heat-treatment during the production of high strength grades.

Ductile iron can be alloyed by means of ladle additions viz. Mn, Ni, Mo and Cu. Alloying involving these elements may be designed for higher strengths, greater toughness, or increased high-temperature or corrosion-resistant properties. Behaviour of these alloying elements in relation to their influence on the microstructure, heat-treatment cycle and mechanical properties of ductile-irons is discussed in subsequent sections.

Similarly, the presence of some trace elements in

the liquid melt have been found to exert powerful influence either on the shape of graphite spheroids or on the base-matrix. Lead, Titanium, aluminium, antimony, zirconium, bismuth, selenium and tellurium, for instance, have been found to encourage the formation of degenerate graphite shapes. It was shown by Donoho⁽¹⁵⁰⁾ that harmful effects of these trace elements, except selenium and Tellurium, can be neutralised by addition of about 0.02% cerium. On the other hand, Arsenic, Boron, Chromium Tin and Vanadium are known to promote the formation of pearlite and/or iron carbide.

4.4 HEAT-TREATMENT

Ductile iron shows excellent response to heat-treatment. A wide variety of microstructures and therefore corresponding mechanical properties can be produced in ductile-irons. All those microstructures that can be produced in steels can be produced in ductile irons too. The carbon content of matrix may be varied from almost zero to over 0.80% by suitably adjusting the metal-analysis, alloying elements, foundry process control, and/or heat-treatment. As such the microstructures may be all ferrite, ferrite and pearlite, all pearlite (lamellar or spheroidized) martensite, tempered martensite, or bainite and may, in special alloys, contain carbides or an austenite matrix. Proper control of the

processing cycle can yield ductile-iron castings to specification without any heat-treatment. However, most ductile iron castings are normally heat-treated for either stress relieving or for developing the desired microstructure and mechanical properties. Alloying elements in ductile iron behave in the same manner as they do in steels.⁽¹⁷¹⁾ Main types of heat-treatments, applied to ductile irons, are given in brief in the following sub-section:

4.4.1 Stress-Relief:

Used to remove internal stresses in castings by holding at 538° to 675°C for 1 hr. plus 1 hr. per 25 mm. of section thickness.⁽¹⁷¹⁾

4.4.2 Ferritisation:

Used to develop maximum ductility and the best mechinability. The process may be carried out by using any of the following time-temperature cycles.⁽¹⁷¹⁾

(i) heat to 900°C , hold for sufficient period to decompose eutectic cementite fully, cool to 690°C and hold for 5 hr. plus 1 hr. per inch of thickness, and then uniformly cool to room temperature. One of the general ferritisation cycles is: hold at 900°C for 8 hrs. furnace cool to 690°C , hold for 16 hrs. at the temperature, finally furnace cool to room temperature.⁽¹²⁶⁾

(ii) heat to 900°C , and hold as above and furnace cool from 790°C to 650°C at a rate less than 19°C/hr.

(iii) subcritically anneal at 705°C for sufficient period to complete ferritisation. Furnace cool to at least 595°C .

The ferritisation time-temperature cycles mentioned above are, however, greatly influenced by the presence of alloying and trace elements in the base composition. Gilbert⁽¹²⁶⁾ found that ferritic S.G. Iron with 0.96% Cu had some retained pearlite. T. Levin et al⁽⁸⁸⁾ also confirmed that both tin and copper promote pearlite formation in ductile iron without promoting carbides. J. Bradshaw⁽¹⁴⁷⁾ has shown that complete removal of primary cementite during first stage of annealing is important, since any traces remaining in the matrix act as centres of pearlite stabilisation in subsequent second stage annealing. He also found that the last traces of pearlitic cementite were very slow to decompose during isothermal decomposition below the critical temperature range. Most pearlite was found to decompose in just $\sim 1/3$ rd time than required for complete removal of pearlite. Rehder earlier had shown that pearlite can be completely eliminated in shorter overall time by slow cooling through the critical temperature range than by holding at sub-critical temperatures; the maximum cooling rate depending on silicon content, nodule-number and other factors.⁽¹⁴⁷⁾ Bradshaw⁽¹⁴⁷⁾ recommends that two stage annealing process should be used in case of as-cast pearlitic S.G. Iron because it results in the production of softer and more

ductile matrix of ferrite. Higher first-stage annealing temperatures beyond 900°C are to be avoided, as higher temperatures shall promote grain-growth. Also, 700°C is considered satisfactory for the production of ferritic matrix in S.G. Irons. Prolonged second stage annealing is desirable and it has been reported that increasing the first stage annealing temperature from 860°C to 900°C , progressively accelerates the second stage ferritisation. Bradshaw⁽¹⁴⁷⁾ further states that ferritisation of a martensitic or bainitic matrix proceeds more rapidly than that of pearlitic matrix. And decomposition of bainite occurs no faster than that of martensite.

It was shown by G.J. Cox⁽¹⁴⁶⁾ that Ni contents of about 0.8% i.e. the levels found in irons treated with 15% Mg/85% Ni alloy, do not increase the amount of pearlite in the microstructure of as-cast high purity ferritic S.G. Iron or do not render them difficult to anneal. M.J. Lalich and C.R. Loper⁽⁸³⁾ in their recent study have shown the influence of pearlite promoting elements like Mn, As, Cu, Sb and Sn and strong carbide formers like Cr and V on the kinetics of the eutectoid transformation reaction in ductile irons. It is obvious that the presence of these elements has to be controlled in base-compositions which have to be ferritised subsequently.

G.N.J. Gilbert⁽¹³⁶⁾ pointed out that ferritic Nodular irons, like black-heart malleable irons and hardened

low alloy steels, exhibit temper embrittlement.

Maximum embrittlement was found to occur between 450°C and 500°C. Embrittlement in malleable or nodular iron occurs because the transition-temperatures are raised by heating in the temperature range of 350° to 600°C.

4.4.3 Normalising and Tempering:

Used to develop properties in the 100-70-03 and 120-90-02 types of ductile irons. Normalising is generally section size sensitive, and alloying elements such as Ni and Mo may be used to counteract this partially. Normalising is usually carried-out at 870° to 925°C, followed by an air-cool. Subsequently, tempering is carried out at 510° to 620°C for 1 hour⁽¹⁷¹⁾.

A.P. Alexander⁽¹⁴²⁾ found that the hardness of quenched and tempered nodular iron fluctuates widely below 305 B.H.N.. He suggests that this can be avoided by normalising the iron, which can produce hardness levels upto 328 B.H.N.. The hardness variation upon tempering after quenching seems to be due to precipitation of secondary graphite in the heating range from 566° to 593°C. Alexander⁽¹⁴²⁾ further suggests that one stage or two stage normalising can be followed for achieving higher hardness levels like 328 to 330 B.H.N.. Fluctuations in hardness values beyond 305 B.H.N. can, however, be maintained within a 5 point scatter in both quenched and tempered and normalised condition.

Ductile iron castings are usually normalised from a temperature of 900°C. G.J. Cox⁽¹⁴⁴⁾ determined the influence of varying temperature on the microstructure and mechanical properties of pearlitic S.G. Iron. Cox⁽¹⁴⁴⁾ suggests that normalising from about 850°C should be preferred, as it slightly improves ductility and toughness, without sacrificing tensile-strength and also because scaling is likely to be less at lower temperatures. But normalising from temperatures below 850°C is not advantageous, because there is more tendency of grain-boundary ferrite formation, accompanied by fall in tensile-strength though impact-strength and machinability significantly improve. ⁽¹⁴⁴⁾

Ductile irons in alloyed, normalised and normalised and tempered conditions were studied for their mechanical properties by C.R. Isleib and R.E. Savage.⁽¹⁴⁹⁾ They reported that simple co-relations exist between chemical composition, mechanical properties, section size and heat treatment of ductile iron. Suitable combinations can thus be selected from the data to produce high-strength material in sections upto 6" thick, corresponding to ASTM A 396-58 specifications by normalising heat-treatment.

It is known that the ductility, as expressed by percentage elongation, and the impact values are lowered by normalising treatment because of the lamellar pearlitic microstructure of base-matrix. Takeomi Okumoto et al⁽¹⁹⁷⁾

investigated the possibility of developing an optimum normalising process, which would yield high ductility as well as high strength pearlitic ductile iron. They suspected that high austenitising temperatures, usually employed might be causing grain boundary precipitation of primary cementite during cooling and hence low-ductility is resulted. The high temperature before cooling might also cause much of the carbon atoms left dissolved in ferrite in the state of over saturation after cooling, which might again lead to low ductility due to internal strain. A process, called as "Two-step Normalising" was suggested by them as a corrective measure, where austenitising was affected at a relatively high temperature in an intention to fully homogenise the matrix and graphitise the free cementite and then the furnace temperature was slowly lowered to and kept at a temperature immediately above the graphite-ferrite eutectoid temperature before cooling in air in an intention to minimise the carbon concentration in the matrix. It was reported by these workers that, compared to an ordinary normalising from 930°C , the two step normalising gave 1.5 to 2 times higher impact values and only slightly lower strength. Tempering, subsequent to ordinary or two-step normalising is not recommended because the gain in impact-strength is not great enough to justify the loss of strength accompanied by it.

4.4.4 Quenching and Tempering:

As stated in the previous section, A.P. Alexander⁽¹⁴²⁾ found that normalised irons can be readily controlled for their hardness but tempered irons below 310 B.H.N. have wide hardness fluctuations. He found that the hardness drops in a regular pattern upto 566°C, then the plateau occurs in softening pattern untill upto 593°C, and thereafter the hardness drops at a very fast rate. This range was supposedly associated with the precipitation of secondary graphite. The phenomenon of graphitisation during tempering of S.G. Irons was studied in detail by Gupta, Chakravarti and Dass.⁽¹⁵³⁾ They found that the mechanism of tempering of S.G. Iron was different than that of steel. It was found to occur in two steps : (i) precipitation of carbides and nucleation of secondary graphite nodules, (ii) decomposition of carbides into ferrite and graphite. The precipitation reaction was found to be very fast at all temperatures, while carbide decomposition was found to vary greatly with the temperature of treatment. They reported that the time lag between carbide precipitation and its decomposition is higher at 500°C than at 580°C. And at temperatures higher than 580°C, this time lag disappears, because the decomposition of carbides starts almost immediately after the precipitation is over. The findings of Gupta et al⁽¹⁵³⁾ and A.P. Alexander⁽¹⁴²⁾ are thus in agreement with each other.

4.4.5 Other Heat-Treatments:

Other heat-treatments which can be given to ductile iron include austempering, martempering, surface-hardening by flame or induction methods, all of which are similar to steel-heat-treatment.⁽¹⁷¹⁾ F.E. Kusch⁽²⁰⁰⁾ reported that as-cast ductile irons had a fast response to developing maximum hardness in 5 seconds, as required during flame and induction hardening. In this instance, pearlitic matrices are preferred prior to hardening, since they are more readily austenitized.⁽¹⁷¹⁾

4.5 MECHANICAL PROPERTIES:

Different grades and their mechanical properties are listed in Table 4.1, 4.2 and 4.3.

The influence of various parameters such as initial composition, alloying and trace elements, process variables during freezing and related microstructures in as-cast and heat treated condition on the mechanical properties of S.G. Irons can not be over-emphasized.

The presence of trace amounts of Tin^(79,88) Arsenic⁽⁸⁴⁾ Antimony^(189,193) and Lead, Boron and Cerium⁽¹⁸⁹⁾ have been found to influence the microstructure and mechanical properties of thin and thick as cast S.G. Iron sections profoundly. Similarly, alloying elements like copper⁽⁸⁸⁾ Nickel^(146,194) and Molybdenum⁽¹⁹⁴⁾ have been found to exert considerable influence on the microstructure and

mechanical properties of S.G. irons.

J.C. Prytherck and G.N.J. Gilbert⁽⁷⁹⁾ and later T. Levin et al⁽⁸⁸⁾ have reported almost similar results, regarding the influence of tin in trace amounts on the microstructure and influence of tin in trace amounts on the microstructure and mechanical properties of S.G. Irons. The common findings appear to be that 0.08% to 0.1% tin results in fully pearlitic base-matrix in as cast condition and that tin refines the bulk of pearlite, with colonies of fine and coarse pearlite, the latter occurring near the graphite nodules. This coarse pearlite is further refined by a normalising treatment⁽⁸⁸⁾. These workers also reported that tin promotes pearlite stability, without promoting any free carbide formation in as cast or normalised condition, even at highest percentage of tin addition. Tin was found to improve the perfection of graphite nodules according to the previous investigators⁽⁷⁹⁾, while the recent findings⁽⁸⁸⁾ have shown that the shape and size of graphite nodules were relatively unaffected by tin additions. Prytherck and Gilbert⁽⁷⁹⁾ found that the hardness and Proof stress of as-cast as well as normalised ductile iron increases progressively with tin additions at all silicon levels. Their data revealed that high silicon and tin contents together may be undesirable. The embrittling effect of 0.1% tin addition on the ultimate tensile-strength could be over-come by normalising treatment⁽⁷⁹⁾. Similar results were quoted by the later investigators⁽⁸⁸⁾.

T. Levin et al⁽⁸⁸⁾ also reported that tin additions upto 0.15% have no pronounced effect on the mechanical properties of annealed ferritic ductile iron, indicating that tin has no solid-solution-strengthening effect of ferrite. This was further supported by the fact that the micro-hardness of ferrite did not increase with progressive tin additions⁽⁸⁸⁾. But the micro-hardness of pearlite, in both as cast and normalised condition, was found to increase with progressive tin additions, suggesting that tin increases the hardenability of ductile iron⁽⁸⁸⁾.

Detailed investigations conducted by M.J. Lalich et al⁽⁸⁴⁾ have shown that small additions of Arsenic (0.05 to 0.2%) promote pearlite formation in sections upto 2.5" dia, and the Arsenic level needed to promote a fully pearlitic structure is dependent on the section size or the cooling rate of casting. Simultaneously, Arsenic increases the formation of primary carbides in section sizes of 1" or less in diameter. Also the mechanical properties developed were found to be a function of the amount of Arsenic added. Recoveries of greater than 90% were achieved with Arsenic metal additions during these investigations.

The combined effect of trace elements like Lead, Antimony and Bismuth on the morphology of graphite nodules and the base matrix of Fe-Si-Mg inoculated ductile iron was studied by R.K. Buhr⁽¹⁸⁹⁾. The percentage of Cerium present in the inoculant was also varied from 0.0% to a

maximum of 0.45% . He reported that the absence of Ce in the inoculant causes the formation of degenerate graphite and pronounced dendritic growth at 0.003% residual level⁽¹⁸⁹⁾. The presence of Ce was also found to have an effect on the percent pearlite in the microstructure, as the total of these elements (Pb, Sb, and Bi) increased to 0.04% . The pearlite increased from about 15% to over 80% at 0.19% Ce level in the inoculant, as the residual elements increased. At higher Ce levels in the inoculant, for example at 0.45% Ce level the percent pearlite decreased as the residual elements increased. The number of nodules was also found to vary with Ce and residual levels. At a low residual content, more nodules were found at 0.19% Ce level in Fe-Si-Mg alloy than when nil Ce or 0.45% Ce levels were employed. The conditions stated above, refer to the optimum conditions with respect to the mode of freezing, % pearlite present in the matrix, shape, size and number of graphite nodules present in the as-cast structure of S.G. Iron.

E. Compomanes⁽¹⁹³⁾, on the contrary, has pointed out that 20 to 100 ppm of antimony can be usefully employed in the manufacture of thick-sections upto 8" , even at higher silicon levels. This trace quantity of antimony inhibits the formation of chunky graphite, increases nodule count in both light and heavy sections, and therefore, results in superior mechanical properties in heavy ferritic ductile iron castings in sections upto 8"⁽¹⁹³⁾. Antimony has been found to be most effective, when added with (or contained in)

the inoculant. 50 ppm (0.005%) addition is considered optimum. Campomanes⁽¹⁹³⁾ further states that excessive Mg content and other trace elements like lead and bismuth should be avoided, as they cause degeneration of graphite nodules and thus deteriorate the mechanical properties.

Recent work of T. Levin et al⁽⁸⁸⁾ has confirmed earlier findings that Cu functions as a pearlite promoting element and that 1.0% copper eliminates all traces of ferrite from the as-cast matrix, without causing any increase in the amount of free carbides. Also, copper was found to have no effect on the shape and number of graphite nodules. These investigations revealed that the mechanical properties of ductile iron in as-cast, annealed ferritic and normalised condition improved considerably because of Cu addition. The as-cast properties improved mainly because ferrite was completely removed from the base-matrix. The as-cast pearlite is further strengthened and refined because of solid-solution strengthening of ferrite by copper and increased hardenability.

It was shown by G.J. Cox⁽¹⁴⁶⁾ that Nickel content of about 0.8% present in the as-cast or heat-treated ferritic base-matrix, raises the tensile-strength and proof stress, without significantly affecting the room-temperature ductility and impact values, or impact transition temperature range. N.L. Church⁽¹⁹⁴⁾ has reported the development of a new strong and tough ductile iron, using 8% Ni and 0.2% Mo at 2.3% Si levels of base-melt. Nickel is the

element, primarily responsible for the tough structure of lower bainite and martensite, obtained in the as-cast condition. The strength provided by this iron was found to be comparable to the best obtainable in quenched and tempered martensitic irons, while toughness was better. And no high temperature treatment was required. Both Mn and Mo help to maintain this structure in 2" and 4" sections. Mould-cooled keel block castings of such irons, tempered for 4 hr at 316°C, resulted about 119 kgs/mm² ultimate tensile strength, 1-2% elongation and 4 ft-lb charpy V-notch impact energy (0.552 kgm) at room temperature in 1, 2 and 4" thick sections. Decreasing Nickel content results into gradual decrease in strength accompanied by an increase in ductility and toughness. Abrupt loss in toughness occurred at 4% Nickel, because lamellar pearlite appeared in 2" and 4" sections. It was earlier shown by C.R. Isleib and R.E. Savage⁽¹⁴⁹⁾ that a ductile iron alloyed with 3.75% Ni and 0.55% Mo, yields fully acicular martensitic matrix in the as-cast condition. Different grades of ductile irons can be produced from this base matrix by suitable heat treatment. Nickel, in this study, was found to increase the tensile-strength, yield-strength and hardness levels of ductile iron in all section sizes both in as cast and normalised condition. Addition of Ni to ductile iron was found to increase the hardness uniformly in sections from 1" to 6". Mo also improved the mechanical properties. They concluded that Mo reinforces the harde-

ning effect of Ni, alloying higher hardness values to be reached.

Influence of various heat-treatment cycles on the microstructure and mechanical properties of S.G. Irons was partly discussed in section 4.4 and has been generally discussed in this section.

It was shown by J. Bradshaw⁽¹⁴⁷⁾ that the application of two-stage annealing process to as-cast pearlitic S.G. Iron results in the production of softer and more ductile matrix of ferrite. The work of C. Vishnevsky and J.F. Wallace⁽¹⁴⁸⁾ revealed that the use of a Low-temperature quenching treatment of ductile iron that was previously ferritized, results in the improvement in impact resistance compared to ductile irons of similar strengths that were normalised or quenched from higher temperatures. This improvement in toughness was thought to be due to better ductility of the lower-carbon matrix. Thus, low austenitizing temperatures can yield tensile-strengths in the range of 70.0 to 106.0 kgs/mm² at relatively low hardness levels. The ductility in the tensile test also improved. In this connection, the work of Takeomi Okumoto et al⁽¹⁹⁷⁾ should also be mentioned. Their work was aimed at finding an optimum normalising process to obtain high ductility as well as high strength pearlitic ductile iron. It is known that the ductility, as expressed by elongation and impact values is lowered by ordinary norma-

lising treatment, and therefore the application of normalised castings shall be limited to only those cases where impact loads are not involved. A remedy, in the form of "two-step normalising", was suggested by these workers to overcome this difficulty. The details of this process are somewhat similar to the one suggested by C. Vishnevsky and J.F. Wallace.⁽¹⁴⁸⁾ Compared to an ordinary normalising from 930°C, the two step normalising gave 1.5 to 2.0 times higher impact values and only slightly lower strength. Endurance limit in rotating beam fatigue test was found to be almost comparable to that of ordinary single stage normalising. The "Two step normalising" process is fully discussed in 4.4.3.

Raw materials used, melting practice and holding time, have been shown to have a measurable effect on hardness and strength of Nodular-irons.⁽¹⁷⁸⁾

Recently, investigations were carried out by A. Hazari-dis et al⁽¹⁹⁶⁾ and R.K. Nanstad et al⁽¹⁸⁰⁾ to obtain data for fail safe design of nodular iron components and to determine whether or not the fracture toughness test is a more sensitive test for measuring toughness than the more conventional impact tests. The principles of linear elastic fracture mechanics (LEFM) and the dynamic tear (DT) instrumented impact tests were utilised in such studies. Some of their important findings are summarised here. They found that nodularity had no pronounced effect on the

fracture toughness of ductile-irons within the range of their study. Grey irons had very low fracture toughness. Fracture of the ferritic nodular irons was accompanied by plastic-deformation. Pearlitic and austempered nodular irons exhibit a high K_{Ic} (Plane strain fracture toughness) value, but this is believed to be nullified by the higher yield-strength levels of these materials. They failed, therefore, in a brittle manner even at room temperature. The interface nodule between ferritic ring in a regular pearlitic iron was found to be a crack nucleating site by simple decohesion. But when the ferritic-ring itself becomes fairly thick, ductile fracture takes over. No effect of strain-rate was observed. It was concluded from these studies that K_{Ic} (Plane strain fracture toughness) values can be used for fail-safe design by applying the principles of fracture mechanics. Fracture toughness of as-cast ferritic Nodular irons was found to be severely degraded by higher than normal (2.5%) silicon levels. The NDT (Nil ductility temperature) values obtained for nodular irons using the dynamic tear test were similar to those obtained by means of charpy V notch impact test.

4.6 MANUFACTURING TECHNIQUES AND PROBLEMS:

Composition limits pertaining to the liquid melt, that can be inoculated to produce S.G. Iron, were outlined by C.K. Donoho⁽¹⁵⁰⁾ and discussed in section 4.3. Typical Indian problems in this regard were discussed by

(151)

S.N. Anantnarayan . Excessive amount of sulphur (0.12 to 0.13%) present in the Indian pig iron, due to high ash content in the coke, has been the main problem, which warrants either effective de-sulphurisation in two or three stages or the production of syntnetic iron from 100% mild steel scrap. J.H. Sale⁽¹⁷⁵⁾ discusses one established practice of utilising junked automobile shredded scrap in the cupola charge to the extent of 75.5%, for the manufacture of centrifugally cast ductile iron pipes in fully ferritised condition. Liquid iron at cupola spout had 0.09/0.15 percent sulphur, which was later decreased to less than 0.010% level by desulphurisation with a mixture of Ferrosilicon graphite and calcium carbide in a Rheinstahl Stirrer. Other elements like carbon and silicon were raised to the desired level by ladle additions. It was shown by R.S. Lee⁽¹⁷⁸⁾ that the melting materials, melting practice and holding time had a measurable effect on hardness and strength of Nodular irons.

Several important developments have so far taken place in the production techniques. Use of Magnesium-wire injection technique has recently been advocated by M.C. Ashton et al⁽¹⁷⁶⁾. They state that this technique has several advantages over the prevailing practice of Mg-alloy additions. Comparatively, metallic Mg is cheaper, undesirable additions of Ni and Si to the melt are avoided and the steps of desulphurisation and nodularisation can be combined in one process. The use of metallic magnesium,

however, causes a violent reaction, which can be partly or fully suppressed by using such techniques viz. treatment in pressurised vessels, controlled reaction of Mg with liquid melt in a tilting reactor provided with a refractory dam, use of Magnesium impregnated coke or Fe-Mg briquettes or the injection of powdered Mg. M.C. Ashton et al⁽¹⁷⁶⁾ found that the Mg recovery in wire-injection process may be assumed to be nearly 40%. While average recovery for 9% Mg alloy is slightly less than 40% and under 45% for 5% Mg alloy. Recoveries were found to be rather better, around 50% in case of bulk magnesium used in tiltable reactor or in pressure vessels. The required residual Mg in all these cases for proper nodularisation is between 0.03 to 0.05%. Residual Magnesium contents beyond this level have been found to be deleterious⁽¹⁸³⁾. It was shown by P.K. Basutker et al⁽¹⁸³⁾ that the spheroidal graphite degenerates to spiky graphite when residual Mg level exceeds 0.075% in heavy section ductile iron castings.

In their recent investigations, S. Yamamoto et al⁽¹⁷⁹⁾ have shown that spheroidal graphite cast iron can be produced by suspending gas bubbles of H₂, N₂, CO₂, and Ar inside the molten cast-iron. They found that graphite nodules can be obtained by the addition of Ce, La, Y, Ti and Zr, when they have absorbed a large amount of H₂.

Though the general practice has been to inoculate liquid iron subsequent to the Mg treatment, E. Campomanes and R. Goller⁽¹⁸⁵⁾ have shown that adding inoculant along

with Mg treatment alloy to the melt yields similar results as in the previous case, provided that the inoculant is added at the same temperature in both cases. They have referred to this practice as "one-step treatment". These workers have claimed that the Magnesium treatment can thus be carried out at lower temperatures, eliminating the need for a treatment ladle, and resulting into higher Mg recoveries.

Efforts have been made in the recent years to develop 'New-Generation Alloys' for the Mg-treatment of liquid melt such that there is essentially no flame or smoke emission during the treatment. One of such alloys is described by P.D. Reuscheh and N.L. Church⁽¹⁸⁶⁾. This alloy consists of 94% Ni, 4.5% Mg and 1.5% C and being heavier, sinks into the liquid melt so that it remains out of contact with air after addition. Mg recoveries of 90% or more have been reportedly obtained from this alloy. Only small addition of this alloy (about 1% of bath weight) would, therefore, be required in the process. Thus, the problems of dross and high residual Mg contents is minimised in this case. The treatment procedure is also simplified in this case, since the alloy can be simply dropped directly on the melt surface. This method of addition adds substantial flexibility to the timing of Mg treatment and permits treatment near the point of pouring. Thus, the advantage of both the factors viz. the relatively low metal temperature and short pouring time, can be taken to obtain high Mg recoveries. This alloy was also found to dissolve in the melt in a

relatively steady manner, because the carbon in the alloy produces a eutectic structure with a continuous high melting point Nickel skeleton and reduced Magnesium (12%) in the Ni-Mg-C compound.. N.L. Church and Paul D. Merica⁽¹⁸⁷⁾ have further investigated the possibility of using Ce in various combinations with Mg. Also, they have discussed various other sinking alloys e.g. Ni-Mg and Ni-Fe-Mg alloys. They concluded that Ce might be added to the molten iron prior to Mg treatment. This Ce pre-treatment shall decrease the Mg requirements for producing S.G. Iron by decreasing the sulphur content of bath to very low levels.

Fading of Mg and Nodularity poses a serious problem during storing of Mg treated melt for extended periods periods^(182,195,198). Under many circumstances, it becomes necessary to hold the treated metal for some period. But if the liquid metal is not poured within 10-20 minutes after treatment, the Mg content, and consequently the formation of spheroidal graphite, decreases rapidly, a phenomenon known as "Mg-fading". G. Bylund et al⁽¹⁸²⁾ have discussed several methods of holding the Mg treated iron for various lengths of time without causing undue Mg fading. The treated metal could be tapped upto 90 minutes at 145^oC, when the bath was protected by a ceramic cover floating over the bath. The holding time could be extended from 15 minutes to 30 minutes at a tapping temperature of 1450^oC by providing an Ar or N₂ cover over the bath. Holding experiments reported from USA⁽¹⁸²⁾ in a 80 ton channel induction-furnace have

shown that Mg treated iron can be successfully held for 9 hrs under the protection of a slag-cover. Mg content when poured was about 0.1%, but it decreased during holding to between 0.026 and 0.01%. In spite of this low residual Mg content, the castings were reported to be of good nodular quality⁽¹⁸²⁾. R.S. Lee⁽¹⁹⁵⁾ also suggested that the treated metal could be stored in a channel induction furnace for periods longer than 3 hrs, since they found that Mg fading was a function of temperature loss. They have also suggested various combinations of rare-earth elements, rare-earth compounds and Fe-Si for ladle inoculation at the time of tapping, which were found to promote upto 100% nodularity and excellent mechanical properties even after a holding period of 3 hrs.⁽¹⁹⁵⁾ J.F. Janowak and C.R. Loper⁽¹⁹⁸⁾ also dealt with this problem and determined the influence of various operating variables such as holding temperature in a coreless induction furnace, furnace refractory and protective atmospheres on the fade rate of the Mg and Si additions. They found that Mg losses during extended holding would be minimised, provided lowest practical holding temperatures are maintained a non-agitating heating vessel is used and the melt is kept covered by a slag or dross cover that is non-reactive with Mg and is impervious to Mg vapour or Oxygen diffusion.

R.W. Heine⁽¹⁸⁸⁾, P.K. Basutkar and C.R. Loper Jr.^(190, 191) E.F. Runtz. Jr, et al⁽¹⁹²⁾ and R.W. Heine and C.R. Loper Jr.⁽²⁰¹⁾ have very usefully corelated the ductile

iron cooling curves with several important process variables viz. carbon-equivalent, solidification process, section thickness, resulting microstructures and mechanical properties in as-cast condition. "Thermal Analysis technique" as it is called, has thus become a very useful tool in ductile iron process control. Apart from other advantages, this technique is mainly employed in practice to predict the as-cast microstructures, that would result from a given treated melt.

Prior to the development of "sinking-type" or "New Generation Mg Alloys", the technique of "Inmould Nodular" was developed in order to make the inoculating process relatively smoke, flare and violence free, while using conventional Ni-Mg or Ni-Mg-Si alloys. "Inmould Nodularising" process offers not only these advantages, but also it eliminates the problems of Mg or Nodularity fade. These techniques have been discussed in details by R.S. Lee⁽¹⁸⁴⁾, M. Remondino et al⁽¹⁷⁴⁾ and G. Fr. Hillner and K.H. Kleeman⁽²⁰²⁾.

Problems involved and the mechanical properties developed during hot-rolling and forging of S.G. Iron have recently been reported by L.A. Newmeier et al⁽¹⁷³⁾. Advantages and limitations of permanent mould casting of S.G. irons have been discussed by C.A. Jones and J.C. Fisher⁽¹⁹⁹⁾. These investigators have shown that sound ductile iron castings can be consistently produced using irons with a carbon-equivalent of 4.5 or above and pouring post-inoculated iron at about 1375°C into acetylene blackened moulds at 370-425°C.

and malleable iron in several applications. They also forecast that by the year 1990, ductile iron castings should contribute about 44% of the total of ductile iron and steel castings and 62% of the total of the ductile and malleable iron castings produced in India. On the whole, it might be inferred that, for very intricate and heavy sections less than 3", malleable iron may be preferred for similar mechanical properties⁽¹⁶⁸⁾.

CHAPTER-5

DEVELOPMENT OF HIGH-STRENGTH, SHORT CYCLE, PEARLITIC MALLEABLE IRONS.

5.1 INTRODUCTION

A critical examination of the research carried out so far in the area of pearlitic malleable irons shows that some aspects have either not been investigated fully or they still remain controversial. They are as follows:

1. The concept of mottling and its influence on the mechanical properties is under constant scrutiny. Controversy exists over the cast white iron structure. According to some investigators, the white iron structure is required to be completely free from primary graphite, while the others state that graphite particles nucleate during solidification and thus, the cast-structure already has graphite specks. In a conventional sense, therefore, such a structure should be termed "Mottled".

The mechanism through which these primary graphite specks form in the cast structure is again controversial. The concept of mottling, therefore, needs revision. Also, it is not known, whether such graphite specks would influence the mechanical properties of ferritic as well as pearlitic malleable irons adversely. The basic question would be whether such graphite specks could be

permitted in the cast structure and whether or not such a structure could be termed "mottled".

2. Different views exist regarding the amount of copper partitioning to the eutectic cementite phase, as the average copper content of base-melt increases. It is important to ascertain this fact in order to evaluate the influence of copper on the thermodynamic stability of eutectic cementite. Change in the copper content of eutectic cementite during the progress of FSG reaction needs to be determined again as the data reported is inadequate in this regard. Such studies would reveal the basic characteristics of Cu-alloyed eutectic cementite phase.

3. Tempering characteristics of copper alloyed
pearlitic malleable irons have not been investigated in detail, though such detailed characteristics have been reported in case of copper containing low alloy constructional steels (68,169). The Precipitation hardening characteristics of Fe-Cu system could be usefully employed for strengthening the base-matrix. The loss in hardness of a fully hardened base-matrix, as it is being drawn, is expected to be partly counter balanced by simultaneous precipitation of copper from the supersaturated solid solution of copper

in α iron. This phenomenon may allow comparatively higher hardness values to be retained on tempering. The tempered structure may thus result into superior mechanical properties, compared to an unalloyed composition.

4. Influence of copper on FSG and SSG periods has been reported by several workers. But the effect of copper on FSG periods incorporating various pre-treatments have not been reported. It would be expected that FSG period would further be shortened by this combination in individual compositions. Such studies would prove to be of practical significance.
5. Data on the mechanical properties of age-hardened copper alloyed pearlitic malleable irons is not plentiful. The influence of copper precipitation during tempering of copper alloyed pearlitic malleable irons on their mechanical properties, need be investigated, since this effect would be expected to yield comparatively higher hardness on tempering and therefore better mechanical properties.

Data on pearlitic malleable irons, made from Indian raw materials, would also be of interest for local conditions.

In the present work it was intended to obtain necessary data on the aspects outlined above, with a specific

object of developing "Superduty" pearlitic malleable irons. Also, it was intended in the present work to employ commercial Indian raw materials, rather than high purity metals and alloys, so that the results of this study could be of more practical significance.

5.2 THE APPROACH

Basically, a strong and tough matrix, with adequate ductility will have to be obtained for the purpose. A tempered martensitic base-matrix, containing adequate amount of carbon should prove to be appropriate for the purpose. Fully martensitic base-matrix may be obtained on quenching, subsequent to FSG completion, or by following several other time-temperature cycles, which can further be tempered to the desired hardness. Nodular shaped temper carbon nodules should also contribute positively towards this aim. A pearlitic malleable iron thus obtained should be able to meet the highest standards of strength requirements in this class of iron.

The processing cycle could best be shortened by a combination of composition adjustment, hot-stripping, alloying, pre-treatments and a high temperature FSG treatment.

Simultaneous precipitation of copper from copper containing as-quenched martensitic base-matrix, as it is being tempered, could also be used to strengthen the base-

matrix. This could further help in achieving superior mechanical properties in pearlitic malleable irons. Temperature ranges known to cause temper-brittleness in such cases could be safely avoided. Superior hardenability obtained due to copper and Mn alloying could be usefully employed particularly in case of thicker sections.

Controversies pertaining to the as-cast microstructure would not matter in the development of high strength pearlitic malleable iron, so long as graphite is present in the form of fine specks at the cementite austenite interface in the cast-condition. But any coagulation of graphite in the form of a cluster or irregular elongated shapes, formed during freezing (mottling), would be highly deleterious for the final mechanical properties of heat-treated product.

5.3 BASIC CONSIDERATIONS IN THE SELECTION OF COMPOSITION.

5.3.1 Base Metal Composition

The influence of variations in composition, alloying and trace elements on the graphitisation kinetics of white irons was discussed in detail in section 2.3.2. The influence of these factors on the mechanical properties of high duty pearlitic malleable irons was summarised in later sections 3.2 to 3.4.

Fundamentally, the base-metal composition had to be such, that would freeze fully white in sections upto 20 mm in dia. graphitise fast during first and second stages

of graphitisation and shall also yield high strength pearlitic malleable iron on suitable heat-treatment. Commencing from typical pig iron and mild steel sheet scrap, the final composition had to be suitably adjusted in line with the above requirements. Also, the alloying and trace elements, selected for the addition, had to be such that would primarily fulfill the metallurgical requirements and yet be cheap and easily available.

Though various combinations of total carbon and silicon may be used to obtain fully white as-cast structure, but lower carbon and higher Si levels have been preferred in practice for various reasons (128, 166). Such a combination, primarily graphitises faster during FSG and SSG reactions and also it yields superior mechanical properties. Higher shrinkage encountered in this case would, however, warrant a modification in gating and feeding system. Thus, total carbon could preferably be fixed between 2.2 and 2.4 wt% and silicon between 1.4 and 1.6wt% for optimum results. A very strict control has to be exercised on silicon levels and freezing conditions, so as to ensure that no primary graphitisation occurs during freezing.

Vast technical information available in the literature clearly shows that Mn and Sulphur must be properly balanced to form MnS, particularly in case of ferritic malleable production, (Table-2.1), since Mn and S both function as carbide stabilisers. Requirements in case of pearlitic

malleable production, however, are different. Excess manganese, of the order of 0.8 to 1.3 wt%, is preferred since pearlitic microstructure is aimed in the end-product, which is obtained either by interrupting the process after FSG completion or by braking the SSG reaction in continuous annealing type furnaces. Mn has always been preferred for this purpose also because it is cheap, easily available, and imparts good hardenability. "Interrupted-annealing" technique was to be employed in the present study. Mn and Si both were to be maintained at medium level (0.5/0.6 and 0.8/0.9 wt% respectively) in copper containing alloys, in order to study the influence of mainly Cu on the graphitisation characteristics and mechanical properties of pearlitic malleable irons. A higher Mn/S ratio of more than 5 and upto 12 could be used because sulphur content of such synthetic irons is easily held between 0.05 and 0.09 wt%. Such higher Mn/S ratios would also not retard the "Interrupted Annealing" process, since SSG is not carried out in this case. Si content in unalloyed irons, with and without Bismuth additions, was planned to be varied between 0.8% and 1.6 wt%.

Phosphorus content of base-melt was planned to be maintained between 0.05 and 0.15 wt % for obvious and very well known reasons (166,171).

5.3.2 Alloying Elements

5.3.2.1 Mottling Considerations

Elements that promote primary graphitisation will have

to be carefully balanced by carbide promoters in order that a fully white structure is obtained in as-cast condition. And yet, the cast composition had to be such that would graphitise fast in the solid state.

In addition to balancing the total carbon and silicon in view of the above, certain trace elements like Bi and Te will have to be used as inoculants, which are known to suppress primary graphitisation strongly. Bi being more common of the two, was used in the present work, in the range from 0.01 to 0.02 wt %.

Table-2-1, page 14, summarises typical characteristics of commonly used elements in this regard. For various reasons, discussed at appropriate places, copper was selected as an alloying element in the present study. Results of various workers summarised in Table-1 indicate that copper mildly promotes primary graphitisation in white-iron compositions. It is estimated that 1.7% Cu is nearly equivalent to about 0.2% Si in this regard^(89,166). The problem of mottling, however, could not be that serious in the present study, since total carbon was maintained on the lower side and also silicon was kept at medium level in the base-melt. Copper in amounts upto 2.0 wt % were planned to be investigated in the present work, since the data reported in the literature at lower carbon and medium silicon levels were found to be meagre.

5.3.2.2 Shortening of FSG and SSG

Shortening the annealing cycle was one of the primary objectives of present investigation. Different investigators listed in Table-21 generally agree on the point that Cu shortens FSG as well as SSG periods. But the data reported on the graphitisation characteristics of copper alloyed, low carbon, medium Mn and Si type white irons is meagre and warrants further study. It would, however, be expected that both these graphitisation reactions would be shortened in this instance too, but exact characteristics need be evaluated. Further, the graphitisation characteristics of copper alloyed white irons of this type and inoculated by Bi for mottle control, had to be determined. The basic idea was to determine whether FSG was going to be unduly prolonged under these-composition-parameters, as-only-this-factor--- was vital for the manufacture of high duty pearlitic malleable irons. However, the determination of SSG characteristics was not planned in this work.

5.3.2.3 Response to Pre-treatments

The basic idea of any such pre-treatment at sub-critical temperatures is to increase the number of nodules in the matrix prior to the commencement of proper FSG reaction. Graphitising elements are known to promote this tendency. It would, therefore, be expected that elements like Si and copper, when present in adequate amounts, would result into the formation of large number of tiny nodules

during pre-treatment. It is, thus, obvious that diffusion distances for carbon atoms released from FSG reaction, would be cut-down due to closer spacing of these tiny graphite nuclei, formed in large numbers during pre-treatment. Number of nodules so formed are also a function of the type of the pre-treatment employed. For actual casting geometries, however, pre-baking treatment may be considered most suitable.

5.3.2.4 Nodule Number, Shape and Size.

Alloying and trace elements have been found to influence this factor profoundly. Number of nodules/mm³ (Nv), their shape and size have also been reported to influence the mechanical properties of ferritic as well as pearlitic malleable irons. These aspects have been discussed in detail in previous sections 2.3.2, 2.3.4, 2.3.5, 3.2 and 3.4. Keeping in view the present aims, it would be desirable to obtain a large number of temper carbon nodules, almost spherical in shape. This microstructure would then roughly correspond to that of nodular irons.

Copper, like other graphitising elements, is known to increase the number of stable nuclei, which grow to form temper carbon nodules. But there appears to be some disagreement regarding the influence of copper on the shape and size of temper carbon nodules. This aspect, therefore, needs further verification. Nevertheless, copper in combination with about 1.0 wt % silicon could be expected to

fulfill the requirements outlined above.

5.3.2.5 Partitioning in Different Phases:

It is known that basically all the alloying elements partition themselves between eutectic cementite and austenitic base-matrix, to a lesser or greater extent, depending upon their graphitising or carbide-forming nature. It is also known that such a partitioning behaviour influences the thermodynamic stability of eutectic cementite phase.

Copper has been found to partition in the same manner between eutectic cementite and austenite^(28,51). Sandoz^(28,51) reported that small but measurable quantities of Cu are dissolved in the cementite phase at the beginning of FSG reaction and that Cu content of cementite does not increase with the progress of FSG reaction. But further, Sandoz has shown that the amount of copper partitioning to the cementite phase increases with an increase in average Cu content of base-iron. There appears to be some disagreement on this point in the literature, since Albert De Sy⁽⁷³⁾ stated that only few copper atoms can be dissolved in cementite, and therefore, the properties of cementite, would largely remain unaffected due to copper addition. Earlier it was hypothesised by Brown and Hawkes⁽⁸⁾ that graphitisers like Co, Ni, Cu and Si substitutionally dissolve in orthorhombic cementite lattice. The resonance bond between each carbon atom and its Si near-neighbour iron atoms is already weak and it is further weakened by being stretched due to the substitution of graphitiser. This makes cementite all

the more unstable.

It appears from the arguments mentioned above that copper can be substituted in the cementite phase only to a limited extent, unlike the results reported by Sandoz. But severe non-equilibrium cooling conditions during freezing and subsequently upto near critical temperatures, may cause Cu segregation in the cementite grains. The extent of copper segregation in the cementite grains shall also be influenced by the diffusion rates of Cu within this phase. On the whole, it would be expected that considerable number of Cu atoms would also remain trapped in the cementite grains due to the conditions stated above. Average copper content found in cementite grains would thus be higher than normally expected under equilibrium cooling conditions. These trapped atoms, however, shall not influence the thermodynamic stability of cementite phase.

It is obvious that the partitioning behaviour of Cu between eutectic cementite and austenite, in different alloys containing varying amounts of copper, in as cast as well as at different stages of FSG reaction, warrants a detailed study in order to confirm whether or not the amount of copper partitioning to the cementite phase changes with a change in average copper content of base-melt.

5.3.2.6 Hardenability Considerations:

Fully hardened structures were required in as-quenched condition, subsequent to FSG completion, so that superior mechanical properties could be developed on tempering.

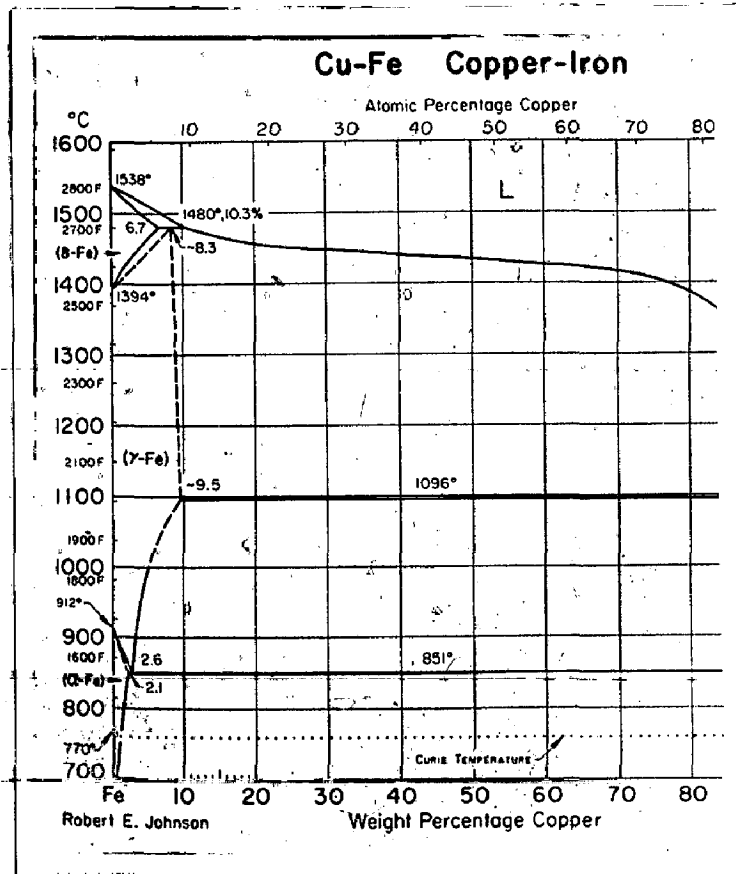


Fig. 5.1 - Iron-Copper equilibrium phase diagram. Metals Handbook, Vol.8, p.293.

Since Mn was maintained at medium level in the present work, copper alone was required to impart adequate hardenability to sections upto 20 mm in thickness in air or oil-quenched conditions. Normally, air or oil quenching techniques only are to be employed in practice, because of many practical problems associated with water-quenching as outlined in previous sections 3.2, 3.3 and 3.4.

P.B. Burgess⁽⁹⁰⁾, B. Thyberg⁽¹²⁸⁾, R.W. Heine⁽⁸⁹⁾ and others have shown that copper improves the hardenability of pearlitic malleable iron.

Copper in amounts upto 2.0 wt% present in the base-melts of this investigation, would, therefore, be expected to yield fully hardened structures at least in sections upto 15 mm in diameter in oil-quenched condition. This hardened structure could then be suitably tempered to obtain a strong and tough pearlitic malleable iron.

5.3.2.7 Strengthening due to Precipitation-hardening:

Iron copper system (Fig.-5-1) is known to exhibit precipitation hardening characteristics. This phenomenon has been utilised in strengthening ferritic malleable irons^(67,89,159). Pearlitic malleable irons also have been age hardened to obtain superior mechanical properties^(89,90). The phenomenon of simultaneous precipitation of copper, as tempering proceeds at sub-critical temperatures, has been reported in copper bearing nodular irons and steels^(152,153,162,169).

It was thought to utilise this phenomenon of copper precipitation during tempering of copper bearing hardened (martensitic) malleable irons in the present work. The drop in hardness, caused by tempering, could thus be partly counter-balanced by simultaneous precipitation of copper from the base-matrix. Pearlitic malleables, alloyed with nearly 1.4 wt% copper (solubility of Cu in Fe-Cu system at 850°C as determined by lattice-parametric method, Fig.-5-1), are going to be particularly useful in this regard. Higher hardness, so retained by the tempered martensitic structure, should correspond to superior U.T.S. and Y.S. values. Copper alloyed pearlitic malleables, so treated, should therefore, yield superior strength properties compared to the unalloyed ones of comparable hardness-values.-

5.3.2.8 Ductility and Toughness

Reasonable ductility and toughness value along with high strength is a prime requirement of strong and tough materials. But, minimum toughness requirements of various ferritic as well as pearlitic grades, have not been specified by either Indian or foreign standard specifications, though other important mechanical properties have been laid down (Tables 3-1 and 3-2).

Interest in the present work was centered around obtaining about 5% elongation corresponding to nearly 85 kgs/mm² UTS value and a higher YS/UTS ratio. This

objective could be achieved, if the temper carbon nodules remained in nearly spherical shape, embedded in a properly tempered martensitic base matrix. Copper, in addition to several other desirable characteristics discussed in the previous sections, also causes the graphite nodules to increase in number and simultaneously renders them partly spherical in shape. Comparatively, therefore, Cu alloyed high strength pearlitic malleable iron grades can be expected to possess higher elongation values.

Data pertaining to the impact properties of either ferritic or pearlitic malleable irons appears to be scarce in the literature, though some information has been compiled in a handbook "Malleable-iron castings⁽¹⁶⁶⁾". Nevertheless, the importance of toughness characteristics of either ferritic or pearlitic malleable irons in actual casting design considerations can not be underestimated. Typical impact values of both ferritic and pearlitic malleable irons were recently summarised by F.W. Jacobs and F.L. Preston⁽¹⁶⁸⁾. Also, it was emphasized by P.B. Burgess⁽¹¹¹⁾ that tempered martensitic structures possess superior toughness and ductility compared to lamellar pearlitic structures of comparable hardness.

It would be clear from above that copper alloyed pearlitic malleable irons, having a tempered martensitic base matrix, should be adequate enough to achieve the stipulated mechanical property targets, set in this work.

5.3.3 As Cast Structure:

5.3.3.1 Basic Requirements

As a standard practice, the as-cast structure of white irons is required to be free from primary graphite, and also the eutectic cementite is required to be in finer distribution (greater surface area/unit volume) as it helps in faster graphitisation of massive carbides during FSG annealing. Both these requirements are met by suitably controlling the process variables viz. composition, cooling rate, section-thickness, alloying and trace additions.

5.3.3.2 Influence of Cooling Rate:

Section-sensitivity of cast irons i.e. the influence of cooling-rate on their-cast structures,—is—used to advantage in case of white irons.

" Hot-stripping" is usually resorted to in white irons within minutes of pouring the casting, in order to meet the basic requirements of cast structure, as outlined in the previous section. A fully white structure is thus assured, provided other variables are also suitably controlled.

5.3.3.3 Influence of Graphitisers

This would basically mean a control of initial composition. Carbide stabilising and graphitising tendencies have to be carefully balanced in the base melt,

keeping in view the subsequent broader aims.

Silicon, being a strong graphitiser, was to be maintained at medium level i.e. 1.0 wt %, since Cu upto 2.0 wt % was to be used as an alloying element in the present study, for strength and other reasons. However, unalloyed compositions were planned to have silicon upto 1.6 wt %, inoculated simultaneously by 0.01 or 0.02 wt % Bi for mottle control. Mottle control by Bi inoculation was also to be exercised in case of alloys containing 2.0 wt % copper.

5.3.3.4 Concept of Mottling

As stated in sections 5.1 and 5.2 earlier, it would not matter if fine graphite specks (grown nuclei) are present at cementite austenite interface in the cast-structure, since the presence of such fine graphite particles would not adversely affect the mechanical properties of finished product. But the mechanical properties of malleable irons would be adversely affected, as soon as free graphite precipitates in the form of a spiky cluster, since large and almost mutually connected weak areas (graphite phase) would then be present in the structure. The fractured surface of such a specimen would show visible tiny black dots, because of large coagulation of free graphite at a place. In fact, only such a structure should strictly be termed as "Mottled".

The previous case, however, when only graphite specks are formed at the austenite/cementite interface during cooling, may not be strictly considered as "mottled". Such a structure, on fracture, may not reveal usual black dots, since these individual graphite specks would be too small to be visible to the naked eye. But the standard practice of examining an unetched or lightly etched (0.5% Nital) specimen at 100 or 200 X may be usefully employed in the present case to study the location, shape and size of graphite specks. If this structure is etched in a normal manner with 2% or 4% Nital, the tiny graphite nodules are likely to get mixed-up with the dark etching pearlite phase. But if the graphite coagulation is very large and spiky in nature i.e. the structure is "mottled", even a normal etching should make no difference, since blocky graphite would be easily visible in the micro-structure.

As stated earlier in section 5.3.3.1, the delicate equilibrium between carbide stabilising and graphitising tendencies will have to be so carefully balanced that large and spiky graphite does not precipitate in the cast structure.

Possible causes of the formation of tiny graphite particles at the austenite/cementite interface during freezing are discussed in a subsequent chapter. Their presence in the cast structure was not considered deleterious in the present work.

5.3.3.5 Response of As-Cast Structures to Pre-treatments.

Various pre-treatments discussed in 2.3.5 and 5.3.2.3 are one of several known methods of shortening the malleabilisation cycle.

All such pre-treatment time-temperature cycles were to be tried on unalloyed and copper alloyed compositions in the present work in order to determine their influence on FSG kinetics. Optimum pre-treatment cycles could thus be determined for individual compositions. Practical problems viz. quench-cracks, distortion of casting geometry, influence of pre-treatment time on total malleabilisation period etc. have to be kept in mind, while deciding the optimum and most practical pre-treatment cycle for any such composition.

Influence of pre-treatment on SSG kinetics was not of particular interest in the present work, since this step of malleabilisation cycle was not involved in the development of high duty pearlitic malleable irons.

5.4 THE HEAT TREATMENT

5.4.1 FSG Completion

In principle, the "Interrupted Annealing!" technique was to be adopted in the present work.

Further, efforts were to be made to shorten the FSG period as much as possible. All possible and known means of shortening the FSG period were to be employed in the

present work. The influence of such individual methods on the kinetics of FSG reaction was to be evaluated in order that their relative influence on individual alloys could be quantified. Also then, the practical applicability of all such methods to actual castings was to be considered. Thus an optimum method of shortening the FSG cycle could be worked-out, keeping in view all the considerations.

It would appear that considerable shortening of FSG period could be possible if the process variables viz. the base-metal composition, the cast microstructure, alloying and trace additions, the pre-treatments, FSG temperature, furnace atmosphere etc. are suitably controlled.

It was also thought in the present work to obtain FSG data on thin (10 mm section) as well as thick (16 mm section) specimens. The thick specimens were to be sliced from the ring portion of an actual wheel casting, made out of the same melt, as used for thin specimens.

5.4.2 Further Heat-treatment

Subsequent to the completion of FSG reaction, the specimens were to be furnace cooled to near eutectoid temperature in order that the carbon content of austenite may be reduced and brought close to the eutectoid composition.

Various quenching media may then be employed to transform this austenite into a fully hardened (Martensitic)

structure. But certain quenching media like still air, may not be able to yield a fully hardened structure. In principle, the transformation of austenite into various phases would be a function of the TTT characteristics of different unalloyed and alloyed compositions. And the depth of hardening shall be controlled by the hardenability characteristics of individual alloys. It was^{, however,} not aimed in the present work to evolve these basic characteristics of different alloys under question.

It would, however, be expected from the results of previous workers that at least copper alloyed compositions (0.7 to 2.0 wt % Cu) would yield fully hardened structures on oil-quenching. Thin specimens (9 mm. sections) of these compositions may be expected to yield hardened structures even on air-quenching with forced draft. Unalloyed compositions would be expected to yield a variety of microstructures in thin and thick specimens on quenching in water, air and oil.

For many practical reasons outlined in sections 3.3 and 3.4, usually air quenching (still or forced air draft) is preferred to either oil or water-quenching in actual practice. In the present investigation, however, all these quenching media were to be employed in order to study the resulting microstructures. The same practice had to be followed for the preparation of tensile-specimen blanks.

Neutral or slightly reducing atmosphere had to be maintained in the furnace till FSG cycle and subsequent furnace cooling to near eutectoid temperature was completed. This would be required to prevent the scaling of castings, because the oxidised layers, when formed, interfere seriously with the efficacy of quench (110,111).

Tempering of these quenched structures at subcritical temperatures was planned in a closely controlled salt bath furnace. Various tempering temperatures and periods would be expected to yield a variety of microstructures. These tempering cycles again will have to be optimised keeping in view the high strength requirements of the finished product.

Further, in case of copper alloyed compositions, it would be expected that the drop in hardness due to the graphitisation of martensitic structure during tempering shall be partly counter balanced by simultaneous precipitation of copper from the base-matrix. Copper would be held in supersaturation in the base-matrix upon quenching from the austenitic temperature range. On tempering, the copper would commence precipitating from the supersaturated solid solution. And this precipitation of copper would continue for considerable period during tempering, till the stage of "Overageing" is reached. In practice, however, the process of tempering is terminated much earlier than the stage of overageing and controlled in a

manner that the desired hardness and microstructure is obtained. This controlled tempering of copper alloyed compositions would be expected to yield superior mechanical properties.

CHAPTER VI

EXPERIMENTAL PROCEDURE

6.1 ALLOY PREPARATION

Alloys listed in Table 6.1 were prepared in a 25 Kg indirect Arc-furnace. Foundry grade pig iron, mild-steel sheet punchings, charcoal, Ferro-manganese, Ferro-silicon, E.C. grade copper and Bismuth metal were employed to obtain the desired compositions. Melting was done under a normal basic slag cover and no special atmospheres were employed. Unalloyed compositions O-8, O-9 and B-1 were also prepared in graphite crucible in a forced draught coke-fired pit furnace. The graphite crucible in this case, was kept fully covered from the top during the melting period. Similarly, the alloyed composition A-5 was again prepared in a high frequency induction furnace, utilising sintered magnesia crucible. This synthetic iron was prepared from 100% mild steel sheet punchings, charcoal and usual ferro-alloys. All these alloys were well superheated and tapped in the temperature range of 1500° to 1530°C after holding for 10 minutes at the temperature. Heats were poured only after the test-fracture had shown no signs of mottle even in a 20 mm dia section. Copper, being a heavy element has a tendency to sink in the melt and therefore, special care was exercised during pouring of "A" series (copper alloyed) melts.

Table 6.1

ANALYSIS OF ALLOYS

Composition by wt %.	Unalloyed Series					Alloyed Series				
	0-8	0-9	0-10	0-11	B-1*	A-1	A-2	A-3	A-4	A-5
Total Carbon	2.27	2.40	2.24	2.30	2.54	2.38	2.48	2.14	2.28	2.64
Silicon	0.89	1.23	1.40	0.95	1.63	0.93	0.89	0.73	0.81	0.80
Manganese	0.44	0.55	0.55	0.60	0.66	0.66	0.50	0.33	0.55	0.60
Sulphur		0.05	0.08	0.05	0.09	0.08	0.10	0.07	0.04	0.10
Phosphorus	0.11	0.18	0.19	0.08	0.06	0.17	0.09	0.10	0.07	0.06
Copper	-	-	-	-	-	1.13	0.70	1.25	1.95	2.10
Bismuth (added)	-	-	-	-	0.02	-	-	-	-	0.02

*B-1 : Series composition corresponds to the TELCO practice.

The melt was well stirred before being poured into the individual moulds.

Both dry sand moulds as well as chill moulds were employed for making the test specimens and castings. The test specimens were poured in finger moulds, made out of washed and graded pure silica sand. The individual fingers (127x25x9 mm) were connected to a common runner, 30x30 mm in section, through a 6x20 mm section ingate. Individual finger castings were sliced into 6 mm thick specimens for subsequent graphitisation and other studies. Simultaneously, from the same melt, a wheel casting was poured in dry sand mould. Some chill-cast cylindrical specimens of 15 mm dia and 100 mm length were also cast in mild-steel chill moulds in case of induction melted A-5 composition.

All these castings were stripped red hot after 5 minutes of pouring and allowed to cool to the ambient temperature in still air.

The alloys were then chemically analysed using wet-methods and Strohlein C and S apparatus. The results are shown in Table 6.1. All possible precautions were observed during these estimations. The accuracy of results could be expected within ± 2 to 3%.

6.2 AS CAST STRUCTURES:

Completely white fracture of the test slug (20 mm di

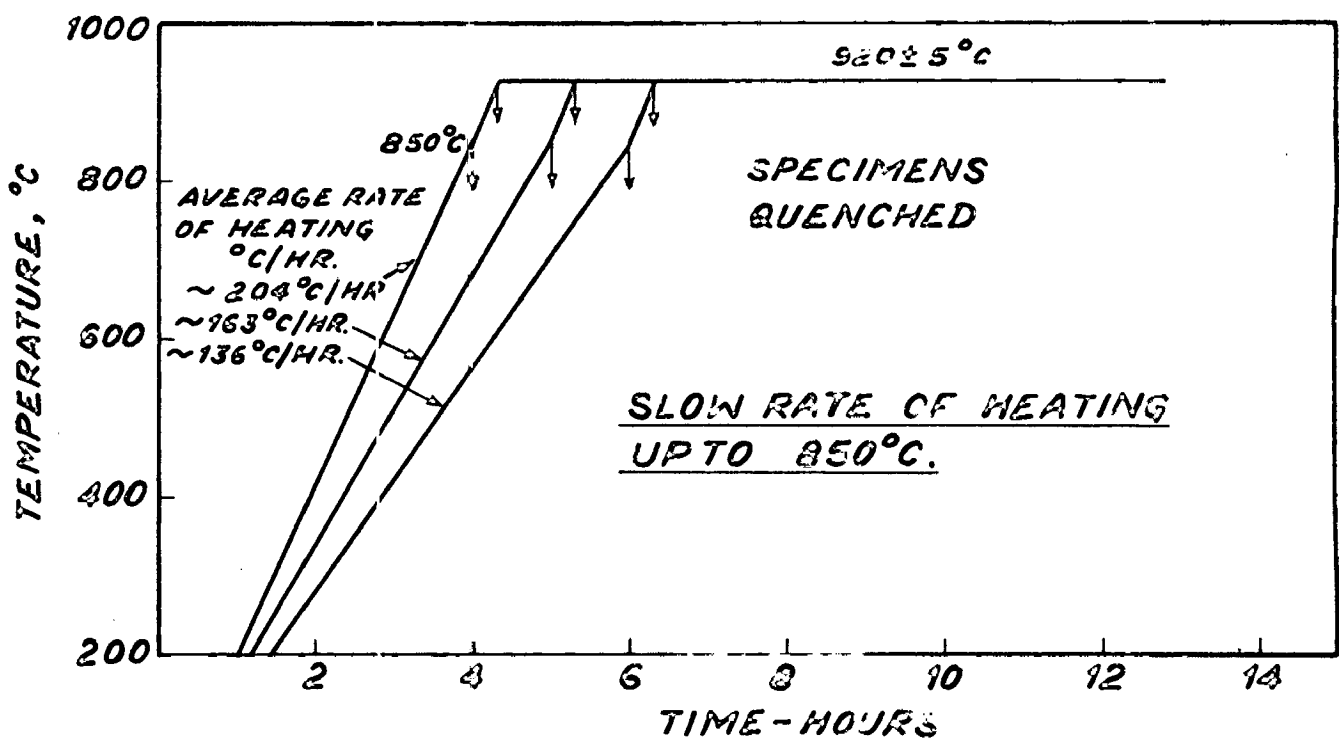
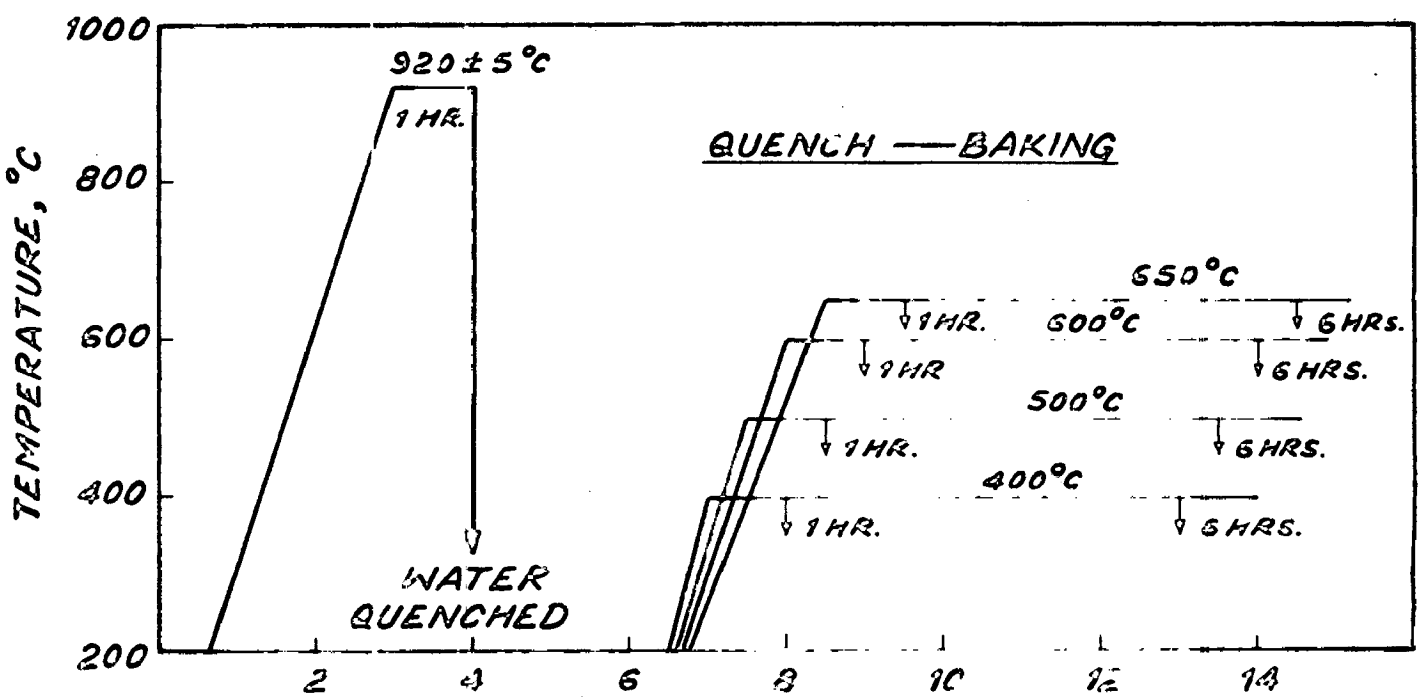
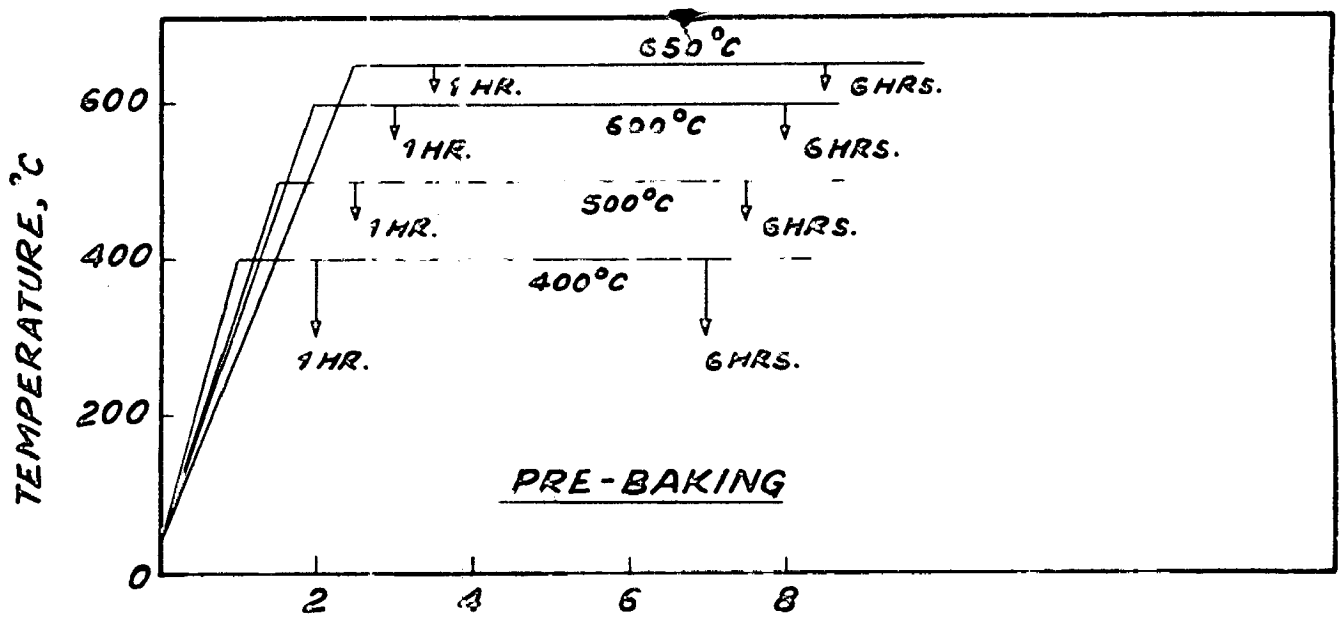


FIG-6.1 TIME-TEMPERATURE CYCLES OF VARIOUS PRE-TREATMENTS.

was a pre-requisite to pouring, in all the heats listed in Table 6.1.

Microstructures of thin as well as thick cast specimens were examined in each case prior to commencing the graphitisation studies on them. These cast specimens were also examined without etching and with light (0.5% Nital) etch. Primarily it was intended to examine the distribution of eutectic cementite in the cast structure by normal (2% Nital) etching. Light etched and unetched specimens were examined to detect the presence and location of graphite specks, if any.

Structure of Chill Cast, Synthetic white iron of A-5 composition, made in high frequency induction furnace, was also examined by EM-300 Phillips Electron Microscope. The intention was only to detect the presence of tiny graphite nuclei in the cast structure, not detected by normal optical microscopy. Two stage replication technique was followed for the purpose. This technique is discussed in section 6.4.2 in detail.

6.3 THE HEAT-TREATMENT:

6.3.1 Pre-treatments:

The pre-treatments carried-out in the present work are summarised in Table 6.2 and schematically shown in Figure 6.1.

Table 6.2

DETAILS OF PRE-TREATMENTS

Sl. No.	Pre-treatment	Details	Temperature °C	Duration hrs.
1.	Pre-baking	Specimens raised from ambient temperature to the temp. of pre-treatment, held at the temp. for pre-determined period and then water-quenched.	400, 500, 600 and 650	1 and 6
2.	Quench-baking	(a) Specimens raised from ambient temp. to the FSG temp., held for 1 hr. and Water-quenched.	FSG temp. 920	1
		(b) Specimens again raised from ambient to the pre-treatment subcritical temps., held for pre-determined period and then Water-quenched.	400, 500, 600 and 650	1 to 6
3.	Slow rate of heating	(a) Raised from ambient to 850°C in a pre-determined period, longer than the usual period of heating upto 920°C.	from ambient to 850°C	in 4.5 and 6 hrs.
		(b) heating from 850°C to 920°C at the usual fast rate.		
		(c) held at 920°C for FSG completion studies.		

The specimens, after quenching, were polished and etched in a regular manner for metallographic examination. The objective of these observations was to determine the No. of graphite nodules/Sq. mm. and their size (average dia) in individual specimens. These measurements were

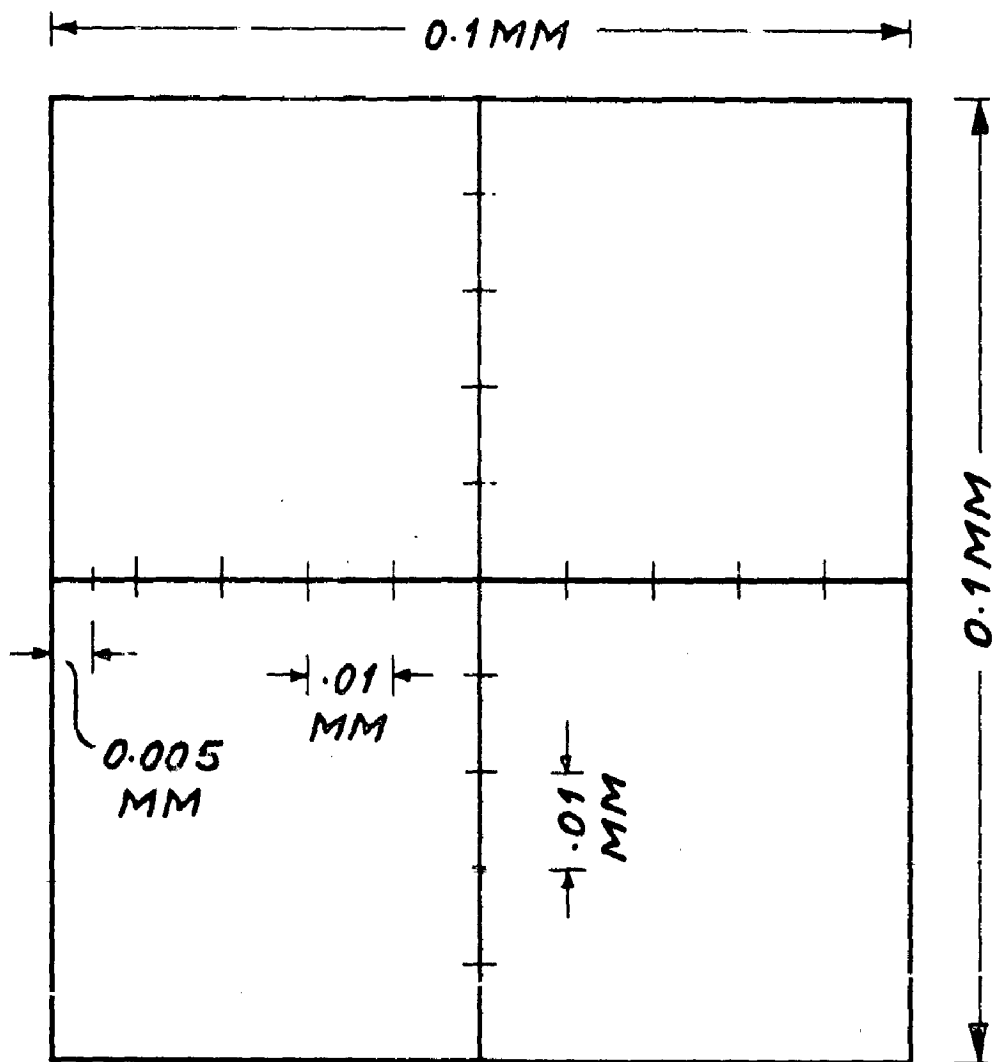


FIG. 6-2 SQUARE AREA GRADUATION ON FROSTED GLASS SCREEN OF NEOPHOT-2 PROJECTION MICROSCOPE.

carried out on Neophot-2, projection microscope, provided with a projection screen, graduated eye-piece and other such accessories, required for the purpose. The frosted glass plate of the projection system was calibrated by the help of a standard 1 mm. grid (1 mm. divided into 100 divisions). This calibration was done at 1000 X to suit the existing dimensions of frosted glass screen, such that 0.01 Sq. mm. area on the sample would cover nearly 75% area of the frosted glass screen at 1000 X. Thus a square area, with 0.1 m.m. each side, was marked on the frosted glass screen with ink. The centre-line of this square was further sub-divided into smaller divisions of 0.005 mm. least count in order to measure the average dia of tiny graphite nodules formed during the pre-treatment. ~~This graduation is shown in Fig. 5.2.~~

1000 X magnification was employed for these measurements, so that even tiny nodules could be clearly visible, which would not be the case at lower magnifications like 100 or 150 X. Higher magnification has been preferred for such measurements by other workers too⁽²⁹⁾ in the recent years for similar reasons.

Total number of nodules falling within this marked square of 0.01 sq. mm. area, were counted, and also the average diameter of smallest as well as the largest nodule in this group was measured. Such observations were recorded at 8 or 10 different areas of the same specimen. Number of

nodules were then converted into per sq. mm. Average of these values was then taken, to yield N_A (No. of Nodules/Sq.mm) term of Schwartz-Saltykov formula, given below:

$$N_V = 2.38 \times N_A^{1.6} \dots (1)$$

where,

$$N_V = \text{Number of nodules/mm}^3$$

$$N_A = \text{Number of nodules/mm}^2$$

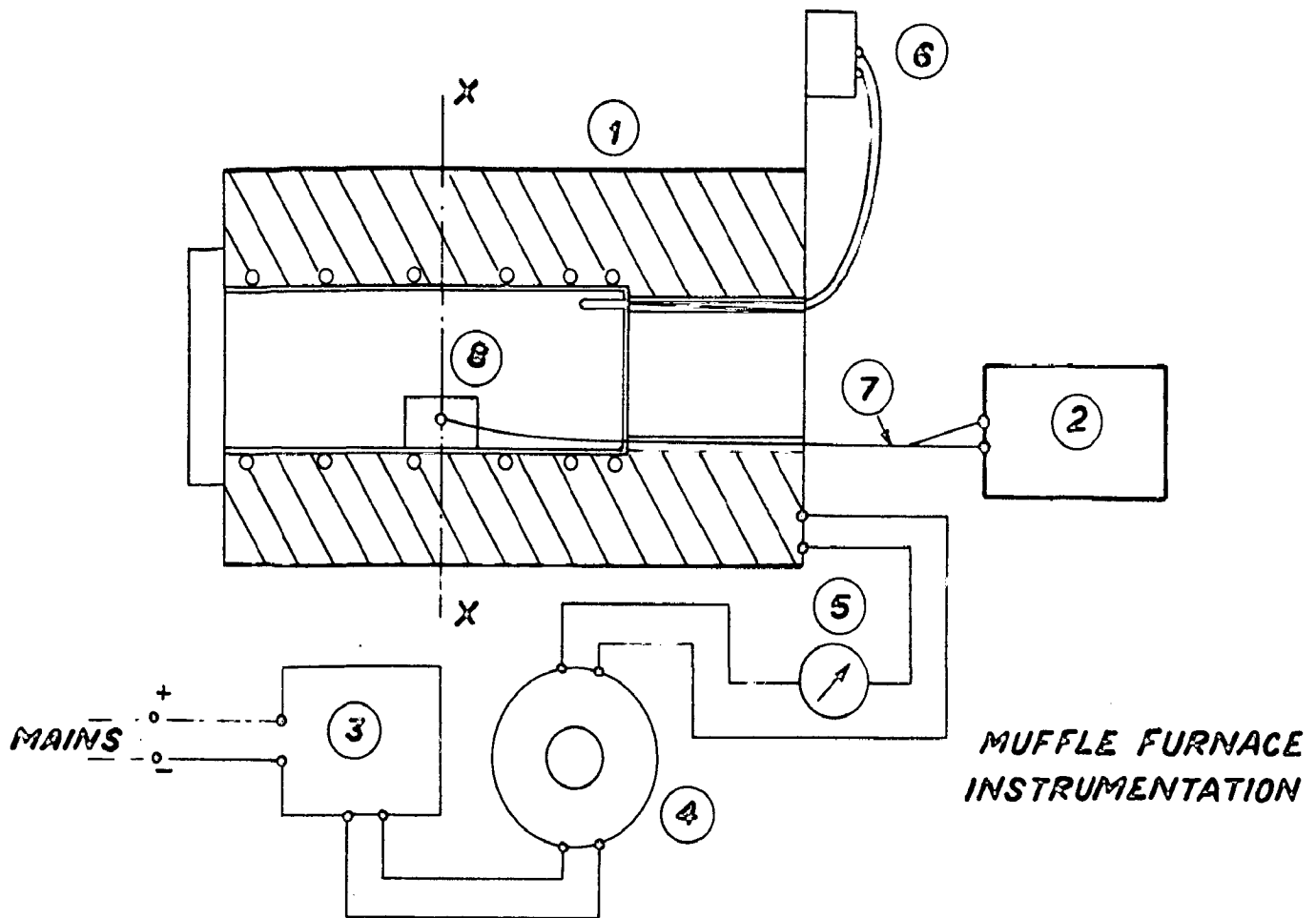
Thus, finally the number of graphite nodules/mm³ and their average dia were determined in individual cases. It must be stated here that graphite nodules less than 0.005 mm. in size were not considered in the present work for size measurements, though many of them were found to exist in pre-treated specimens. Such tiny nodules were, however, considered in N_A measurements. Also, it should be stated that such studies were best carried-out in unetched or lightly etched (0.5% Nital etch) condition.

This technique of determining N_A values has generally been termed as "Point counting technique" of quantitative metallography.

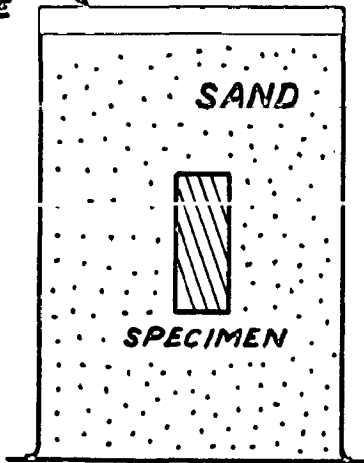
6.3.2 FSG and SSG Estimations:

Quantitative metallography and dilatometric techniques employed for such studies were discussed in detail in sections 2.2 and 2.3.1.

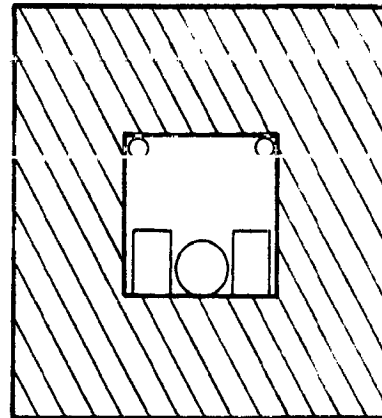
Metallography techniques were employed in the present work to determine the completion of FSG and SSG reactions



FIRECLAY
+ GRAPHITE
PASTE TO
SEAL THE
END.



PACKING OF SPECIMEN
IN STEEL CYLINDER



X-X SECTION THROUGH THE
MUFFLE FURNACE

INDICATIONS

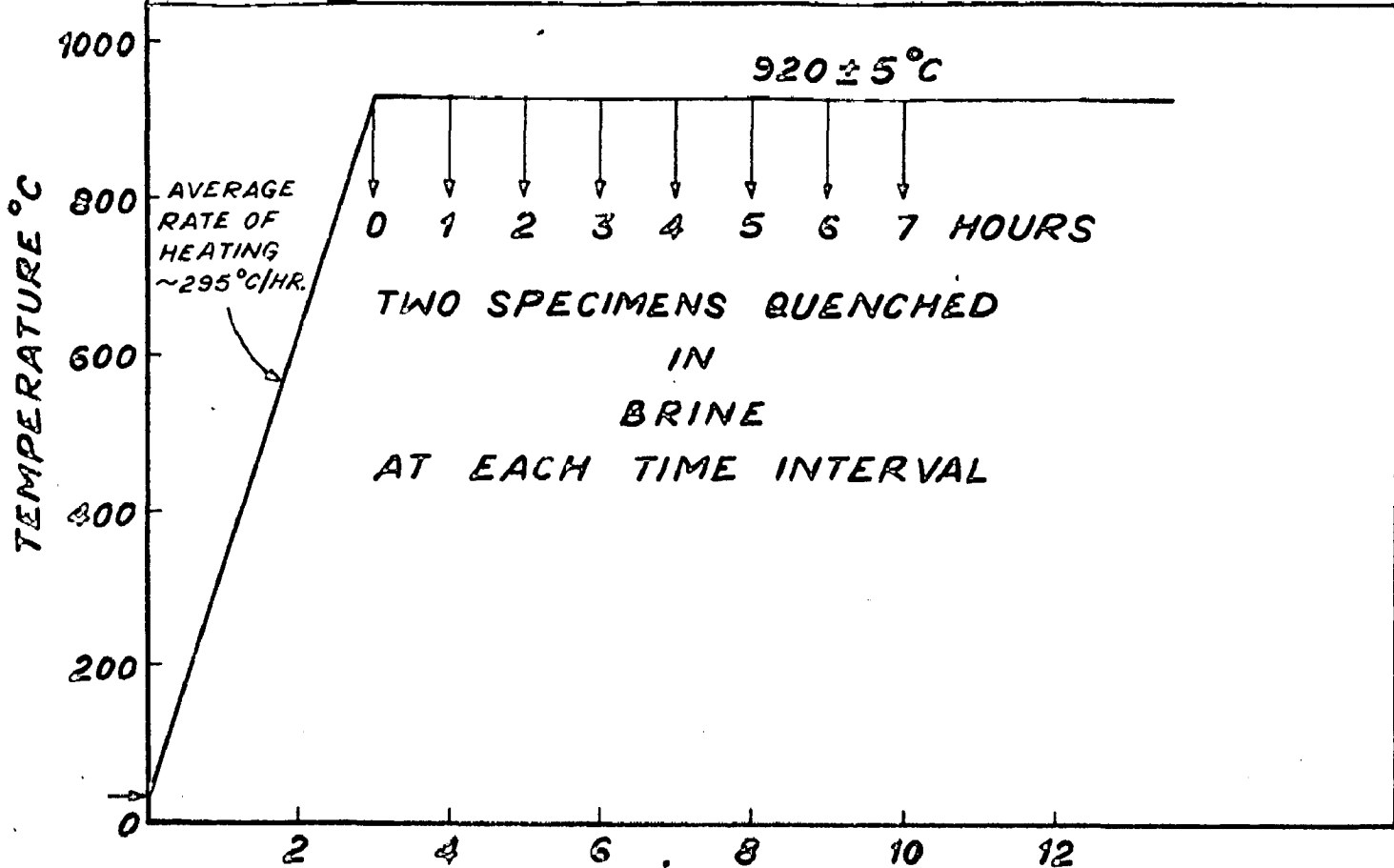
1. MUFFLE FURNACE - 4 kW.
2. POTENTIOMETER - LEAST COUNT 0.0001 MV.
3. VOLTAGE STABILISER - 6 KVA; $\pm 2\%$
4. AUTO-TRANSFORMER - 0-270V, 15 AMPS.
5. AMMETER, 0-15 AMPS.
6. C_r-AL TEMP. INDICATOR, 0-1000°C.
7. C_r-AL THERMOCOUPLE
8. BLANK CYLINDER TO MONITOR THE TEMPERATURE WITHIN THE CYLINDER.

FIG.-6-3 GENERAL ARRANGEMENT OF MUFFLE FURNACE INSTRUMENTATION.
ALSO SHOWING THE PACKING OF SPECIMEN IN STEEL CYLINDER.

in various cases. The general arrangement of muffle furnace and its controls, used in this study, is shown in Fig.-6-3. The following procedure was followed for these estimations:

FSG Period

1. One specimen each of the size (width-25 mm., length-6 mm., thickness-9mm.), sliced from finger castings of the dimension 127x25x9 mm, was packed in dried sand in a mild steel cylinder container (dia-30 mm I.D. and about 65 mm. length) along the longitudinal axis. This steel cylinder was then completely sealed from both the ends by a paste of fireclay and graphite. This was done to ensure that the specimen reacted under a neutral atmosphere.
2. As shown in Fig. 6-3, a blank mild-steel pipe of 30 mm. I.D. was also packed with sand and sealed on both ends by graphite and fireclay paste, but without any specimen contained in it. Instead, a medium-gauge chromel-alumel thermocouple was planted at the centre of this blank-cylinder. This cylinder was then placed horizontally at the centre of the hot-zone of resistance wound muffle-furnace. The thermocouple leads were then taken out of the furnace through the rear opening provided in the muffle for the purpose. The arrangement is shown in Fig. 6-3. This blank cylinder was required to monitor the



"QUENCH METHOD" OF ESTIMATING FSG PERIOD.

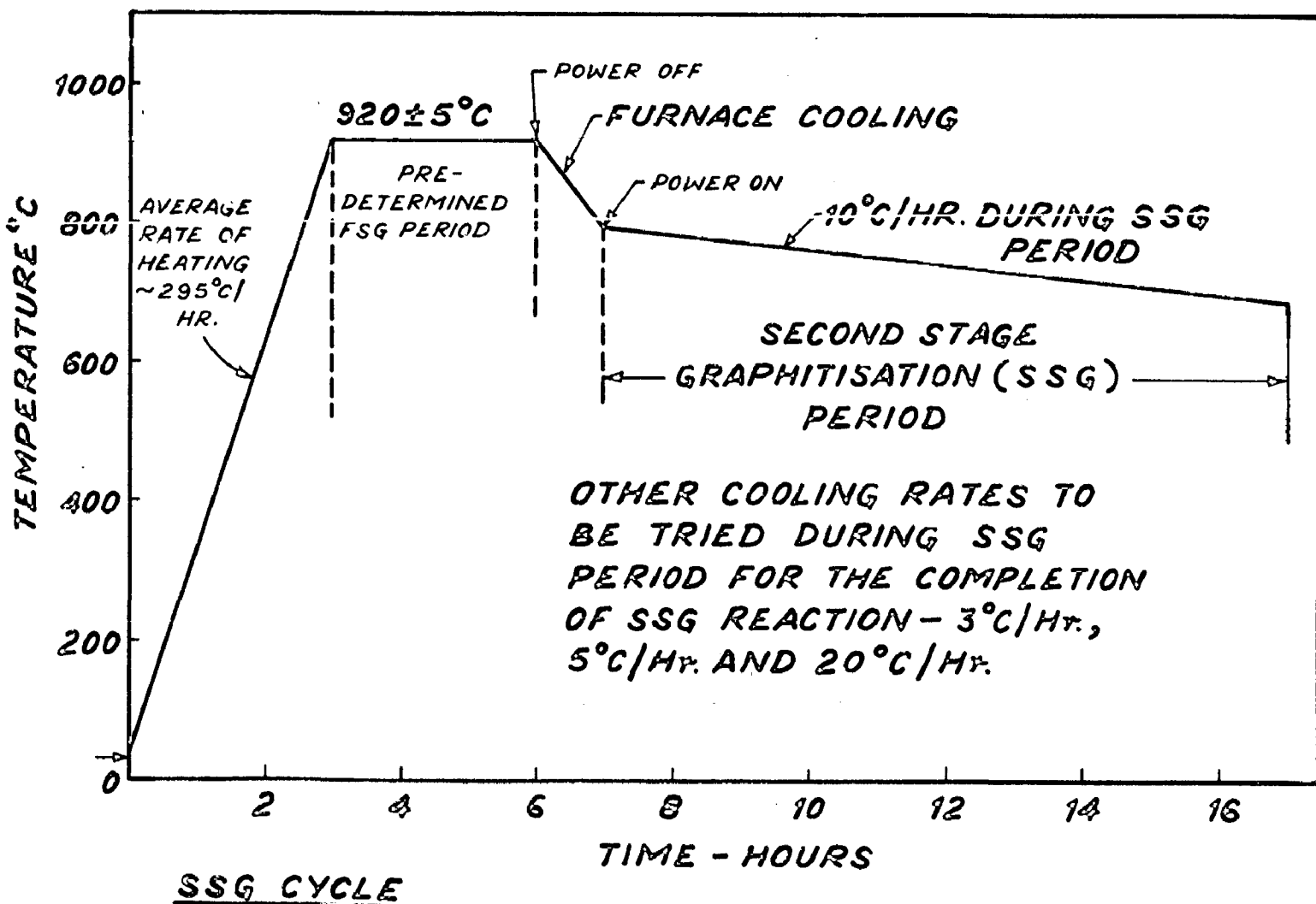


FIG.-5-A FSG AND SSG TIME - TEMPERATURE CYCLES.

temperature at the centre of cylinders, placed in the hot-zone. Thermocouple leads from the blank-cylinder were connected to a potentiometer through compensating leads to give accurate temperature readings.

The furnace was first calibrated, before using it for actual FSG or SSG runs.

3. The sealed cylinders, containing one specimen each, were then kept vertically and arranged on both sides of the blank cylinder in the muffle, the cylinders being as close to the blank cylinder as possible.
4. The furnace was then turned 'on' at full energy and allowed to reach 920°C , after which, the temperature was controlled at this level and maintained within ± 3 to 4°C throughout the completion of FSG reaction.

Specimens were drawn from the furnace at pre-determined intervals, as shown in Fig.6-4, and quenched in water after breaking the end seal quickly.

5. The specimens were then polished and etched for metallographic examination.

Presence of less than 2/3% eutectic carbide particles in the matrix was considered to be the criterion

for the completion of FSG reaction. Quenched specimens corresponding to specific periods of FSG reaction were thus examined for the presence of any eutectic carbide particles in the matrix. The reaction period, corresponding to which, the quenched specimen microstructure showed no traces of eutectic cementite particles, was taken to be the FSG completion period. The same procedure was adopted in all the cases to determine the FSG completion period.

SSG period

1. Four specimens, packed in the manner stated above, were run through a predetermined FSG period in case of individual alloys. The entire cycle is shown in Fig.6-4. Extra 30 minutes at 920°C were provided in all the cases to ensure that the FSG reaction was completely over.
2. The furnace was switched 'off' at this stage and the specimens were furnace cooled to 850°C .
3. The furnace was again put 'on' and controlled very precisely onwards. The specimens were allowed to cool very slowly, at a pre-determined rate, between 800° and 695°C (critical temperature range). These cooling rates were selected based on the base-composition. Two or three different cooling rates were tried in case of individual alloys, in an effort to determine the critical cooling rate, that would result in a fully ferritic base-matrix.

Furnace control in the present study was manual due to non-availability of such sophisticated temperature control

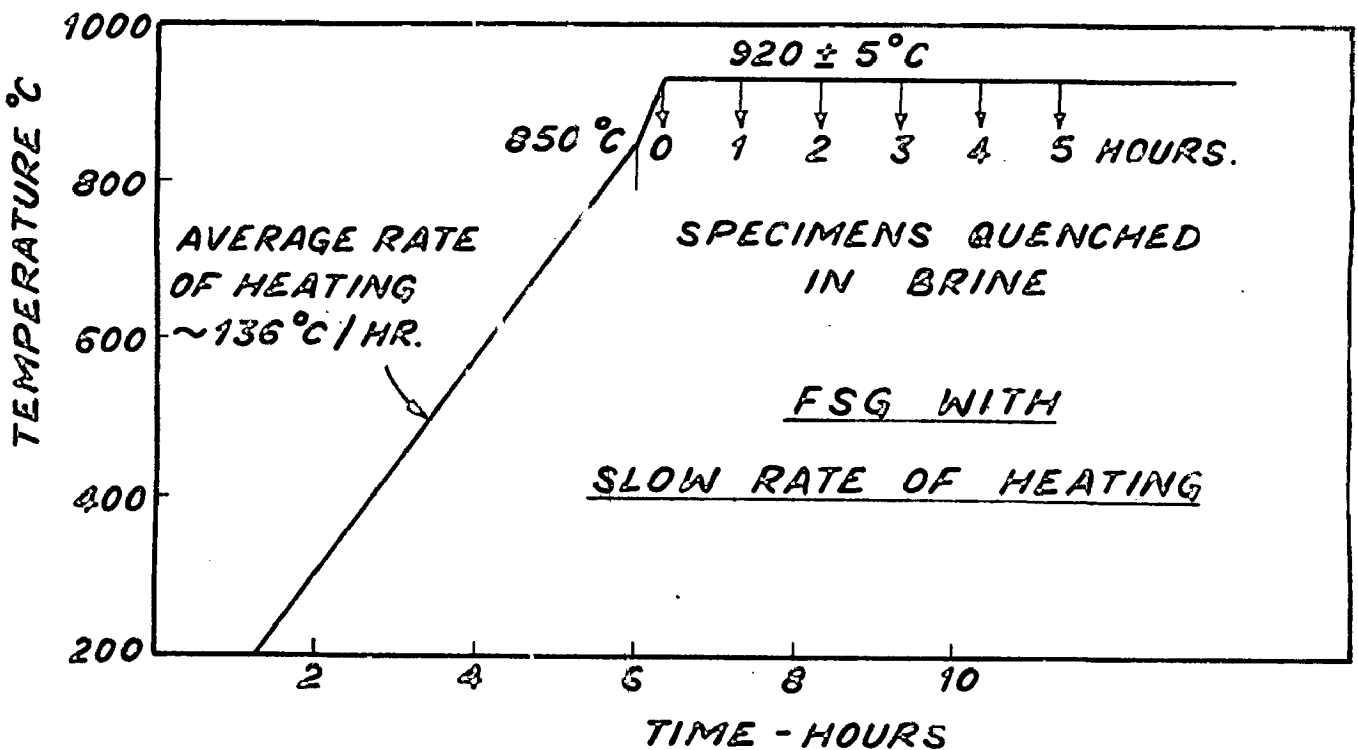
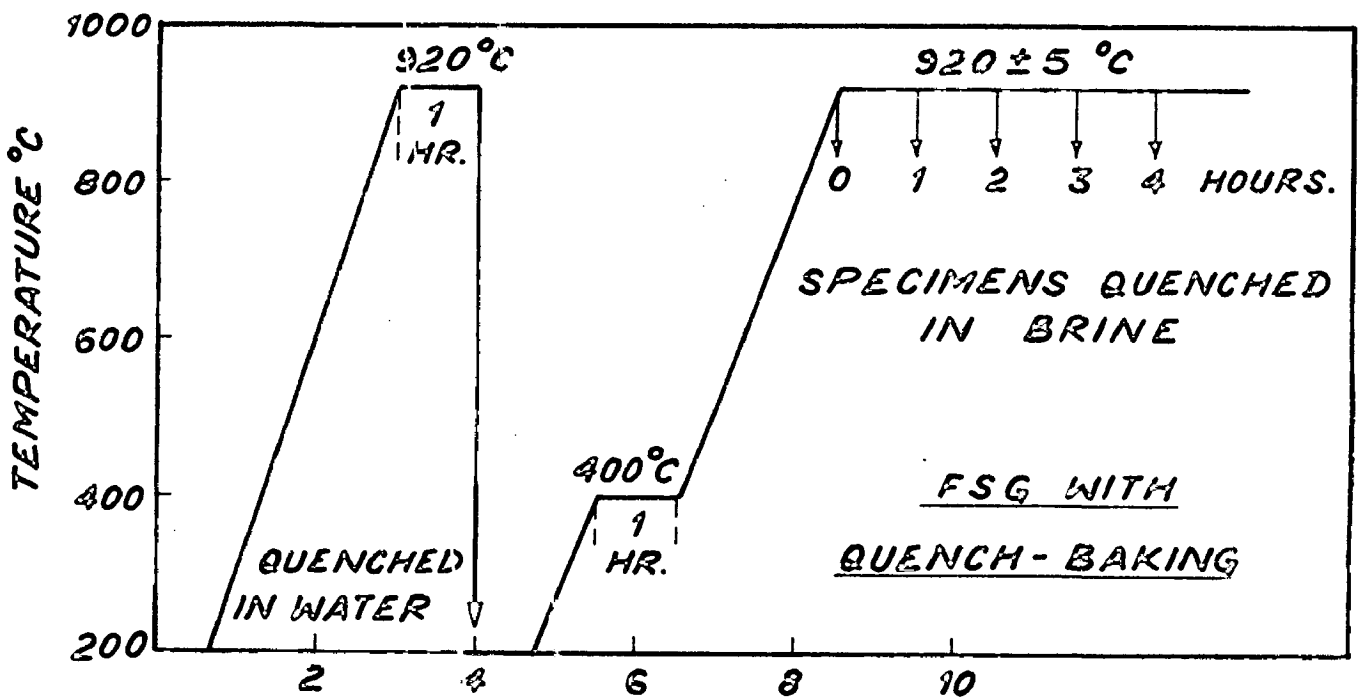
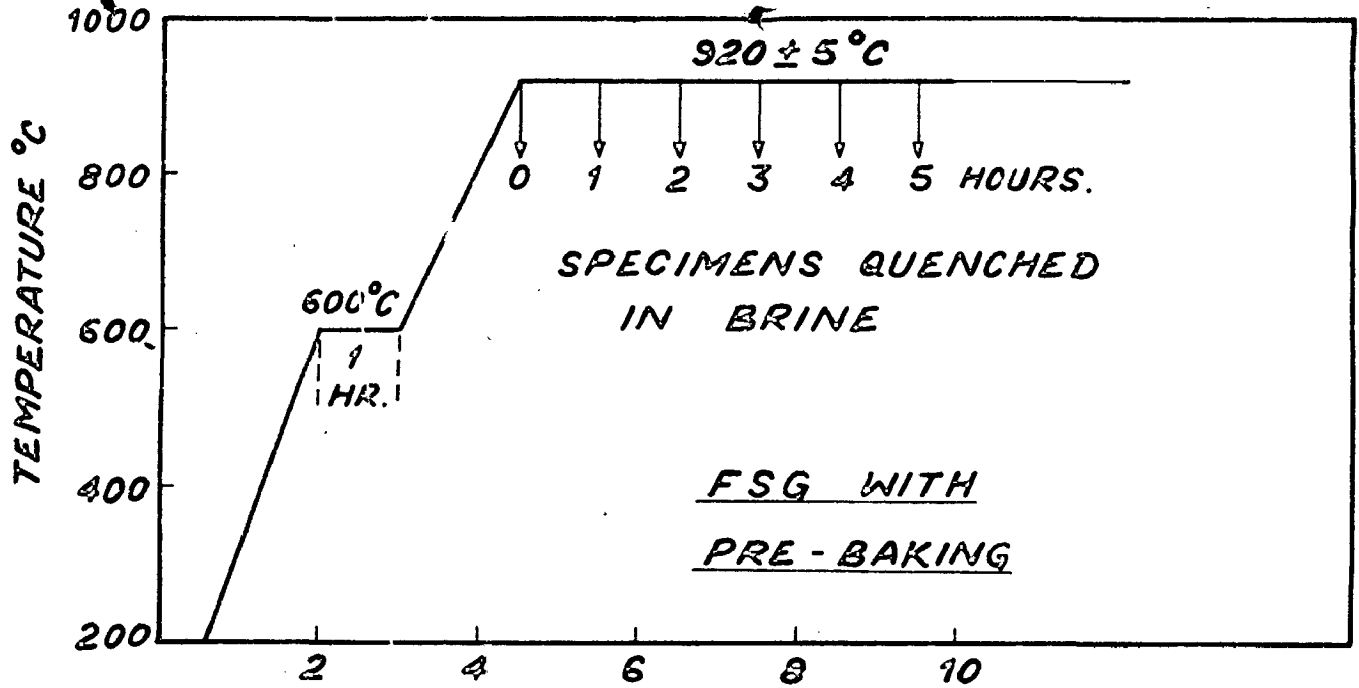


FIG.-6-5 FSG TIME-TEMPERATURE CYCLES WITH VARIOUS PRE-TREATMENTS.

instruments as to give pre-determined rate of heating or cooling within an accuracy of ± 0.5 °C/hr. However, proper calibration of the furnace was done prior to running the SSG cycles and it was found possible to control the temperatures within an accuracy of ± 3 °C with available instruments.

4. - The specimens were prepared for metallographic examination after the completion of SSG cycle. A microstructure showing fully ferritic base matrix along with tempered carbon nodules was taken to be the criterion for completion of SSG reaction.

6.3.3 FSG with pre-treatments

Details of such individual cycles are shown in Fig.6-5.

Methods of determining FSG periods and the experimental techniques were the same as described in the previous section.

Optimum temperature and period of the pre-treatment in individual cases was determined based on earlier experimental results. The criterion was that the selected temperature and period of pre-treatment would correspond to maximum number of nodules formed in the base-matrix. Simultaneously, the average diameter of largest nodules was required to be more than 10μ (microns).

Percentage shortening in FSG period, so obtained, was then calculated.

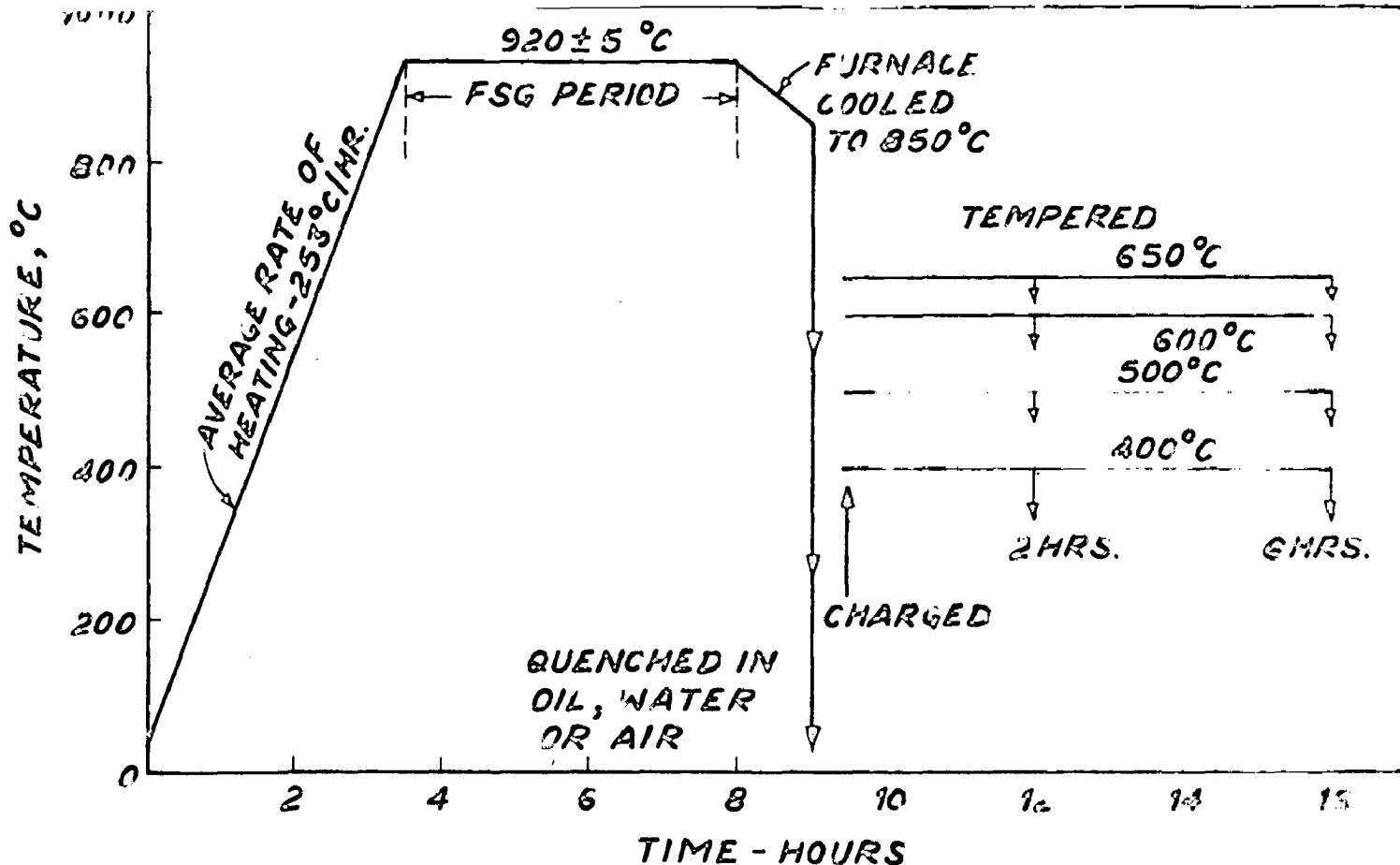
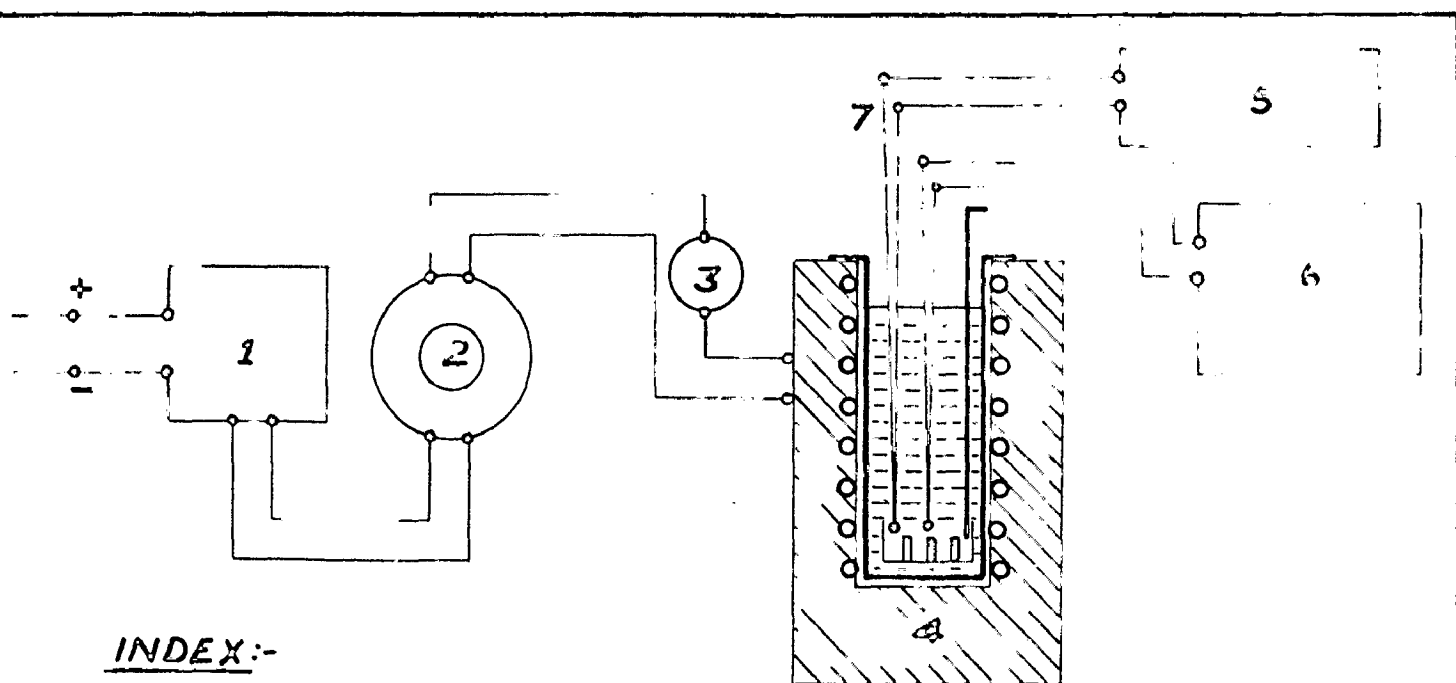


FIG.-6-6(i) TIME-TEMPERATURE CYCLE FOLLOWED IN CASE OF "INTERRUPTED ANNEALING" PROCESS.



INDEX:-

1. VOLTAGE STABILISER - 2KVA ± 2%
2. AUTO-TRANSFORMER, 0-270 VOLTS
3. AMMETER, 0-15 AMPS.
4. RESISTANCE WOUND FURNACE - 1.5 KW.
5. TEMPERATURE INDICATOR - Cr-Al, RANGE - 0-1200°C.
6. POTENTIOMETER, LEAST COUNT - 0.0001 MV.
7. CHROMEL - ALUMEL - THERMOCOUPLE.

FIG.-6-6(ii) SALT BATH FURNACE SET-UP.

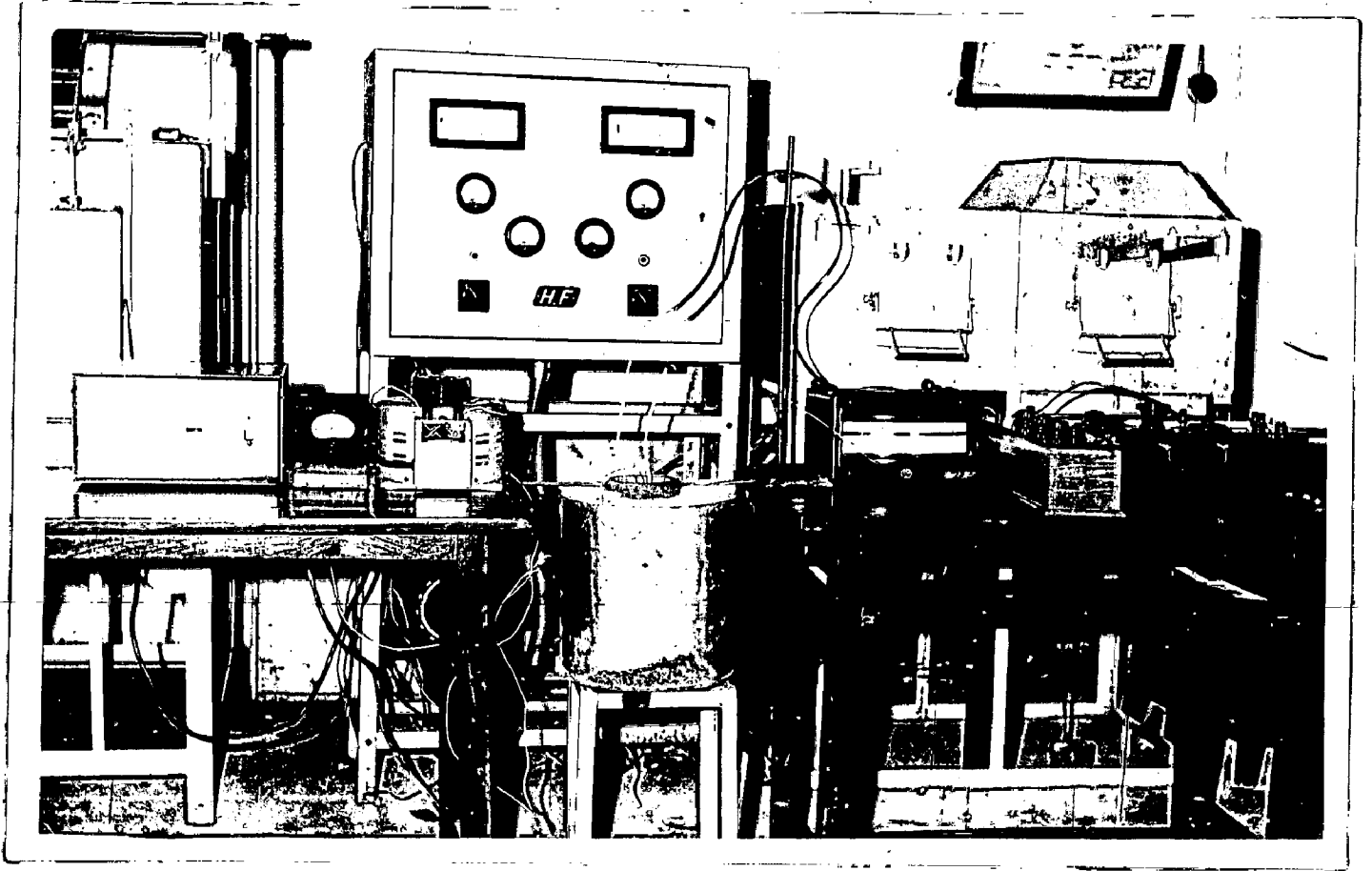


Fig. 6.7 - General arrangement of Salt-bath furnace Set-up.

6.3.4 Quenching after FSG Completion and Tempering

'Interrupted annealing' or tempering subsequent to FSG completion and quenching was the technique employed in the present work to study the microstructure and mechanical properties of pearlitic malleable irons made from different alloys. Quenching media of air, water and oil were used in this study. Quenched specimens were later tempered at various temperatures for different lengths of time. Time-temperature cycles employed and the experimental set-up used in this study are shown in Fig.6.6.

Instrumentation and general layout of salt-bath furnace, employed for the tempering work, is shown in Fig.6.6 and 6.7 respectively.

Hardness measurements coupled with metallographic examination were used to determine the effect of tempering temperatures and periods on the properties of tempered specimens. Hardness (VHN at 30 kg load with a diamond of 136° apex angle and 100X magnification), was measured in case of all the tempered and as-quenched specimens. At least six indentations were taken on a single specimen as a matter of routine practice. Some spread in hardness values was thus obtained.

These hardness values were then plotted against tempering periods for individual tempering temperatures. Such studies were conducted for thin (9 mm thick) as well as thick (15 mm thick) specimens. In most cases, the hardness values corresponding to 2 and 6 hours of tempering were

determined from these plots.

Later on, full length tensile test bars of 15 mm. dia. and about 130 mm length were subjected to full FSG anneal and quenched in different media (Fig.6-6). These dimensions of the test bars were selected in accordance with IS:2640-1964 (Indian Standard Specification for pearlitic malleable iron castings). Tensile test bars, subjected to this annealing treatment, belonged to the series O-8, O-10, B-1 and A-1 to A-5 (Table 6-1). Small blanks (9 mm thick) sliced from these quenched test bars were then subjected to tempering treatment at various temperatures for periods of 2 and 6 hours. As usual, their hardness was measured after tempering. These values provided also a check on earlier values, found in case of thin rectangular specimens.

The balance length of tensile-test bars was then sliced into two equal lengths, suitable for making Instron tensile-test specimens, and subjected to a pre-determined tempering cycle. Based on the earlier results, the tempering cycle was so adjusted that the hardness in tempered tensile specimens could be maintained between 290 and 315 HV₃₀ after 2 hours of draw period at a temperature. Complete tempering work of tensile specimens too was carried out in the salt-bath furnace (Fig.6-6).

Tempered micro-structures obtained in different tensile specimens have been discussed in relation to their

corresponding mechanical properties in subsequent chapters (7.0).

6.4 METALLOGRAPHY

6.4.1 Optical Microscopy

Optical microscopy was the most common method of examining the microstructure in the present work. Common metallographs employed for the purpose were Neophot-2 projection microscope and Japanese tube microscope. Magnifications upto 1260X could be obtained by Neophot-2 microscope, while the Japanese microscope could be used upto a magnification of 1000X.

Etching with 2% Nital (prepared in Ethyl Alcohol) was the common practice adopted to examine the microstructures. Also 0.5% nital etch was commonly employed to study the as-cast microstructures of white irons. This light etch was found to delineate only the eutectic-Cementite/Austenite grain boundaries without attacking the body of grains. This practice was used to locate the position of graphite specks in the cast white iron structure. These cast white iron specimens were also examined under the microscope in just polished condition and without any etching. Such an examination was to reveal the presence of graphite specks in the cast structure, if any, since it is known that graphite, if present in the structure, shall be clearly visible under the microscope in just polished condition only. Such a practice of examining the shape and size of graphite flakes

in gray cast irons is common. This practice was extended to the examination of malleable white iron structures because it was feared that tiny graphite specks, if present in the cast-structure, would get mixed-up with the dark-etching base-matrix, in case of normal etching with 2% Nital. Again, care was taken to repolish these cast specimens at least three times, every time nearly one mm metal being ground-off on the rough wheel before being finally polished for examination under the microscope. Thus, every cast structure was examined at least three times before any conclusions were drawn.

Normal metallographic practice of preparing the specimens for microstructural examination was followed in all the cases.

Optical photomicrographs in the present work were mostly taken on the Japanese microscope, because of its superior resolving power. The fractographs of as-cast white-irons were taken on the stereo-projection microscope at 2X or 16X. Optical microscopy was extensively used to follow the change in microstructures at various stages of graphitisation, quenching, and subsequent tempering.

Neophot-2 projection microscope was also extensively used to determine N_V (number of tempered carbon nodules/ mm^3) and the average size of largest graphite nodules in different cases. Such studies were conducted in case of pre-treated and partially reacted specimens at FSG

temperature, belonging to various compositions given in Table 6.1. The detailed procedure of calibrating the instrument for the purpose was discussed in the previous section 6.3.1, and also shown in Fig.6.2.

6.4.2 Electron Microscopy

6.4.2.1 Introduction

EM-300 Phillips Electron Microscope, having the following essential characteristics was used during these studies:

Resolution - $3\overset{\circ}{\text{A}}$

fully transistorised

Accelerating potentials - 20, 40, 60, 80 and 100 KV.

Magnification range - upto 500,000X with 100% utilisation of screen area.

It is known that suitable techniques for preparing thin-films of cast irons have not been developed to date for obvious reasons. However, double-replication technique has recently been used to study the sub-structures in cast irons. It was intended to use this technique (replica) in the present work.

It was thought to locate the presence of sub-microscopic tiny graphite nuclei in the cast structure, which could be in the early stages of growth. Also, it was thought to identify the copper precipitates in tempered specimens alloyed with copper, besides studying the sub-structure of tempered martensite in these cases.

6.4.2.2 Replica Preparation

Two stage carbon replicas were prepared in the present work. The following cases were chosen for replica preparation:

- (i) A-5 (2.0 wt% Cu and 0.02% Bi) white iron, chill cast, in 15 mm diameter rounds.
- (ii) A-5, Rectangular specimens (25x9x6 mm), oil quenched subsequent to FSG completion, and tempered at 600°C for 1/2 hr. and 9 hours.
- (iii) A-2, Rectangular specimens (25x9x6 mm), oil quenched (0.70 wt% Cu) subsequent to FSG completion, and tempered at 600°C for 1 hour and 14 hours.

The specimens were ground and polished to a very ^{fine} finish employing usual metallographic techniques. Only A-5 chill cast specimen was replicated in un-etched condition, while rest of the specimens were etched with 2% Nital and then replicated. Every care was taken to see that the etched surface was just fresh and free from any oxide and other films before replication. Also, it was made sure that the etched structure was distinctly visible under optical microscope.

A piece of special plastic tape, meant only for electron-microscopy work, was then dipped into acetone three or four times and applied onto the specimen surface, prepared for replication. Some more acetone was applied at the interface

of specimen surface and the plastic tape so that the tape sticks properly to the surface of specimen. After this, the plastic was allowed to dry onto the specimen at least for a period of 24 hours. The plastic was then carefully removed from the specimen.

A small quantity of carbon was then evaporated in a high vacuum chamber by striking an arc between a pair of graphite rods for 2 to 3 seconds only, and deposited on the plastic replica. The plastic replica was later dissolved in acetone to obtain the carbon replica. The carbon replica was then thoroughly washed in acetone to remove any traces of adhering plastic. This washed replica was then picked-up on specimen grids for examination under the Electron microscope.

6.4.2.3 Examination of Replicas:

Replicas taken on specimen grids were then mounted in EM-300 Electron-microscope, and examined at an accelerating potential of 80 or 100 KV. Magnifications upto 100,000X were employed in the present work. But in most cases, a magnification of 30,000X was found adequate to reveal the sub-structural details. All the micrographs were taken on a 35 mm. film and later enlarged three times to make electron-microphotographs.

6.5 FRACTURE STUDIES

As cast and tensile fractures were studied by the help of stereo-projection microscope at 5 X and 16 X. Some of

typical fractures were also photographed on 35 mm film. The cast white-iron fractures were examined to detect the presence of any mottle, while the tensile fractures were examined to ascertain whether the failure had occurred through ductile or brittle fracture.

6.6 PARTITIONING OF ALLOYING ELEMENTS

6.6.1 Electron Probe Micro-analysis

Electron-probe-micro-analyser, used in the present work, had the following technical specifications:

Excitation voltage	= 25 KV
Beam dia.	= 1 μ
Depth of penetration	= 1 μ^3 (analysing volume)
Analysing crystal	= Mica.
Detector	= Proportional counter,
Sample current	= 10 Micro-Amps.
Standard	= Pure Cu, spec. pure upto 4 nine.
equipped with Pulse Height discriminator.	
Size of specimen	= 14x8x7 mm. provided with X-Y strip chart-recorder for Cu intensities, obtained during scanning of specimen by electron beam.
Specimen speed past electron beam	= 0.25 μ /sec.
Chart speed	= 4 cm/min.

The aim of the work was to determine quantitatively the amount of copper partitioned to the eutectic cementite

and pearlite phases. Such estimations were carried out in as-cast as well as partially reacted FSG specimens belonging to five different compositions containing copper (A-1 to A-5 series).

14x8 mm phase of 14x8x7 mm size specimens was polished and etched with 2% nital in a regular manner. Eight such prepared specimens were loaded at a time in the specimen holder, the etched phase facing the electron gun. The etched surface could thus be examined with the help of a microscope attached to the instrument. Any particular phase, sought to be analysed, could be fixed under the cross-wires, or the specimen could also be moved past the electron-beam at a fixed speed as desired. At least seven or eight grains of eutectic cementite and a similar number of base-matrix locations were analysed for their Cu content in case of every specimen. X-ray intensities so recorded for any phase in a specimen were averaged and computed for their percentage copper, considering the intensity of standard copper sample as the reference (100% Cu). As a matter of precaution, X-ray intensity of standard copper sample was recorded before commencing with the analysis of every alternate specimen. Most of these specimens were also scanned by the electron-beam across different cementite and pearlite grains at a relatively slow specimen speed of 0.25 μ /sec. X-Y plots of relative Cu intensity vs the width of individual grains were thus obtained. Scanning data was recorded primarily to observe the variation of copper content

within the individual grains of eutectic cementite as well as the base-matrix.

Since the diameter of electron-beam could not be narrowed down to less than 1μ by this instrument, the beam was made to bombard well within the cementite grain in order to avoid the risk of electron beam partly falling on the base-matrix, whose copper content was found to be much higher than the cementite grains. This procedure was followed to ensure that the Cu concentration of cementite grains was measured as accurately as possible.

Necessary corrections were applied to these observations as discussed in the subsequent section and the Appendix.

- Table 6-3 shows the details of specimens subjected to this study:

Table-6-3

Specimens subjected to Electron-probe
Micro-Analysis.

S.N.	Series	Specimen details
1.	A-1	As cast, FSG - 2, 3, 4 and 5 hrs.
2.	A-2	As cast-far end and ingate end, FSG - 3, 4, 5 and 6 hrs.
3.	A-3 [*]	As cast FSG - 0, 1, 2 hrs.
4.	A-4 [*]	As cast-far end, ingate end. FSG - 1 and 2 hrs.
5.	A-5 [*]	As cast-far end and ingate end. FSG - 1, 2 and 3 hrs.

* Note - Cementite grains of partly reacted FSG specimens, beyond the periods indicated, were found to be smaller than 1μ and hence, no further analysis was found possible.

6.6.2 Error Analysis

Mainly, the following correction factors have to be applied to the observations of electron-probe micro-analyser, in order to obtain the correct concentration of element under question in the sample⁽²⁰³⁾:

$$K_i = C_i \cdot Z \cdot A \cdot F \quad \dots (1)$$

where

K_i = Relative X-ray intensity.

C_i = Mass concentration of i^{th} element in the sample.

Z = Atomic Number correction factor.

A = Absorption correction factor.

F = Fluorescence correction factor.

and

$$K_i = \frac{I_i^{\text{sample}}}{I_i^{\text{std.}}}$$

where,

I_i^{sample} = intensity of the characteristic ray of i^{th} element in the sample,

$I_i^{\text{std.}}$ = intensity of the characteristic ray of i^{th} element in the standard.

(i) Absorption Correction Factor (A)

Philibert absorption correction-

$$A = \frac{f(\chi_M \text{ sample})}{f(\chi \text{ stand})} = \frac{f(\chi_M)}{f(\chi_{100} \text{ Cu})} \quad \text{for Cu } K\alpha \text{ radiations only.}$$

and the value of $f(\chi)$ has been given by Philibert as

$$f(\chi) = \frac{1}{\left[\left(1 + \frac{\chi}{\sigma}\right) \left\{ 1 + \frac{\chi}{\sigma} \frac{h}{1+h} \right\} \right]} \quad \dots (2)$$

where the value of χ and h changes for pure elements (i) and the matrix (M).

$$\chi_{\text{std.}} = \mu_{ii} \operatorname{Cosec} \theta$$

where

θ = Take-off angle,

μ_{ii} = Mass absorption coefficient of element i for its own characteristic radiation

and $\chi_{\text{sample}} = \mu_{Mi} \operatorname{Cosec} \theta$

where μ_{Mi} = mass absorption coefficient of matrix M for the characteristic radiation of element i.

$$= \mu_{1i} C_1 + \mu_{2i} C_2 + \dots$$

$$h_{\text{std}} = \frac{1.2 A_i}{Z^2} \left\{ \begin{array}{l} A = \text{atomic weight of standard} \\ Z = \text{atomic number of standard} \end{array} \right\}$$

$$h_{\text{samp}} = \frac{1.2}{\sum (C_i Z_i^2 / A_i)}$$

σ = Lenard coefficient

The best present estimate is as given by Birk

$$\sigma = \frac{4.5 \times 10^5}{(V - V_i)^{1.65}}$$

where,

V = Electron beam voltage (Excitation Voltage)

V_i = Critical excitation voltage.

(ii) Atomic Number correction factor (Z)
Duncumbs and Reed Expression

$$Z = \frac{R_M \cdot \bar{S}_i}{R_i \cdot \bar{S}_M} \dots (3)$$

R is called as the back-scatter coefficient

R_i are provided in standard tables.

$$R_M = \sum C_i R_i$$

\bar{S} is the mean electron stopping power and is given by

$$S = \frac{Z}{A} \cdot \ln \frac{1.1\bar{V}}{J}$$

where

$$\bar{V} = \frac{V+V_i}{2} \text{ in volts}$$

$$\bar{S}_M = \sum C_i S_i$$

J = Mean Ionisation potential (given in standard tables)

different values of J given by different workers are:

$$J = 11.5 \quad (\text{Philibert})$$

$$J = Z \left[14.0(1 - e^{-0.17}) + \frac{75.5}{Z^{2/7.5}} - \frac{Z}{(100+Z)} \right] \text{ Duncamb and Reed.}$$

$$J = 9.76Z + 58.5 \cdot Z^{-0.19} \quad \text{Berger and Seltzer.}$$

(iii). Fluorescence Correction Factor (F)
Castaing and Reed expression

$$F = (1 + Y_i) \dots (4)$$

where,

$$r_i = \sum_j P_{ij} \cdot C_j \left(1 + \frac{1}{J_i}\right) \left(\frac{U_j - 1}{U_i - 1}\right)^{1.67} \cdot \frac{W_j}{2} \cdot \frac{\mu_{ij}}{\mu_{Mj}} \times$$

$$\frac{A_i}{A_j} \left[\frac{\ln(1+u)}{u} + \frac{\ln(1+v)}{v} \right]$$

where

$$\begin{aligned}
 P_{ij} &= \text{Constant} \\
 &= 1 \text{ for } P_{KK} = P_{LL} \\
 &= 4 \text{ for K radiation exciting L fluorescence (P}_{LK}\text{)} \\
 &= 0.25 \text{ for L radiation exciting K} \\
 &\quad \text{fluorescence (P}_{KL}\text{)} \\
 U_j &= V/v_j \\
 U_i &= V/v_i \\
 J_i &= \text{Jump factor of element i (tabulated)} \\
 W_j &= \text{Fluorescence yield for element (tabulated)} \\
 U &= \frac{\mu_{Mi} \operatorname{cosec} \theta}{\mu_{Mj}}
 \end{aligned}$$

where,

μ_{Mi} = Mass absorption coefficient of matrix M for the characteristic i radiation.

μ_{Mj} = Mass absorption coefficient of matrix M for characteristic j radiation.

$$v = \frac{\sigma}{\mu_{Mj}} \quad \text{where } \sigma = \text{Lenard coefficient.}$$

Correction procedures outlined above were applied to four different known hypothetical compositions containing copper in order to determine K_i values from known C_i values. Details of these calculations are shown in the Appendix. Calibration curve was then drawn between K_i and C_i values. K_i values obtained by Electron-probe-microanalyser in case of various specimens listed in Table 6-3 were corrected by the help of calibration curve to give C_i values. Such corrected values of Cu concentration were found for cementite

as well as the base-matrix in case of every specimen.

6.7 MECHANICAL TESTING

6.7.1 Hardness and Microhardness tests:

Vicker's hardness (VPN) was calculated based on the following formula:

$$H_v = \frac{1.854 \times P}{d^2} \text{ kgs/mm}^2 \dots\dots (5)$$

where,

H_v = Vicker's hardness expressed in number (VPN).
Values expressed as HV_{30} .

P = Load applied in kgs (30 kgs in the present work).

d = Diagonal of the indentation in mm.

(The diamond indenter had on apex angle of 136° in the present work and the diagonal was measured at 100 X).

Micro-vickers hardness (HV_M) was calculated by the same expression as used for normal VPN calculations, except that the different terms would be defined as under:

HV_M or H_M = Micro-Vicker's hardness, expressed in number.

P = Load applied in grams (44.8 gms. in case of Neophot-2 micro-hardness attachment and 50 gms. in case of Table type model).

d = Diagonal of the indentation in μ (microns) (read by the help of cross-wires in terms of drum divisions, which when multiplied by the least-count, would give the length of diagonal in μ)

diagonal length measured at 200 X in case of Neophot-2 and at 487 X in case of table-type-model.

DIMENSIONS IN MM.

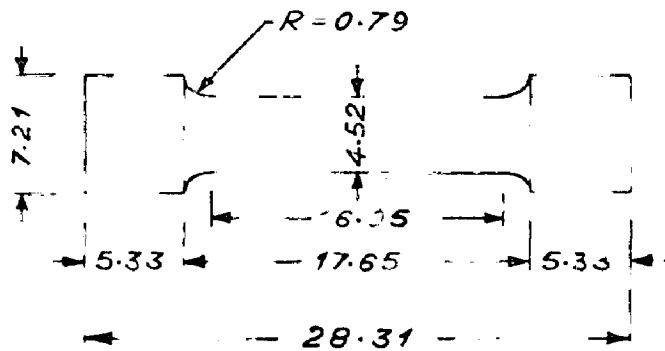


FIG.-6-8 HOUNSFIELD TENSOMETER SPECIMEN.
GAUGE-12

USED ON INSTRON UNIVERSAL TESTING MACHINE

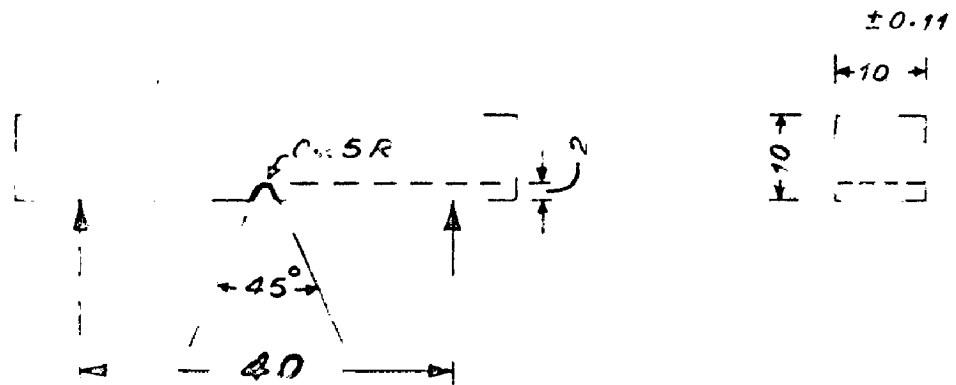


FIG.-6-9 CHARPY V NOTCHED BEAM TYPE
IMPACT TEST SPECIMEN.

Micro-hardness determined by Neophot-2 attachment was cross checked by the help of Table-type micro-hardness tester. Observations made by the latter instrument were expected to be more accurate since the indentation diagonal was measured at a higher magnification i.e. 487 X and also because the specimen was held firmly on the base-plate of instrument and therefore, there could be no relative motion between the specimen and the indenter in this case.

Indentations were taken at least at eight different locations of a sample, each for eutectic cementite and the base matrix to ensure accuracy. H_M values were calculated for all these diagonals independently to find the spread in values. The same practice was adopted in case of normal VPN measurements.

6.7.2 Tensile Testing:

Standard Hounsfield Tensometer specimens of gauge-12 (Fig.6-8) were tested on INSTRON Universal testing machine at slow strain-rates. Essential features of the Instron machine were as under:

Full scale sensitivity (Load-Range) = 0.2 gms to 5000 kgs.

Cross-head speed = 0.005 to 5 cm/min.

Chart speeds = 0.2 to 50 cm/min.

Load Cell - Tension and compression type upto 5000 kgs.

Model - Floor model (TT-CM-L)

Stress-strain curves for most specimens were obtained under the following conditions:

Cross-head speed = 0.01 cm/min.

Chart speed = 10 cm/min.

Resulting magnification on chart = 1000 X.

Load range used = 0.5 to 2 m.T.

In addition to measuring the UTS values, yield-strength was also calculated at 0.2% and 0.5% off-set values and reported in terms of kgs/mm^2 . Also percentage elongation (% Elong.) on standard 16.05 mm gauge length was determined using stress-strain curves. At least two to three specimens were tested for an individual case of heat treatment. Percentage reduction in area was not recorded in the present study since the material under investigation was of high strength and comparatively less ductility.

6.7.3 Impact-Testing:

Beam type standard V-notched specimens (Fig. 6-9) were tested by Charpy Impact testing machine at room-temperature. The results were reported in terms of kg.f.m.

CHAPTER-7

RESULTS AND DISCUSSION

7.1 AS CAST STRUCTURE

7.1.1 Optical Microstructures

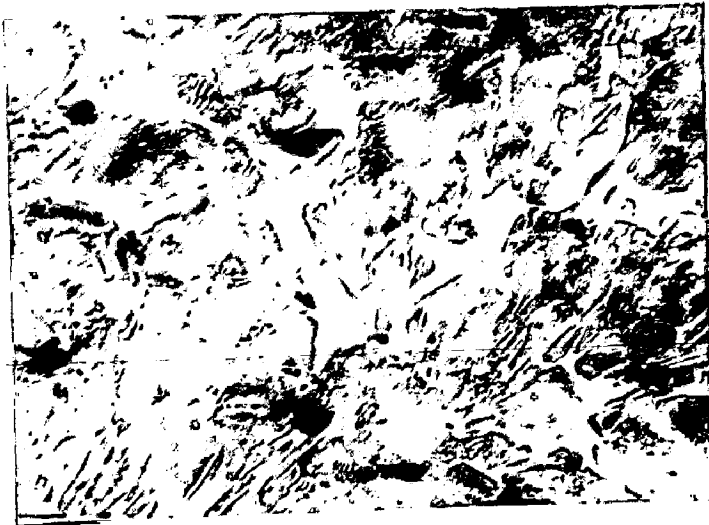
Figures 7.1 to 7.4 show the microstructures of O-8 (thin), O-8 (thick), A-5 (thin), A-5 (thin) induction-melted and A-5(thick) cast specimens. These photo-micrographs were taken in un-etched, lightly etched (0.5% Nital) and normal etched (2% Nital) condition. Chemical composition of these alloys is given in Table-6.1 (page-133). Apart from the microstructures shown here, all the alloys listed in Table 6.1 were examined in the same manner for the presence of tiny primary graphite nodules in thin as well as thick cast sections.

Figure 7.3(d and e) shows also the microstructure of a chill cast, A-5 composition, cast in about 15 mm round bar geometry. As stated earlier, this composition was prepared from mild-steel sheet scrap in a magnesia lined high frequency induction furnace under a basic slag cover and recarburised suitably by charcoal.

Microstructures after light etching (0.5% Nital) were examined in all the cases at higher magnification in order to study the location and shape of tiny graphite nodules in the cast-structures. Fig. 7.4 (b and c) shows



a) Unetched, X 250

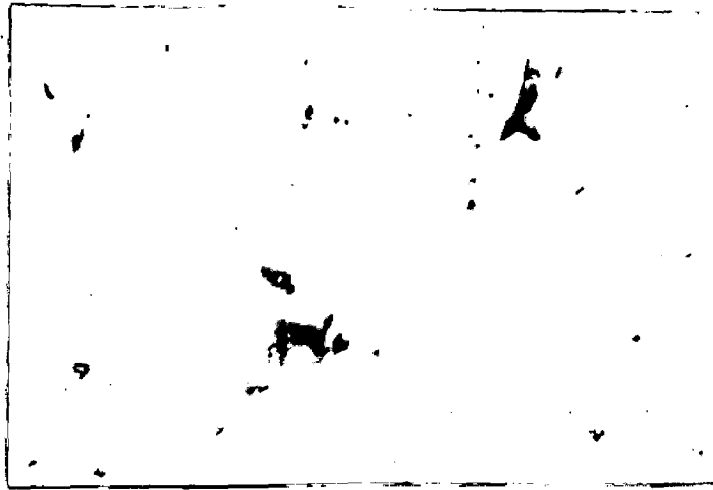


b) 0.5% Nital etch, X 250

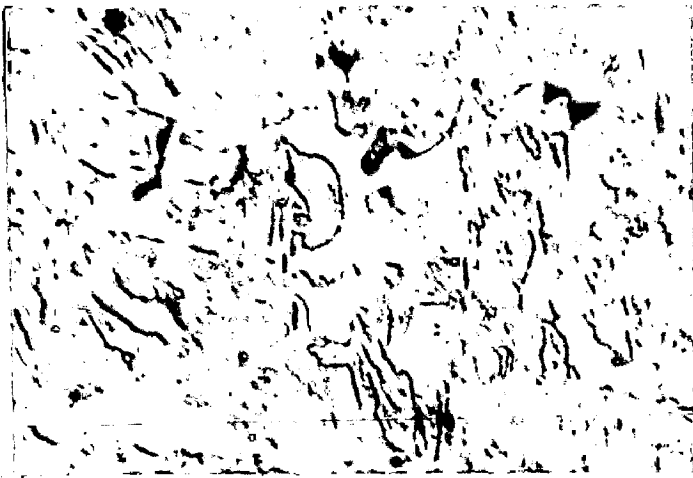


c) 4% Nital etch, X 1000

Fig. 7-1 - 0-8, As Cast, Thin specimen.



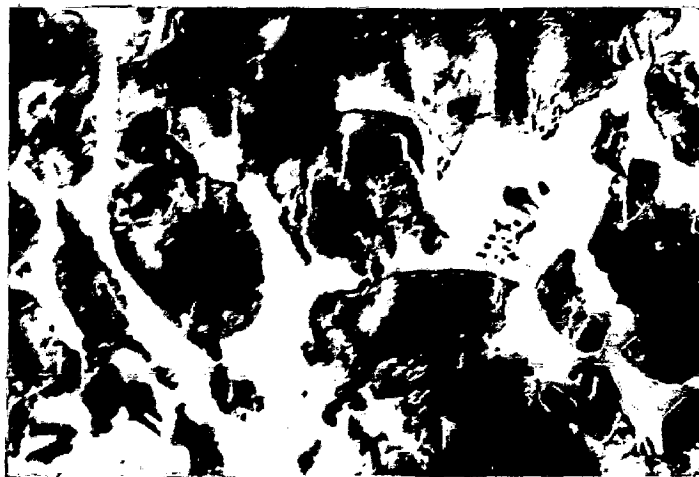
a) Unetched, X 250



b) 0.5% Nital etch, X 250



c) 0.5% Nital etch, X 250



d) 2.0% Nital etch, X 250

Fig. 7-2 - 0-8, As cast, Thick specimen



(a)

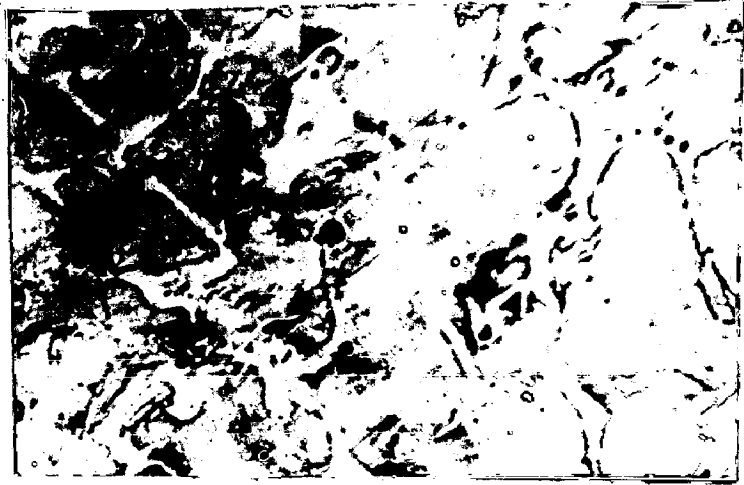


Fig. 7.3.(i): A-5, As Cast,
thin specimen.

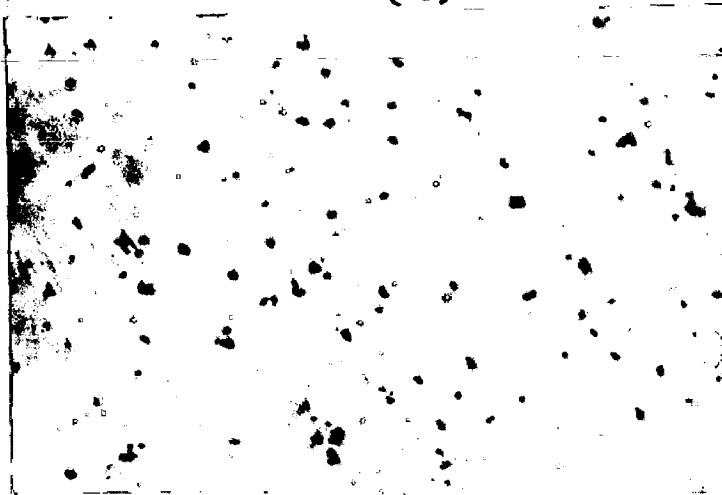
a) Unetched, X 250

b) 0.5% Nital etch, X 250

c) 2.0% Nital etch, X 250



(b)



(c)



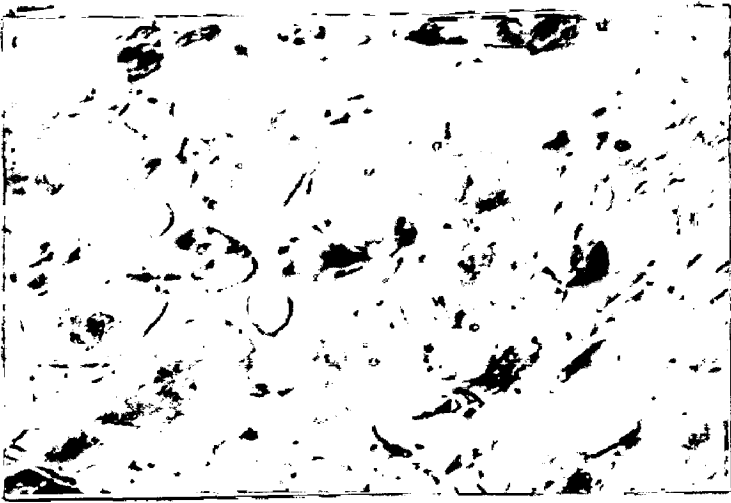
Fig:7-3(ii): A-5, Induction
melted, Chill Cast

a) Unetched, X 157

b) 0.5% Nital etch, X 628

c) 2.0% Nital etch, X 628





a) 0.5%. Nital etch, X 250.



b) 0.5%. Nital etch, X 1000.



c) 0.5%. Nital etch, X 1000.



d) 2.0%. Nital etch, X 250.

Fig. 7-4 - A-5; As Cast, thick specimen.

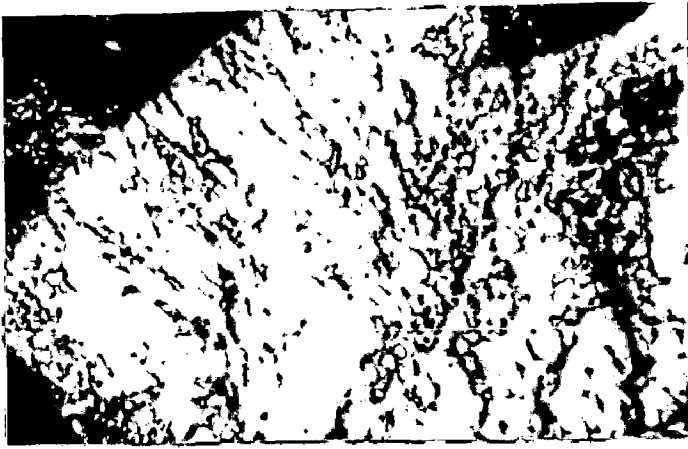
such a microstructure in case of A-5(thick) cast specimen at 1000X.

It was found from these observations that tiny graphite nodules of the order of 2 to 5 μ (measured at 1000 X) in size were present in the cast structure. Also, these nodules, were found located at eutectic cementite/Austenite interface in all the cases. Even thin sections of 0-8 composition, that contained only 0.89 wt % Si and 2.27 wt % total carbon, displayed the presence of such tiny graphite nodules in the cast structure (Fig. 7-1-a and b).

It was stated in section 6.2 earlier that thin as well as thick sections of all the alloys were allowed to cool in the sand mould for a period of 3 to 4 minutes subsequent to pouring, after which, all the castings were stripped and allowed to cool in still air. Only the synthetic white iron made in the induction-furnace was chill cast in 15 mm dia rounds.

These chill cast-specimens were also found to contain tiny free graphite nodules at cementite/austenite interface (Fig. 7-3-d and e), except for the difference that these nodules were comparatively smaller in size.

It should be mentioned that these tiny graphite nodules get mixed-up with the dark etching base-matrix, when the specimen is examined after normal etching with 2% or 4% Nital. This is shown in Figs. 7-1 to 7-4. Hence, these tiny graphite nodules are not easily detected in a



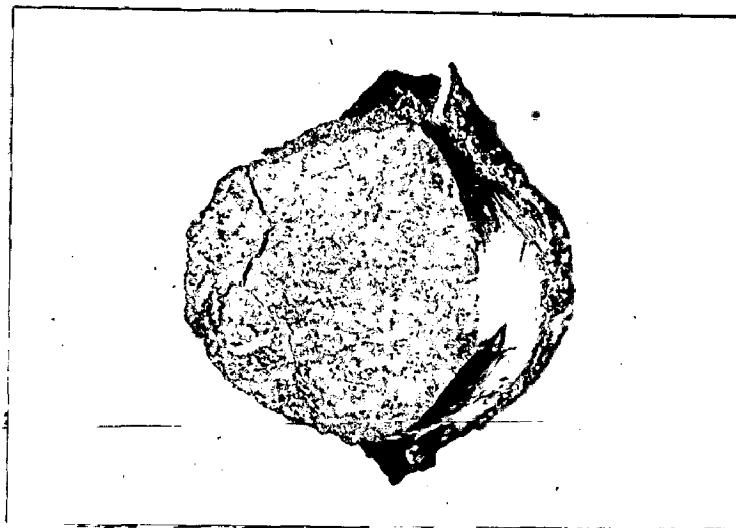
a) Stereo-projection Fracto-graph, X 2.
A-5, Induction, melted, chilled.



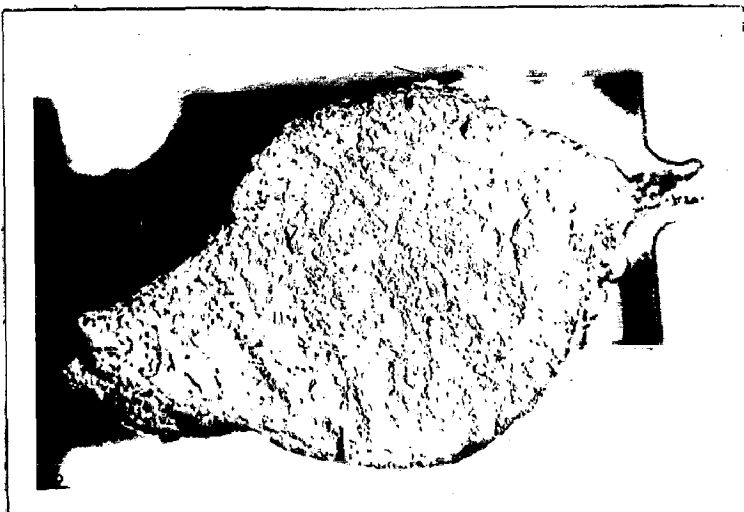
b) Stereo-projection-fractograph, X 2.
A-5, Induction melted, chilled.



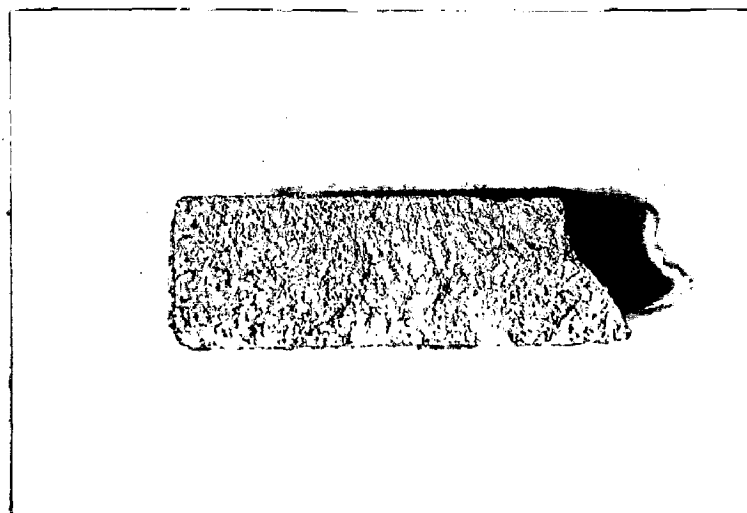
c) A-5, Chill-Cast, Induction melted.



d) A-4, thick specimen (25 mm dia).



e) A-4, thick specimen (25 mm dia).



f) A-4, thin specimen.

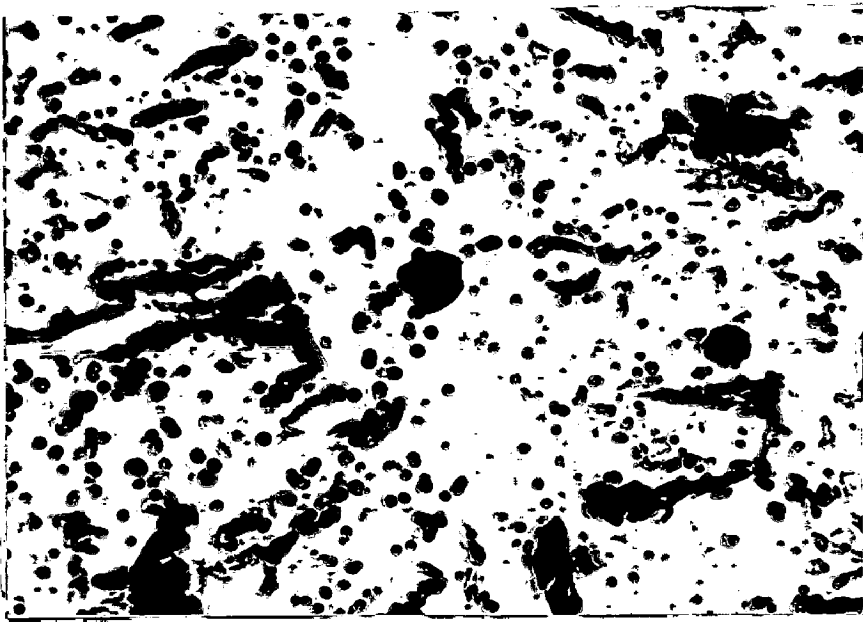
microstructure etched with 2% Nital.

Chill cast specimens and thin and thick specimens cast in sand mould, as outlined above, bring out qualitatively the influence of cooling rate on the formation of these very small graphite nodules in the cast structure. It is also obvious that considerable growth has already occurred in these small graphite nodules, commencing from the initial nuclei stage, since they are easily visible under optical microscopy. And yet, such individual nodules would be too small to be visible to the naked eye. Presence of such tiny nodules in the fractured surface was, therefore, not detected.

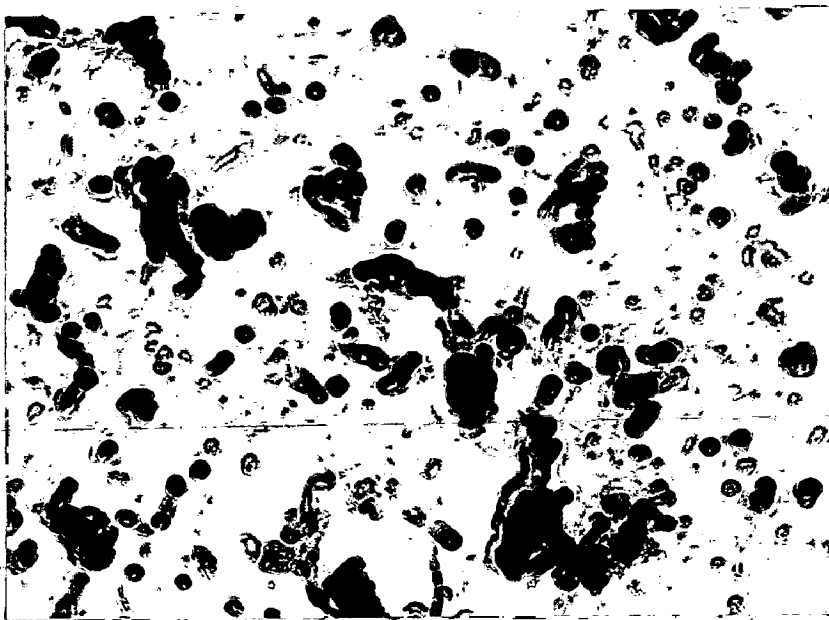
The influence of graphitisers like Si and Cu on the tendency of tiny graphite nodule formation in the cast structure has also been brought out in the present work. As would be expected, even 0.9 wt % Silicon in the base melt (0.8 composition) was found to cause the formation of minute graphite nodules in the cast-structure.

7.1.2 Fracture Studies

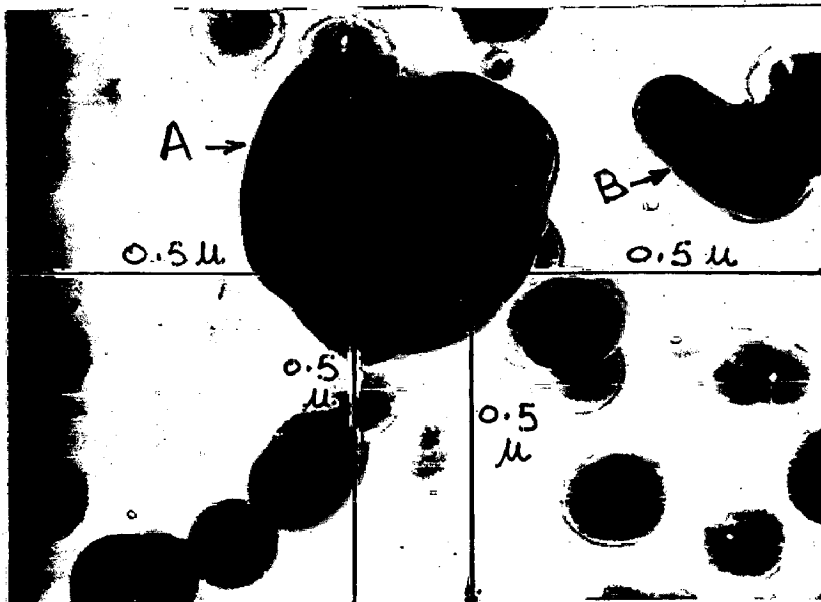
As stated in earlier sections 6.2 and 6.5, none of the compositions listed in Table 6.1 were poured unless the fracture of a 20 mm dia test specimen had shown a completely white fracture (totally free from mottle). These fractures were also examined by a magnifying glass (nearly 2X) prior to pouring in an effort to detect the presence



a) Unetched, X 30,000



b) Unetched, X 30,000



c) Unetched, X 80,000

Fig. 7.6:- Carbon Replica, Electron Micrographs.
A-5, Induction melted, Chill Cast.

of mottle spots, if any.

Fig. 7-5 shows the fractographs of chill-cast A-5 specimens (induction-furnace melted) taken on Stereo. Projection microscope at X2. The fractographs show no evidence of mottling. Fractographs of thin and thick specimens of A-4 alloy are also included in Fig. 7-5 as an example. Fractures of all other alloys listed in Table-6.1 were studied in the same manner under stereo-projection microscope in order to detect the presence of mottle-spots, if any. It was found that none of the cast structures, thin or thick, showed any evidence of mottle-spots on their fractured surfaces.

7.1.3 Carbon-Replica Studies

Fig. 7-6 shows carbon replica electron-micrographs of chill-cast A-5 synthetic white iron. As stated earlier, this synthetic white iron was melted in an induction furnace provided with a magnesia crucible. Two stage carbon replicas were prepared in the manner described in section 6.4.2, and studied by EM-300 Phillips Electron Microscope.

Fig. 7-6(a and b) shows these electron-micrographs at 30,000 X, while Fig. 7-6 (c) gives the micrograph at 80,000 X. These micrographs were first photographed on a 35 mm film (approximately 900 Sq. mm. photograph area), which later were enlarged to 90 x 90 mm size, resulting

in the original magnification to be restored on the enlarged prints.

These electron-micrographs reveal that a large number of tiny graphite nodules are present in the chill cast A-5 structure. Also, it can be seen from the micrographs that the tiny nodules are almost spherical in shape, indicating that they were still in the initial stages of growth.

Average size of these small graphite nodules was found to be approximately 137 \AA . The number of these tiny nodules/sq. mm area was found to be nearly 32. Using Schwartz-Saltykov formula, the volume fraction of these nodules works out to be nearly 609 nodules/Cu.mm. The distance between nodules was found to be varying from 0.033μ to 0.363μ approximately, indicating that they were randomly distributed throughout the whole matrix. Several nodules can be seen blurred in Fig. 7-6(c), showing that such tiny nodules were present throughout the cast-section.

From Fig. 7-6(c) it is also inferred that several tiny nodules of the size 137 \AA diffuse together to make a larger nodule of the size 437 \AA (marked A on figure) approx. Similarly, three tiny nodules (marked B on fig. 7-6-c) can be seen diffusing together to form larger nodule. This was so due to the higher chemical potential of the larger nodule compared with the smaller ones.

7.1.4 Microhardness of Eutectic Cementite and Base Matrix.

Microhardness of eutectic-cementite and base-matrix

Table 7-1

Microhardness of eutectic cementite and the
Base-matrix of cast alloys

(Using Neophot-2 Microhardness attachment)

1 Drum div = 0.455 μ at 200X

Load = 44.8 gms = 20 scales div.

Series	Specimen Details	Microhardness H_m , in kgs/mm ²	
		Cementite	Base Matrix
0-8	Thin, far end	758, 1111, 1003, 1238, 909, 758, 909	550, 368, 327, 263, 327
0-8	Thin, Ingate end	909, 909, 1238, 1238, 1238	327, 327, 347
0-8	Thick	1388, 829, 1238, 1238, 1238.	327, 327, 391, 309
0-10	Thin	1238, 1111, 1238, 1238, 1003	417, 417, 445, 445, 368, 347, 445.
0-11	Thin, Ingate end	1111, 1238, 909, 1238	327, 368, 309, 347
0-11	Thin, Far end	909, 1103, 1111, 696, 909	347, 368, 391
B-1	Thin	1388, 1238, 1238 1238, 1238, 829	391, 417, 368, 417, 445.
A-5	Thin	1388, 1238, 1111 1388, 1238.	391, 445, 368, 391
A-5	Thick	1238, 1003, 1003, 1238	368, 445, 417, 347

was determined in all the cast compositions with a view to ascertain the influence of varying silicon and copper content on the hardness of these micro-constituents.

Table 7.1 shows microhardness values found in case of different alloys. It can be seen from the observation that the microhardness of eutectic cementite in general varied between 909 and 1388 kgs/mm², while that of the base-matrix varied between 263 and 445 kgs/mm². These variations in microhardness values can not be considered very large taking into account the dimensions of individual cementite grains and normal sources of error in making such measurements. It can, therefore, be concluded from the present observations that the microhardness of eutectic cementite is not appreciably influenced by increasing amounts of silicon or copper in the base-melt, probably because these elements do not partition to the eutectic cementite phase in large amounts. Thus it appears that the fixed composition of eutectic cementite is not much altered by silicon or copper additions in the range studied.

Also, it can be noted from the present observations that the eutectic cementite formed in thick sections is no less hard than the one formed in thin sections. And this characteristic remains the same irrespective of higher silicon or copper present in the cast alloy.

7.1.5 Discussion of Results

The basic question, whether tiny nodules of free

graphite are present in the cast white iron structure or not has remained controversial so far. All the more controversial is the mechanism, through which, these small graphite nodules might be forming, if at all they are present in the cast structure. Again, the question is whether such tiny nodules can at all be tolerated in the cast structure, keeping in view the mechanical properties of the final heat-treated ferritic or pearlitic malleable irons. Then, the basic question will be "What should be the fundamental definition of a 'mottled' structure and what must be the basic requirements of a cast white iron structure, required for subsequent malleabilisation, provided it is confirmed that tiny graphite nodules are an integral part of any such cast white iron structure?!"

Unetched and lightly etched (0.5%.Nital) structures shown in Figs. 7-1 to 7-4, confirm that tiny nodules of free graphite are present in the cast white irons, corresponding to the compositions shown in Table 6-1. It is also confirmed that these graphite nodules are masked by dark-etching pearlitic base-matrix in a microstructure etched with 2 or 4%.Nital (Fig. 7-1 to 7-4). These tiny nodules, being of 2 to 5 microns in size, get mixed-up with the dark etching pearlitic base-matrix (2 or 4%.Nital etch), and hence are not clearly visible in such a microstructure. But when these nodules grow to dimensions larger than 15 to 20 μ during subsequent pre-treatment or FSG reaction,

they can be clearly visible in a normal microstructure with 2% Nital etch. It should be mentioned here that Na (No. of nodules/mm²) measurements on pre-treated specimens are also carried-out in an un-etched or lightly etched (0.5% Nital) condition so that every tiny nodule, formed during the pre-treatment, is clearly visible under the microscope. If this practice is not followed, wrong data may result, since many small nodules may be masked by the dark etching base-matrix (in case of 2% or 4% Nital etch.).

These tiny graphite nodules were found to exist at eutectic cementite/austenite interface in all the cases (Fig. 7-1 to 7-4). Even chilled synthetic white iron (A-5) was found to contain these graphite specks at the cementite/Austenite interface.

Carbon replica electron-micrographs (Fig. 7-6) further confirm that very tiny graphite nodules were present even in a chill cast white iron structure. Fully round graphite nodules of the size 137 Å approx. could be seen in Fig. 7-6(c) Fig. 7-6(a and b) clearly shows that a large number of graphite nodules were present in this cast-structure.

It was thus inferred from the present work that a large number of tiny graphite nodules of varying dimensions were present in the cast white iron structure. Their number and size would greatly depend upon the opportunity provided to these tiny nodules to coagulate together and grow.

Most of the earlier workers seemed to think that

graphite nucleation and growth occurs only in the solid state, when the cast structure is heated to austenitic temperature ranges. This has so far been most commonly accepted mechanism of white iron graphitisation. According to this mechanism, most of graphite nucleation occurs in early stages of heating i.e. between a temperature range of approximately 400 to 1000°C. This concept may be termed as the "Classical theory of white iron graphitisation".

This concept, however, does not explain the present observations.

Recently Ashton⁽²⁰⁴⁾ and others have projected the view that tiny graphite nodules are an integral part of a cast white-iron structure, and that these particles form at the boundaries of austenite dendrites during the solidification. According to Ashton⁽²⁰⁴⁾, the growth of these particles is inhibited by the nucleation and rapid growth of the metastable eutectic. He suggests that the graphite particles formed during solidification act as nucleation sites on subsequent first stage graphitisation of white iron. But in a recent work, Bhide and Banerjee⁽²⁹⁾ seemed to disagree with the views of Ashton⁽²⁰⁴⁾. However, they have also expressed contradictory opinions, saying that graphite particles smaller than the spherical cap-shaped particles (1 to 3 μ basal chord length and 1 to 1.5 μ height) may be present in the cast structure and also saying that graphite is detected on holding white iron sample at the

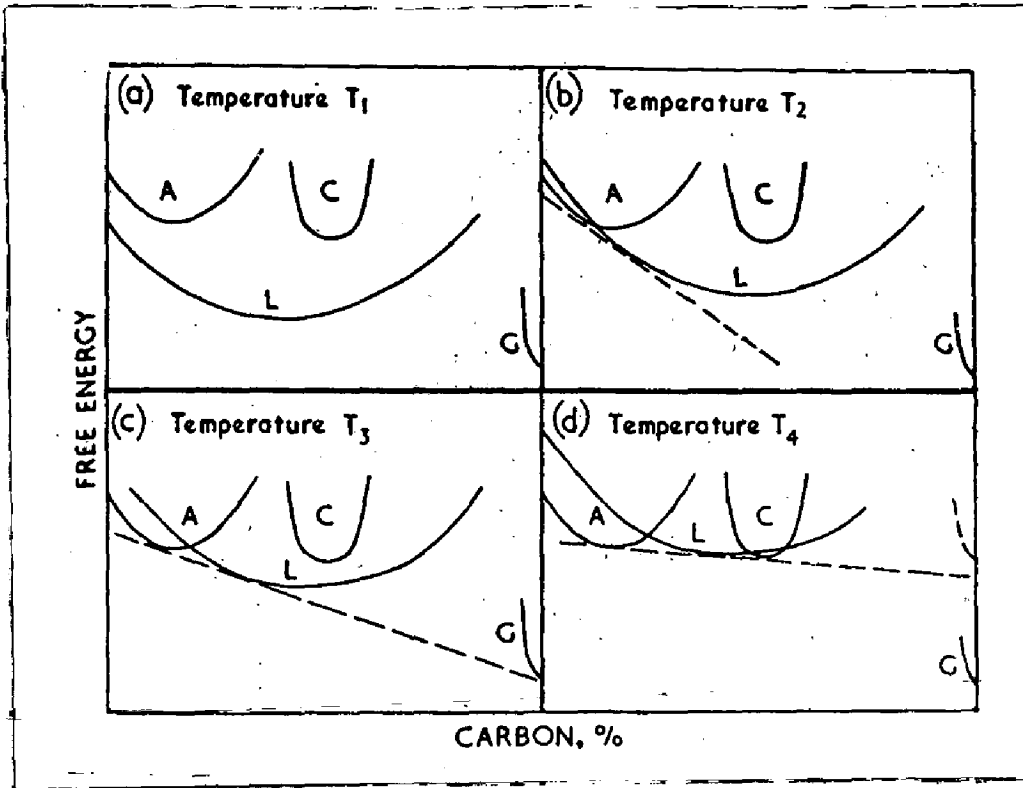
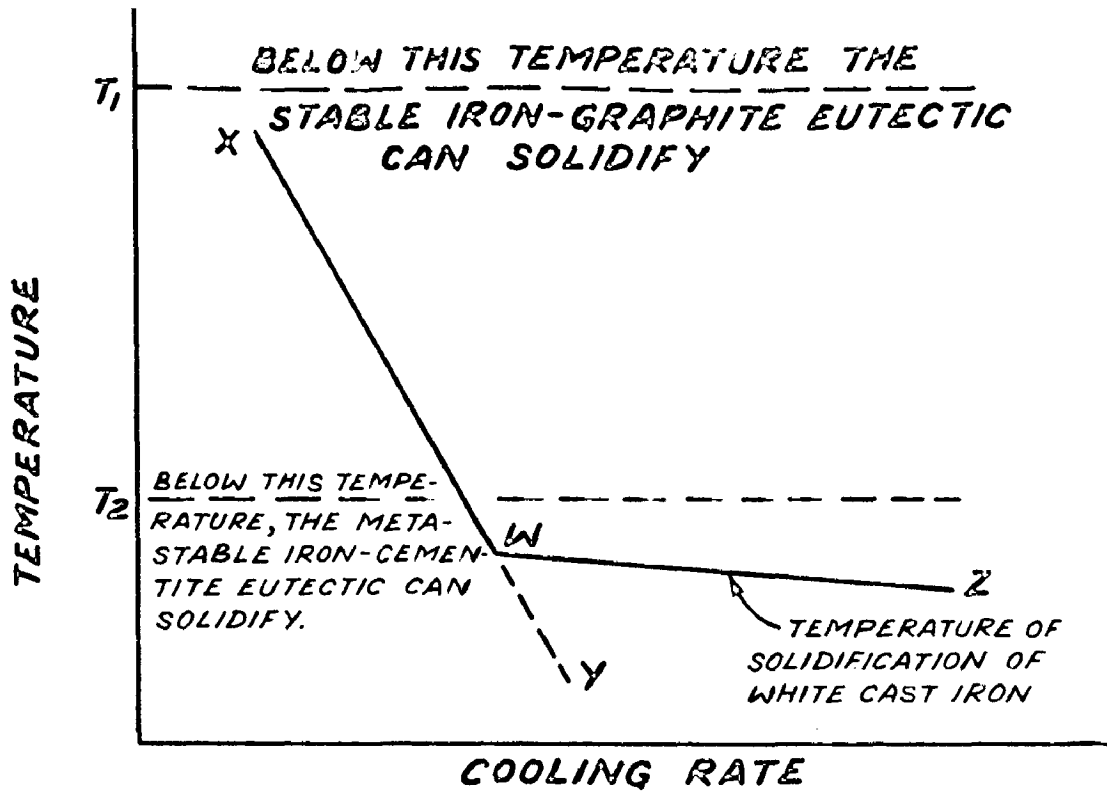
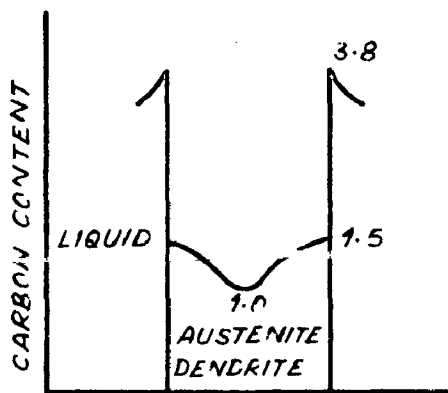


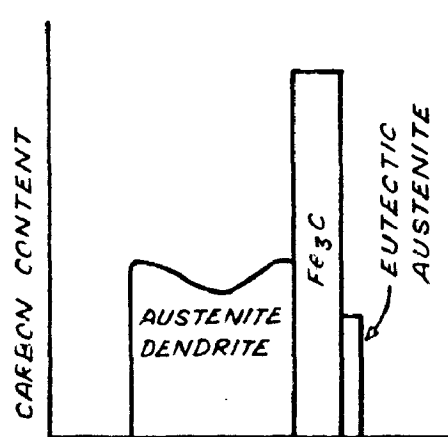
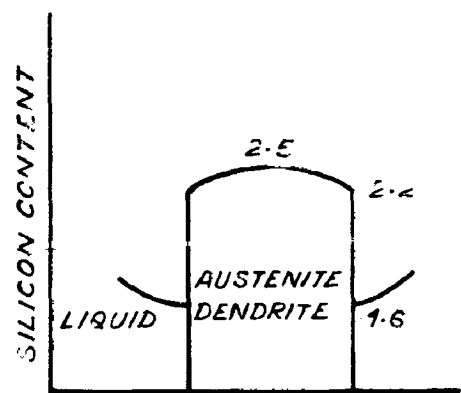
Fig. 7.7:- Free-energy/composition diagram of Fe-C system (Schematic). After Berman and Kondic (30).



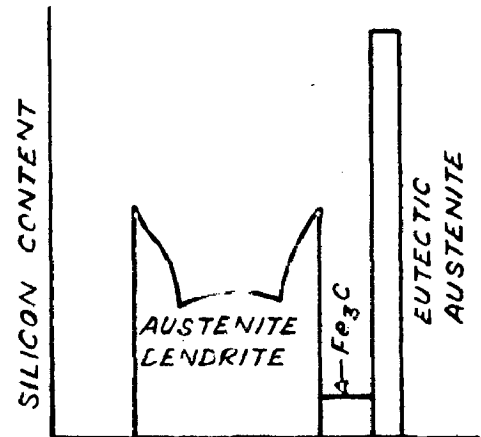
(a) EUTECTIC REGION OF THE DOUBLE Fe-C EQUILIBRIUM DIAGRAMME. (SCHEMATIC). AFTER (ASHTON)⁽²⁰⁴⁾



(A)



(B)



(b) SEGREGATION CHARACTERISTICS OF 3.0% C, 1.8% Si WHITE CAST IRON FREEZING UNDER EQUILIBRIUM CONDITIONS (A) PRIOR TO AND (B) AFTER THE METASTABLE EUTECTIC CONDITION. AFTER (ASHTON)⁽²⁰⁴⁾

FIG. - 7-8

FSG temperatures. The time for the formation of such large spherical cap-shaped particles has been termed as "Incubation period" and the process called as "Nucleation" by Bhide and Banerjee⁽²⁹⁾, which is basically unacceptable because graphite nuclei can not be larger than 10 \AA from fundamental considerations of surface and bulk free energy change required for the formation of graphite nuclei, and when the first particle of graphite is detected under optical microscopy after FSG reaction, it must already be in a grown condition. The terms of "Nucleation" and "Incubation period" have, therefore, been used incorrectly by Bhide and Banerjee⁽²⁹⁾.

The concepts of Ashton⁽²⁰⁴⁾, however, partly explain the present results.

Berman and Kondic⁽³⁰⁾, while working on the problem of origin of D type graphite in Fe-C alloys, made significant observations with regard to the possibility of graphite forming either direct from the liquid state or from the decomposition of cementite at and near the eutectic temperature. They observed that these two reactions occur in Fe-C alloy (3.38% total carbon and 0.1% Cr) under varying degrees of cooling rates.

From Figures 7.7 and 7.8 it is clear that some graphite would always nucleate direct from liquid, even when the melt is chilled from just above the eutectic temperature, because graphite has a lower free energy

than the liquid. The freezing phenomenon being heterogeneous in this case, since it is not a pure metal, the graphite nuclei of comparatively smaller diameter would be stable at greater degrees of under cooling of liquid. Resolution of these graphite nuclei in the base melt, once formed, will be less probable because of lower free energy of graphite compared to the base-melt (Fig. 7-7) and also because of its very high melting point (4830°C). Hence, these graphite particles will remain only in a nuclei stage, if proper conditions for their growth are not provided. Such graphite nuclei of the size $5-10 \text{ \AA}$ will not be resolved by optical microscopy. Austenite dendrites will continue to separate out from the liquid, till the eutectic temperature is reached. Graphite nuclei would form preferentially at the boundaries of austenite dendrites for the reasons stated by Ashton⁽²⁰⁴⁾. Along the line WZ in Fig. 7-8 (corresponding to the condition 'd' in Fig. 7-7), the metastable eutectic starts growing rapidly⁽²⁰⁴⁾. Therefore, even under these circumstances, when graphite nuclei had no chance to grow, normal white iron cast structure will be expected to possess a large number of graphite nuclei.

Growth of these graphite nuclei to different degrees would occur provided adequate conditions for their growth are available either during liquid to solid transformation or during subsequent stages below the eutectic temperature.

From the thermodynamic data discussed by Darken and

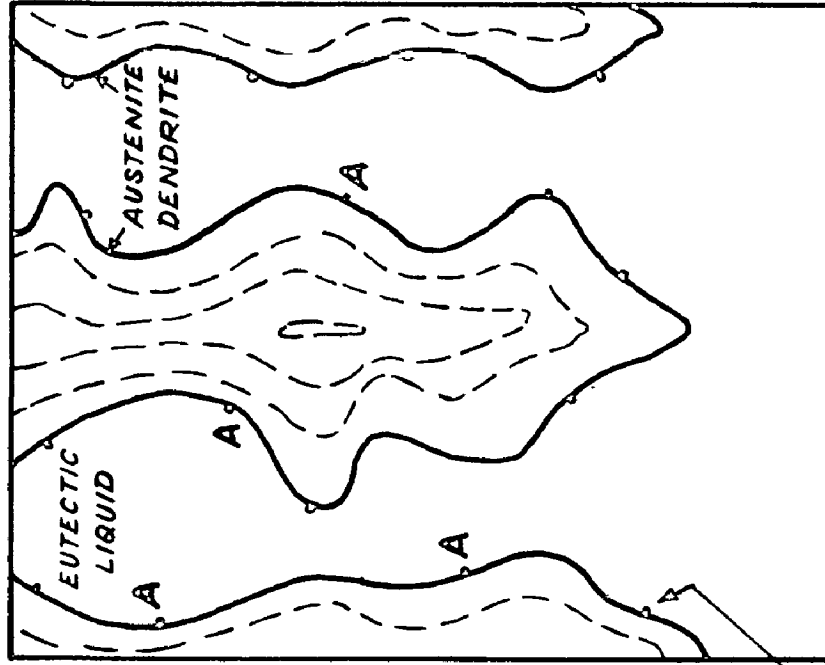
Gurry (Fig. 14-10 and Table 14-1)⁽²⁰⁵⁾ it can be seen that the free-energy of formation of Fe_3C at 25°C is $\Delta F_{298}^\circ = +4.76 \text{ K. Cals}$, which goes on increasing as the temperature increases since $\log a_c$ goes on decreasing with temperature (Fig. 14-10)⁽²⁰⁵⁾. This shows that the degree of instability of cementite increases with temperature. Kondic⁽³⁰⁾ reported that the time required for the decomposition of cementite near the eutectic temperature is of the order of minutes. This period, was found to be only 4 minutes in case of his pure Fe-C alloy (3.38% carbon and 0.1% Cr). Also, it is known that silicon increases carbon activity. Hence, normal white irons containing even 0.6 to 0.8% silicon and 2.2 to 2.4% total carbon must all the more exhibit this tendency of eutectic-cementite decomposition near the eutectic temperature. This process of cementite decomposition should further be hastened due to the presence of graphite nuclei at the boundaries of precipitated austenite dendrites. But in a normal procedure of white-iron manufacture for subsequent malleabilisation, the castings are stripped in air soon after they are frozen. Actual castings may thus be held at the eutectic temperature for only a fraction of minute due to continuous rapid cooling. In such cases, therefore, the carbide decomposition shall occur only to a very limited extent in the vicinity of eutectic temperature. Comparative instability of carbides is further evidenced by the fact that FSG periods are cut short considerably by resorting to relatively higher FSG reaction

temperatures.

Thus, any partial decomposition of eutectic cementite near the eutectic temperature shall release carbon atoms, which will deposit themselves on the existing graphite nuclei, and shall cause their partial growth. Almost a continuous network of cementite Austenite eutectic would have grown rapidly adjacent to the pro-eutectic austenite dendrites just below the eutectic temperature. Concentration profile with respect to C and Si at this stage is shown in Fig. 7.8 b (after Ashton⁽²⁰⁴⁾). Carbon atoms released by the decomposing cementite at the austenite-cementite interface, shall quickly travel to the existing graphite nuclei and get deposited on them, causing their growth. This seems probable because the diffusion rate of carbon near the eutectic temperature is very high.

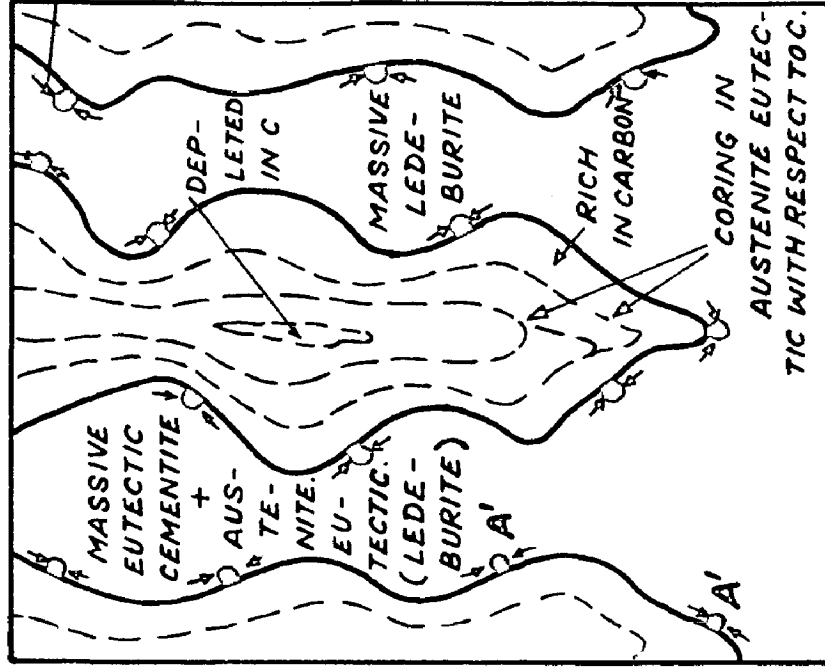
As the cooling progresses, the maximum amount of carbon soluble in austenite decreases along the AC_m - line. Carbon from the outermost layers of austenite will thus start diffusing inward, slowly equalising the carbon content of austenite. Still, austenite may be left inhomogeneous with respect to carbon content, due to usual rapid rates of cooling, since adequate time is not provided for homogenisation under these conditions. This goes to show that the outermost layers of austenite dendrite at any temperature shall be well saturated in C content,

(i) SLIGHTLY ABOVE THE EUTECTIC TEMPERATURE



PARTLY GROWN GRAPHITE NUCLEI FORMED AT AUSTENITE DENDRITE BOUNDARIES DURING FREEZING.

(ii) BETWEEN THE EUTECTIC TEMPERATURE AND $\sim 920^{\circ}\text{C}$



A'; OBTAINED FROM 'A' AFTER GROWTH DUE TO THE "PARTIAL DECOMPOSITION" OF MASSIVE EUTECTIC CEMENTITE.

FIG.-7-9. THE MECHANISM OF FORMATION AND GROWTH OF GRAPHITE PARTICLES IN MALLEABLE WHITE CAST IRON STRUCTURE.

while cooling, along the AC_m line. It is also obvious that the process of homogenisation of austenite dendrites shall also become sluggish with decreasing temperatures. Hence, any additional carbon atoms released by partial decomposition of eutectic cementite shall not be taken-up by already saturated outermost layers of austenite dendrite during the process of cooling. The easiest passage for these carbon atoms would, therefore, be to the graphite nuclei, already existing at the austenite dendrite boundaries. The partial decomposition of cementite would, thus, cause the growth of graphite nuclei, as the cast structure is cooling through the austenitic temperature range. It is obvious that the extent of cementite decomposition and resulting growth of graphite nuclei will be a function of temperature, the process becoming increasingly sluggish with decreasing temperatures till the cast structure approaches eutectoid temperature. Most of this process would have occurred in the temperature range of 1145°C to nearly 930°C . The proposed mechanism of this reaction is shown schematically in Fig. 7-9.

The ease, with which, the eutectic cementite would decompose in the temperature range of 1145°C to 900°C , either during freezing or during re-heating at these temperatures subsequent to freezing, will be a function of its thermodynamic stability. It is known that all the alloying elements partition to the cementite phase, to a lesser or greater extent, depending upon whether they are carbide

stabilisers or graphitisers^(28,51). Also, it is known that graphitisers make the eutectic cementite all the more unstable and conversely carbide stabilisers⁽⁸⁾ make the eutectic cementite more stable. It would, therefore, be expected that the presence of graphitisers or carbide stabilisers in the base melt, would considerably alter the cast white iron structure with respect to the number and size of graphite nodules present in it.

It is inferred from the above discussion that a cast white iron structure may have not only the graphite nuclei but also the graphite nodules of varying dimensions ranging from 0.5 to nearly $6/7 \mu$, depending on their cooling conditions. In general, therefore, it can be stated that graphite (nuclei or nodule) is an integral part of a cast white iron structure.

The mechanism, discussed above, explains the presence of tiny graphite nodules at cementite/Austenite interface in all the cast white iron structures, studied in this work. However, it may again be mentioned that the presence of these tiny graphite nodules in the cast structures can be detected only in unetched or lightly etched (0.5% Nital) condition, since they will be masked by the dark etching base matrix in case of 2.0% or 4.0% Nital etch. Accordingly such white iron compositions, which have total carbon and silicon very much on the lower side, or such cases in which very rapid rates were employed for white iron

freezing, shall possess mostly sub-microscopic particles of graphite along with some grown particles ($6/7 \mu$), which on fracture would reveal a normal white crystalline fracture free from any visible mottle spots, and on etching, would reveal a common white iron microstructure.

From these considerations, it would appear that the prevalent definition of mottled structures needs revision. In the light of the present postulate, only those structures may be considered mottled, which on freezing, would develop such large clusters of graphite, that would be easily visible to the naked eye or at $2/3 X$ on the fractured surface of the cast slug. Such graphite clusters would normally not be less than 100 to 200 μ in size, if they have to be visible at 2 or 3 X. Also, it is thought necessary that the dimensions of cast-slug be standardized for the purpose of studying the mottling behaviour of any composition, since several practices have been followed by different workers for the purpose, and hence it becomes hard to compare their data. Basically, the dimensions of the cast-slug, moulding material, the pouring temperature of the liquid melt and the stripping practice may be standardized and accepted on international basis.

The mechanism proposed in this work explains fully other phenomena too connected with the process of malleabilisation viz. the influence of pre-treatments on the number and size of nodules, formed in the treated cast

structure, varying incubation periods reported by different workers before the onset of graphitisation during FSG period, the influence of composition on the kinetics of FSG reaction etc. These have been discussed at appropriate places.

In conclusion, it may be stated that the presence of tiny graphite nodules of size less than 10 μ in the cast structure at cementite/austenite interface was not considered deleterious in the present work, since, in any case, such nodules were required to develop at cementite/austenite interface during the FSG reaction even according to the conventional concept of solid-state graphitisation. However, the presence of large irregular clusters of graphite in the cast structure, would be highly deleterious for final mechanical properties of the malleabilised product. Therefore, such a cast structure was considered completely unacceptable.

7.1.6 Conclusions:

1. Graphite is an integral part of the malleable white iron cast structures.
2. Formation of graphite nuclei is initiated during liquid to solid transformation. These nuclei grow further to different dimensions, depending upon the opportunity provided to them for growth.
3. Graphite nuclei may grow partly during freezing due to the coagulation of several nuclei together forming

tiny sized nodules. Smaller nodules may further diffuse into larger nodules, because of higher chemical potential of the larger ones causing the growth of these nodules progressively. The extent to which this phenomenon would progress, shall mainly depend upon the severity of cooling during freezing. Under extreme cases of severe cooling, only graphite nuclei may be present in the cast structure, since practically no growth would have taken place.

4. Graphite nuclei or tiny graphite nodules form at austenite dendrite boundaries. Therefore, these tiny nodules are present at austenite/cementite interfaces in a cast white iron structure.
5. On further cooling, just below the eutectic temperature (1145°C), cementite remains in a highly unstable state. Small amounts of graphitising elements partitioning to the eutectic cementite phase, greatly influence its thermodynamic stability. Eutectic cementite undergoes partial decomposition as it traverses from eutectic to the eutectoid temperature during continuous cooling. Carbon atoms released by the partial decomposition of cementite, cause the growth of existing graphite nodules. Cementite is known to be highly unstable, particularly in the vicinity of eutectic temperature. The extent of

growth of pre-existing graphite nodules due to this reaction, will be a function of the cooling rate and the composition of base-melt.

6. The presence of tiny graphite nodules at cementite/Austenite interface in the cast structure is not considered deleterious; rather such tiny nodules are an integral part of a cast malleable white iron structure.
7. Only those structures may be termed as "mottled" which develop very large irregular clusters of graphite of size not less than 100 to 200 μ (microns) so that these spots may be clearly visible to the naked eye or at 2 or 3 X.
8. Microhardness of eutectic cementite in thin and thick cast structures is not appreciably influenced by the presence of increasing amounts of silicon or copper in the base-melt.
9. No "incubation period" is required for the nucleation of graphite particles during pre-treatments and the first stage of graphitisation since graphite nodules of varying dimensions upto a maximum of 4/5 μ in size are already present in the cast structure. The present concept explains the results of some recent workers⁽²⁹⁾. The phenomenon occurring during pre-treatments and the FSG reaction are simply growth of already existing graphite nuclei in the cast

structure. During pretreatment, the smaller particles diffuse into the larger ones, due to the higher chemical potential of larger nodules. Decomposition of cementite will be highly sluggish during pre-treatment. Most of this process would have occurred during early stages of heating in case of normal FSG cycle. During the FSG reaction, growth will mainly occur because of the decomposition of eutectic cementite. In this context, the term "Incubation period" has, so far been loosely used.

7.2 PRE-TREATMENTS AND SHORTENING OF FSG PERIOD

7.2.1 Introduction

Pre-treatments outlined in section 6.3.1 and 6.3.3. (Table 6-2) were carried out in case of all the alloys listed in Table 6-1.

The study was carried out to determine the shortening influence of various pre-treatments on FSG cycle. Percentage shortening of FSG period obtained in case of individual pre-treatments, was later correlated with the amount of silicon or copper present in the cast alloy.

Results obtained have been summarised in Table 7-2 to 7-5 and plotted in Figures 7-10 to 7-16.

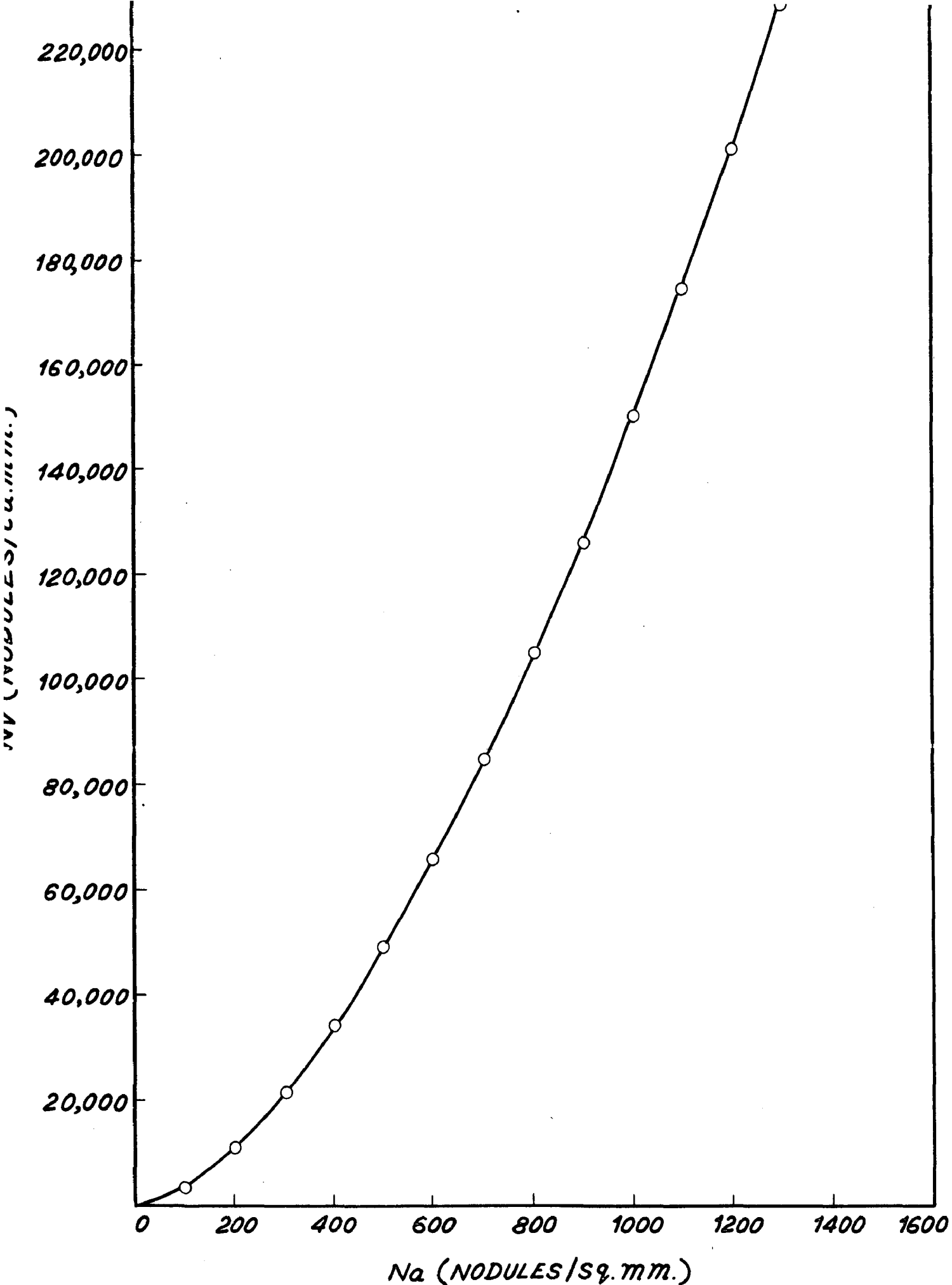


FIG.7-10.SCHWARTZ -SALTYKOV CORRELATION ($N_v = 2.38 \times N_a^{1.6}$) PLOT.

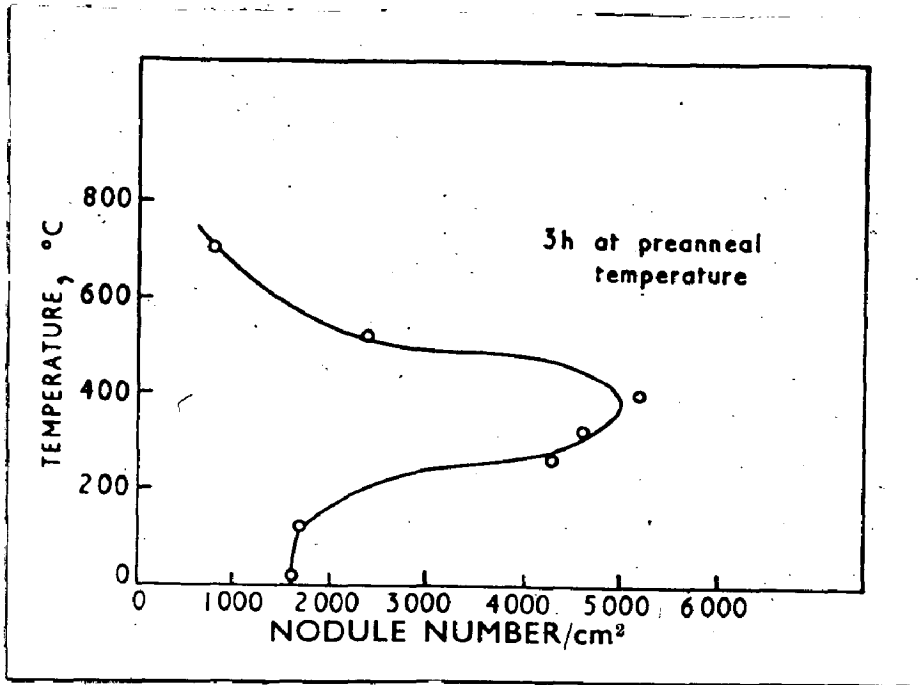


Fig. 7.10(a) (i)- Effect of subcritical heat-treatment on Nodule number. Walker and Kondic⁽¹²⁾.

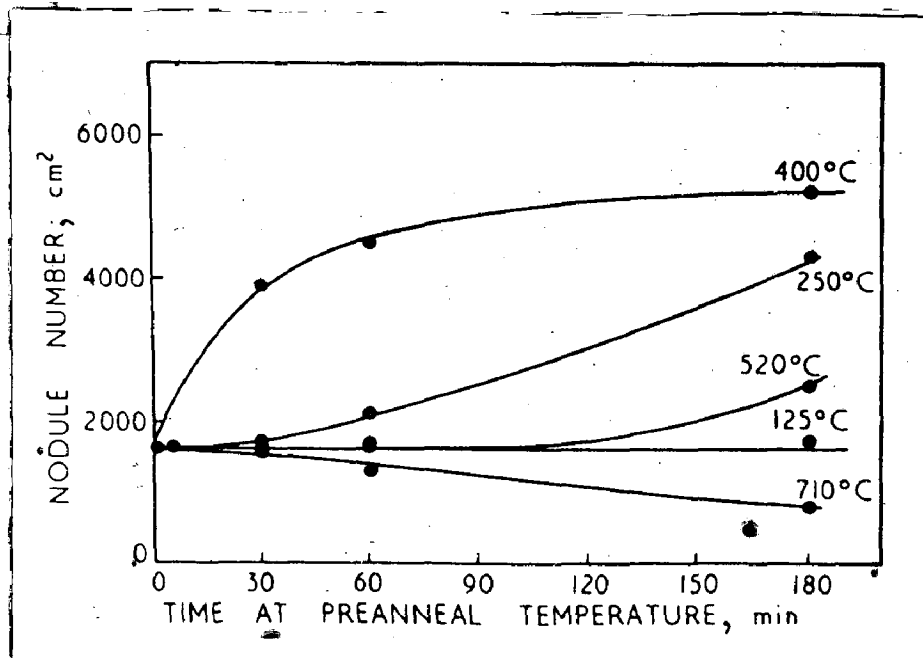


Fig. 7.10(a)(ii)- Effect of time and temperature of subcritical heat-treatment on Nodule number. Walker and Knodic⁽¹²⁾.

7.2.2 Results:

7.2.2.1 Influence of Pre-treatments on N_v and Average Size of Largest Nodules.

Schwartz-Saltykov correlation ($N_v = 2.38 \times N_a^{1.6}$), plotted in Fig. 7-10, was used for obtaining N_v values from N_a (Number of Nodules/mm²) observations. N_v values (Number of Nodules/mm³) and the average size of largest nodules were used as the basis of comparison for the evaluation of different pre-treatment methods.

It was reported earlier that large number of small nodules develop during pre-treatments, which subsequently help in shortening the FSG period, since inter-particle diffusion distances are reduced (4, 12, 33, 35, 44, 54, 166, 171). Keeping basic causes and mechanisms aside, the influence of pre-treatments on FSG kinetics may be usefully utilised in shortening the FSG cycle. But the quantitative data available in this regard is not plentiful. M.C. Mittal et al⁽⁵⁴⁾ have reported some data on this aspect using Indian raw-materials. Walker and Kondic⁽¹²⁾ in a similar study have shown that either a continuous slow rate of heating to malleabilisation temperature or a pre-anneal at 400°C gives rise to a marked increase in nodule-number as compared with a rapidly heated white iron. Some of their results are shown in Fig. 7-10 (a). They suggested that the formation of graphite nodules at sub-critical temperatures is similar to the precipitation of cementite from carbon

Table 7-2

EFFECT OF BAKING AND QUENCH-BAKING AT VARIOUS TEMPERATURES
FOR DURATIONS OF 1 AND 6 HRS. ON NV AND AVERAGE SIZE OF
LARGEST NODULES. ALLOY A-5

Sl. No.	Series	% Alloy	Treatment	Treatment temperature °C	Duration of treatment hrs.	Average Nv [†] (No. of nodules/mm ³)	Average size of largest nodules μ (microns)	Remarks
1.	A-5	Cu=2.10 Bi=0.02	B (Pre-baking)	400	1	20,000	8.6	[†] Nv measured at 1000 X. Neophot-2 projection Microscope used for the measurements
				500	6	24,000	12.5	
				650	1	22,000	10.0	
					6	21,000	17.5	
					1	35,000	11.2	
					6	21,000	16.0	
					1	30,000	10.5	
					6	21,000	14.0	
			QB (Quench-baking)	400	1	26,000	19.4	
				500	6	24,000	27.2	
					1	28,000	28.4	
					6	19,000	31.6	
				600	1	45,000	15.0	
					6	21,000	24.6	
				650	1	25,000	25.9	
					6	22,000	28.7	

Table 7-3

OPTIMUM NV AND AVERAGE SIZE OF LARGEST NODULES IN CASE OF DIFFERENT ALLOYS, AS INFLUENCED BY PRE-BAKING AND QUENCH-BAKING TREATMENT

Sl. No.	Series	Alloying Elements Wt%	Treatment	Temperature of treatments °C	Duration of treatment hrs.	Nv* average (No. of nodules/mm ³)	Average size of largest nodules μ (microns)	Remarks
1	2	3	4	5	6	7	8	9
1.	0-8	Si-0.89	QB	650	1	21,000	23.0	QB-Quench-baking B-Pre-baking. * NV values measured at 1000X. Neophot-2 projection microscope used for the measurements.
			QB	650	6	49,000	23.0	
			B	650	1	37,000	10.8	
			B	650	6	34,000	12.0	
2.	0-11	Si-0.94	B	650	1	35,000	8.4	
			B	650	6	35,000	12.0	
			QB	650	1	21,000	20.6	
			QB	650	6	11,000	33.0	
3.	0-9	Si-1.23	QB	650	1	16,000	30.6	
			QB	650	6	21,000	35.0	
			B	650	1	39,000	12.0	
			B	650	6	26,000	22.3	
4.	0-10	Si-1.40	B	650	1	60,000	14.1	
			B	650	6	85,000	15.5	
			QB	400	1	30,000	37.0	
			QB	400	6	105,000	37.0	

Table contd/-

Table 7-3 (continued)

1	2	3	4	5	6	7	8	9
5.	A-2	Cu-0.70	B	650	1	126,000	7.25	QB- Quench-baking
			B	650	6	105,000	12.5	B - Pre-baking
			QB	600	1	105,000	8.7	
6.	A-1	Cu-1.12	B	650	1	126,000	12.5	★ NV-values measured
			B	650	6	163,000	8.4	at 1000X. Neophot-
			QB	600	1	31,000	20.0	2 projection
			QB	600	6	35,000	19.3	microscope used
								for the
								measurement.
7.	A-3	Cu-1.25	B	650	1	105,000	7.7	
			B	650	6	16,000	15.5	
8.	A-4	Cu-1.95	B	650	1	35,000	15.5	
			B	650	6	21,000	12.5	
9.	A-5	Cu-2.10	B	650	1	35,000	11.2	
		Bi-0.02	B	650	6	21,000	16.0	
			QB	600	1	45,000	15.0	
			QB	600	6	21,000	24.6	
10.	B-1	Si-1.63	B	650	1	35,000	7.3	
		Bi-0.02	B	650	6	66,000	14.8	
			QB	600	1	21,000	25.0	
			QB	600	6	11,000	28.0	

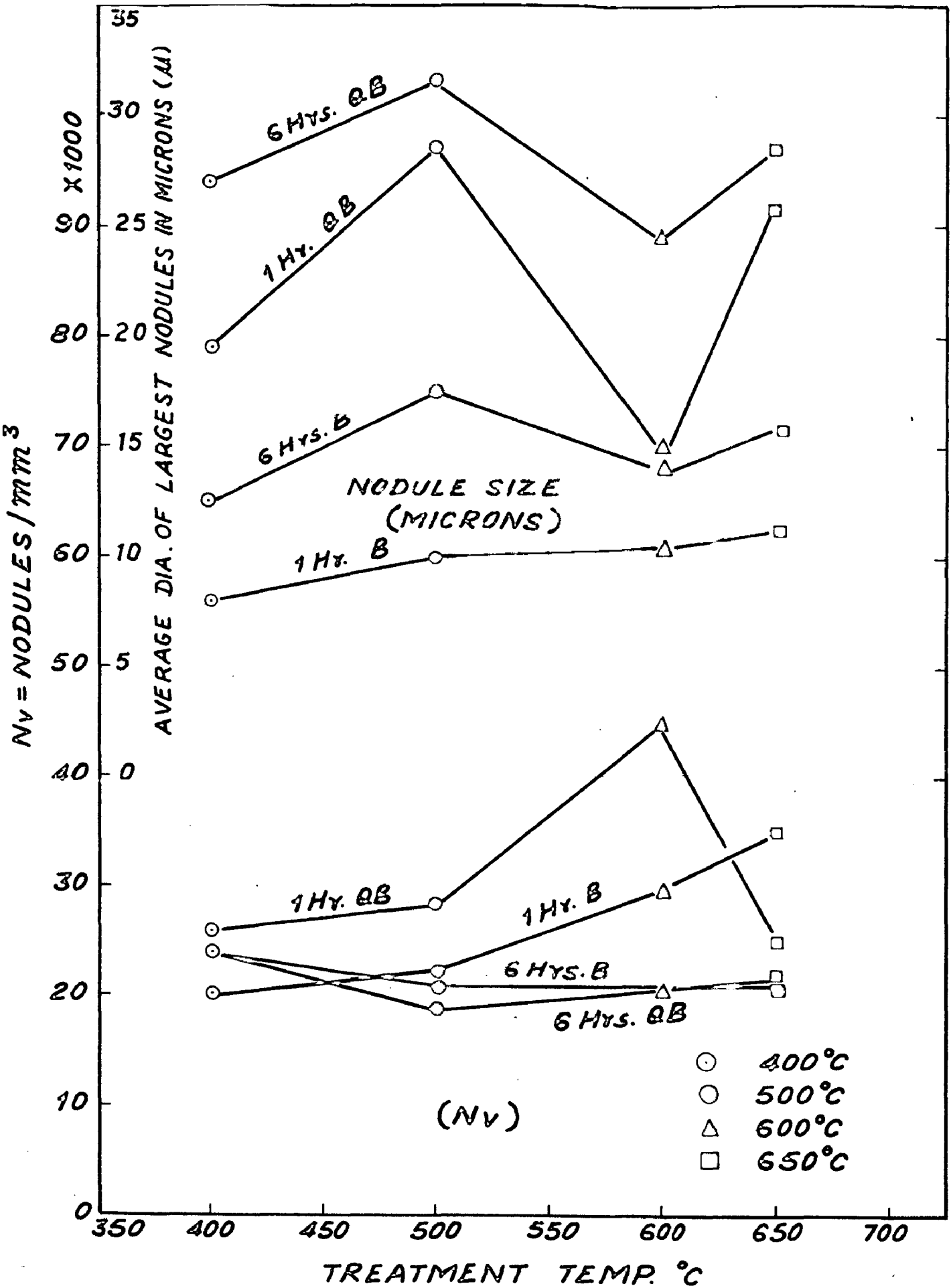


FIG. 7-11. INFLUENCE OF PRE-TREATMENT AT SUB CRITICAL TEMPERATURES ON N_v AND THE SIZE OF LARGEST NODULES DEVELOPED IN CASE OF A-5 ALLOY.

SERIES	Cu%	TREATMENT			
		BAKING		Q. BAKING	
		°C	HRS.	°C	HRS.
A-2	0.7	650	1	600	1
A-1	1.125	650	1	600	1
A-3	1.25	650	1	-	-
A-4	1.95	650	1	-	-
A-5	2.10 + .02 Bi	650	1	600	1

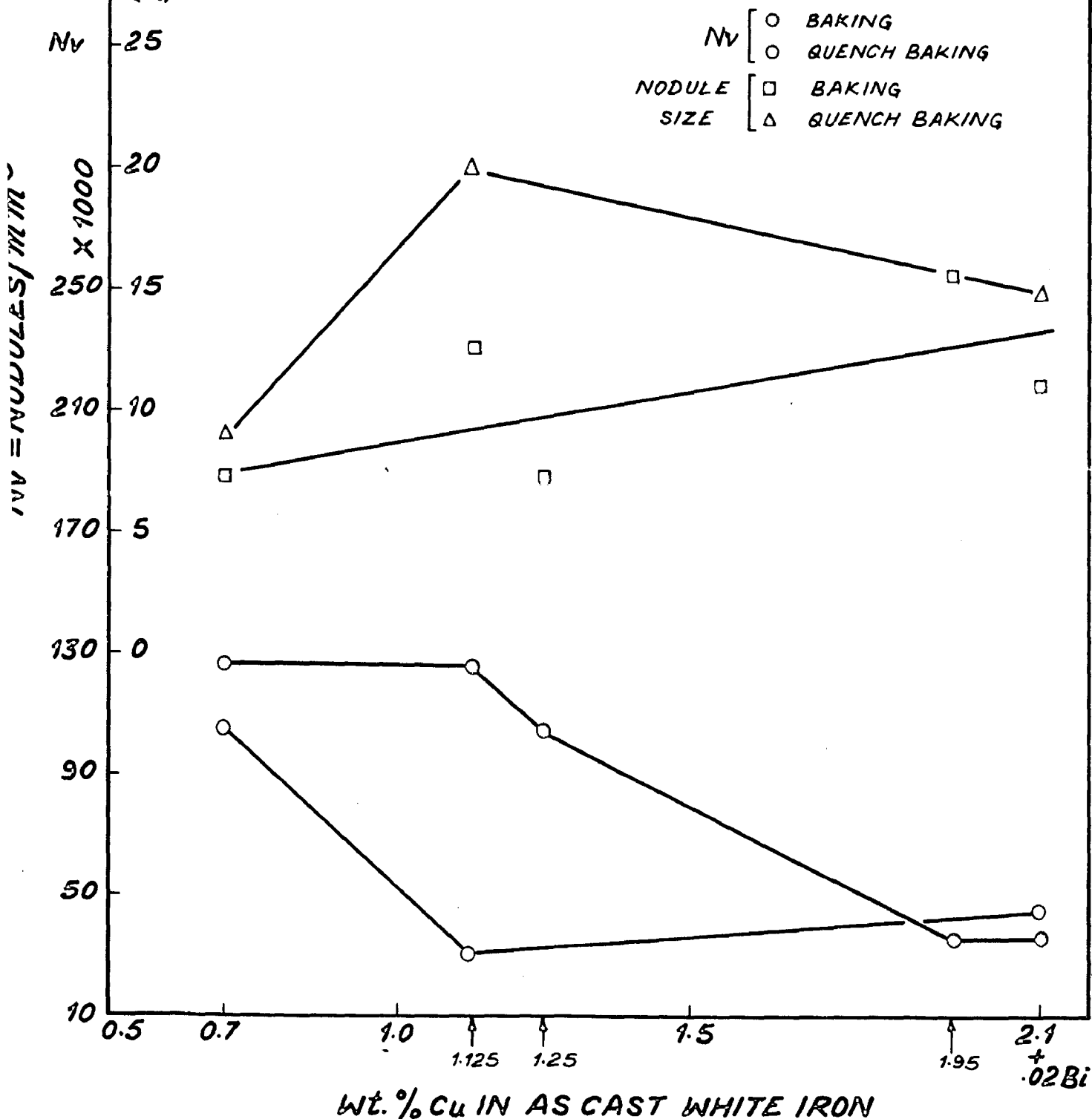


FIG. 7-12 INFLUENCE OF Cu CONTENTS OF AS-CAST WHITE IRONS ON N_v AND SIZE OF LARGEST NODULES DEVELOPED DURING VARIOUS PRE-TREATMENTS.

SERIES	% Si	TREATMENT			
		BAKING		Q. BAKING	
		°C	HRS.	°C	HRS.
O-8	.8873	650	6	650	3
O-11	.943	650	1	650	1
O-9	1.231	650	1	650	1
O-10	1.401	650	1	400	1
B-1	1.631	650	1	600	1
	.02Bi				

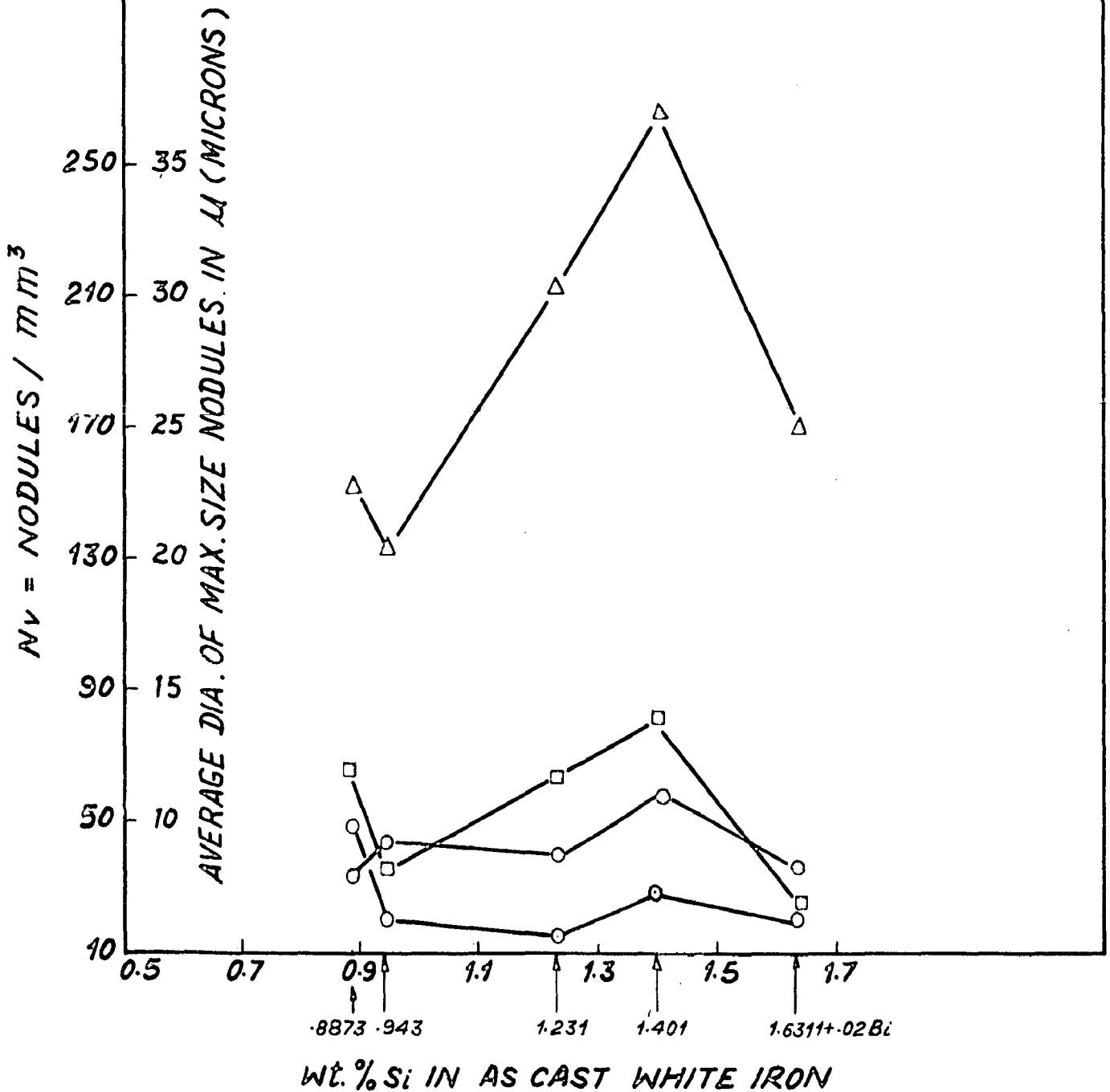


FIG. 7-15 INFLUENCE OF Si CONTENT OF AS-CAST WHITE IRONS ON N_v AND SIZE OF LARGEST NODULES DEVELOPED DURING VARIOUS PRE-TREATMENTS

supersaturated ferrite in case of low C steels. Formation of " pores" , as the graphite produced during pre-annealing dissolves, has been suggested as the possible mechanism by these workers, through which, nucleating sites are created for subsequent graphitisation at higher temperatures. But the influence of these pre-treatments and increased number of nodules on FSG period, was not determined by these workers.

Results obtained in the present investigation have been summarised in Tables 7-2 and 7-3 and plotted in Figs. 7-11, 7-12 and 7-15.

Results obtained in case of A-5 alloy have been summarised in Table 7-2 and plotted in Fig. 7-11. It can be seen from Fig. 7-11, that the maximum number of nodules developed in this alloy at 650°C after 1 hr. of pre-baking, though the average size of largest nodules was found to be only 11.2 μ in dia. The number of nodules decreased at the same temperature of pre-baking with six hours of exposure periods, though the average diameter of largest nodules increased in size. Temperature of pre-treatment corresponding to the largest number of nodules i.e. 650°C and one hour duration in the present case, was considered most suitable for pre-baking. Similarly, it can be seen from Fig. 7-11 that 600°C and one hour treatment duration is most suitable for Quench-baking treatment. In case of quench baking treatment, it may be noted from Fig. 7-11 that the greatest number of nodules/mm³ present in the base-matrix

correspond to the smallest average size of largest nodules.

As stated earlier in section 6.3.1, the criterion for selection of optimum temperature was that the maximum number of nodules/mm³ should correspond to this temperature. Normally, the duration of treatment at any temperature was kept only one hour in practice, since otherwise, if this duration was longer, the total FSG cycle would get unduly prolonged. But in certain cases, e.g. 0-8 alloy, longer periods at highest selected temperature (650°C) had to be used, since no appreciable effect was observed at shorter intervals and at lower temperatures, particularly during pre-baking. However, in most other cases, so far as possible, longer durations of pre-treatments were avoided; rather higher temperatures and shorter durations were preferred.

The procedure that was adopted in case of A-5 alloy for selecting optimum pre-treatment temperature and duration for example was followed in case of other alloys too. Results obtained in case of other alloys are summarised in Table 7-3. These optimum values were later used for FSG studies involving pre-treatments, in an effort to study the percentage shortening of FSG period caused by such pre-treatments.

Figure 7-12 and 7-15 show the relationship between optimum Nv values obtained due to either pre-baking or quench-baking and the alloy content of base composition.

These graphs also show the relationship between the average diameter of largest nodules corresponding to optimum Nv values and the alloy content of base-melt.

It can be seen from Fig. 7-12 that the largest number of nodules ($126000/\text{mm}^3$) developed between 0.7 and 1.125 wt % Cu content during pre-baking, after which the number of nodules declined, as the copper content of base-melt increased upto 2.0 wt % . At the same time, it can be noted that the average diameter of largest nodules continues to increase moderately over the entire range of copper contents investigated. Least number of nodules were found at 1.125 wt % copper content during quench-baking, while the average diameter of largest nodules corresponding to this Nv number ($31000/\text{mm}^3$) was found to be the largest in size (20 μ). Best results were, therefore, found to exist between 0.7 and 1.125 wt% copper content of the base alloys.

Similarly Fig. 7-15 shows that best results were obtained at ~ 1.4 wt % Si with respect to the largest number of nodules obtained/ mm^3 . It can be seen that about 60000 nodules/ mm^3 developed at 1.4 wt % Si, while the corresponding average size of largest nodules was found to be nearly 14 microns. As expected, the average size of largest nodules in case of quench-baking treatment was found to increase sharply as the silicon content of base alloy increased from 0.95 to 1.4 wt % . Average size of the largest nodules, found in this case, was 37 μ

(microns), which is nearly 2.5 times the size of largest nodules found in case of pre-baking. At the same time, the value of Nv in case of 1.4 wt%. (Quench-baking case) silicon dropped to only 30,000, which is only 50% of the Nv value, obtained in case of pre-baking. It may further be noted that both Nv and the average size of largest nodules, found in case of pre-baking and quench-baking of 1.63 wt% silicon white iron inoculated with 0.02 wt% bismuth, dropped considerably, compared to the values obtained in case of 1.4 wt % Si white iron.

7.2.2.2 FSG Period Shortening Due to Various Pre-treatments.

Percentage shortening obtained in FSG period, due to various pre-treatments in case of different alloys, has been summarised in Table 7.4.

This data reveals that maximum shortening of FSG period was caused due to quench-baking treatment in all the alloys. 'Pre-baking' was found to be nearly as effective as the 'slow rate of heating upto 850°C' in cutting down the FSG periods.

It may be noted that Bi inoculation even at 1.63 wt% Si level or at 2.10 wt % Cu level, causes a sharp drop in the extent of percentage FSG shortening obtained due to various pre-treatments.

Values found only in case of pre-baking and slow rate of heating upto 850°C are of practical significance

Table 7-4

PERCENTAGE SHORTENING IN FSG PERIODS OBTAINED
IN CASE OF DIFFERENT ALLOYS DUE TO VARIOUS PRE-TREATMENT

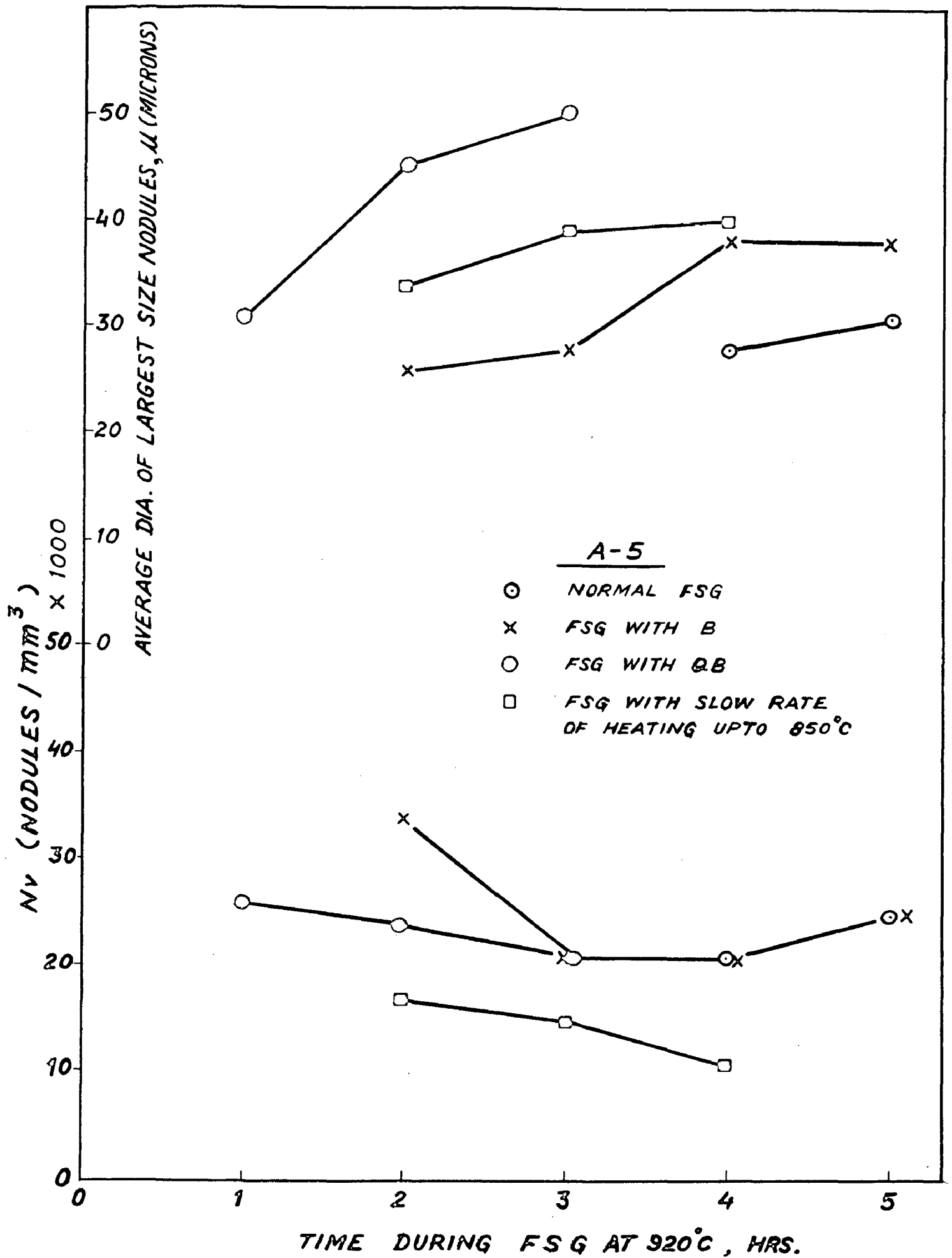
Series	Alloying element Wt. %	FSG period (thin section)		FSG period (thick) section		FSG period with pre-baking		FSG period with quench-baking		FSG period with slow heating upto 850°C		% shortening in FSG period (thin section)		slow rate of heating upto 850°C
		hrs.	hrs.	hrs.	hrs.	hrs.	hrs.	hrs.	hrs.	B	QB			
0-8	Si-0.89	17-18	22	13	12	14	28	33	22					
0-11	Si-0.95	12	18	8	5	8	53	58	33					
0-9	Si-1.23	7½-8	13	4	3	4½	46	62	43					
0-10	Si-1.40	6½-7	12	3	1½	1½	57	77	50					
B-1	Si-1.63 Bi-0.02	7	10	6	5	6	14	28	14					
A-2	Cu-0.70	10	13	9	6	9	10	40	10					
A-1	Cu-1.13	9	13	6	3½	5	33	61	44					
A-3	Cu-1.25	3½	7	1	¾	1	71	79	71					
A-4	Cu-1.95	3½	7	2	1	2	43	71	43					
A-5	Cu-2.10 Bi-0.02	5	7½	4	2	4	20	60	20					

Note:- Detailed composition shown in Table-6-1.

Table 7-5

FSG WITH PRE-TREATMENT, NV AND AVERAGE SIZE OF LARGEST NODULES DEVELOPED AFTER DIFFERENT HOLDING PERIODS AT 920°C (REACTION TEMPERATURE) IN CASE OF A-5 ALLOY.

Alloy series	Composition, wt %	Treatment	Holding period hrs. at 920°C	FSG period hrs.	Average Nv ⁺ (No. of nodules/mm ²)	Average size of largest nodules in μ (Microns)	Remarks
A-5	Cu=2.10	Normal FSG at 920°C ± 3°C	4	5	21,000	28	+Nv values measured at 1000 X with the help of Neophot-2 projection-microscope. FSG temperature in all cases = 920°C ± 3°C.
	Bi=0.02		5		25,000	31	
	(A-5)	FSG with B, (650°C. 1 hr.)	2	4	34,000	26	
			3		21,000	28	
			4		21,000	38	
			5		25,000	38	
		FSG with QB (600°C 1 hr.)	1	2	26,000	31	B = Pre-baking QB = Quench-baking
			2		24,000	45	
			3		21,000	50	
			4		17,000	34	
		FSG with slow rate of heating upto 850°C.	3		15,000	39	
			4		11,000	40	



TIME DURING FSG AT 920°C, HRS.

FIG. 7-14 EFFECT OF REACTION TIME AT 920°C ON N_v AND LARGEST SIZE NODULES IN NORMAL AND PRE-TREATED CASES (A-5 COMPOSITION)

since actual castings are likely to develop quench-cracks during quench-baking treatment.

Data pertaining to A-5 alloy, recorded in Table 7-5 and plotted in Fig. 7-14, shows the influence of pre-treatments on the value of N_v and the average size of largest nodules developed in the specimens, during different holding periods at FSG temperature ($920 \pm 3^\circ\text{C}$). It can be seen from this data that largest number of nodules develop in case of FSG with pre-baking treatment. Also, the nodules of largest average diameter develop during FSG with quench-baking treatment. It may further be noted from Fig. 7-14 that the growth curves of graphite nodules corresponding to different pre-treatments shift to the left on x-axis, as the FSG period is progressively shortened by these pre-treatments.

Data pertaining to A-5 alloy (Table 7-5 and Fig. 7-14) show as a typical example, the mechanism through which various pre-treatments cause the shortening of FSG period.

7.2.2.3 Influence of Graphitisers on the Effectiveness of Pre-treatments

Data recorded in Table 7-4 has been plotted in Figs. 7-13 and 7-16 to show the correlation between the percentage shortening in FSG period obtained due to various pre-treatments and the amount of graphitisers present in the base melt.

Figure 7-13 shows that optimum results, with respect

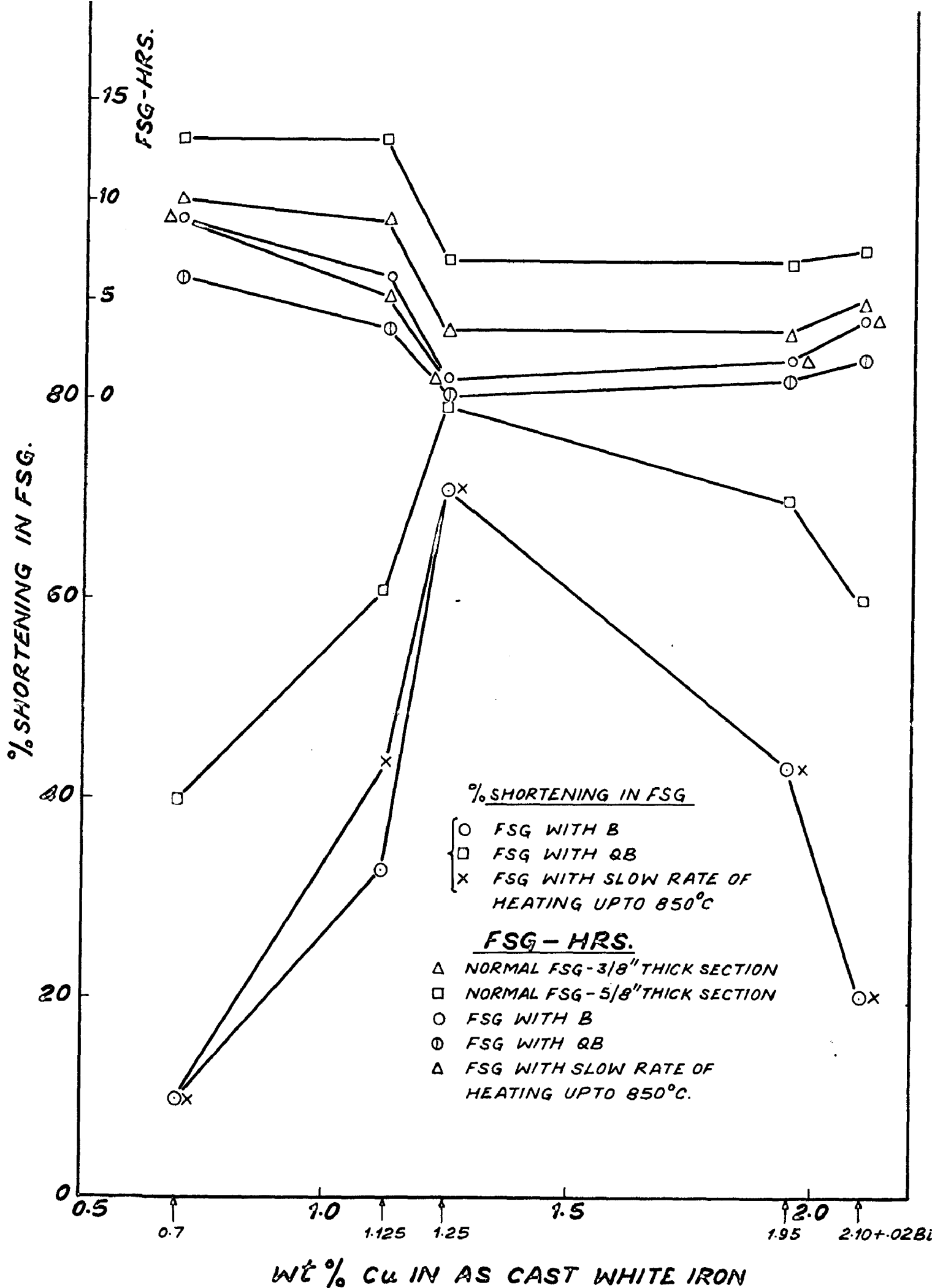


FIG. 7-13 INFLUENCE OF CU CONTENT ON % FSG SHORTENING AND FSG PERIODS OF WHITE IRONS IN CASE OF VARIOUS PRE-

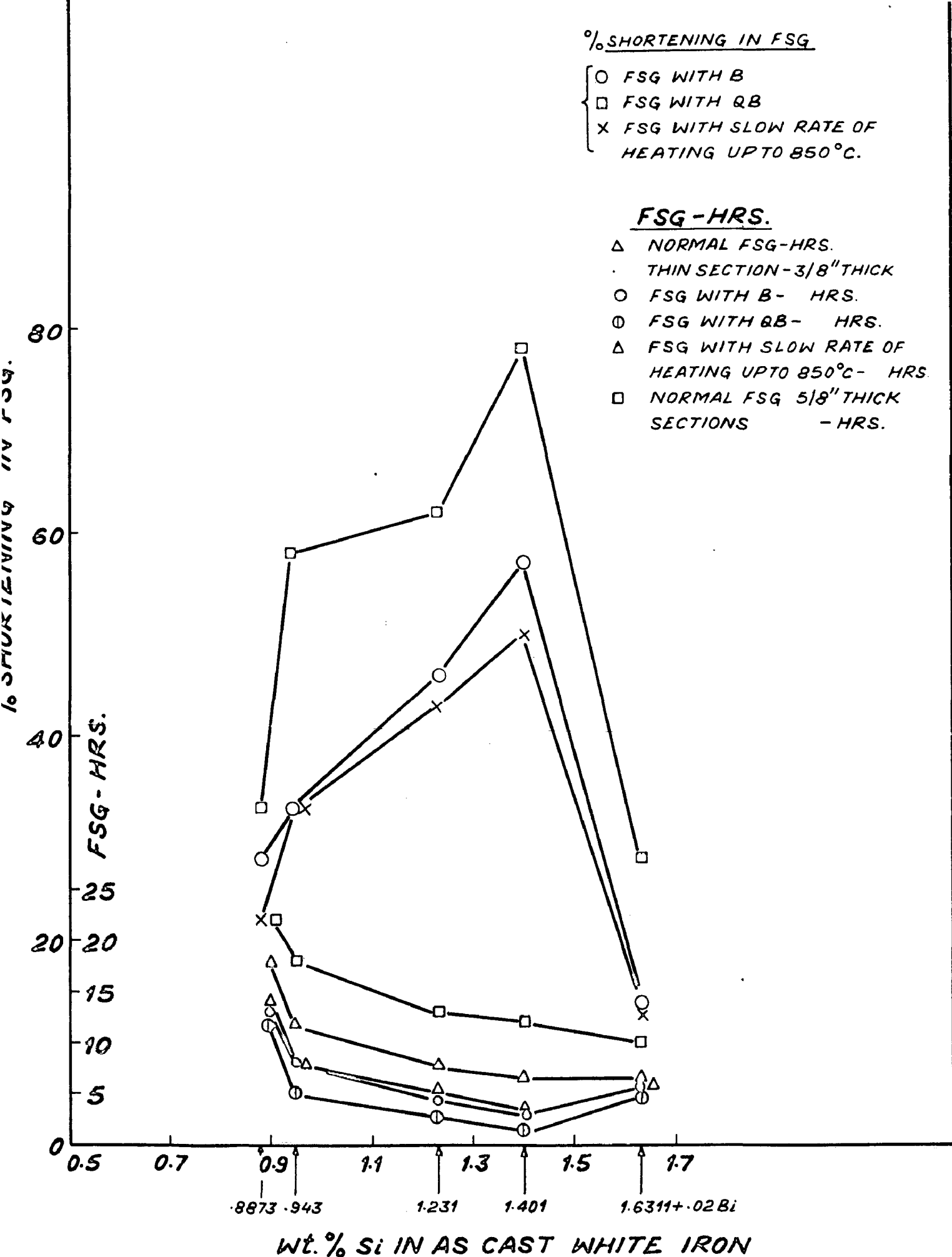


FIG. 7-16. INFLUENCE OF Si CONTENT ON % FSG SHORTENING AND FSG PERIOD OF WHITE IRONS IN CASE OF VARIOUS PRE-TREATMENTS.

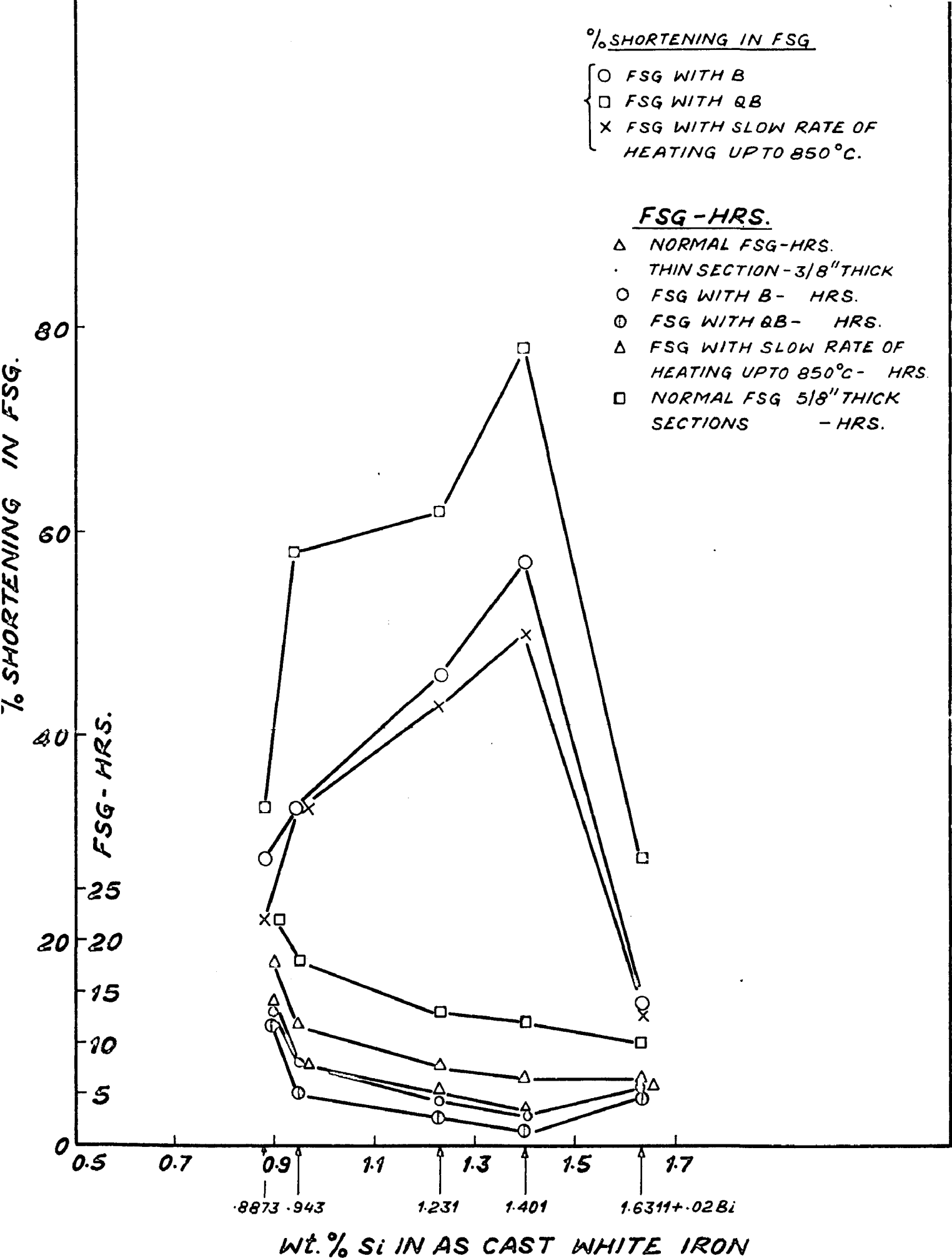


FIG. 7-16. INFLUENCE OF Si CONTENT ON % FSG SHORTENING AND FSG PERIOD OF WHITE IRONS IN CASE OF VARIOUS PRE-TREATMENTS.

to percentage shortening obtained in FSG period due to various pre-treatments, were found at 1.25 wt% copper content of the cast white iron. This indicates that copper contents higher than 1.25 wt% Cu offer no special advantage in this regard. Also, it can be noted from Fig. 7-13 that slow rate of heating upto 850°C is nearly as effective as pre-baking in shortening the FSG period. And the results obtained in case of pre-baking may be considered encouraging, since the percentage FSG shortening found in this case (71%) is quite close to the one obtained in case of quench-baking treatment (79%). It is, thus, inferred from these observations that optimum results in this regard are obtained at 1.25 wt % Cu content of the base alloy.

Figure 7-16 shows that the extent of FSG shortening obtained due to any pre-treatment is a function of the Si content of cast alloy. It can be seen from Fig. 7-16 that the best results were obtained in case of 1.4 wt % Si in the cast alloy. These characteristics deteriorate sharply due to Bismuth inoculation (0.02 wt%) even at 1.63 wt % Si level in the base alloy. Slow rate of heating upto 850°C prior to FSG cycle, was found to be nearly as effective as pre-baking treatment in cutting down the FSG period. Percentage shortening in FSG period ($\sim 57\%$), obtained due to pre-baking at 1.4 wt% Si content of cast alloy, may be considered encouraging for industrial malleabilising cycles. Data presented in Fig. 7-16 shows that

graphitiser influence strongly the effectiveness of pre-treatments.

7.2.3 Discussion of Results:

It was concluded in previous section 7.1, that a large number of tiny graphite particles are already present in the cast structure. It was also shown in Fig. 7-6(c) that single units of grown nuclei have a tendency to diffuse into the larger particles, causing them to grow further. The extent of growth of these larger particles depends upon the opportunity provided for this diffusion phenomenon to occur. Also, this tendency of smaller graphite particles diffusing into the larger ones shall always exist because of higher chemical potential of the larger nodules.

At the same time, the decomposition of eutectic cementite at sub-critical temperatures (usual temperature of pre-treatment) is known to be highly sluggish^(8,33), although it is metastable even at room temperature⁽²⁰⁵⁾. Therefore, the suggestion⁽¹²⁾ that graphite nuclei are formed during sub-critical annealing appears to be less probable. Also, the observation, that the maximum effect occurs at about 400°C during sub-critical annealing since it corresponds approximately with the nose of the C-curve for sub-critical graphitisation of steel^(12,33) is not in line with the present observation.

Results of the present work show that maximum number of nodules developed in the temperature range of 600° to 650°C (Table 7-3). Also, it was found that the maximum number of nodules formed during sub-critical annealing, correspond to a certain Cu percentage in the base-melt (Fig.7-12) or to a specific Si content of the cast-alloy (Fig.7-15).

Pre-baking was found to be more effective in developing the largest number of nodules during sub-critical annealing at all Cu and Si levels of the cast alloy compared to quench baking treatment, while the reverse was true for the average size of largest nodules developed during these pre-treatments. Also, bismuth inoculation, even at highest silicon and copper contents of the cast alloy, was found to render these pre-treatments considerably less effective.

The hypothesis put forward in this work (formation of sub-microscopic graphite particles at austenite dendrite boundaries during freezing and their limited growth due to partial decomposition of massive eutectic cementite in the temperature range of 1140° to nearly 920°C on further cooling) explains the results of present investigation.

It was shown in Fig.7-6 that a large number of tiny graphite particles are present even in a chilled white iron, indicating that the nucleation of graphite might have taken place above the eutectic temperature. Some of these nuclei are able to grow and coagulate together on further cooling, forming larger microscopic particles. The cast structure, therefore, contains not only a large

number of sub-microscopic graphite particles, but also a considerable number of already grown particles.

Thermal energy supplied during pre-baking activates the process of diffusion and coagulation of sub-microscopic graphite nuclei, forming comparatively larger particles. Simultaneously, already grown graphite particles shall grow to still larger sizes by the same mechanism at sub-critical temperatures. The period during which, several graphite nuclei coagulate together to form particles of microscopic size, may be termed, for convenience, the " Incubation period". Though in strict sence, as discussed in section 7.1.5, even this period can not be termed as " Incubation period", since the nucleation of graphite had already taken place, and all that happens during the so called " Incubation period" is only growth of these nuclei through mutual coagulation. The growth of these tiny graphite nuclei, first continues at sub-microscopic level and then is carried forward at microscopic levels too. Thus, the period during which sub-microscopic growth of graphite nuclei continues, may be termed as the " Incubation period".

According to this postulate, the cast white iron will be expected to possess a large number of graphite particles in partially grown condition with respect to both sub-microscopic as well as microscopic levels.

On pre-baking, both sub-microscopic as well as microscopic graphite particles shall continue to grow into comparatively larger particles. Thus, a large number of new

graphite particles would appear on pre-baking, since sub-microscopic particles would have grown to the microscopic sizes, and therefore, they can be visible at 1000 X. Higher magnifications like 1000 X to 1800 X should be preferred for Nv measurements, since as already pointed out by Bhide and Banerjee⁽²⁹⁾, numerous tiny nodules are not visible at lower magnification like 150 X, and therefore, erroneous data was reported by several previous workers in this regard, since they employed lower magnification (150 or 200 X) for such studies.

From the view point of microscopic levels; therefore, it can be stated that the process of nucleation and growth continues during the entire process of pre-baking. Obviously, as more number of tiny particles coagulate together to form larger particles, a stage would come, when growth and not the nucleation, would become the dominating phenomenon. Again, this phenomenon of nucleation and growth will be a function of the temperature of pre-treatment, holding period at the temperature, the percentage of graphitisers present in the cast alloy, and the number of nuclei present in the cast structure . Fig. 7-11, for example, shows that the number of nodules continue to increase in case of pre-baking for one hour holding period upto 600°C, after which the value of Nv drops sharply at 650°C, while the average size of largest nodules continues to increase steadily upto 650°C. For six hours of holding period, however, Nv

does not increase at any temperature of pre-treatment, since the process of nucleation is counter-balanced by growth because of the large holding period provided at individual temperatures.

The strong influence of silicon on nucleation of graphite particles (Nv values) appears to be acting through its influence on iron-graphite and iron-cementite eutectic temperatures, as suggested by Ashton⁽²⁰⁴⁾ and also through its influence on the stability of eutectic cementite as suggested by Sandoz⁽⁵¹⁾. The net effect, however, is that much larger number of tiny graphite particles nucleate in the cast structure as the Si content is progressively increased in the base-alloy. This results into the largest number of graphite nodules associated with the highest silicon content in the base-alloy (Fig.7-15). Moreover, the presence of largest number of nodules corresponding to nearly 1.4 wt % Si in the present work, caused greatest shortening in FSG period (Fig.7-16) in all the cases of pre-treatments, since diffusion distances for carbon atoms are reduced due to closer spacing of graphite nodules. Another factor of prime importance, that causes the shortening of FSG period, is the influence of Si content on the stability of eutectic cementite. Greater is the silicon content of base melt, greater will be the instability of eutectic cementite in the temperature range of 1140° and 920°C, and therefore, greater will be the extent of "partial decomposition of cementite" which will

ultimately result into much larger number of graphite particles at cementite/austenite interfaces. The cast structure would thus contain a large number of graphite particles at cementite/austenite interfaces. And the size of these particles may vary from sub-microscopic to microscopic dimensions.

The influence of Cu content of the base alloy, on Nv values obtained during pre-baking and quench-baking, appears to be limited (Fig.7-12). The optimum effect was found at ~ 1.13 wt % copper in this regard. Also, the maximum percentage shortening in FSG period, obtained due to various pre-treatments, was found to exist at nearly the same Cu content of base-alloy (Fig.7-13). This was presumably so, because copper is known to be a mild graphitizer compared to Silicon^(28,51,73). Simultaneously, it is known that the maximum solubility of copper in iron is nearly 9.5 wt % at 1096°C, which decreases to a maximum of nearly 2.6 wt % at 815°C (Fig.5-1). Dissolution of copper in γ iron (both of f.c.c. structure), shall cause the precipitation of excess carbon atoms from γ iron at the boundaries of austenite dendrites. This argument is in line with the fact that graphitisers like copper increase the activity of carbon. This probably, could be the mechanism, through which, copper addition upto a certain extent causes an increase in Nv values.

Slow rate of heating upto 850°C over a period of 5,6

and 7 hours respectively was found to be nearly as effective as pre-baking in shortening the FSG cycle. Average rate of heating during these cycles respectively would be 164°C/hr. , 157°C/hr. and 117°C/hr. approximately. That would mean that the approximate period of retention of the specimen in the temperature range of 400° to 650°C , corresponding to these heating rates respectively would be nearly 1.5 hrs. 1.6 hrs. and 2.15 hrs.. These durations with progressively increasing temperatures will cause considerable nucleation and growth of graphite particles in the base-matrix. Increased number of relatively grown graphite nodules must have caused faster graphitisation during FSG reaction, which would naturally result in a shorter FSG period. On the whole, therefore, pre-baking works out to be a shorter pre-treatment cycle compared to the slow rate of heating upto 850°C .

7.2.4 Conclusions:

1. Sub-microscopic graphite particles (partially grown graphite nuclei) coalesce together to form microscopic size particles on getting thermally activated. Duration required for their growth into the microscopic sizes may be termed as "incubation period" in the microscopic sense. This appears to be the mechanism through which a large number of microscopic graphite particles from in the pre-treated specimens at sub-critical

temperatures, meaning clearly that both sub-microscopic as well as microscopic size graphite particles already exist in the cast structure.

2. Graphitisers cause a considerable increase in the number of graphite particles in the pre-treated specimens. This effect of graphitisers may be due to (i) their action on the eutectic temperatures of Fe-Fe₃C and Fe-graphite eutectics and (ii) their effect on the carbide stability, thereby influencing the extent of partial decomposition of eutectic carbide in the temperature range of 1140°C to nearly 920°C.
3. In every case, particular time-temperature combination can be found, at which, the net balance of nucleation and growth phenomenon is such, that a maximum number of nodules/mm³ are present in the pre-treated specimen. This combination can be incorporated in FSG cycle with either pre-baking or quench-baking, as the case may be.
4. Generally, maximum number of nodules were obtained in case of pre-baking in the temperature range of 600-650°C compared to quench-baking, though the size of nodules was found to be smaller in case of pre-baking compared to quench-baking.
5. In case of the alloys under study, maximum number of nodules were found at 1.4 wt% Si (unalloyed series) during pre-baking as well as quench-baking, while

this maxima was found between 0.7 and 1.12 wt % copper contents in copper alloyed series during these pre-treatments. Present observations show that copper is instrumental in increasing the number of nodules during pre-treatments only upto an addition of ~1.2 wt % Cu. Higher copper contents give no additional advantage.

6. Maximum shortening of FSG period obtained due to any of these pre-treatments, was found to correspond to ~1.4 wt % Si contents (unalloyed series) and to ~1.2 wt % Cu contents (alloyed series).
7. Quench-baking was found to be most effective in shortening the FSG period, followed by pre-baking and slow rate of heating upto 850°C in this regard. Slow rate of heating upto 850°C was found to be nearly as effective as pre-baking in shortening the FSG cycle. Maximum shortening in FSG period due to pre-baking was, found to be nearly 57% in case of unalloyed series, while it was found to be nearly 70% in case of copper alloyed series. The values quoted above are applicable only for thin sections (10 mm. thickness). Results obtained in case of pre-baking treatments can be of interest to industrial malleabilising cycles. Quench-baking treatment is not considered suitable for practical purposes.

7.3 PARTITIONING OF COPPER IN DIFFERENT PHASES:

7.3.1 Introduction:

Sandoz⁽⁵¹⁾ found that most of the alloying elements, present in white iron, partitioned themselves between eutectic cementite and the base-matrix to different extents, depending on whether the concerned alloying element was a carbide stabiliser or a graphitiser. This partitioning behaviour of different alloying elements was found to influence the decomposition characteristics of cementite, affecting ultimately the kinetics of white iron graphitisation⁽²⁸⁾.

Partitioning studies with respect to copper were undertaken in the present work in order to find a plausible explanation of the typical graphitisation characteristics of copper alloyed malleable irons, found in the present studies. These graphitisation characteristics have been discussed in the previous section 7.2.

7.3.2 Results:

7.3.2.1 Electron-Probe Partition Data:

Results of partition data are summarised in Table 7-7. Appendix shows the method of calculation adopted in the present work for determining K_i values from known C_i values.

K_i = Mass concentration of copper found by probe-Analyser.

C_i = Mass concentration of copper in the sample.

Table: 7-6

Calculated K_i values from known C_i values in case of hypothetical white-iron compositions- alloyed with copper

C_i	K_i	Error	% Error
Mass concentration of copper in the sample.	Mass concentration of copper found by the Probe Analyser	$\pm(K_i - C_i)$	\pm
0.005	0.00425	-0.00075	-15.0
0.010	0.0084933	-0.0015067	-15.067
0.02	0.01705	-0.00295	-14.75
0.03	0.02562	-0.00438	-14.60

Table: 7-7

Electron-Probe Micro-Analysis Data

Series	Treatment	Cu actually added by wt %	Cu analysis method	Micro-probe analysis (k _i)			Probe corrected Data (C _i) % Cu		
				Cementite	Base Matrix	Graphite Nodule	Cem.	Matrix	Module
1	2	3	4	5	6	7	8	9	10
A-1	As cast	1.2	1.125	0.7	1.2	-	0.825	1.425	
	FSG-2 hrs			0.8	1.6	1.0	0.950	1.900	
	FSG-3 hrs			0.8	1.8	-	0.950	2.125	
	FSG-4 hrs			0.8	1.5	0.6	0.950	1.775	
	FSG-5 hrs			0.7	1.2	-	0.825	1.425	
A-2	As cast, far end	0.8	0.70	0.67	0.99		0.80	1.175	
	As cast, ingate end			0.64	0.98		0.80	1.175	
	FSG-3 hours			0.63	1.04		0.75	1.212	
	FSG-4 hours			ND	1.23		ND	1.45	
	FSG-5 hours			ND	1.32/1.39		ND	1.5625/1.65	
	FSG-6 hours			0.76	2.66		0.90	3.125	

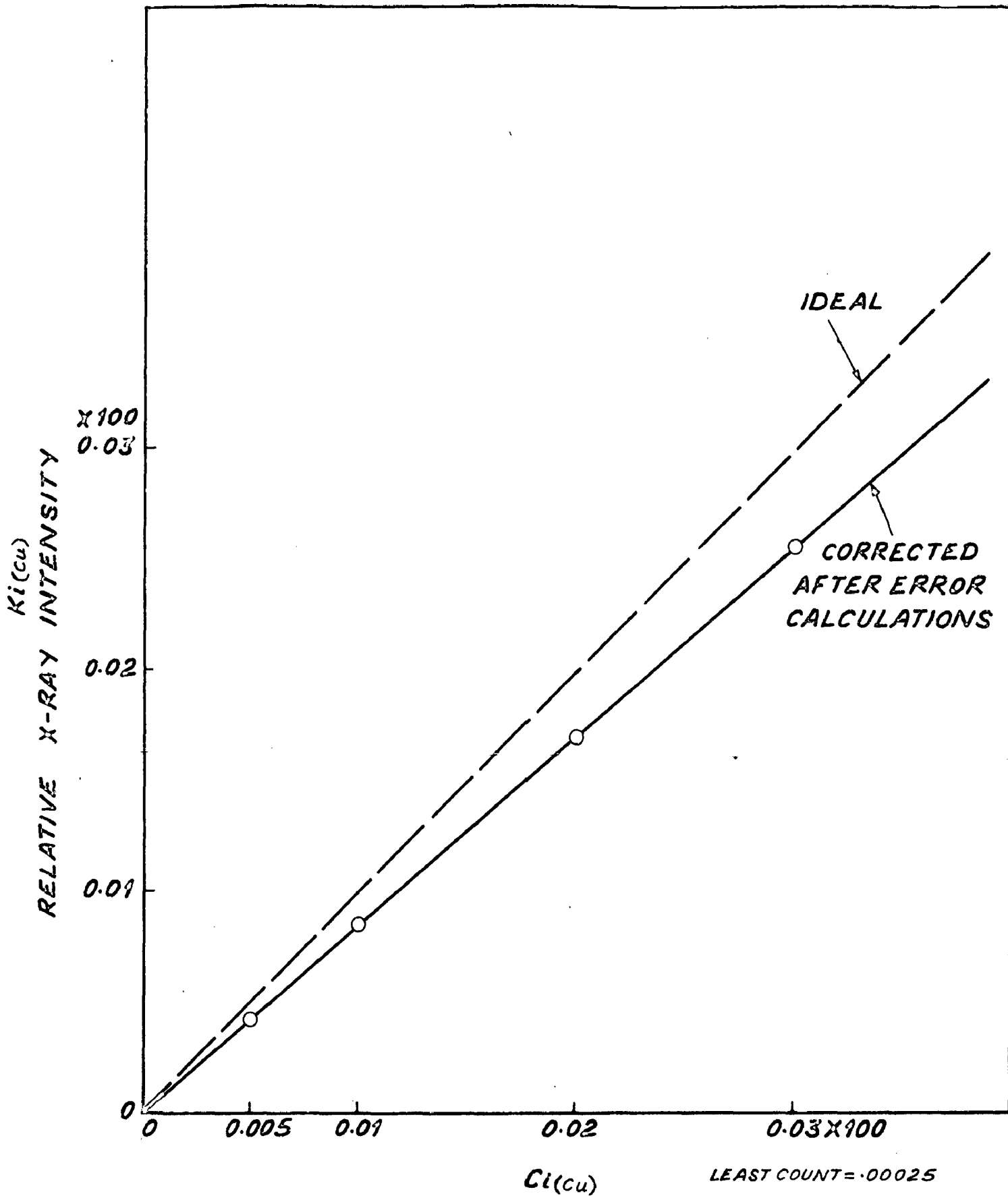
Table continued

ND - Not determined.

Table 7-7 continued

1	2	3	4	5	6	7	8	9	10
A-3	As cast	1.6	1.25	0.79	2.38		0.95	2.8	
	FSG - 0 hr.			0.81	1.86	0.85	0.95	2.175	
	FSG - 1 hr.			0.78	1.68	-	0.95	1.975	
	FSG - 2 hrs.			0.85	1.65	1.36	1.00	1.95	
A-4	As cast, Far end.	2.0	1.95	0.904	2.40/2.67	-	1.06	2.825/3.125	
	As cast, Ingate end			0.78	2.45		0.95	2.825	
	FSG - 1 hr.			0.67	2.46		0.80	2.83	
	FSG - 2 hrs.			0.69	2.40		0.825	2.825	
A-5	As cast, Ingate end	2.0	2.10	0.82	2.60		0.95	3.05	
	As cast, Far end			0.90	4.05		1.06		
	FSG - 1 hr.			0.77	2.56		0.91	3.00	
	FSG - 2 hrs.			0.77	2.53		0.91	2.975	
	FSG - 3 hrs.			0.77	2.44	0.79	0.91	2.825	

N.D. - Not determined.



MASS CONCENTRATION OF i^{th} ELEMENT (Cu)
 IN SAMPLE

FIG.7-17. CALIBRATION CURVE FOR Cu ANALYSIS BY ELECTRON PROBE MICRO-ANALYSER.

Wt. % Cu IN CEMENTITE AND AUSTENITE
AFTER 2 HRS. AT 920 °C

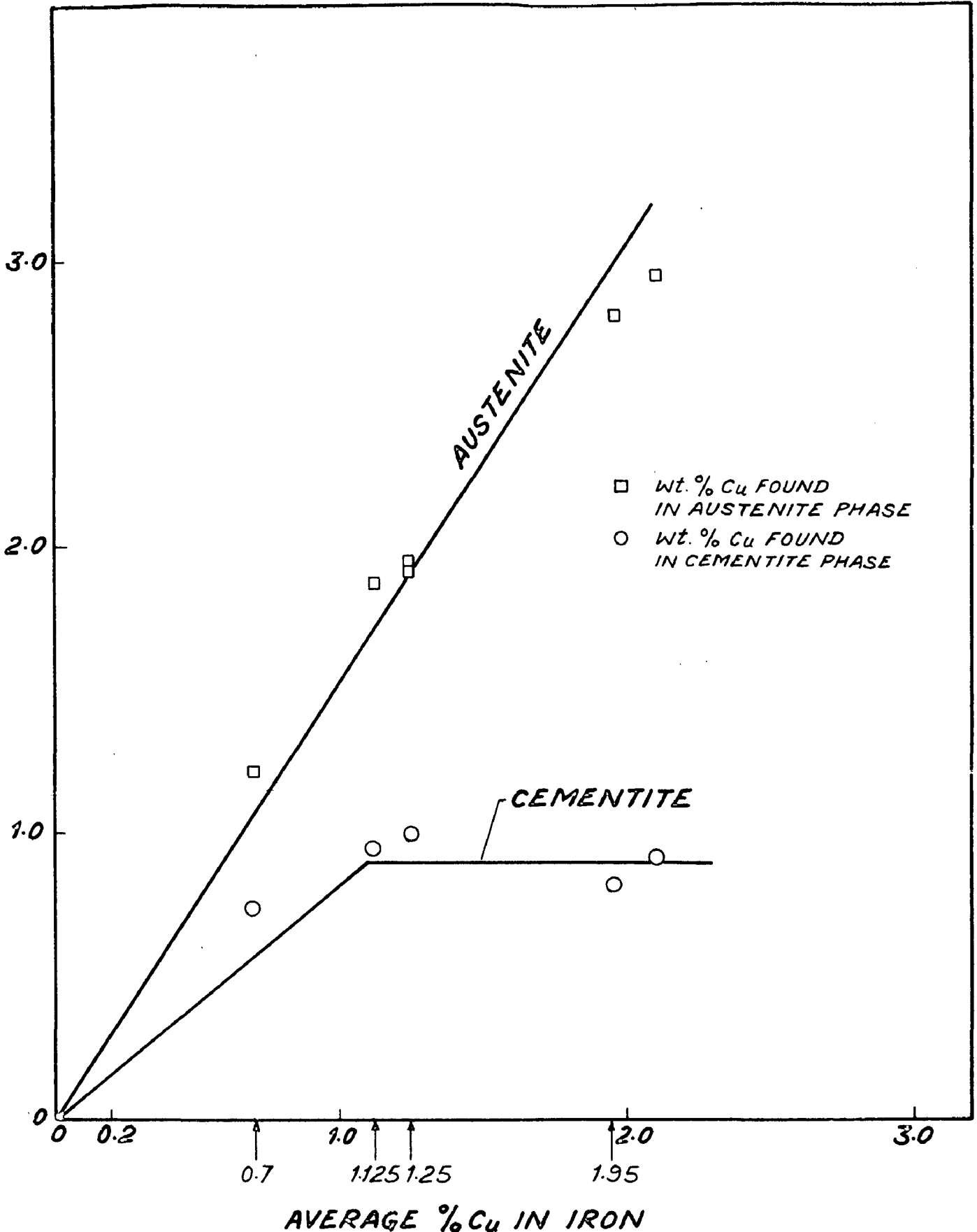
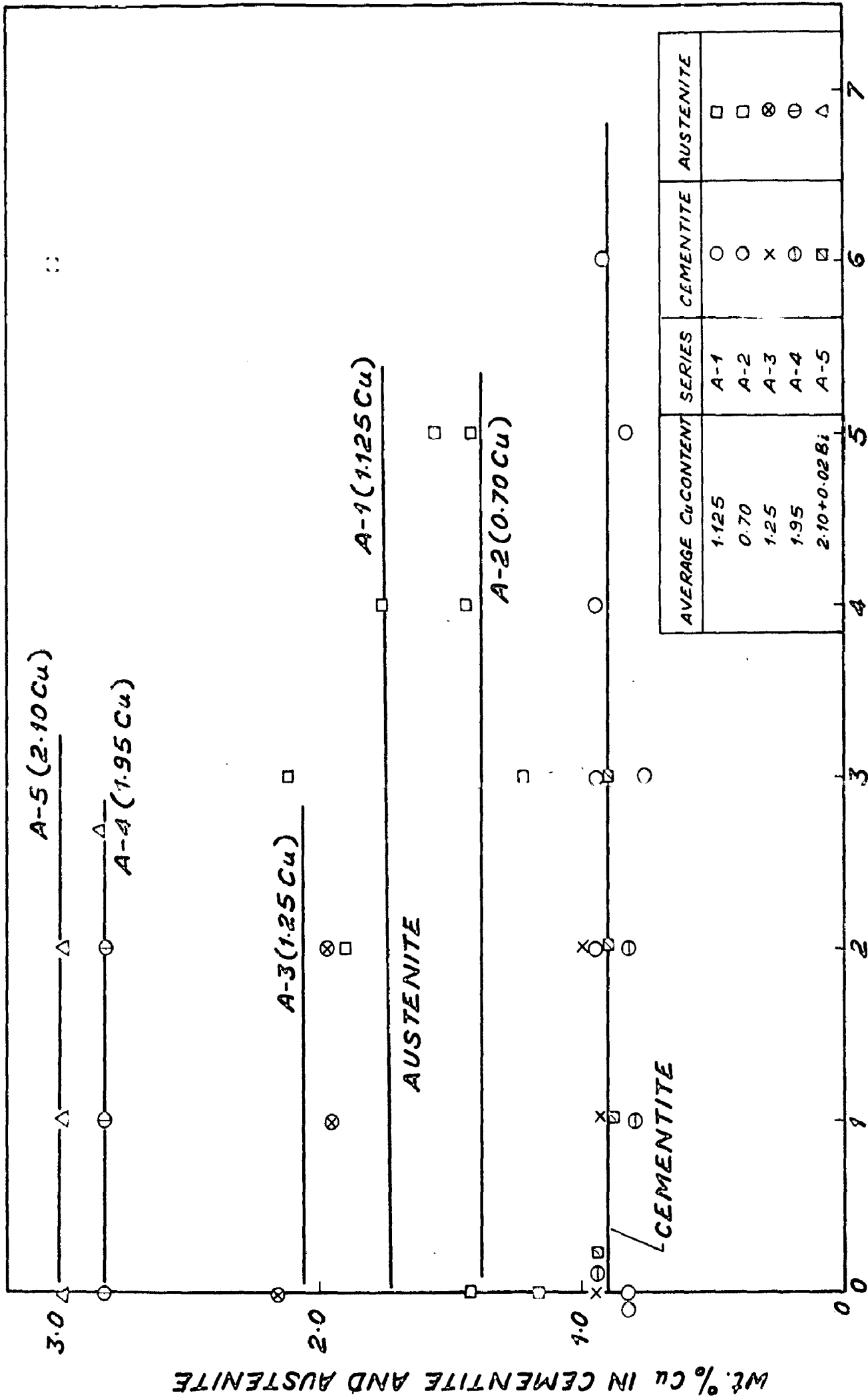


FIG. 7-18. Wt. % Cu FOUND BY ELECTRON PROBE MICRO-ANALYSER IN CEMENTITE AND AUSTENITE PHASE OF DIFFERENT ALLOYS AFTER 2 HRS. HEATING AT 920 °C.



HYS. AT FSG TEMP. (920°C)

FIG. 7-19. PARTITIONING OF Cu BETWEEN CEMENTITE AND AUSTENITE PHASE OF DIFFERENT Cu BEARING WHITE IRONS WITH THE PROGRESS OF FSG AT 920°C.

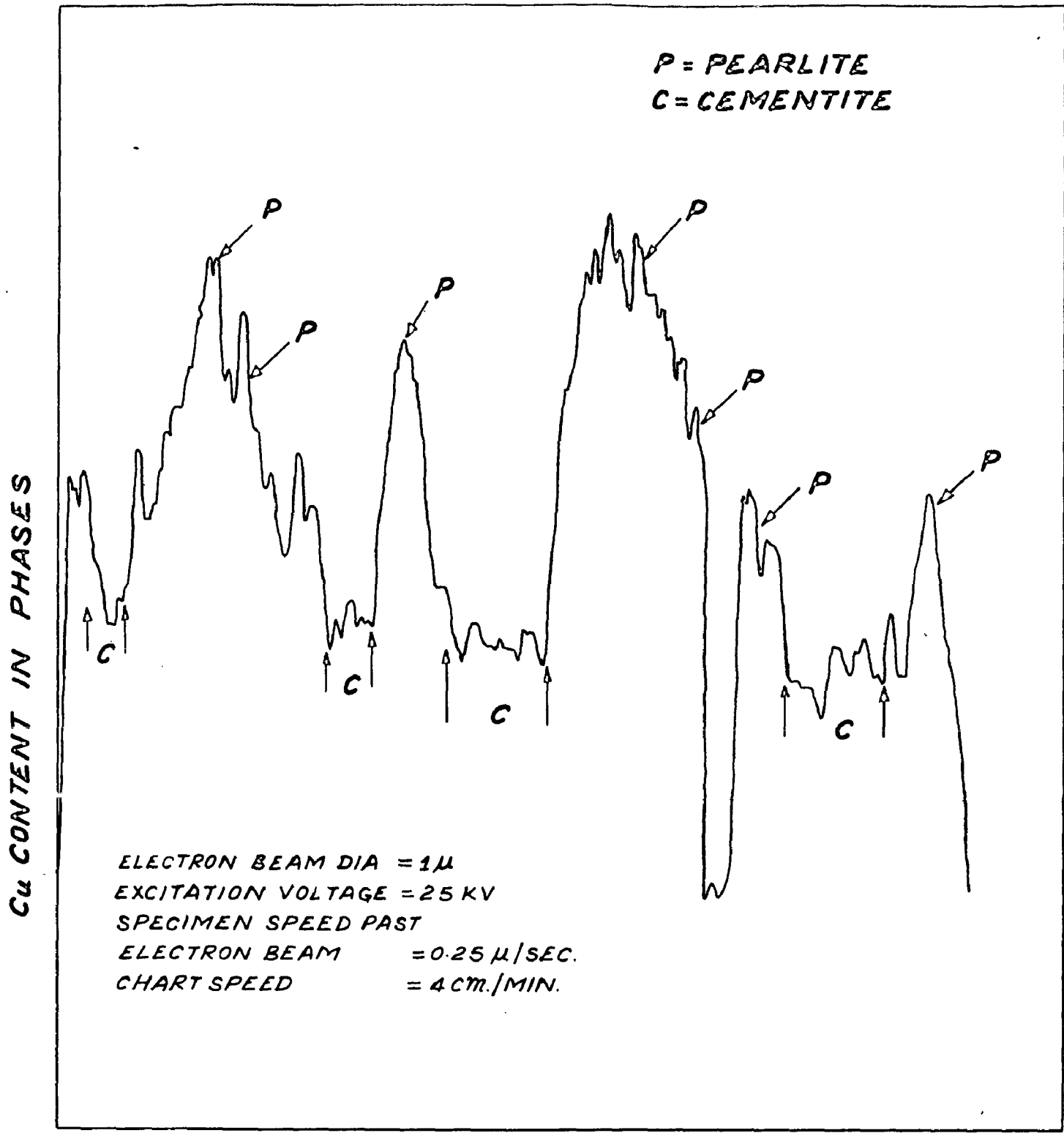
Results of these calculations at various copper contents in the hypothetical sample are summarised in Table 7-6 and plotted in Fig. 7-17. Partition data summarised in Table 7-7 has been plotted in Fig. 7-18 and 7-19.

Data in Table 7-6 and Fig. 7-17 show that an error of nearly 15% is introduced in the probe-observations due to various sources, discussed in section 6.6.2. These error calculations have been shown in the appendix.

Observed data from the probe-analyser was thus corrected to yield C_i (Mass concentration of copper in the samples) values, recorded in Table 7-7. Calibration curve shown in Fig. 7-17 was directly utilised for the purpose.

It can be seen from Fig. 7-18 that copper mainly partitions to the austenite phase. Only small quantities of copper partition to the cementite phase. From the present observations, it can be noted that a maxima in the amount of copper partitioning to the cementite phase occurs at about 1.1 to 1.25 wt % average copper content, beyond which, no further amount of copper partitions to the cementite phase, even when the average copper content is increased upto 2.10 wt %.

Fig. 7-19 shows the partitioning of copper in cementite and austenite phases in case of different alloys with the progress of FSG reaction at 920°C . It is seen that copper content does not increase in either cementite



WIDTH OF PHASES SCANNED

FIG.7-20 VARIATION OF Cu CONTENT IN CEMENTITE AND AUSTENITE PHASES OF A-2 (AVERAGE Cu = 0.7 Wt %) AT FSG = 0 Hrs., AS DETECTED BY ELECTRON PROBE MICRO-ANALYSER, SCANNING ATTACHMENT.

or austenite phase of any alloy with the progress of graphitization reaction at 920°C . Also the copper content of cementite phase, in case of all the alloys, was found to be nearly 0.95% , which remained practically constant throughout the entire period of graphitisation. Of course the amount of copper partitioning to the austenite phase of different alloys was found to be in proportion with the average copper content of base-alloys (Fig. 7-18).

7.3.2.2 Probe-Scan Data:

The main aim of carrying out this work was to ascertain, whether eutectic cementite grains had marked segregations with respect to copper, since it was feared that rapid cooling due to air-stripping within minutes of pouring, could have caused such copper segregations at least in the cast structure.

All the specimens shown in Table 7-7 were subjected to this study by the help of Electron-probe-microanalyser scanning attachment.

Typical scanning curve found in case of A-2 specimen at the start of FSG reaction is shown, as an example, in Fig. 7-20.

No appreciable Cu segregation in the cementite phase of any alloy, listed in Table 7-7, was found.

7.3.3 Discussion of Results:

Maximum number of nodules formed between 1.1 and 1.2 wt%.

copper during pre-treatments (Fig. 7-12); shortest FSG periods found corresponding to nearly 1.2 wt% Cu in normal as well as pre-treated cases and maximum percentage shortening in FSG period obtained due to any pre-treatment at the same wt% copper (Fig. 7-13); coincide fully with the partitioning data found in the present work. Optimum results of graphitisation stated above, thus coincide with a specific average copper content of base-alloy (1.1-1.2 wt% Cu), at which, the maximum amount of copper partitions to the eutectic cementite. Obviously, eutectic cementite will be most unstable corresponding to this composition. Since partitioning behaviour of copper does not change beyond this percentage, the FSG period is held constant after 1.25 wt% Cu content in thin as well as in thick sections (Fig. 7-13), meaning that Cu additions beyond 1.25 wt% and upto nearly 2.0 wt % do not help in reducing the FSG period. Nearly the same trend is maintained in pretreated specimens too. Thus, it can be clearly seen that the results of present investigation, with regard to both, the graphitisation characteristics of copper alloyed white irons upto 2.0 wt % copper content, as well as the partitioning behaviour of such white irons, are fully in agreement with each other.

Partitioning data of Sandoz⁽⁵¹⁾ with respect to copper going to cementite phase has been reproduced in Table 7-8 and replotted in Fig. 7-22. Original plot of Sandoz is shown in Fig. 7-21. It can be seen from Fig. 7-21 that Sandoz has

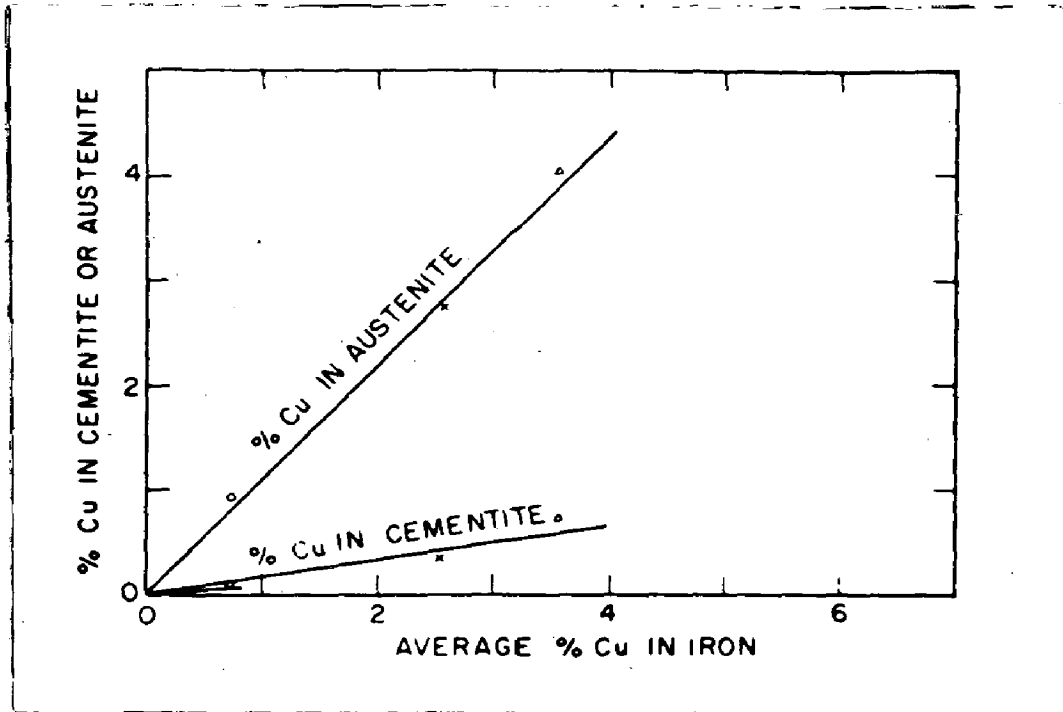


Fig. 7.21: - The partition of copper near the beginning of the first stage reaction Sandoz (28,51).

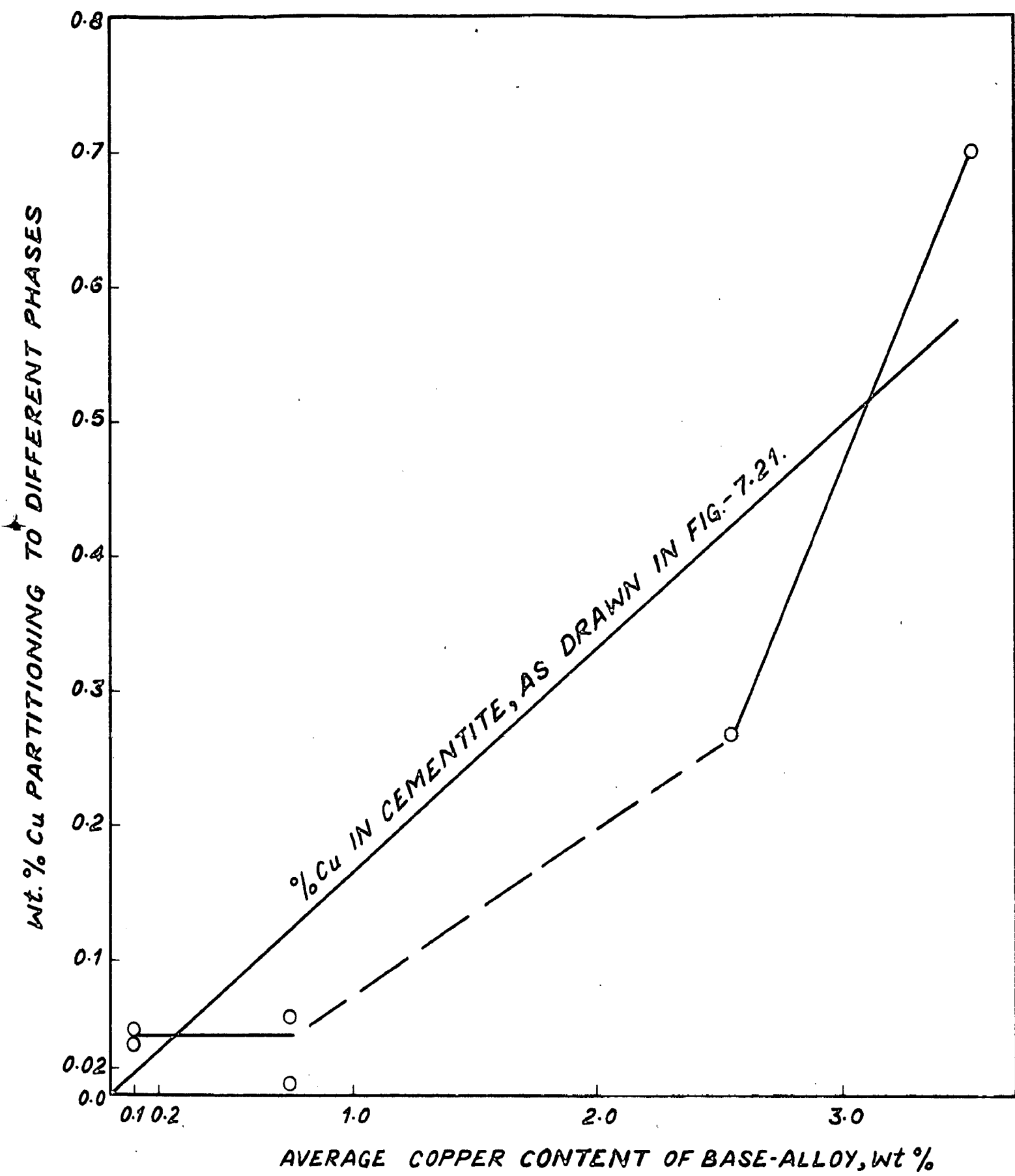


FIG.-7-22. PARTITION-DATA OF SANDOZ^(28,51) REPLOTTED.

drawn a straight line through two points corresponding to 2.55 and 3.53 average percentage copper in iron, neglecting the points corresponding to 0.74 and 0.10 average percentage copper in iron, with regard to copper partitioning in cementite. Straight line denoted by "percent Cu in cementite" in Fig.7-21, has therefore, been taken by him as average partitioning behaviour of Cu in cementite. True representation of his data in this regard is shown in Fig.7-22.

The curve is horizontal between 0.1 and 0.74 average % Cu in iron, no data is available between 0.74 and 2.55 average % Cu in iron, beyond which, there is a steep rise in copper content of eutectic cementite. "percent copper in cementite" line shown in Fig.7-21 has been super-imposed on Fig.7-22.

Even if the data of Sandoz in this regard is taken to be correct, the FSG period must continuously decrease with increasing percentages of copper in the base alloy, which was not the case in the present investigation. Even Sandoz has not reported any graphitisation data beyond 1.21 wt % Cu content of base-alloy, though he has reported partitioning data upto 3.53 wt % average Cu content⁽²⁸⁾.

It must be stated that the graphitisation data found in the present work upto 1.25 wt % Cu content is in complete agreement with most workers including Sandoz^(28,51) Heine et al⁽⁸⁹⁾, B.Thyberg⁽¹²⁸⁾ and other reports⁽¹⁶⁶⁾. It may be only incidental that Sandoz⁽¹²⁸⁾ did not investigate the graphitisation characteristics of copper bearing

white irons beyond a percentage of 1.21 wt % copper; Or it may be that interest in the graphitisation characteristics of copper bearing white irons did not exist beyond a copper content of 1.25 or 1.30 wt % , since the optimum mechanical properties were found at nearly this copper content by most investigators like P.B. Burgess⁽⁹⁰⁾, B.Thyberg⁽¹²⁸⁾ and Heine et al⁽⁸⁹⁾.

Slight increase in FSG periods at 1.95 wt % copper in all the pre-treated cases compared to the one found at 1.25 wt % copper (Fig.7-13), may be attributed directly to the lower Nv values found at 1.95 wt % copper (Fig.7-12). FSG periods further increase in case of 2.1 wt % copper, when the melt was inoculated with 0.02 wt % Bi, because Bi is known to have a strong carbide stabilising effect and also because Nv has lowest value corresponding to this composition. Nv values decrease at copper contents beyond 1.1 to 1.2 wt % copper even though copper partitioning to the cementite phase at 1.95 or 2.1 wt % average Cu contents is the same as at 1.1 or 1.21 wt % Cu contents (Fig.7-18), meaning that cementite phase is equally destabilised at these two different percentages, because copper contents beyond the critical value of ~1.2% cause the precipitation of copper atoms at austenite/cementite interfaces during cooling, which present a barrier to the diffusion of carbon atoms^(65,166), and therefore, the phenomenon of nucleation is partially inhibited. Lower Nv values or increased diffusion distances would ultimately lower the rate of

Table 7-8

PARTITIONING DATA OF SANDOZ*

Heat No.	No. of samples	Time at 900°C hrs.	C		Si		Mn		S		P		V		Cr		Cu		Ni	
			Ave	Cem.	Ave	Cem.	Ave	Cem.	Ave	Cem.	Ave	Cem.	Ave	Cem.	Ave	Cem.	Ave	Cem.	Ave	Cem.
H-104-F	1	0.25	2.18	0.85	0.28	0.08	-	0.03	-	0.005	-	0.19	1.03	0.37	1.48	0.74	0.06	-	-	-
H-104-F	1	30	2.18	0.85	0.25	0.08	-	0.03	-	0.005	-	0.19	1.16	0.37	1.70	0.74	0.01	-	-	-
H-72-B	3	0.25	2.20	1.10	0.29	0.05	-	0.025	-	0.008	-	-	-	-	-	2.55	0.27	-	-	-
L-56-A	2	0.25	2.20	0.78	0.14	0.13	0.200	0.02	-	0.011	-	-	-	-	-	0.10	0.04	-	-	-
L-56-B	2	0.25	2.20	0.78	0.22	0.13	0.16	0.02	-	0.011	0.038	-	-	-	-	3.53	0.70	-	-	-
L-56-L	3	0.25	2.20	0.78	0.20	0.13	0.12	0.02	0.010	0.011	-	-	-	-	-	0.10	0.05	2.88	0.95	-

* Sandoz (51) - NRL Report 5268, Feb. 16, 1959, page-6

cementite decomposition, causing an increase in FSG period.

Partitioning behaviour of copper in austenite phase found in this work at increasing average copper contents, is identical in nature with the investigations of Sandoz⁽⁵¹⁾, ~~except~~ ^{that some} marginal shift in the values can be noted. These marginal shifts may be attributed to the cumulative errors.

It can be seen from the data of Sandoz⁽⁵¹⁾ (Table 7-8) that the amount of silicon partitioning to the cementite phase at 0.78 average Si content is nearly 0.22%. (L-56-B alloy) and 0.20%. (L-56-L alloy), while the amount of copper partitioning to the cementite phase at 0.74 average Cu content has been reported to be only 0.06% and 0.01% in the same H-104-F alloy respectively at 0.25 and 30 hours of exposure at 900°C. These results, however, are not compatible with the established fact that silicon is a far more strong graphitiser compared to copper. Copper would, therefore, be expected to go more in solution with eutectic cementite to give graphitising effect compared to silicon. The results of present investigation are in line with this argument. Moreover, the partition data found in the present investigation is in complete agreement with the graphitisation characteristics of copper bearing white irons reported in section 7.2 of this work.

7.3.4 Conclusions:

1. Copper partitions between eutectic cementite and austenite phases in definite proportions.
2. Maximum copper partitions to the eutectic cementite phase at an average copper content of nearly 1.2 wt%.. No further amount of copper partitions to the cementite phase at higher average copper contents of base-alloy.
3. Copper partitioning to the austenite phase increases in proportion to the increase in the average Cu content of base alloy.
4. Copper content of either austenite or cementite phase of any alloy does not change with the progress of graphitisation at 920°C.
5. No appreciable copper segregation was found in the cementite phase of any alloy under study.
6. Partition data determined in the present study was found compatible with the graphitisation characteristics of white irons containing 0.7 to 2.10 wt % copper contents.

7.4 UNALLOYED AND COPPER-ALLOYED PEARLITIC MALLEABLE IRON

7.4.1 Introductory:

Unalloyed as well as Cu-alloyed compositions were subjected to the "Interrupted annealing and tempering" treatment, outlined in previous sections 5.4 and 6.3.4, in order to make pearlitic malleable irons from these alloys.

Mechanical properties of these pearlitic malleable irons were determined in accordance with the procedure detailed in section 6.7.

Metallographic specimens prepared out of pulled tensile test pieces were examined under optical microscope and then representative microstructures were photographed. Few specimens tempered for short as well as long periods were replicated and studied under the electron microscope for their sub-structures. These microstructures were then correlated with the mechanical properties of pearlitic malleable irons.

Basically, it was aimed in this work to determine the tempering characteristics of unalloyed as well as copper alloyed pearlitic malleable irons in detail and to find the copper content, that would correspond with the optimum mechanical properties of such irons. It was natural further to compare the mechanical properties of unalloyed pearlitic malleable irons with those of copper alloyed pearlitic malleable irons, heat-treated in the

same manner approximately to 290-310 HV₃₀ hardness values.

7.4.2 Results:

7.4.2.1 Tempering Characteristics:

Tempering characteristics of unalloyed and alloyed pearlitic malleable irons are summarised in Table 7-9 to 7-13 and plotted in Figs. 7-23 to 7-38. Figs. 7-35 to 7-38 were plotted based on the data derived from Figs. 7-23 to 7-34. Hardness values obtained after 2 and 6 hrs. of tempering at various draw temperatures were plotted separately in individual cases in order to avoid the over crowding of points on a consolidated graph.

It can be seen from Figs. 7-23 to 7-34 and Tables 7-9 and 7-10 that the spread in hardness values obtained in all the cases (Oil, Water and Air quenched, thin and thick specimens) was minimum at 600°C after 2 and 6 hrs. of tempering. Approximately similar was the trend at 680°C, except that the range of hardness variation obtained was slightly in the lower hardness levels. Variation in hardness values obtained at 600°C and 680°C draw temperatures are summarised in Table 7-13. This range of hardness variation at 600°C draw temperature has been plotted in Fig. 7-38. Fig. 7-37 shows the relationship between the range of hardness variation obtained at 600°C and 680°C after 2 and 6 hrs. of draw periods and the copper content of base alloys.

Table-7-9

Resulting hardness (HV₃₀) in thin and thick sections of different alloys at various draw temperature

Alloy	Section	Hardness as quenched HV ₃₀	Quenching Media	HV ₃₀ after 2 hrs of tempering at draw-Temperatures °C				
				400°C	500°C	550°C	600°C	680°C
A-1 (1.125% Cu)	thin	763-810	Oil	-	-	-	290	260
	thick	383	Oil	-	-	-	365	305
	thick	348	Air	-	-	-	300	245
A-2 (0.7% Cu)	thin	705-752	Oil	-	-	-	280	225
	thick	415	Oil	-	-	-	348	300
	thick	311	Air	-	-	-	305	250
A-3 (1.25% Cu)	thin	705-730	Oil	325	310	-	240	230
	thick	314	Air	-	-	-	280	235
A-4 (2.0% Cu)	thin	639-666	Water	455	380	330	330	270
	thin	661	Oil	-	-	-	325	275
	thick	543-598	Oil	-	-	-	295	280
	thick	323	Air	-	-	-	290	245
A-5 (2.1% Cu + 0.02% Bi)	thin	635-685	Water	450	415	320	295	260
	thin	644-725	Oil	475	425	-	285	269
	thin	450	Air	400	390	-	305	-
	thick	639	Oil	-	-	-	295	275
	thick	348	Air	-	-	-	275	235
B-1 (0% Cu + 0.02% Bi)	thin	350	Air	-	330	-	300	240
	thin	406	Oil	-	-	-	275	260
	thick	280	Oil	-	-	-	260	210
	thick	297	Air	-	-	-	255	245

Table 7-10

Resulting hardness (HV_{30}) in thin and thick sections of different alloys after 6 hours of tempering at various draw temperatures.

Alloy	Section	As quenched hardness HV_{30}	Quenching Media	HV_{30} after 6 hours of tempering at various draw temperatures				
				400°C	500°C	550°C	600°C	680°C
A-1 (1.125% Cu)	thin	763-810	Oil	-	-	-	290	260
	thick	383	Oil	-	-	-	245	300
	thick	348	Air	-	-	-	300	223
A-2 (0.7%Cu)	thin	705-752	Oil	-	-	-	275	225
	thick	415	Oil	-	-	-	344	300
	thick	311	Air	-	-	-	305	236
A-3 (1.25% Cu)	thin	705-730	Oil	315	300	-	220	208
	thick	314	Air	-	-	-	276	223
A-4 (2.0% Cu)	thin	639-666	Water	450	380	315	310	260
	thin	661	Oil	-	-	-	312	265
	thick	543-598	Oil	-	-	-	290	250
	thick	323	Air	-	-	-	275	211
A-5 (2.1% Cu+ 0.02% Bi)	thin	635-685	Water	430	400	295	275	250
	thin	644-725	Oil	460	375	-	265	257
	thin	450	Air	400	370	-	297	-
	thick	639	Oil	-	-	-	285	255
	thick	348	Air	-	-	-	260	210
B-1 (0% Cu+ 1.63% Si+ 0.02% Bi)	thin	350	Air	-	270	-	240	204
	thin	406	Oil	-	-	-	255	220
	thick	280	Oil	-	-	-	200	180
	thick	297	Air	-	-	-	200	144-180

Table 7-11

Drop in hardness between 2 hours and 6 hours of tempering in individual cases at 600°C.

Alloy	Hardness details at 600°C.	Thin specimens			Thick specimens	
		Water quen- ched	Oil quenched	Air quenched	Oil quenched	Air quenched
A-1 (1.125% Cu)	HV ₃₀ after 2 hrs.	-	290		365	300
	HV ₃₀ after 6 hrs.		290		345	300
	Drop in hardness numbers.		0		20	0
	% drop in hardness.				5.5	0
A-2 (0.7% Cu)	HV ₃₀ after 2 hrs.		280		348	305
	HV ₃₀ after 6 hrs.		275		344	305
	Drop in hardness.		5		4	0
	% drop in hardness		1.8		1.1	0
A-3 (1.25% Cu)	HV ₃₀ after 2 hrs.		240			280
	HV ₃₀ after 6 hrs.		220			276
	Drop in hardness number.		20			4
	% drop in hardness.		8.3			1.4
A-4 (2.0% Cu)	HV ₃₀ after 2 hrs.	330	325		295	290
	HV ₃₀ after 6 hrs.	310	312		290	275
	Drop in hardness number.	20	13		5	15
	% drop in hardness	6	4		1.7	5.2
A-5 (2.0% Cu + 0.02% Bi)	HV ₃₀ after 2 hrs.	295	285	305	295	275
	HV ₃₀ after 6 hrs.	275	265	297	285	260
	Drop in hardness number.	20	20	8	10	15
	% drop in hardness	6.8	7.0	2.6	3.4	5.4
B-1 (0% Cu +1.63Si +0.02% Bi)	HV ₃₀ after 2 hrs.		275	300	260	255
	HV ₃₀ after 6 hrs.		255	240	200	200
	Drop in hardness number.		20	60	60	55
	% drop in hardness.		7.3	20	23	21.5

Table 7-12

Drop in hardness between 2 hrs. and
6 hrs. of tempering in individual
cases at 680°C

Alloy	Hardness details at 680°C	Thin specimens			Thick specimens	
		Water quen- ched	Oil quen- ched	Air quen- ched	Oil quen- ched	Air quen- ched
A-1 (1.125% Cu)	HV ₃₀ after 2 hrs.		260		305	245
	HV ₃₀ after 6 hrs.		260		300	223
	Drop in hardness number		0		5	22
	% drop in hardness.					9
A-2 (0.7% Cu)	HV ₃₀ after 2 hrs.		225		300	250
	HV ₃₀ after 6 hrs.		225		300	236
	Drop in hardness number		0		0	14
	% drop in hardness.					5.6
A-3 (1.25% Cu)	HV ₃₀ after 2 hrs.		230			235
	HV ₃₀ after 6 hrs.		208			223
	Drop in hardness number		22			12
	% drop in hardness.		9.5			5.1
A-4 (2.0% Cu + 0.02% Bi)	HV ₃₀ after 2 hrs.	270	275		280	245
	HV ₃₀ after 6 hrs.	260	265		250	211
	Drop in hardness number.	10	10		30	34
	% drop in hardness.	3.7	3.6		10.7	14
A-5 (2.0% Cu)	HV ₃₀ after 2 hrs.	260	269		275	235
	HV ₃₀ after 6 hrs.	250	257		255	210
	Drop in hardness number.	10	12		20	25
	% drop in hardness.	3.85	4.5		7.3	10.6
B-1. (0% Cu + 1.63% Si +0.02% Bi.)	HV ₃₀ after 2 hrs.		260	240	210	245
	HV ₃₀ after 6 hrs.		220	204	180	160
	Drop in hardness number		40	36	30	85
	% drop in hardness.		15.4	15	14.3	34.7

Table 7-13

Range of hardness variation in Oil, Water and Air quenched cases of different alloys, thin and thick sections at 600 and 680°C after 2 and 6 hours of tempering periods.

Alloy	Range of hardness (HV ₃₀) in Oil, Water and Air quenched cases, thin and thick section						
	Draw temperature 600°C		Draw temperature 680°C		Net variation		
	2 hrs.	6 hrs.	2 hrs.	6 hrs.	2 hrs.	6 hrs.	
A-1 (1.125% Cu)	348-810	290-360	290-345	290-360	245-305	223-300	223-300
A-2 (0.7% Cu)	311-752	275-345	280-345	275-345	225-300	225-300	225-300
A-3 (1.25% Cu)	314-730	240-280	200-275	200-280	230-235	200-223	200-235
A-4 (2.0% Cu)	323-666	290-330	275-310	275-330	245-280	211-265	211-280
A-5 (2.0% Cu + 0.02% Bi)	348-725	275-305	260-300	260-305	235-275	210-257	210-275
B-1 (0% Cu + 1.63% Si + 0.02% Bi)	297-406	255-300	200-255	200-300	210-260	160-220	160-260

TEMPERED - 2 Hrs.

A-1

- OQ (THIN)
- OQ (THICK)
- AQ (THICK)

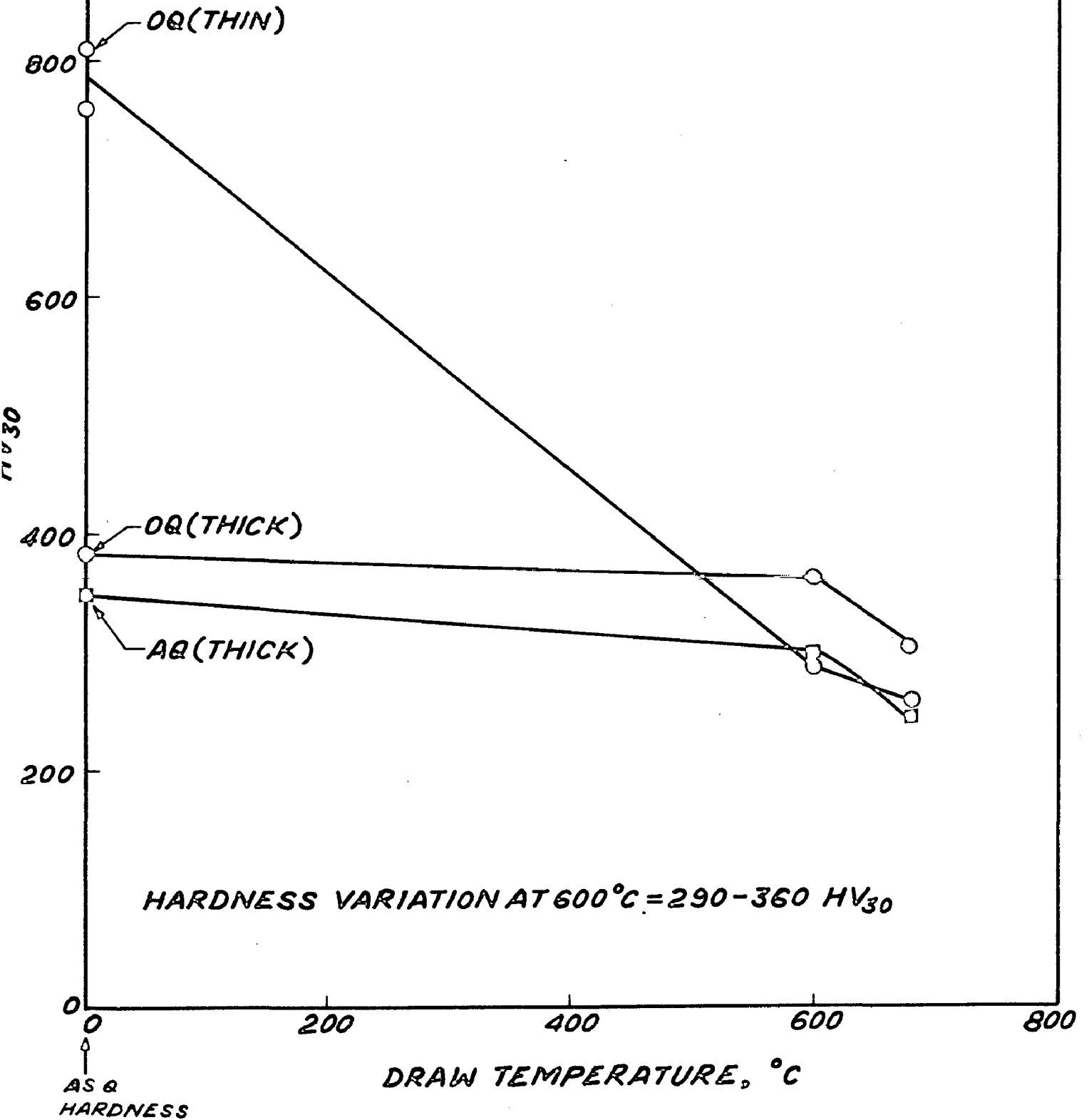


FIG. 7-23, VARIATION IN HARDNESS OBTAINED AFTER 2 Hrs. OF TEMPERING AT DIFFERENT DRAW TEMPERATURES, A-1 SERIES, THIN AND THICK SPECIMENS, OQ AND AQ CASES.

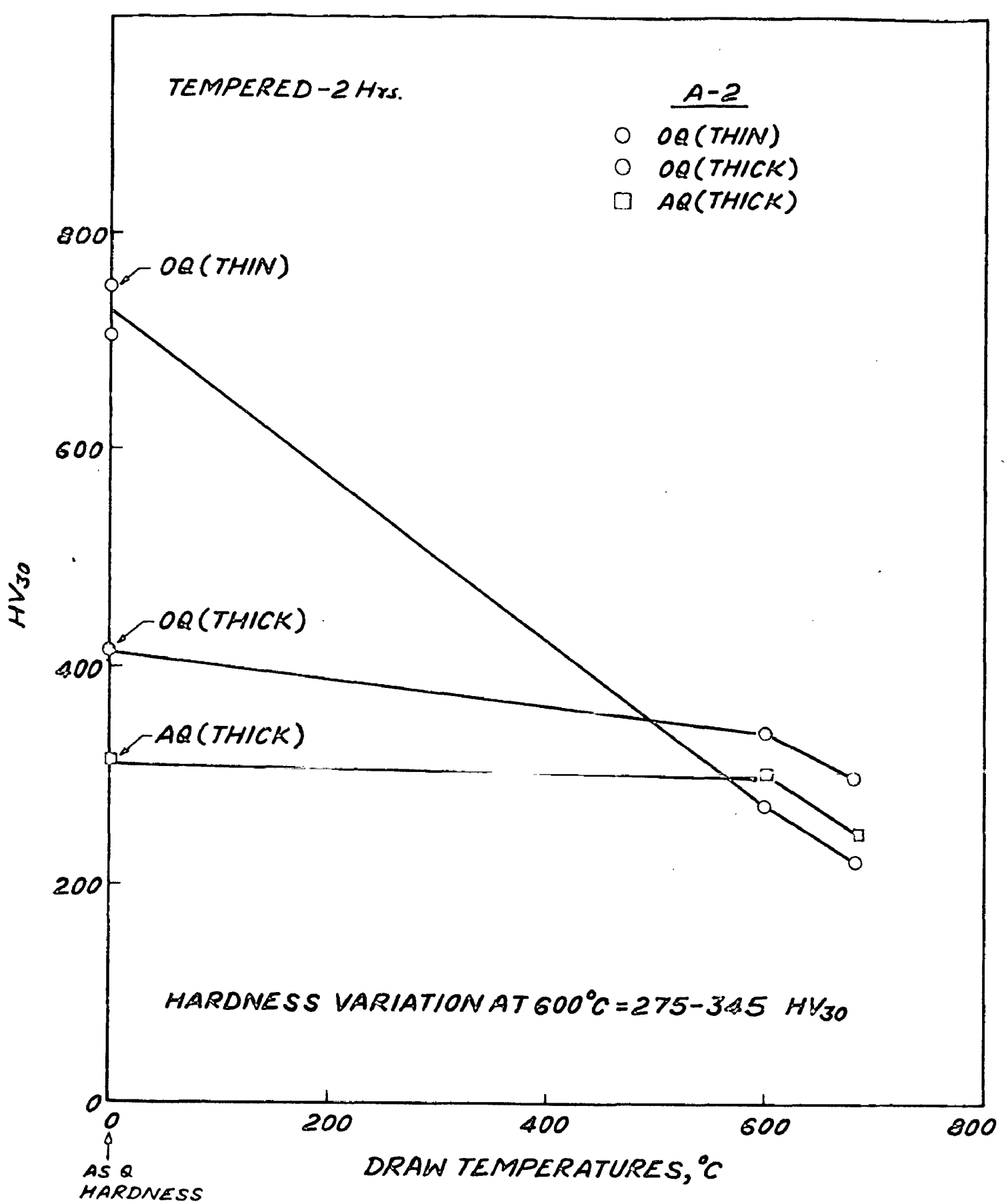


FIG. 7-24. VARIATION IN HARDNESS OBTAINED AFTER 2 Hrs. OF TEMPERING AT DIFFERENT DRAW TEMPERATURES, A-2 SERIES, THIN AND THICK SPECIMENS, OQ AND AQ CASES.

TEMPERED - 2 Hrs.

A-2

- OQ (THIN)
- AQ (THICK)

HV₃₀

800
600
400
200
0

OQ (THIN)

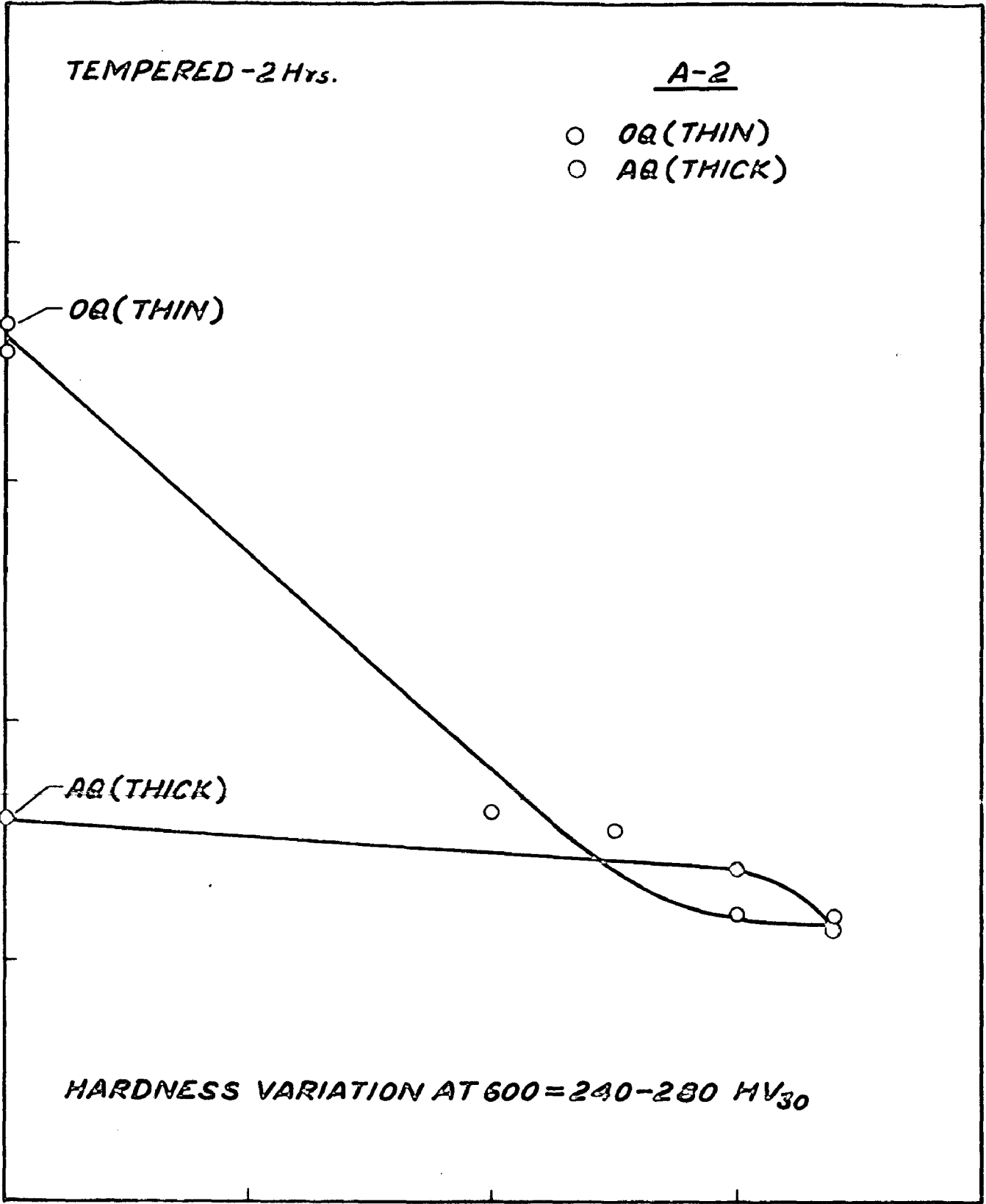
AQ (THICK)

HARDNESS VARIATION AT 600 = 240-280 HV₃₀

DRAW TEMPERATURES, °C

AS Q
HARDNESS

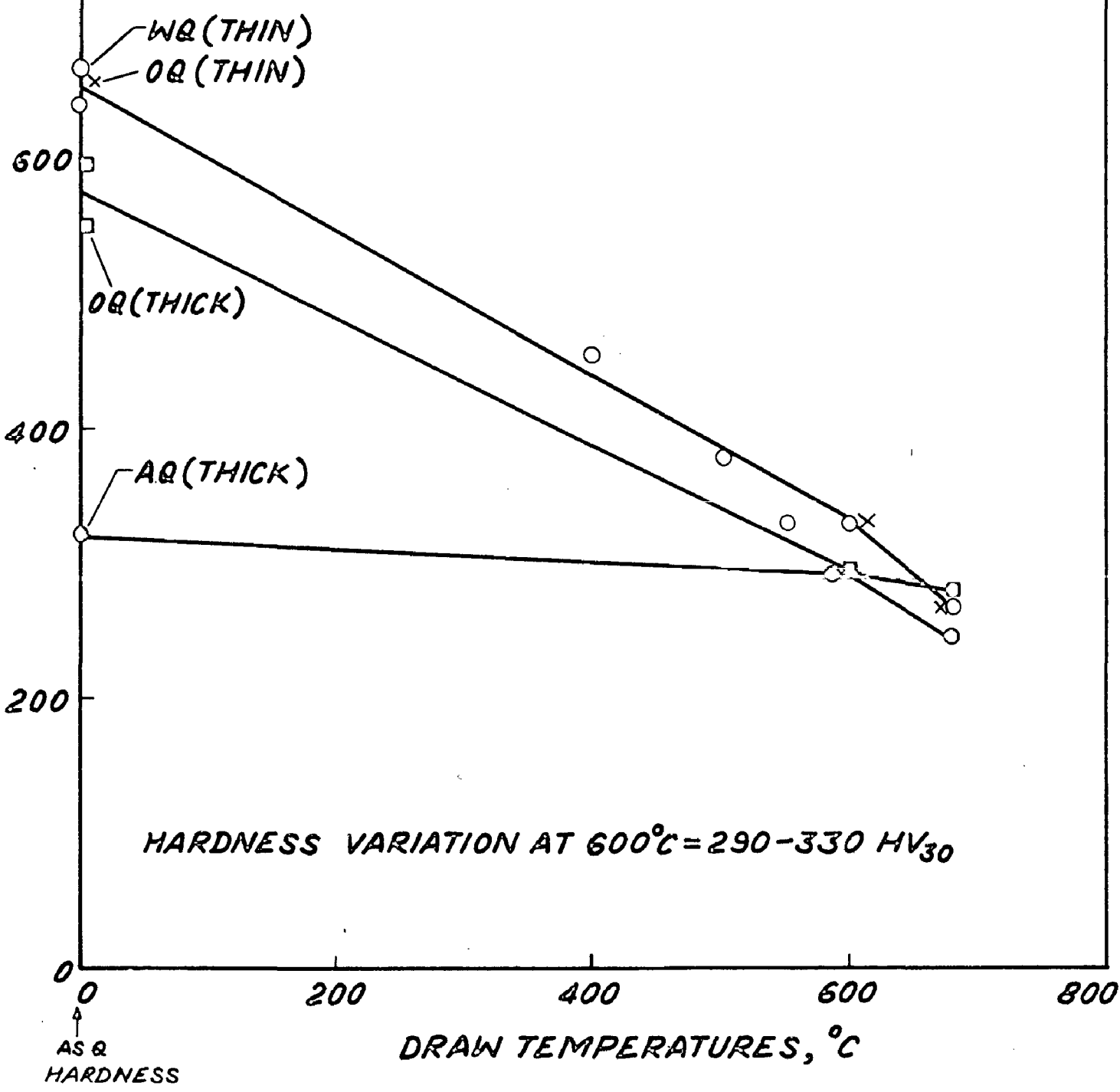
FIG. 7-25. VARIATION IN HARDNESS OBTAINED AFTER 2 Hrs. OF TEMPERING AT DIFFERENT DRAW TEMPERATURES, A-2 SERIES, THIN AND THICK SPECIMENS, OQ AND AQ CASES.



TEMPERED - 2 Hrs.

A-4

- WQ (THIN)
- × OQ (THIN)
- OQ (THICK)
- AQ (THICK)



HARDNESS VARIATION AT 600°C = 290-330 HV₃₀

FIG.7-26.VARIATION IN HARDNESS OBTAINED AFTER 2 Hrs. OF TEMPERING AT DIFFERENT DRAW TEMPERATURES, A-4 SERIES, THIN AND THICK SPECIMENS, WQ, OQ AND AQ CASES.

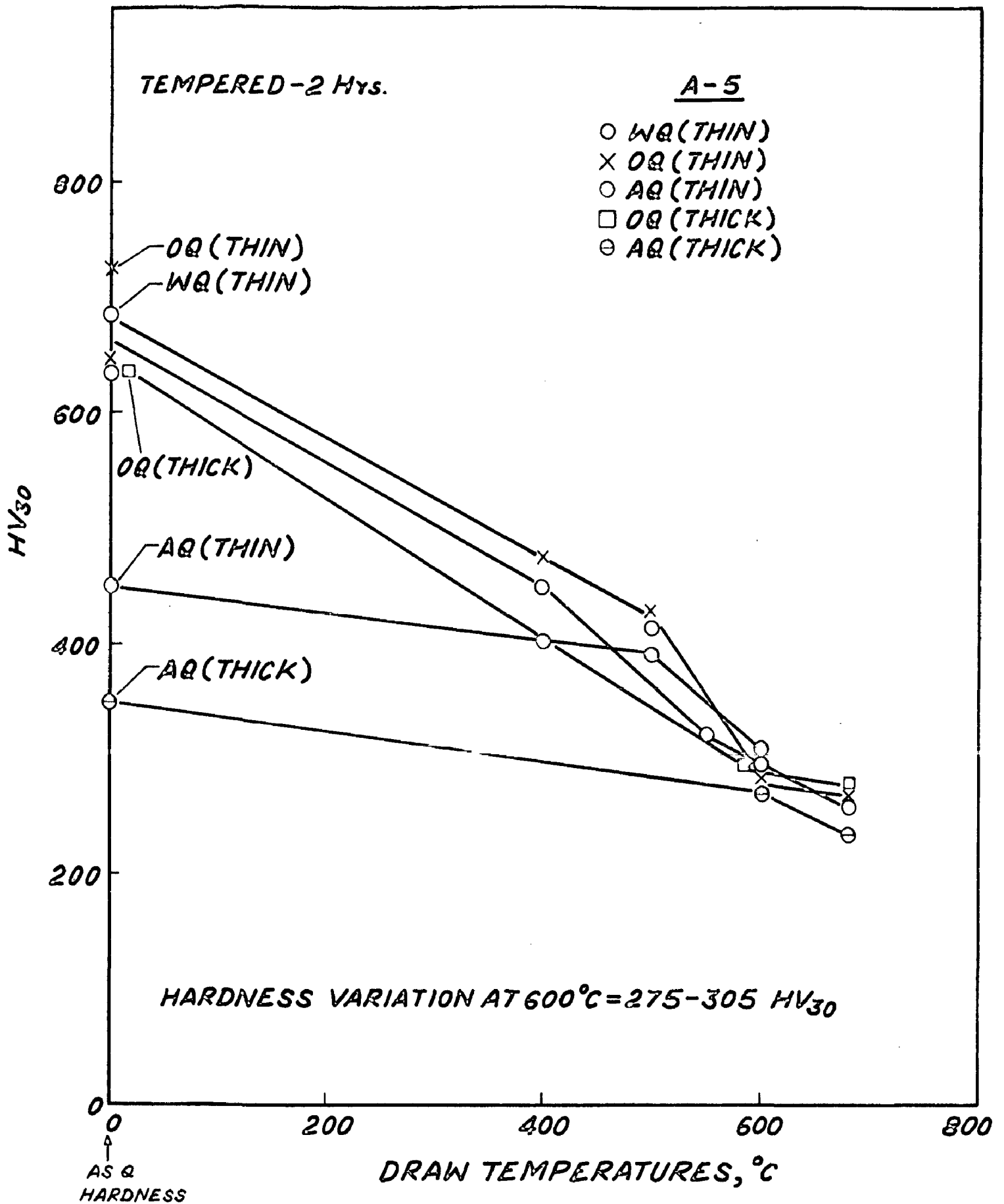


FIG. 7-27 VARIATION IN HARDNESS OBTAINED AFTER 2 Hrs. OF TEMPERING AT DIFFERENT DRAW TEMPERATURES, A-5 SERIES, THIN AND THICK SPECIMENS, WQ, OQ AND AQ CASES.

TEMPERED-2 Hrs.

B-1

- OQ (THIN)
- × AQ (THIN)
- OQ (THICK)
- AQ (THICK)

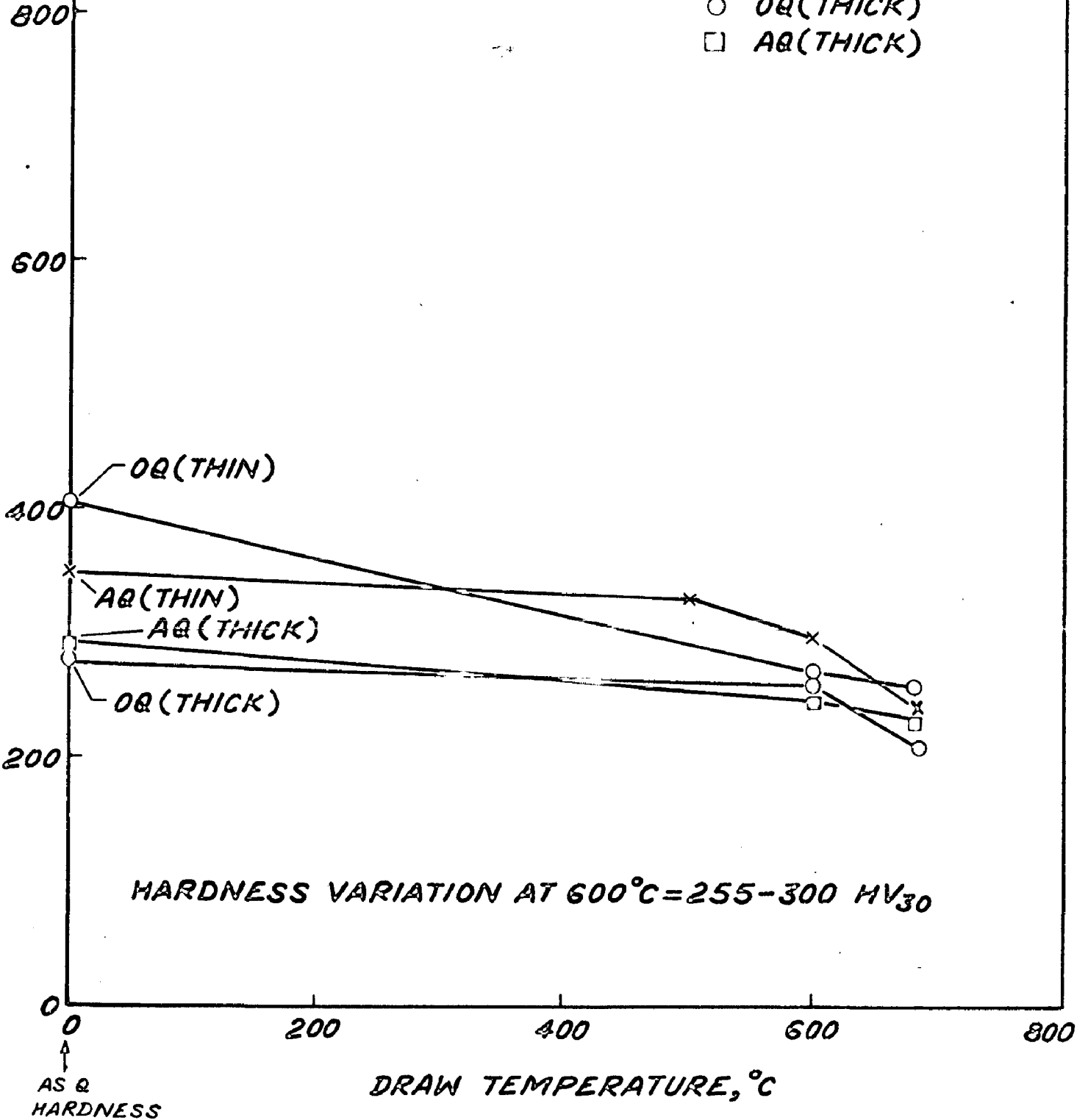


FIG.7-28 VARIATION IN HARDNESS OBTAINED AFTER 2 Hrs. OF TEMPERING AT DIFFERENT DRAW TEMPERATURES, B-1 SERIES, THIN AND THICK SPECIMENS, OQ & AQ CASES.

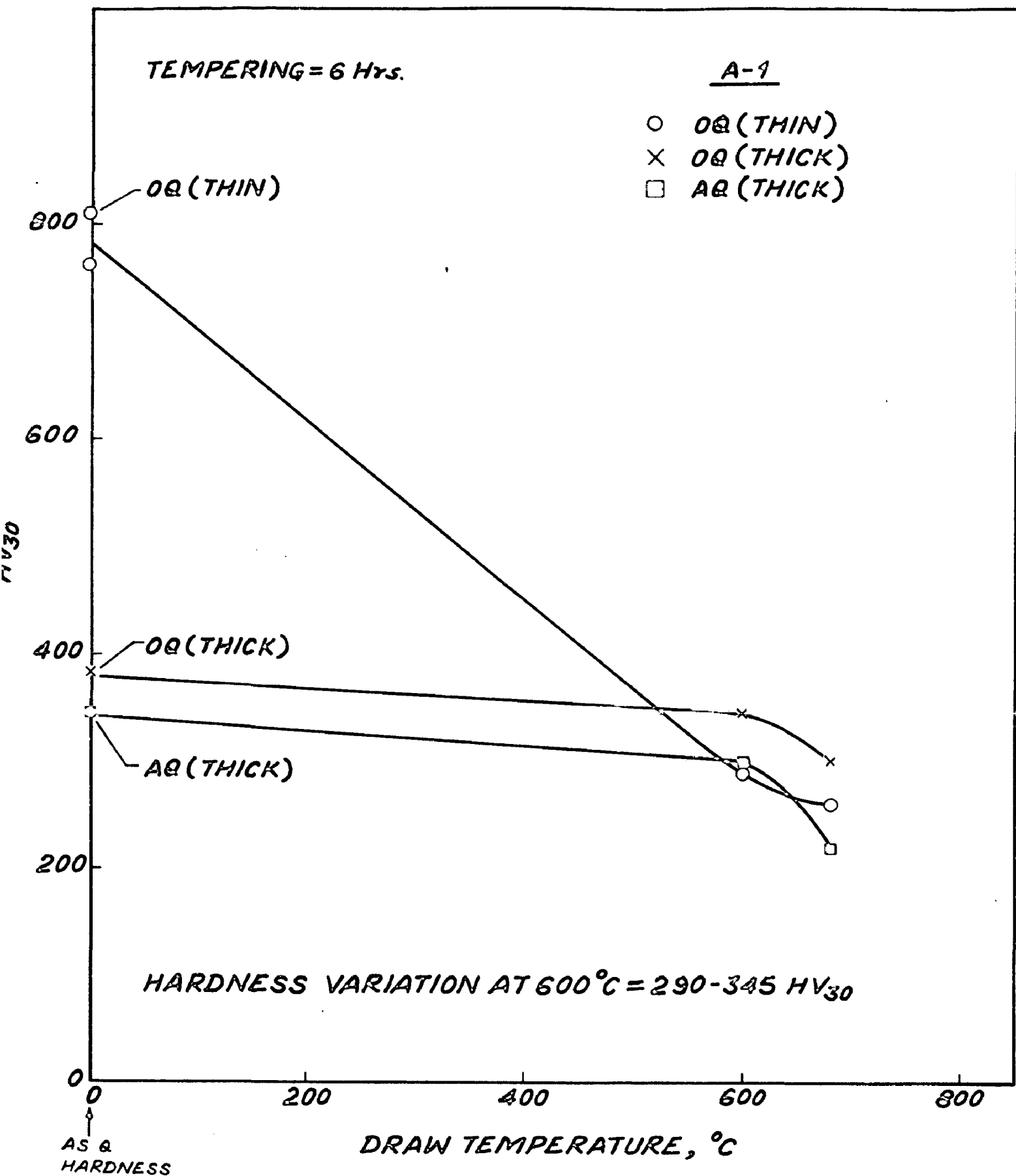


FIG. 7-29 VARIATION IN HARDNESS OBTAINED AFTER 6 Hrs. OF TEMPERING AT DIFFERENT DRAW TEMPERATURES, A-1 SERIES, THIN AND THICK SPECIMENS, OQ AND AQ CASES.

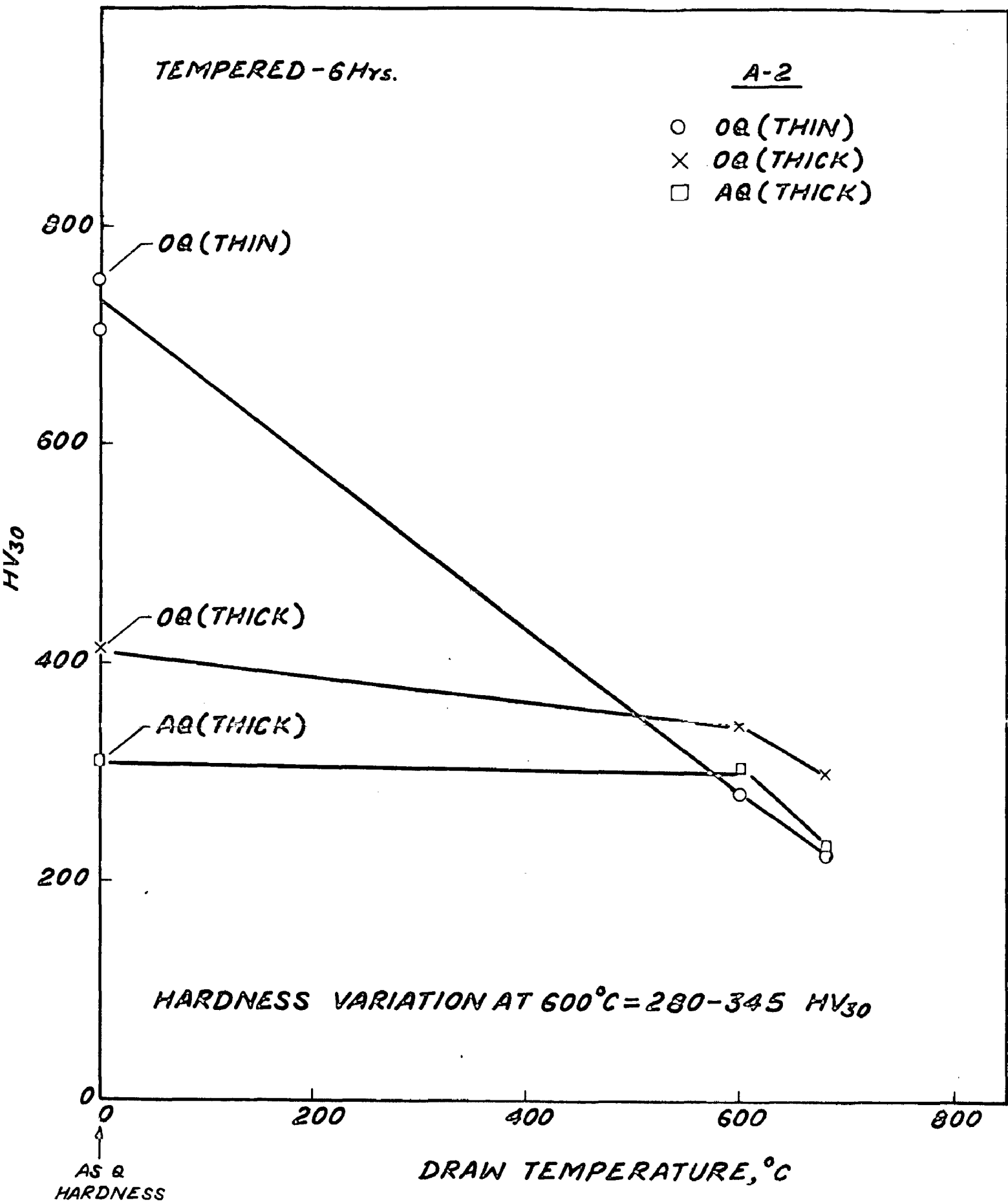


FIG.7-30 VARIATION IN HARDNESS OBTAINED AFTER 6 Hrs. OF TEMPERING AT DIFFERENT DRAW TEMPERATURES, A-2 SERIES, THIN AND THICK SPECIMENS, OQ AND AQ CASES.

TEMPERED - 6 Hrs.

A-3

○ OQ (THIN)
× AQ (THICK)

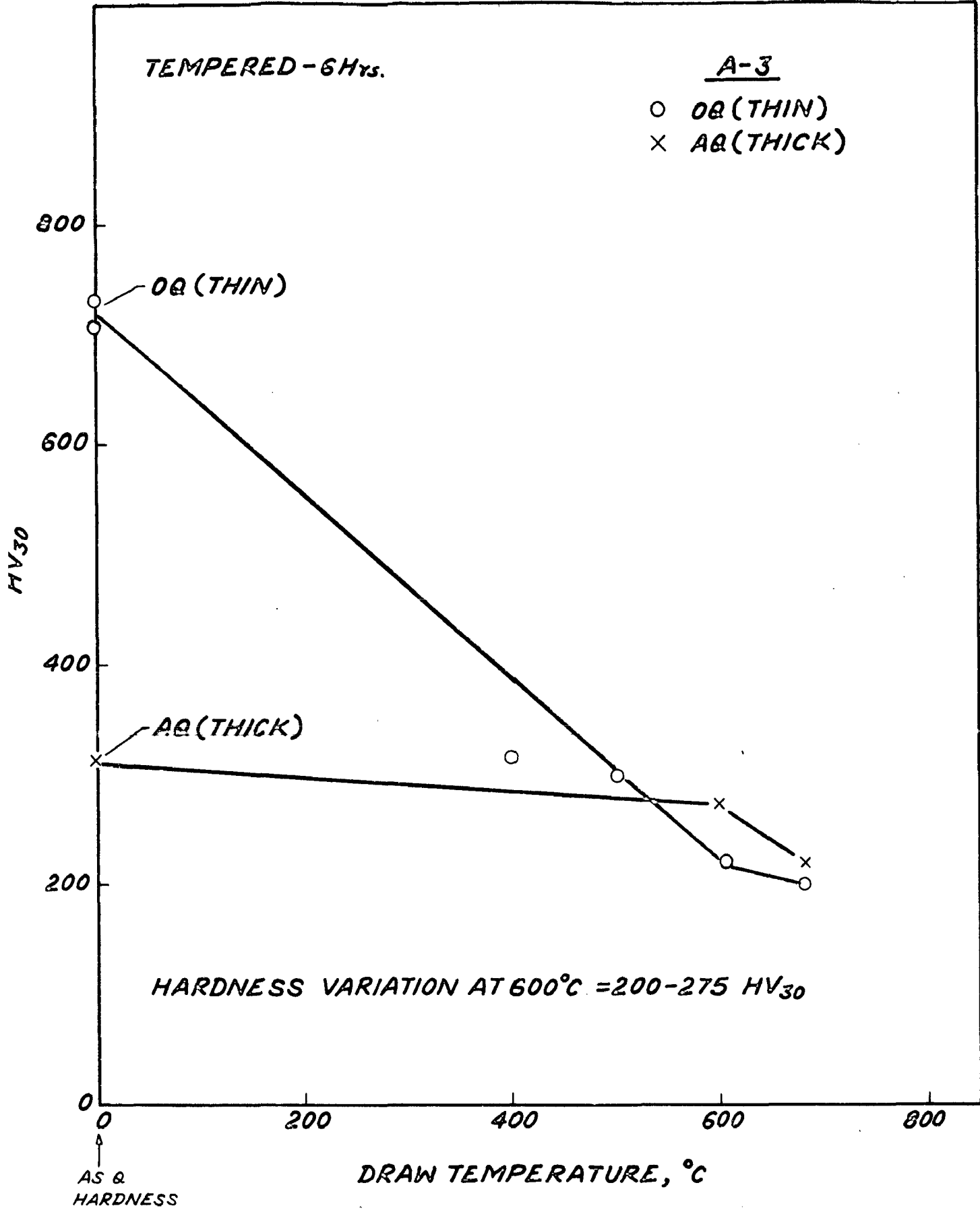


FIG.7-31 VARIATION IN HARDNESS OBTAINED AFTER 6 Hrs. OF TEMPERING AT DIFFERENT DRAW TEMPERATURES, A-3 SERIES, THIN AND THICK SPECIMENS, OQ AND AQ CASES.

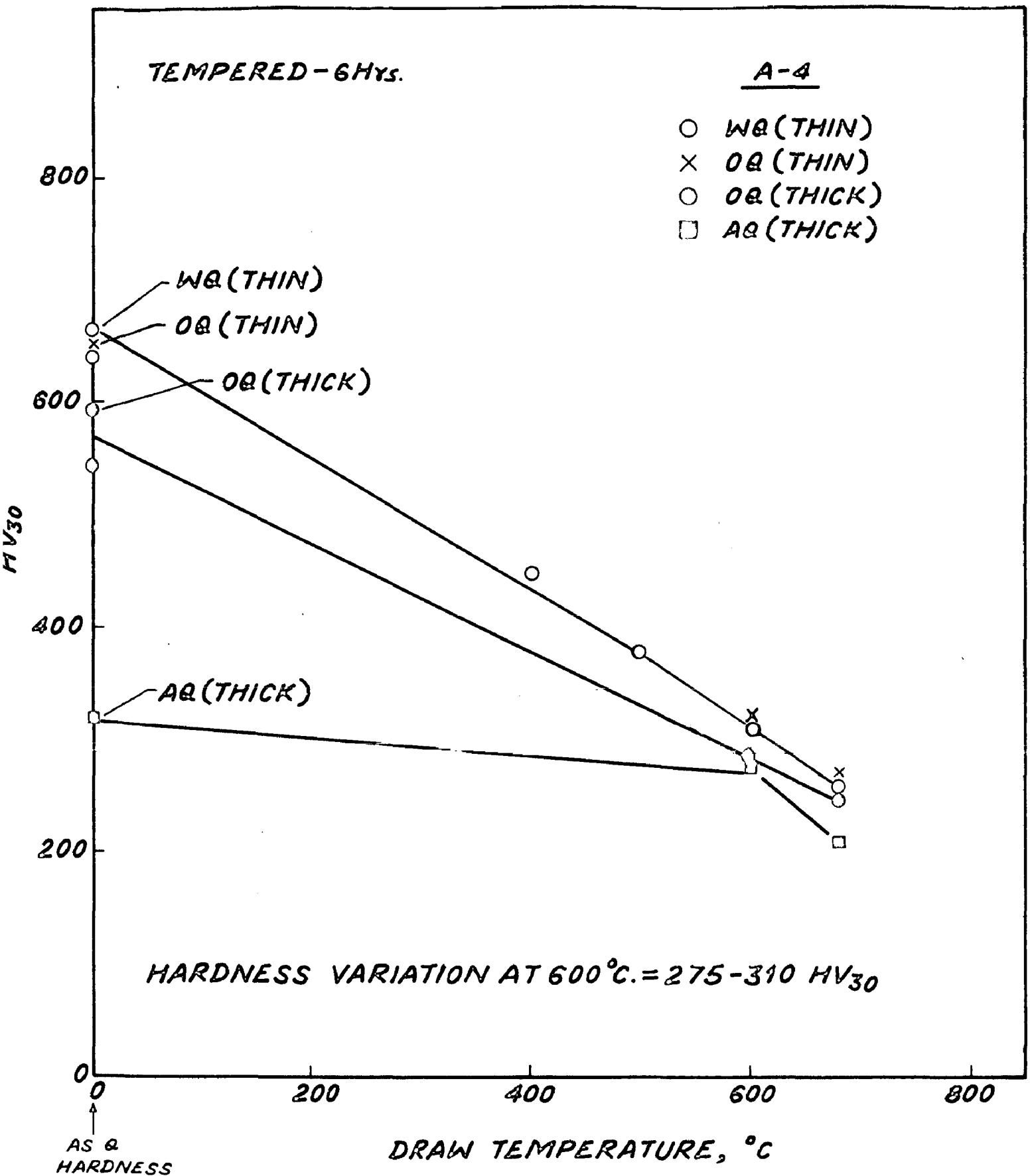


FIG.7-32 VARIATION IN HARDNESS OBTAINED AFTER 6 Hrs. OF TEMPERING AT DIFFERENT DRAW TEMPERATURES, A-4 SERIES. THIN AND THICK SPECIMENS, WQ, OQ AND AQ CASES.

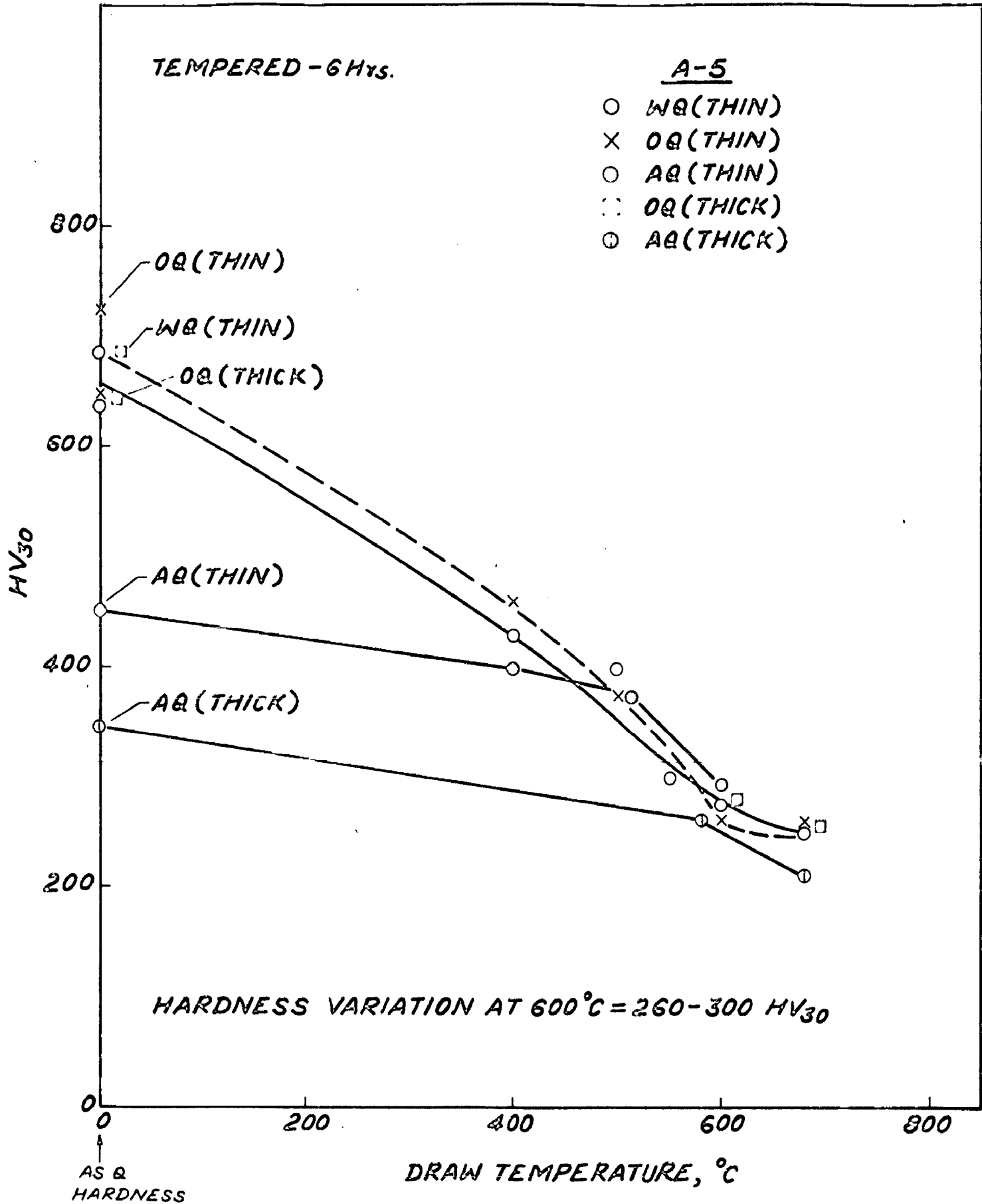


FIG.7-33 VARIATION IN HARDNESS OBTAINED AFTER 6 Hrs. OF TEMPERING AT DIFFERENT DRAW TEMPERATURES, A-5 SERIES, THIN AND THICK SPECIMENS, WQ, OQ AND AQ CASES.

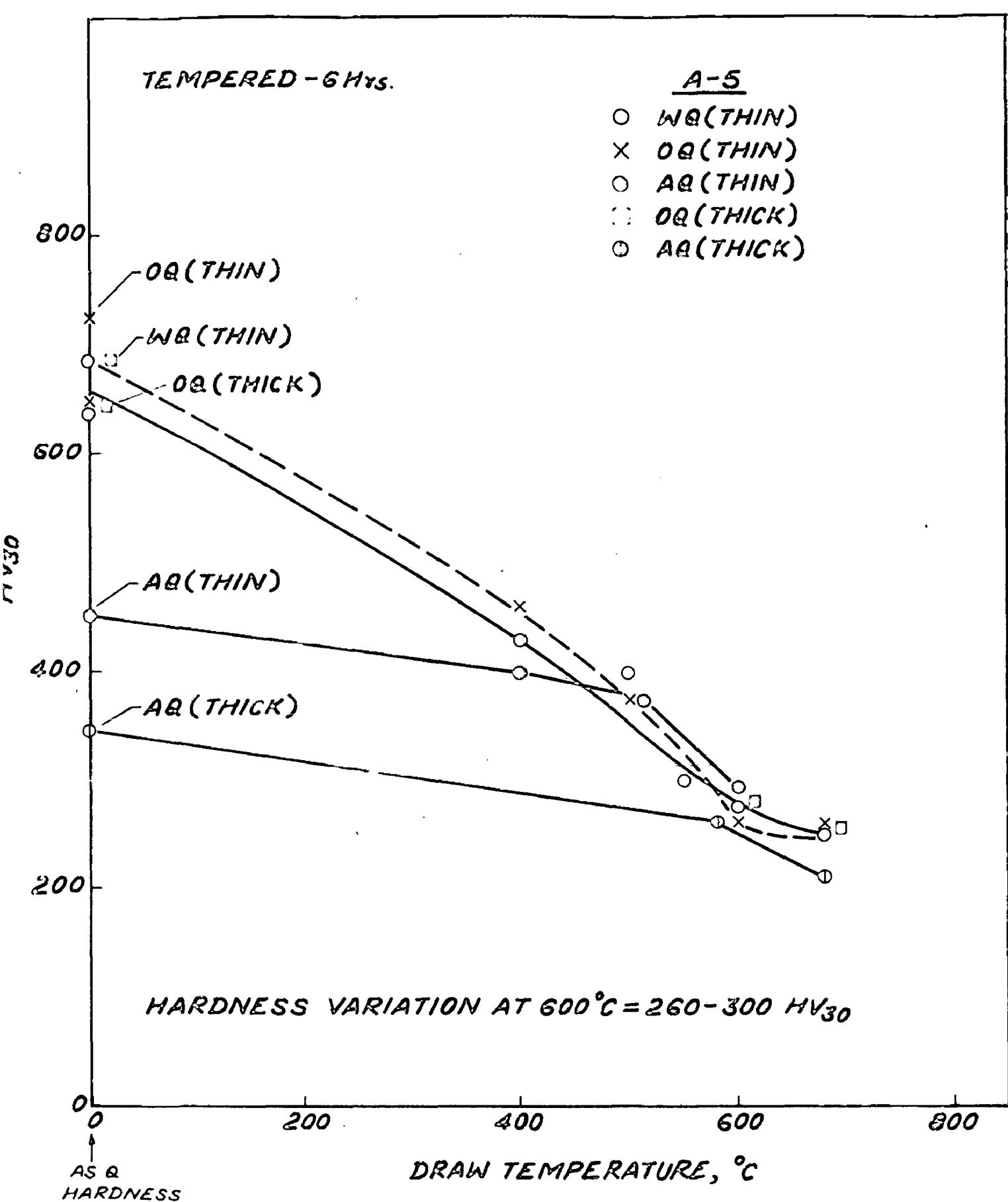


FIG.7-33 VARIATION IN HARDNESS OBTAINED AFTER 6 Hrs. OF TEMPERING AT DIFFERENT DRAW TEMPERATURES, A-5 SERIES, THIN AND THICK SPECIMENS, WQ, OQ AND AQ CASES.

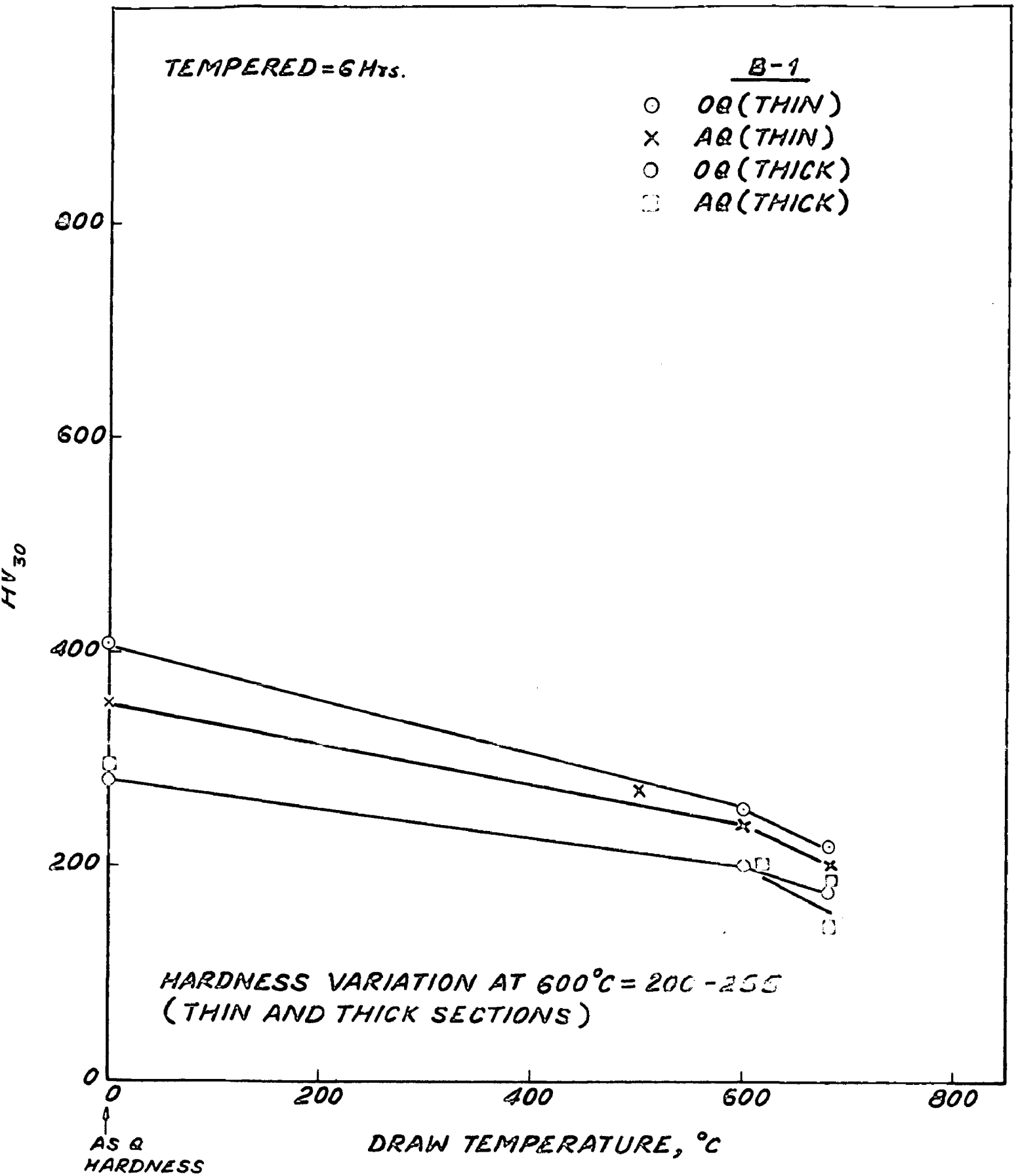


FIG. 7-34 VARIATION IN HARDNESS OBTAINED AFTER 6 Hrs. OF TEMPERING AT DIFFERENT DRAW TEMPERATURES; B-1 SERIES, THIN AND THICK SPECIMENS, OQ, AND AQ CASES.

RANGE OF DROP IN HARDNESS DURING TEMPERING BETWEEN 2 Hrs AND 6 Hrs AT 600°C (THIN AND THICK SPECIMENS)

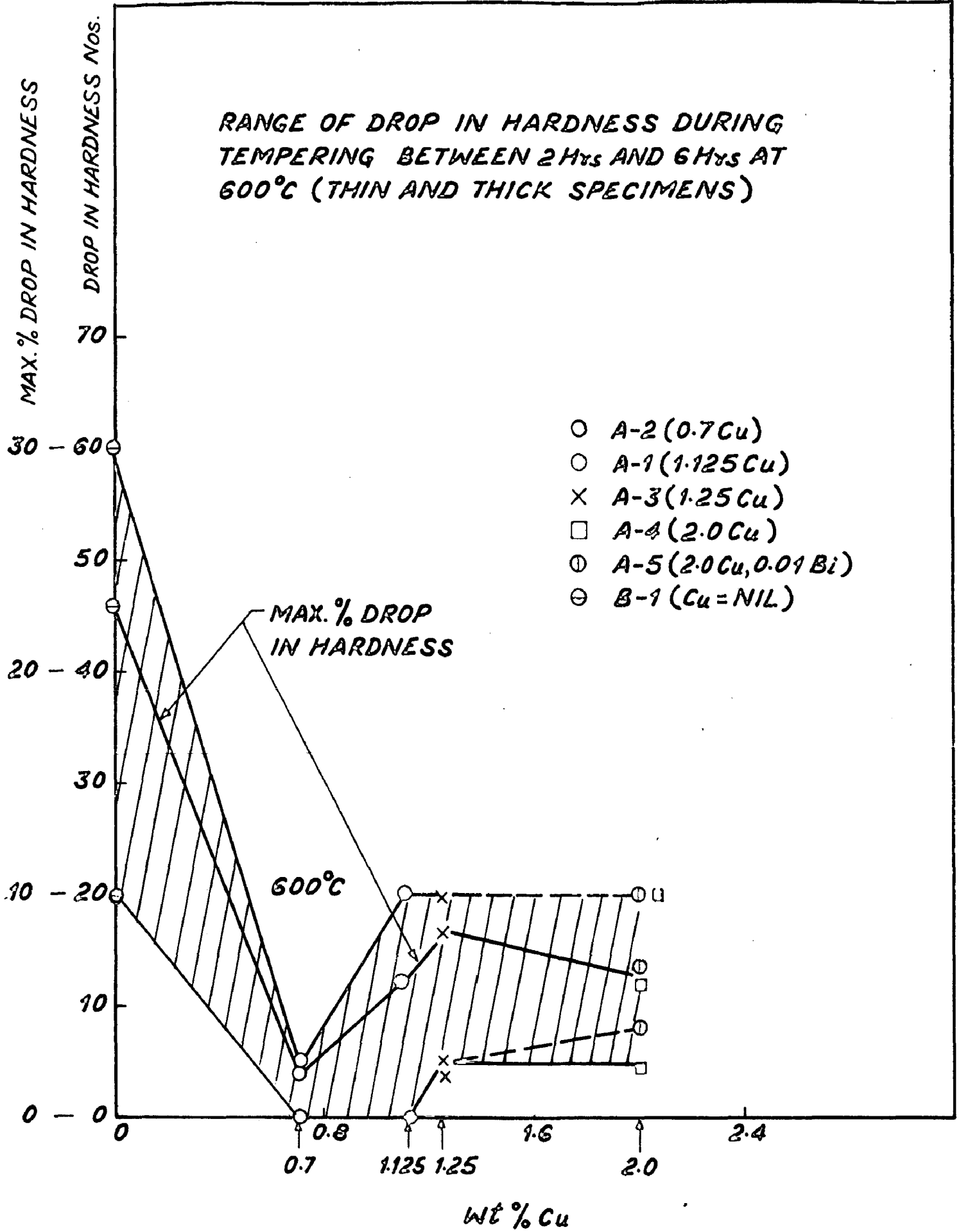


FIG.7-35 RANGE OF DROP IN HARDNESS BETWEEN 2 Hrs. AND 6 Hrs. OF TEMPERING AT 600°C IN UNALLOYED AND Cu ALLOYED CASES, THIN AND THICK SPECIMENS, A@, W@ AND O@ CASES CONSIDERED.

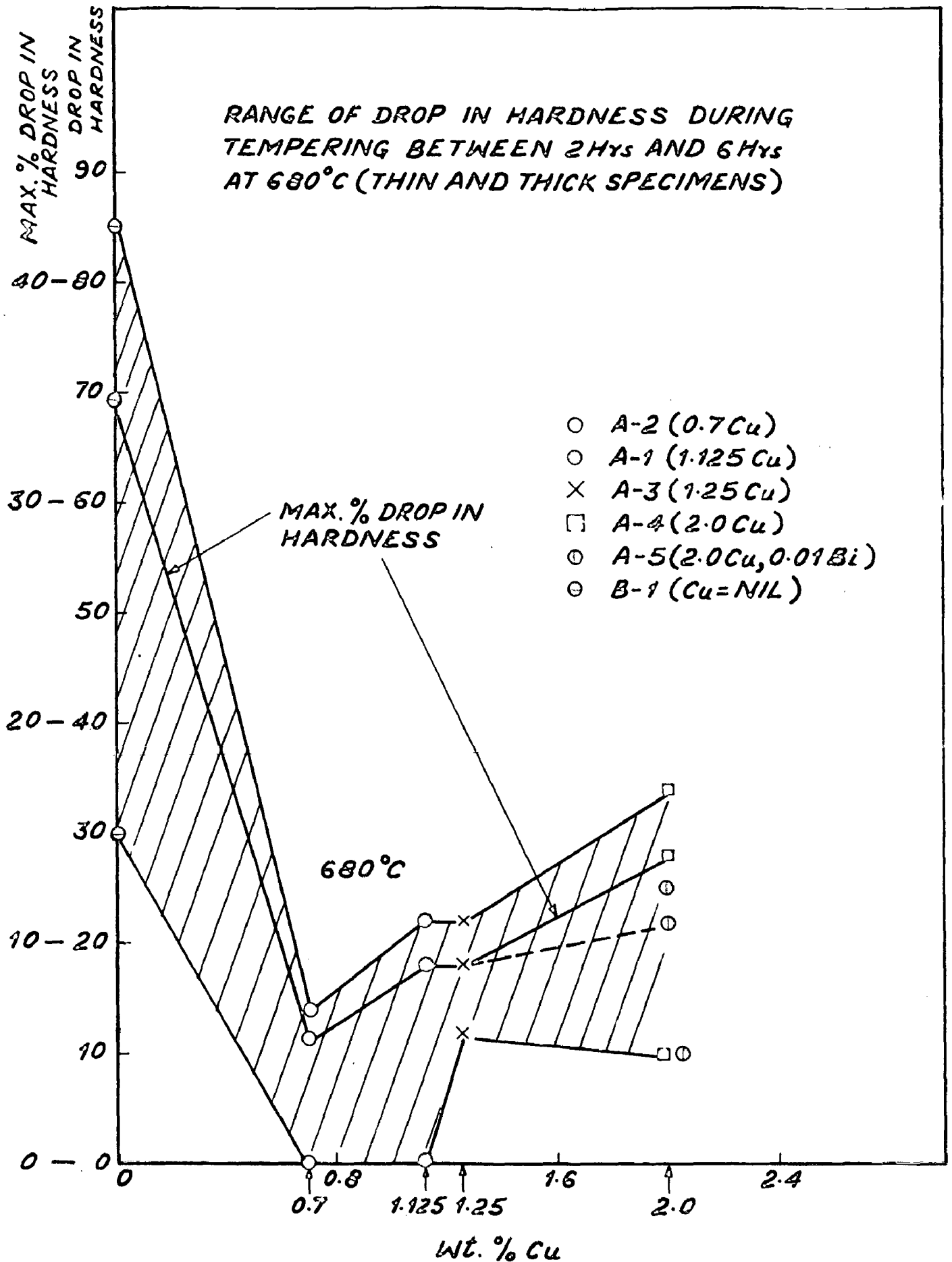


FIG. 7-36 RANGE OF DROP IN HARDNESS IN UNALLOYED AND Cu ALLOYED CASES DURING TEMPERING AT 680°C BETWEEN 2 Hrs. AND 6 Hrs., THIN AND THICK SPECIMENS CONSIDERED.

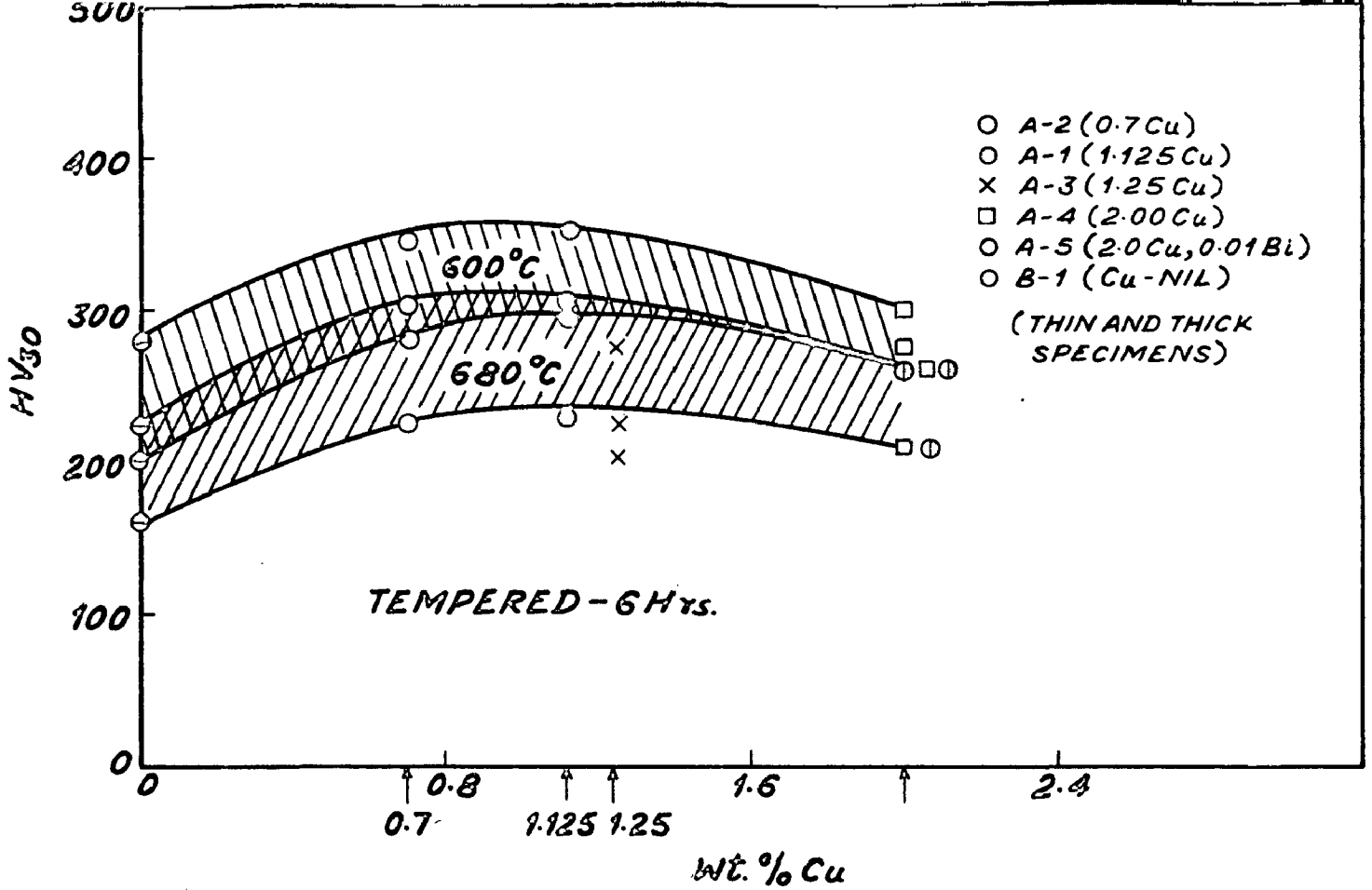


FIG. 7-37. RANGE OF HARDNESS VARIATION AT DIFFERENT Cu CONTENTS OF BASE WHITE-IRON; THIN AND THICK SPECIMENS, A@, W@ AND O@ CASES; TEMPERED AT 600 & 680°C FOR 6 Hrs.

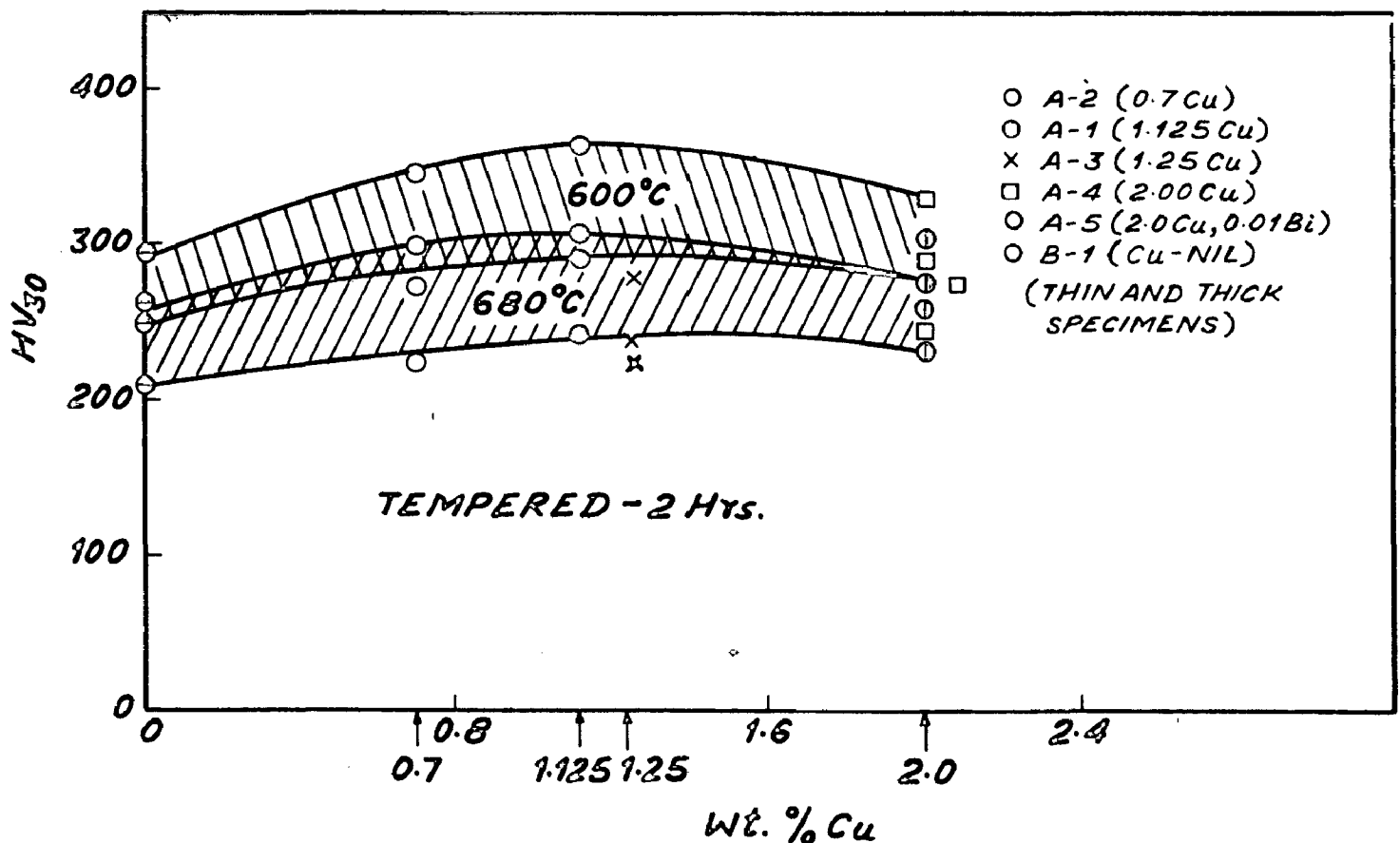


FIG. 7-37. RANGE OF HARDNESS VARIATION AT DIFFERENT Cu CONTENTS OF BASE WHITE-IRON; THIN AND THICK SPECIMENS, A@, W@ AND O@ CASES, TEMPERED AT 600 AND 680 FOR 2 Hrs.

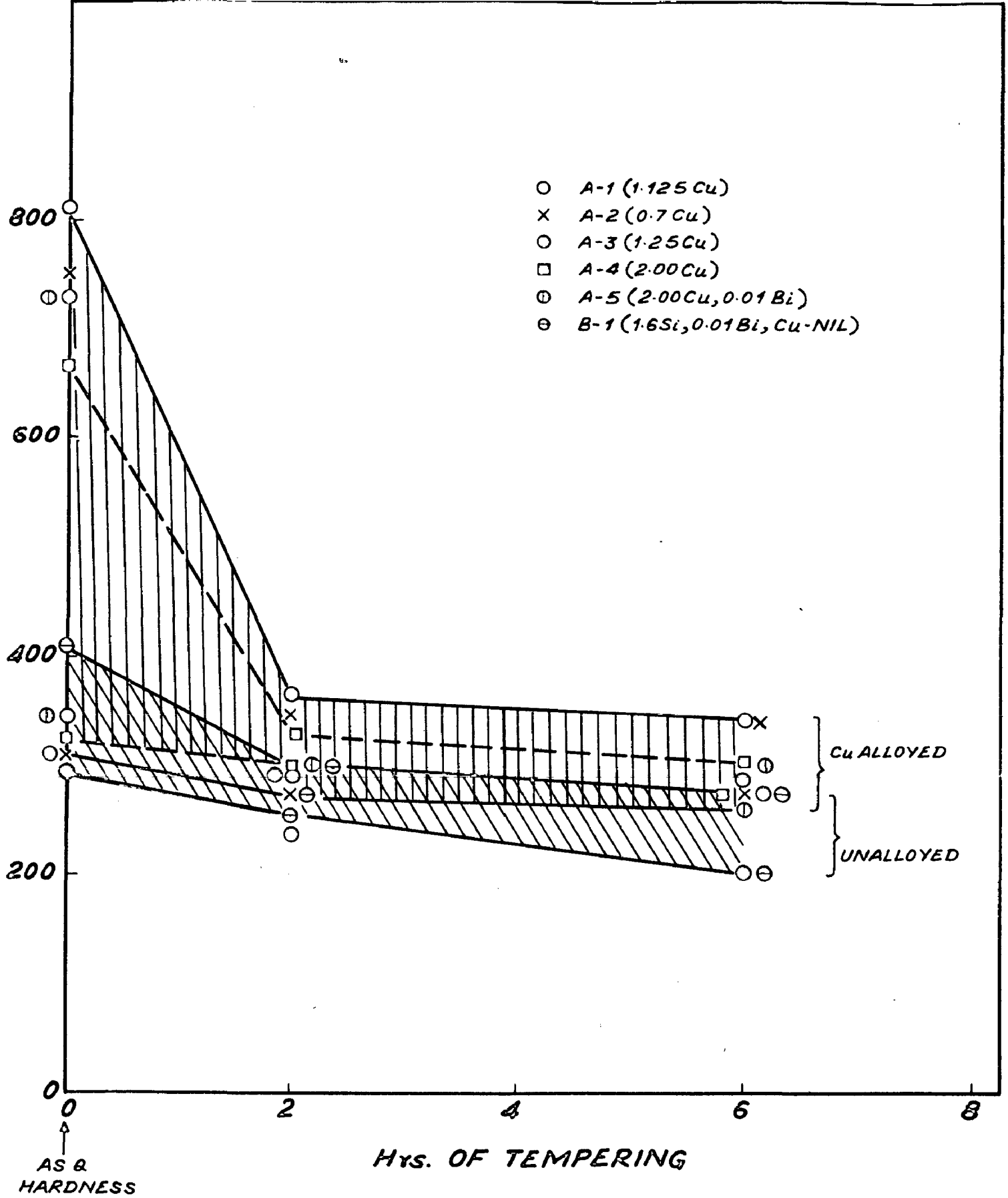


FIG. 7-38 RANGE OF HARDNESS VARIATION DURING TEMPERING AT 600°C, AQ, OB AND WQ CASES, THIN AND THICK SPECIMENS.

These observations show that highest tempered hardness is obtained between 1.0 and 1.2 wt % copper content of base alloy, both at 600° and 680°C draw temperatures as well as at 2 and 6 hrs. of draw periods.

These tempering characteristics indicated that a draw temperature of 600°C and a draw period of about 2hrs. would be adequate to yield a hardness of 290-320 HV₃₀ in most cases. Tempered hardness in this range would be expected to yield high strength pearlitic malleable irons. A variety of microstructures may be associated with this hardness range, which are discussed in subsequent sections.

Tables 7-11 and 7-12 show the drop in hardness between 2 and 6 hrs. of tempering in different cases at 600°C and 680°C respectively. These results have been plotted in Figs. 7-35 and 7-36. Simultaneously, percentage drop in hardness numbers was calculated from these values. This factor has been recorded and plotted in respective tables and graphs, referred to above. These observations show that the minimum drop in hardness between 2 and 6 hrs. of tempering occurred at 0.7 wt% copper content of the base alloy, both at 600° and 680°C draw temperatures. It can be seen from Figs. 7-35 and 7-36 that the extent of drop in hardness corresponding to 0.7 wt % copper content, was larger at 680°C compared to the one obtained at 600°C. The drop in hardness increases to a maximum of 20 points at 600°C corresponding to 1.125 wt % copper content and thereafter

it becomes constant. While, this drop in hardness continues to increase at 680°C beyond 0.7% copper content. Consequently, the minima in maximum % drop in hardness was associated with 0.7 wt% copper content, both for 600°C as well as for 680°C draw temperatures. Also, the drop in hardness, found in case of unalloyed composition was much more ^{large} compared to the one found in case of copper alloyed compositions; both at 600°C as well as at 680°C draw temperatures.

7.4.2.2 Mechanical Properties

Mechanical properties of unalloyed and copper alloyed pearlitic malleable irons have been summarised in Table 7-14. Tensile specimens for these studies were prepared using the 'continuous pearlitic malleable heat-treatment process' described by P.B.Burgess⁽¹¹⁰⁾. Influence of copper content on the mechanical properties of air-quenched and tempered pearlitic malleable irons is shown in Fig.7-39. Fig. 7-40 shows the influence of copper content on the mechanical properties of air, water and oil quenched and tempered pearlitic malleable irons. Only minimum and maximum value have been plotted on both these graphs, revealing the range of variation in individual properties.

Fig. 7-39 shows that optimum mechanical properties result at about 1.1 wt% copper content. Nearly 81 to 84 kgs/mm² UTS is developed in air-quenched and drawn pearlitic malleable at this copper content with corresponding Y.S.value

TABLE 7-14

MECHANICAL PROPERTIES OF UNALLOYED AND ALLOYED PEARLITIC MALLEABLE IRONS.

Sl. No.	Alloy	Heat Treatment	Mean Hardness HV ₃₀	Specimen Dimensions		Max. Load kgs.	Load in Kgs.				UTS kgs/mm ²	R E S U L T S		Pot. Elongation	YS/UTS Ratio
				Gauge dia mm.	Gauge length mm.		0.1% off-set kgs.	0.2% off-set kgs.	0.5% off-set kgs.	Y.S. kgs/mm ²					
										0.1%		0.2%	0.5%		
1	0-8	WQ	281	4.41	16.05	1000	980	-	-	-	65.41	64.13	-	4.5	0.97
		OQ	297	4.53	16.00	670	650	-	-	-	41.46	40.22	-	3.3	0.97
		AQ	307	4.52	16.00	680	-	-	-	-	42.08	-	-	4.0	-
2	0-10	WQ	279	4.55	16.05	920	-	860	900	-	56.56	52.87	55.33	5.2	0.93
		OQ	317	4.57	16.00	1030	1015	-	-	-	62.77	61.85	-	4.4	0.98
		AQ	310	4.58	16.05	1280	-	1160	1240	-	77.66	70.38	75.23	5.87	0.9/0.96
				4.56	16.00	1030	-	1018	-	-	63.04	62.31	-	4.50	0.98
3	B-1 (0% Cu + 1.63% Si + 0.02% Bi)	WQ	295	4.58	16.00	760	-	-	-	-	46.11	-	-	3.8	-
		OQ	304	4.54	16.00	800	760	-	-	-	49.39	46.92	-	3.8	0.94
				4.57	16.00	1020	-	950	-	-	62.16	57.89	-	4.8	0.93
				4.54	16.00	910	880	-	-	-	56.19	54.33	-	4.0	0.96
		AQ	306	4.57	16.00	1025	-	-	-	-	62.47	-	-	5.25	-
				4.46	16.05	1150	-	1040	1120	-	73.58	66.54	71.66	6.30	0.9/0.97
				4.50	16.00	995	-	-	-	-	62.53	-	-	-	-
4	A-1 (1.125% Cu)	OQ	288	4.51	16.00	1280	-	1050	1150	-	80.1	-	71.96	6.75	0.82/0.84
		AQ	311	4.57	16.05	1210	-	1025	1100	-	73.8	-	67.1	6.75	0.84/0.91
				4.52	16.00	1300	-	1260	-	-	80.98	-	-	5.65	0.96
				4.56	16.00	1360	-	1240	-	-	84.00	-	-	5.90	0.91
5	A-2 (0.7% Cu)	WQ	301	4.55	16.04	1210	-	1060	1140	-	74.38	-	70.08	6.87	0.87/0.91
		AQ	306	4.56	16.00	1225	-	1060	1100	-	75.00	-	67.32	6.87	0.86/0.88
				4.53	16.00	1300	-	1100	1200	-	80.6	-	74.42	6.3	0.84/0.91
				4.56	16.05	1250	-	1050	1200	-	76.51	-	73.45	5.6	0.83/0.91

Table continued

Table 7-14 (continued)

1	2	3	4	5	6	7	8	9	10	11	12	13	14	15	16
6	A-3 (1.25% Cu)	WQ	301	4.60	16.00	1080	-	-	-	64.96	-	-	-	4.8	-
				4.52	16.00	1025	980	-	-	63.85	61.05	-	-	4.5	0.95
		OQ	295	4.58	16.05	1000	-	-	-	60.67	-	-	-	4.4	-
		AQ	302	4.61	16.00	1030	-	-	-	61.68	-	-	-	4.3	-
				4.61	16.00	1040	-	-	62.28	-	-	4.5	-		
7	A-4 (2.0% Cu)	WQ	318	4.62	16.05	1000	-	980	-	59.62	-	58.2	-	4.2	-
		OQ	311	4.62	16.00	1300	-	1210	1285	77.52	-	72.1	76.6	6.0	0.93/0.98
				4.61	16.00	1130	1065	-	-	67.67	63.78	-	-	4.7	0.94
		AQ	306	4.61	16.05	1140	1065	-	-	68.27	63.78	-	-	5.0	0.93
8	A-5 (2.1% Cu + 0.02% Bi)	WQ	307	4.60	16.00	1280	-	1150	1230	76.99	-	69.17	73.98	6.4	0.89/0.96
		OQ	311	4.58	16.04	1140	1080	1120	-	69.17	65.52	67.95	-	5.4	0.94/0.98
		AQ	309	4.61	16.00	1220	1110	1160	-	73.06	66.47	69.47	-	5.3	0.9/0.95
				4.62	16.05	1300	-	1220	-	77.51	-	72.74	-	6.0	0.93

... Continued/-

NOTE-- (1) Heat Treatment

- (a) Quenched in water, oil, and Air subsequent to FSG completion and furnace cooling upto 850°C.
- (b) Tempered at 600°C to approximately 300 HV₃₀.

(2) Notations

WQ = water-quenched and tempered; OQ = Oil quenched and tempered.

AQ = Air quenched and tempered.

Chart speed = 10 cm/min.

(3) Instron M/C Operating Details

Cross head speed = 0.01 cm/min.

Resulting magnification on chart = 10/0.01 = 1000 X.

Load Range = 1-2 m.t.

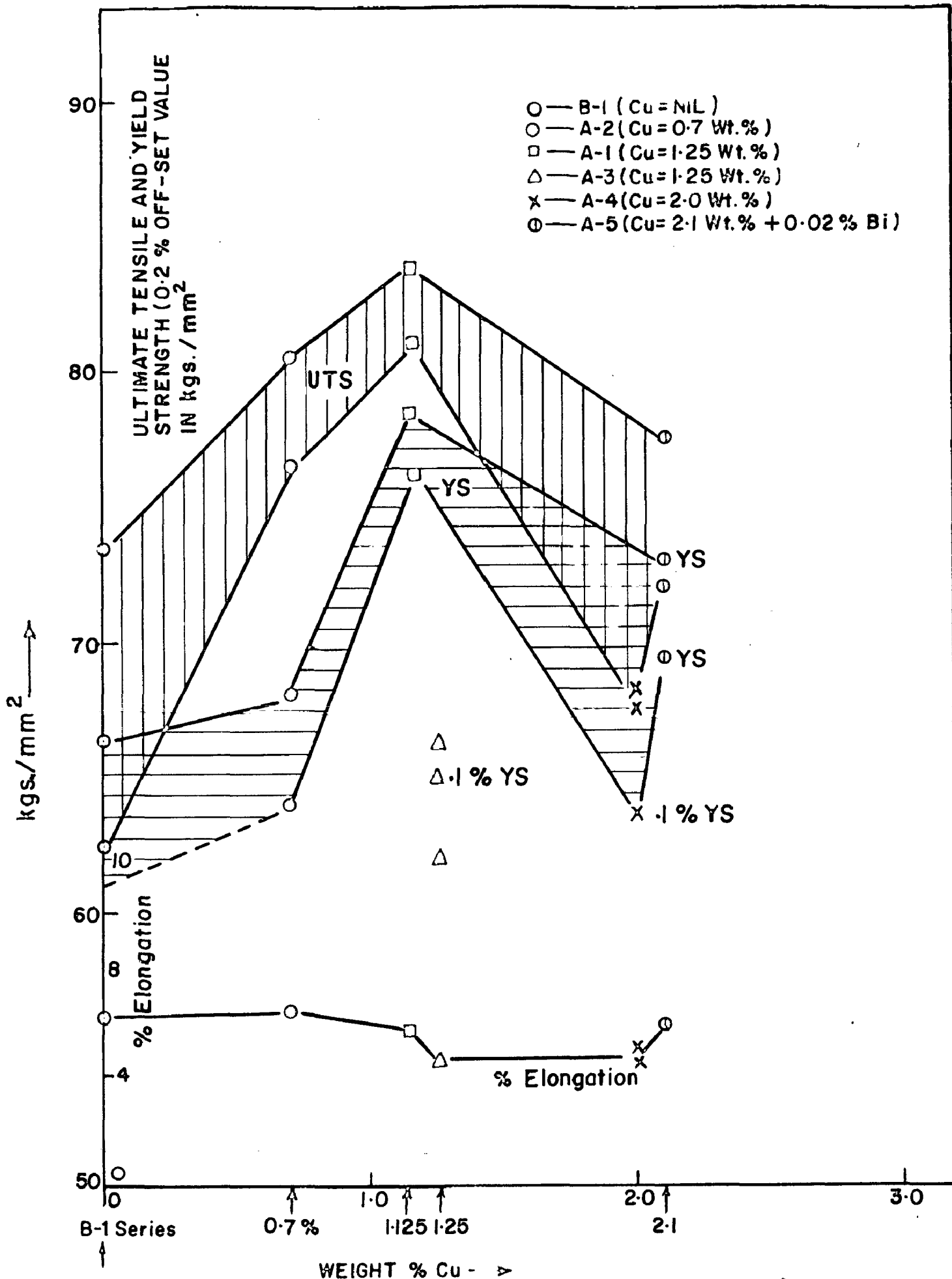


FIG. 7-39 INFLUENCE OF Cu CONTENT ON THE MECHANICAL PROPERTIES OF AIR-QUENCHED PEARLITIC MALLEABLE IRON, DRAWN AT 600°C BETWEEN 1 AND 2 HOURS.

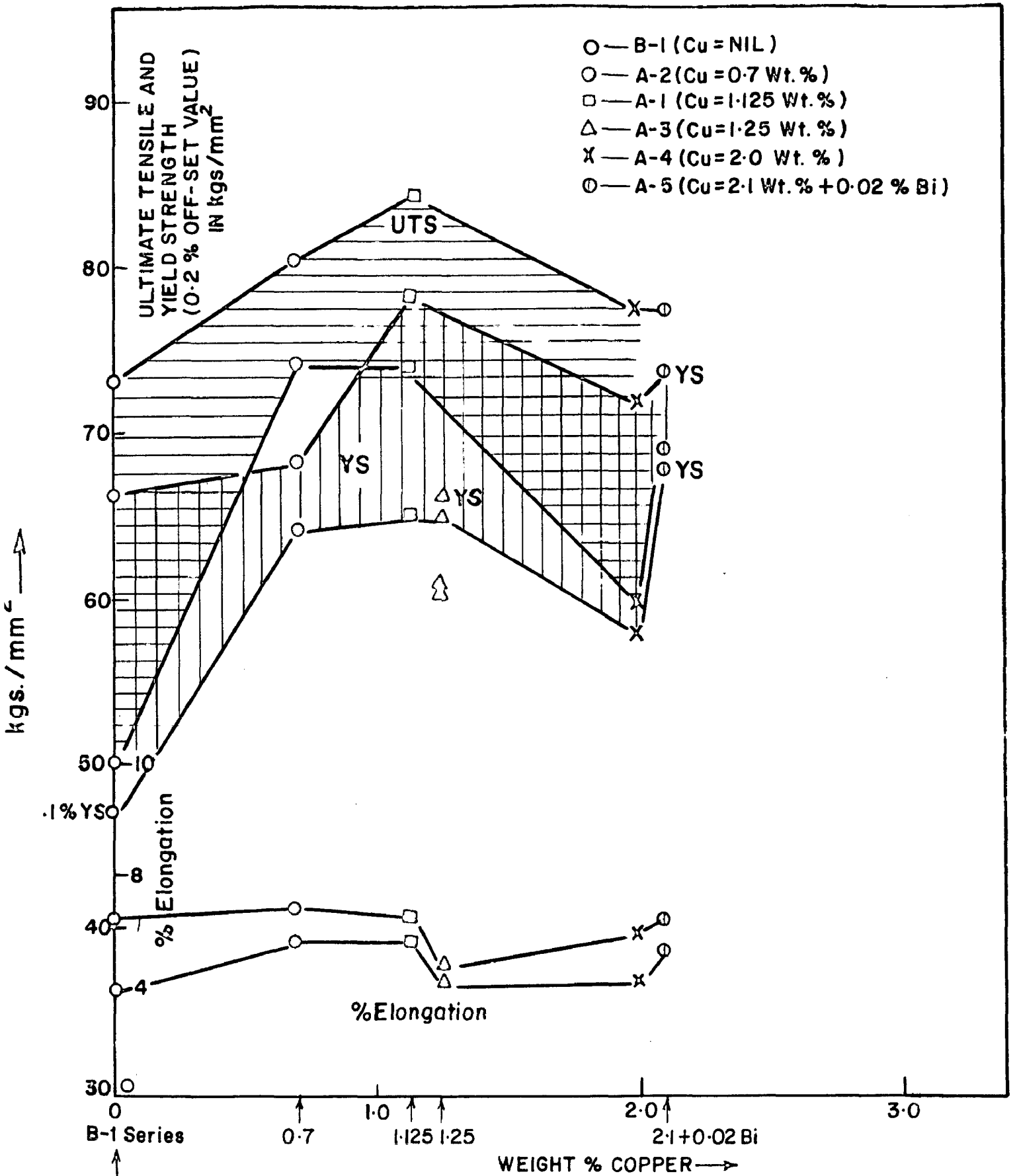


FIG. 7-40 INFLUENCE OF COPPER CONTENT ON THE MECHANICAL PROPERTIES OF AIR, WATER AND OIL QUENCHED PEARLITIC MALLEABLE IRONS, DRAWN AT 600°C BETWEEN 1 AND 2 HOURS.

of nearly 76 to 78 kgs/mm² and percentage elongation of nearly 6%. Resulting YS/UTS ratio in this case would be around 0.94. These properties would be superior to unalloyed pearlitic malleable of highest silicon content in this series, by nearly 13% in UTS and by nearly 16% in Y.S. at almost the same level of percentage elongation. Copper contents beyond 1.1 or 1.2 wt.% do not seem to yield any special advantage. Rather, the mechanical properties are found to deteriorate beyond this copper content. Results of this study are in agreement with the findings of P.B. Burgess⁽⁹⁰⁾ and B. Thyberg⁽¹²⁸⁾.

Fig. 7-40 shows the range of mechanical properties found in case of oil, water and air quenched specimens, tempered at 600°C between 1 and 2 hours. It can be seen that optimum mechanical properties were found again at nearly 1.1 wt% copper content. The UTS of this copper content was found to be nearly 15% higher than the maximum UTS obtained in case of unalloyed iron (B-1 series), while the yield-strength improved by nearly 12% at approximately the same percentage elongation (~6%). Improvement in the mechanical properties was, therefore, roughly of the same order as found in air-quenched and tempered cases. Spread in UTS as well as Y.S. values of unalloyed irons was found to be fairly wide compared to the one found in case of copper alloyed irons at about 1.1 wt.% copper content.

Data recorded in Table 7-14 and plotted in Fig. 7-40

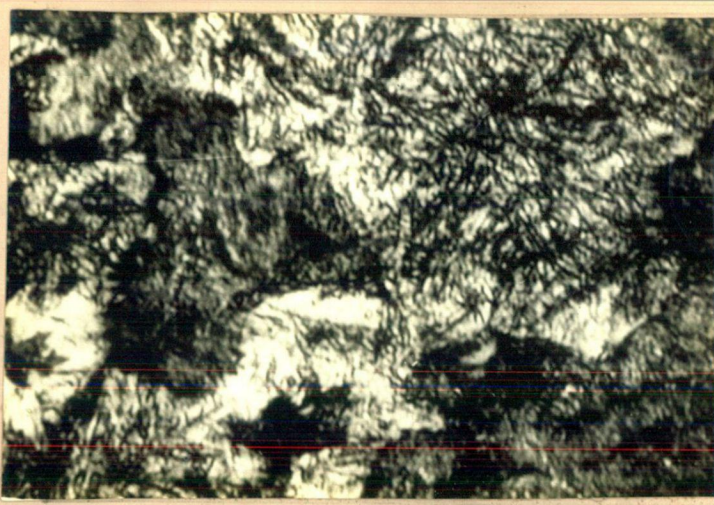
also show that the mechanical properties found in case of oil-quenched specimens is almost similar to the one found in case of air-quenched specimens within the limits of experimental errors.

7.4.2.3 Optical Microstructures

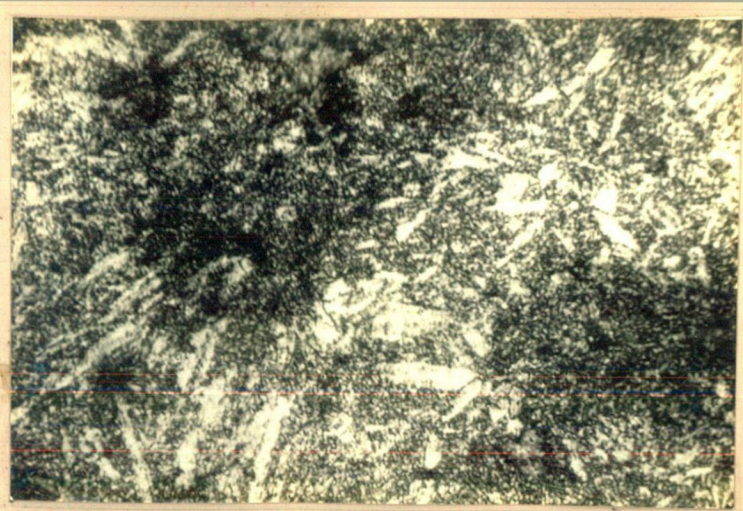
Microstructures shown in Figs. 7-41 to 7-46 give as quenched and tempered structures of unalloyed and copper alloyed tensile test bars of 15 mm dia. Individual figures show water, oil and air-quenched cases and their respective tempered structures. As stated earlier, all these specimens were tempered at 600°C in salt bath furnace for a duration of nearly 1 to 2 hours, subsequent to their FSG completion and furnace cooling upto 850°C, such that a tempered hardness of nearly 300 HV₃₀ was obtained in every case.

As expected, martensitic structures were produced on water-quenching in all the cases (Figs. 7-41 to 7-46). Also, martensitic structures were produced on oil-quenching in copper alloyed compositions. Unalloyed composition (B-1 series, Fig. 7-41), however, did not produce martensitic structure on oil-quenching. Instead, a fine pearlitic base-matrix was obtained on oil-quenching in this case. Pearlite formed on air-quenching in B-1 composition was coarser than the one formed on oil-quenching.

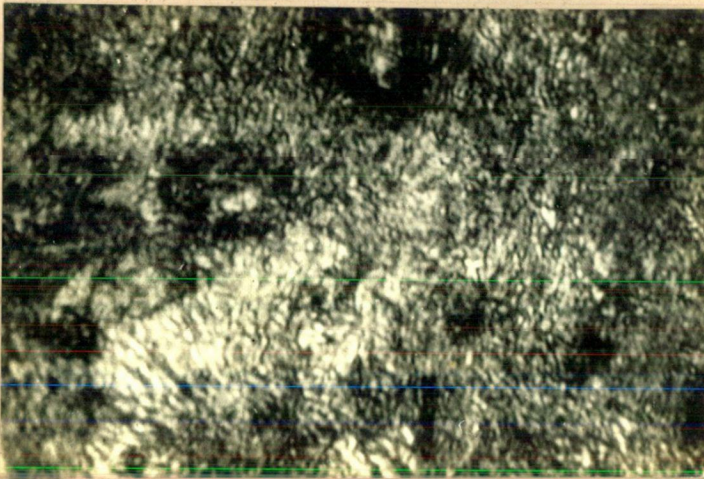
It can be seen from as-quenched and tempered microstructures of copper alloyed compositions (Figs. 7-42 to 7-46), that alloys containing 1.0%, or more copper, yield martensitic structure on oil quenching. Alloys containing 2.0 wt % copper



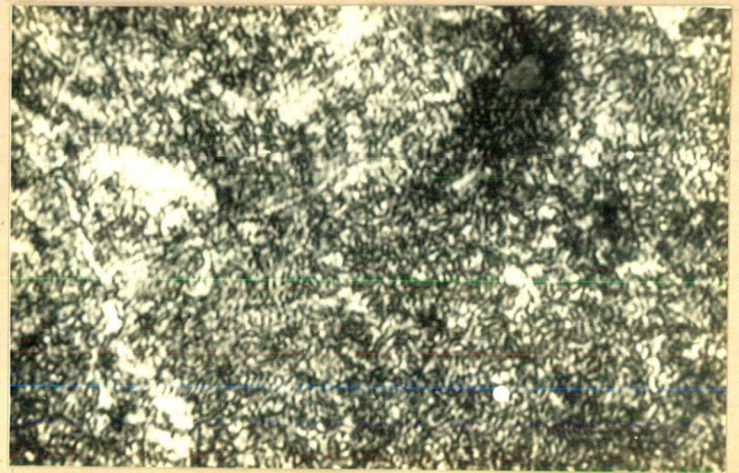
Water quenched, X 1000



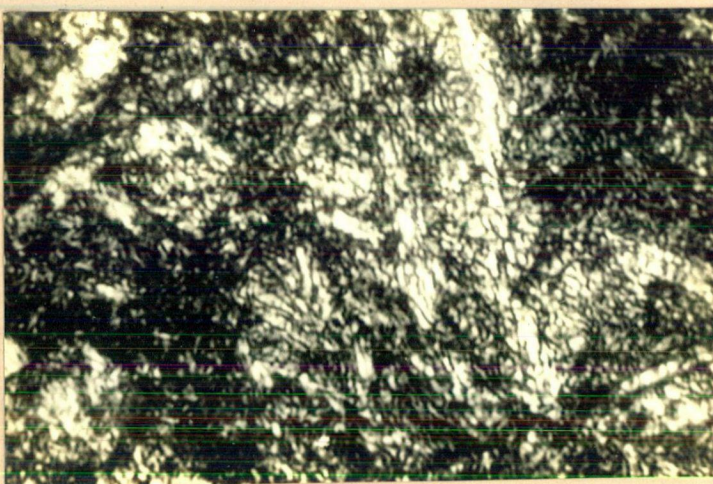
Tempered, X 630



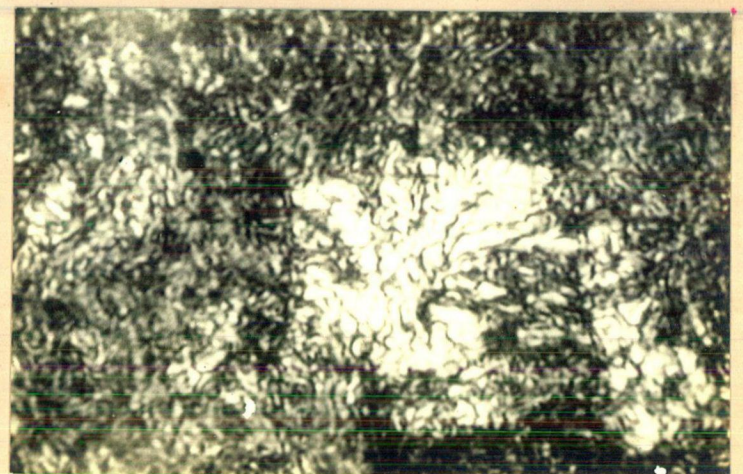
Oil quenched, X 1000



Tempered, X 1000



Air quenched, X 1000

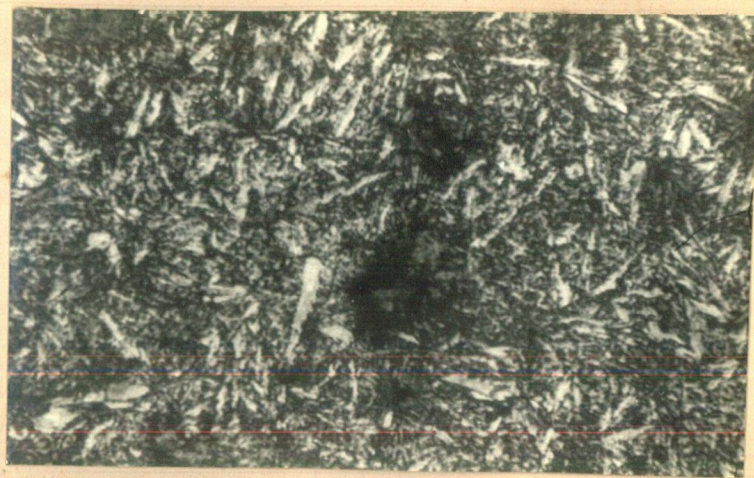


Tempered, X 1000

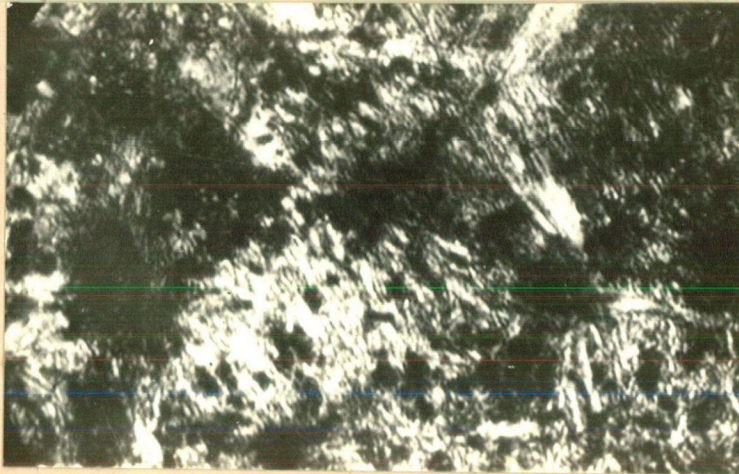
Fig. 7.41:- B-1, Air, Water and Oil quenched and tempered at 600°C between 1 and 2 hrs. subsequent to FSG completion and furnace cooling upto 850°C .



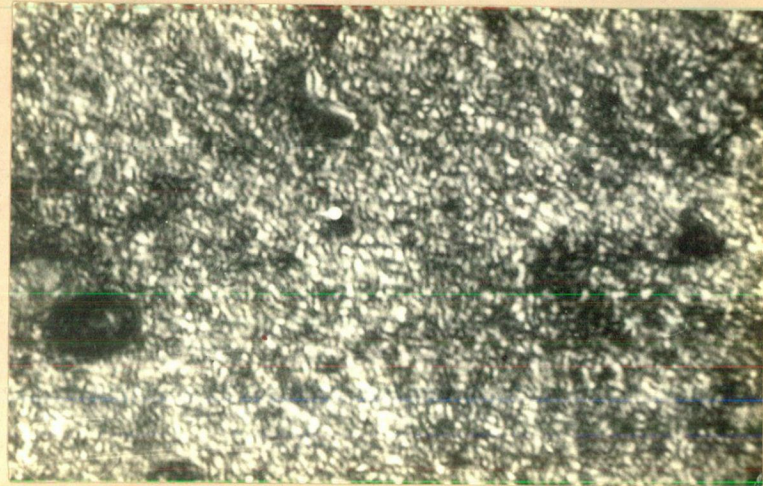
Water quenched, X 1000.



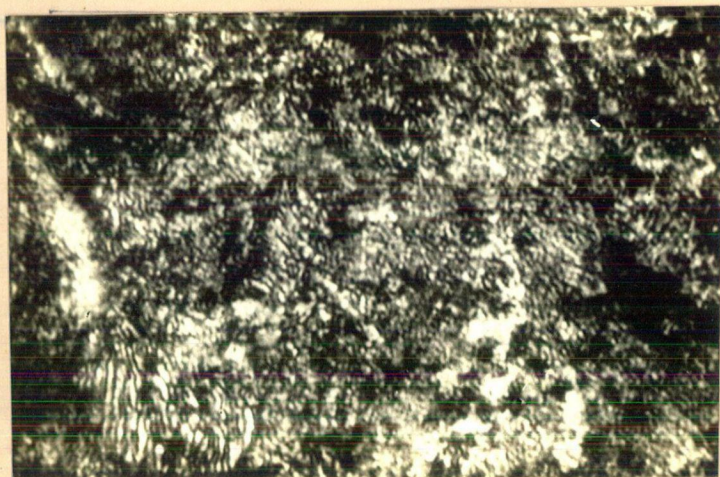
Tempered, X 250.



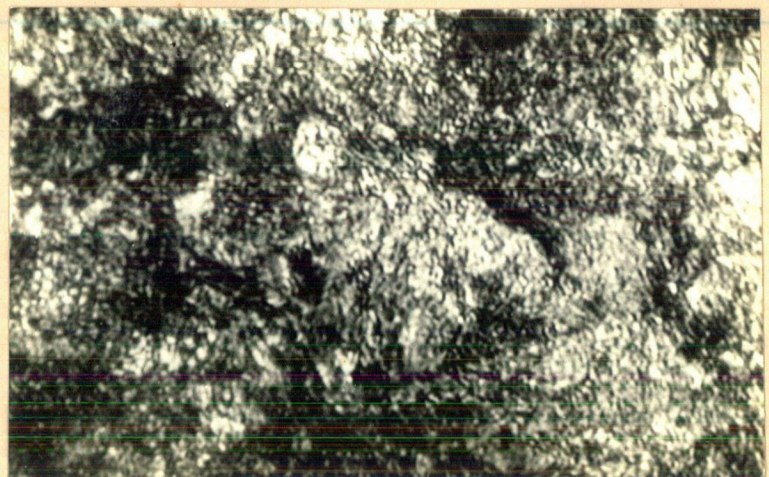
Oil quenched, X 1000



Tempered, X 1000

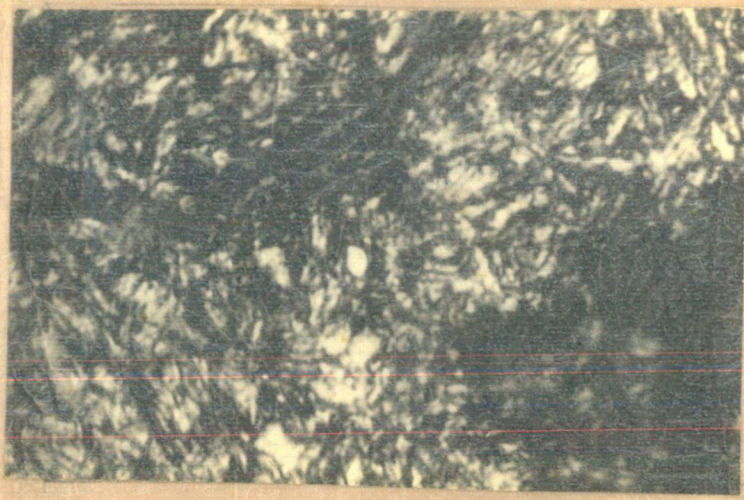


Air quenched, X 1000

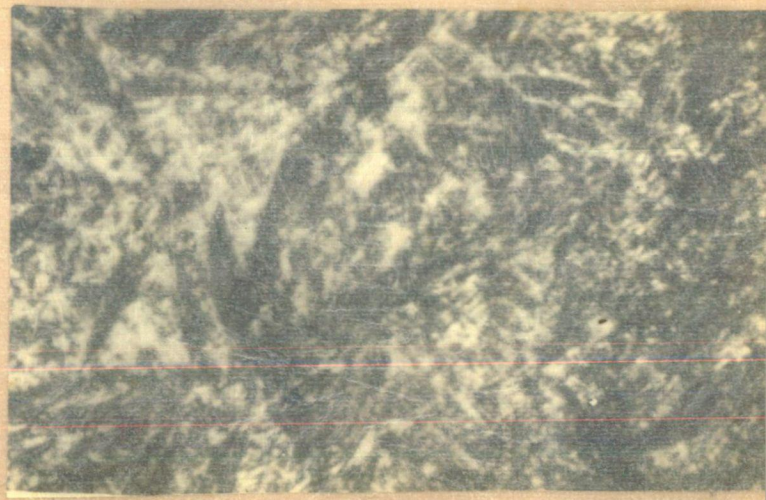


Tempered, X 1000

Fig. 7.42:- A-1, Air, Water and Oil quenched and tempered at 600°C between 1 and 2 hours subsequent to FSG completion and furnace cooling upto 850°C., 4% Nital etch.



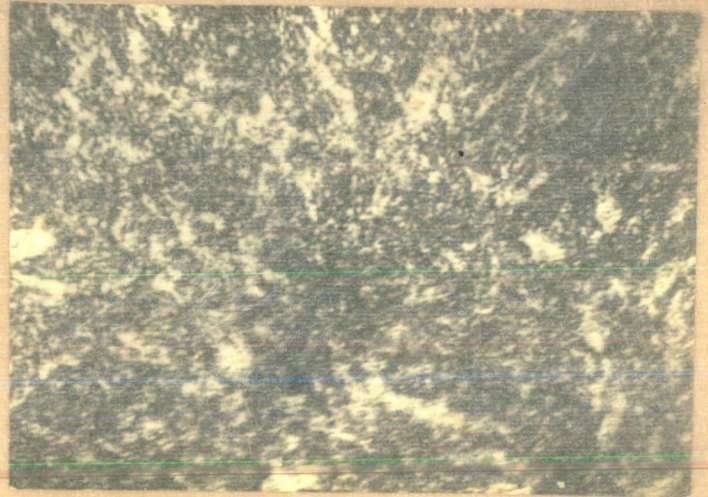
Water quenched, X 1000



Tempered, X 1000



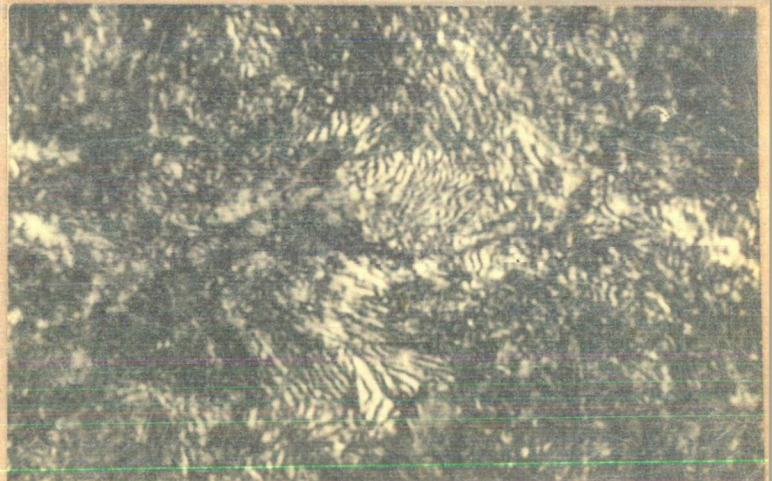
Oil quenched, X 1000



Tempered, 6X 630



Air quenched, X 1000

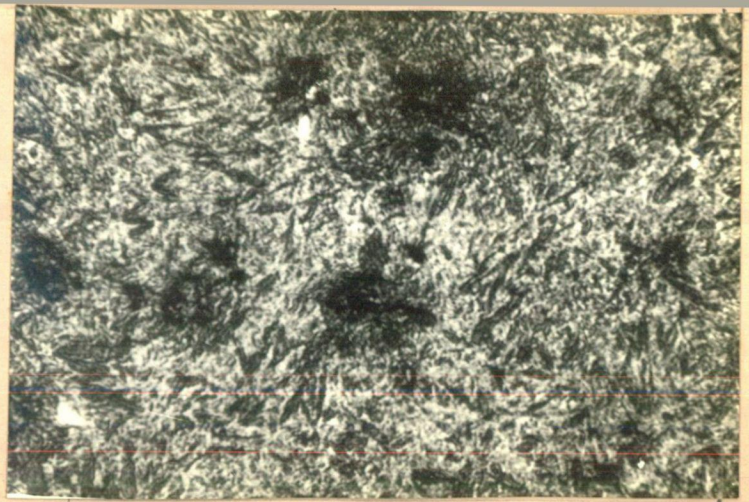


Tempered, X 1000

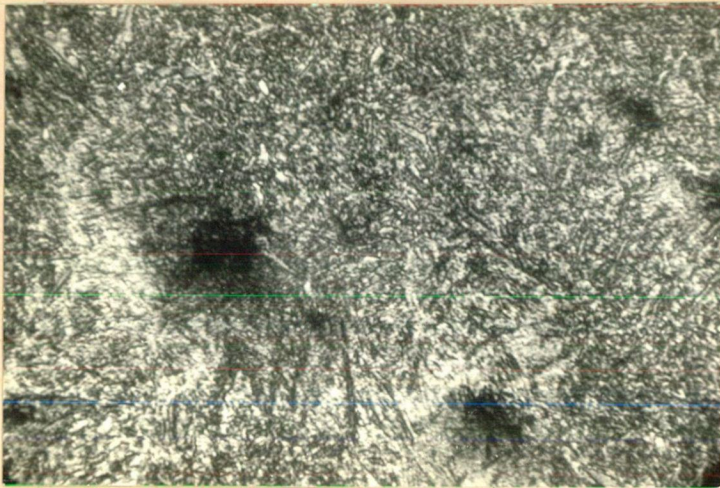
Fig. 7.43 - A-2; Air, Water and Oil quenched subsequent to FSG completion and furnace cooling upto 850°C . Tempered at 600°C between 1 and 2 hrs. Etched 4% Nital.



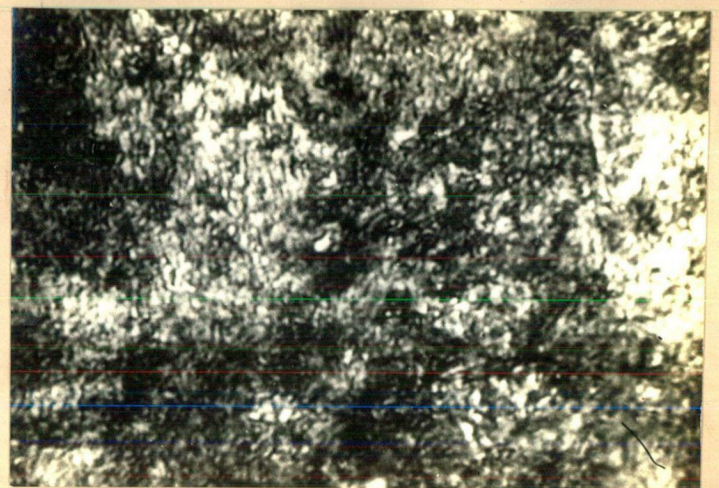
Water quenched, X 1000



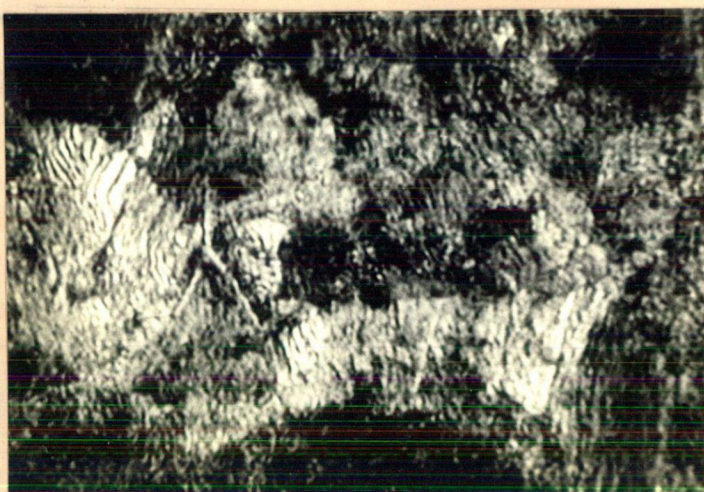
Tempered, X 250



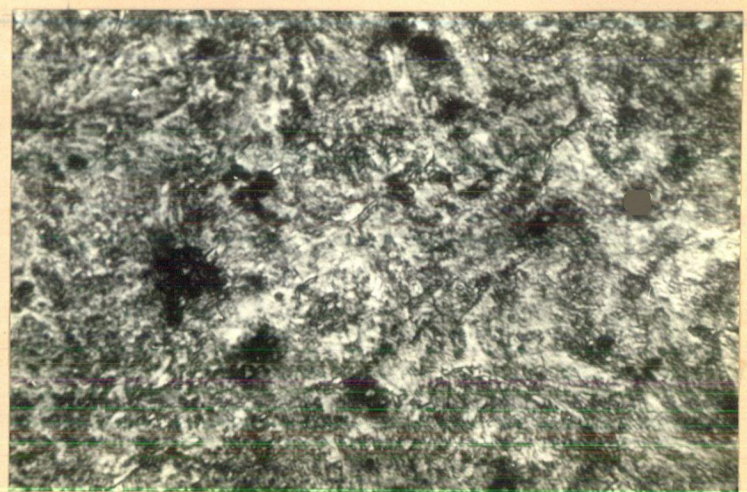
Oil quenched, X 250



Tempered, X 250

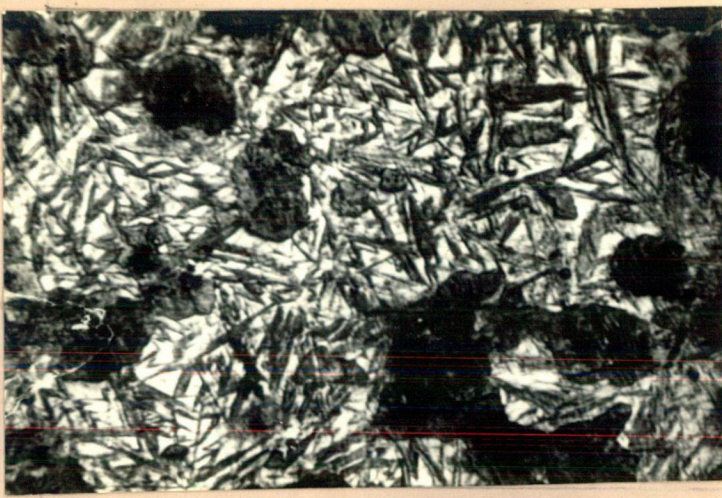


Air quenched, X 1000

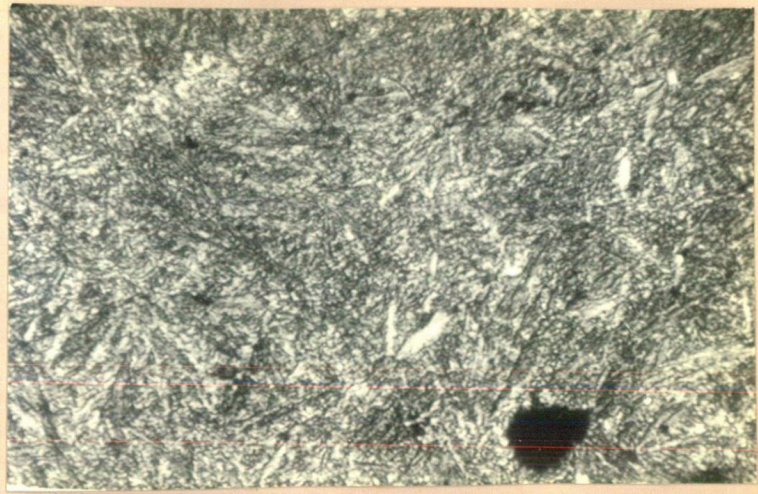


Tempered, X 250

Fig. 7-44:- A-3, Air, water and oil quenched subsequent to FSG completion and furnace cooling upto 850°C Tempered at 600°C between 1 and 2 hrs. etched-4% Nital



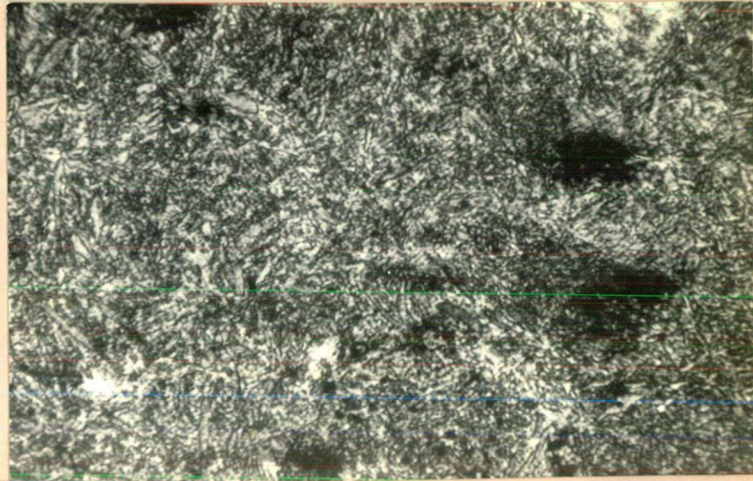
Water quenched, X 250



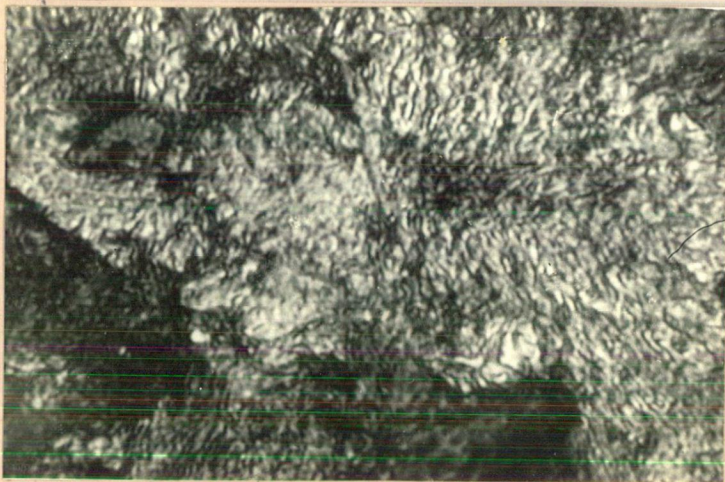
Tempered, X 250



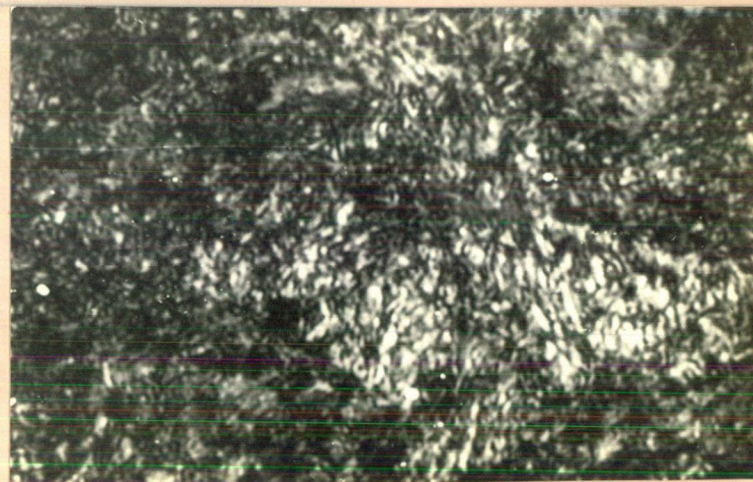
Oil quenched, X 1000



Tempered, X 250

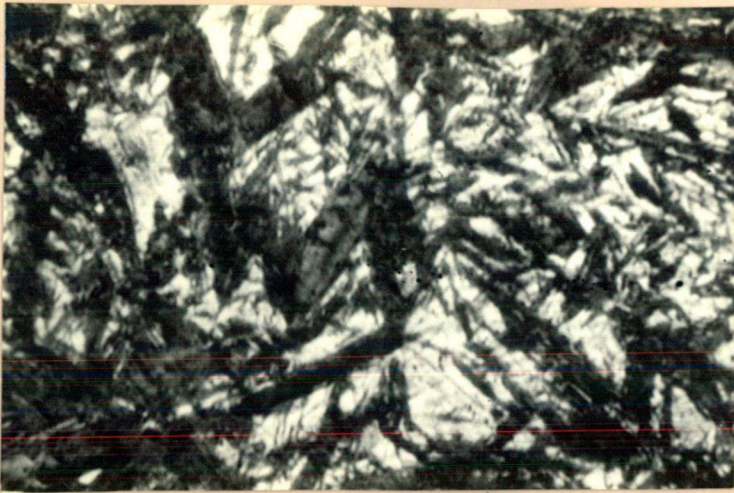


Air quenched, X 1000

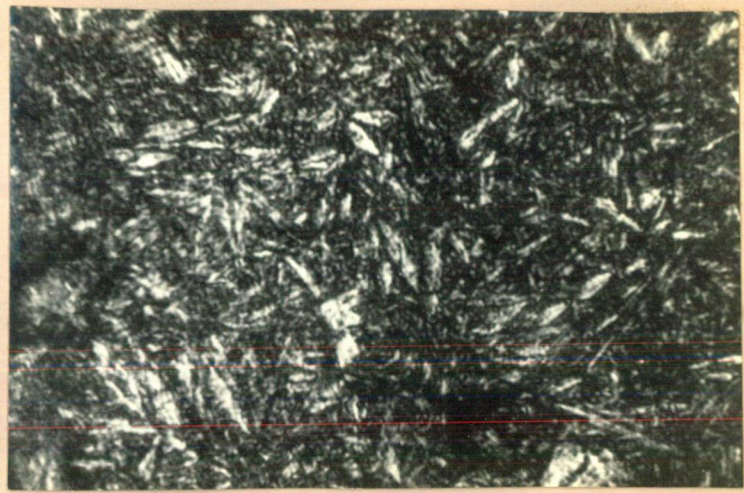


Tempered, X 1000

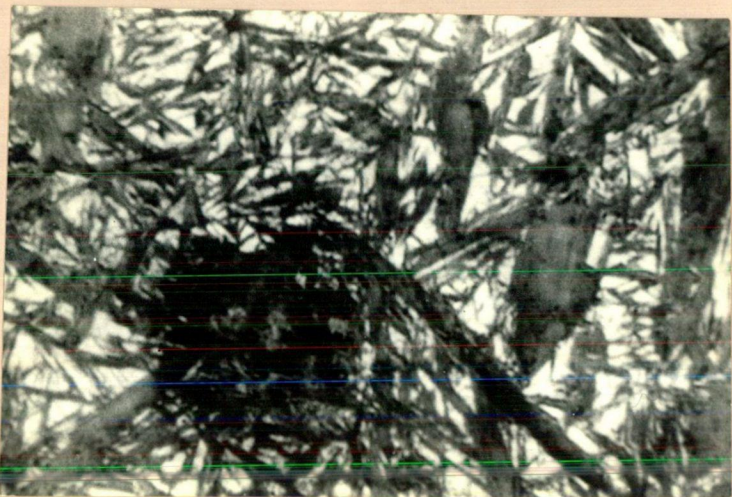
Fig. 7-45 - A-4, Air, Water and Oil quenched subsequent to FSG completion and furnace cooling upto 850°C. Tempered to 300 ± 5 HV₃₀ at 600°C between 1 and 2 hrs. Etched, 4% Nital.



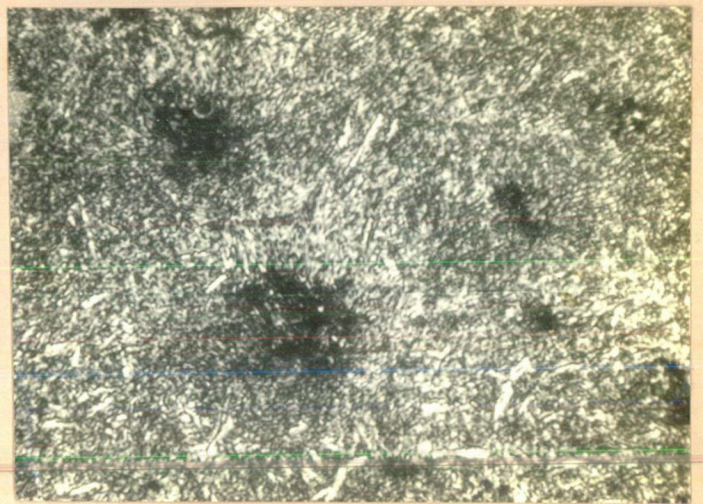
Water quenched - 1000 X



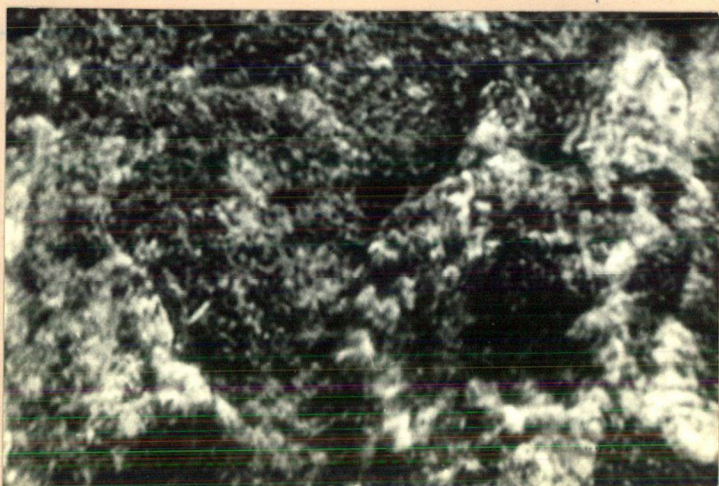
Tempered - 250 X



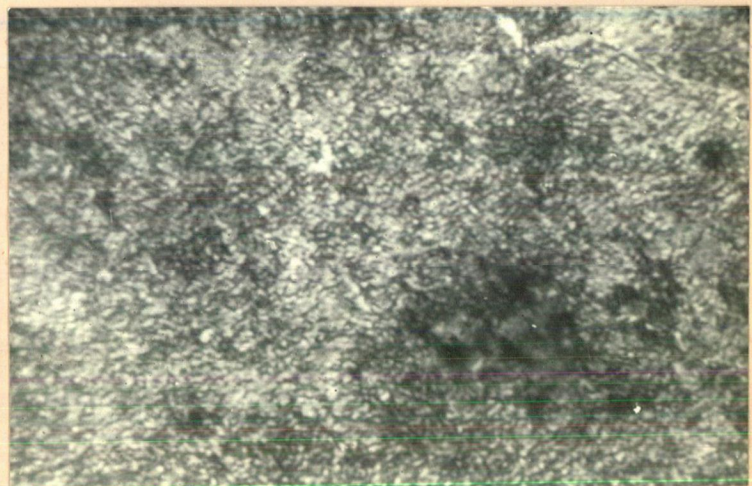
Oil quenched - 1000 X



Tempered - 250 X

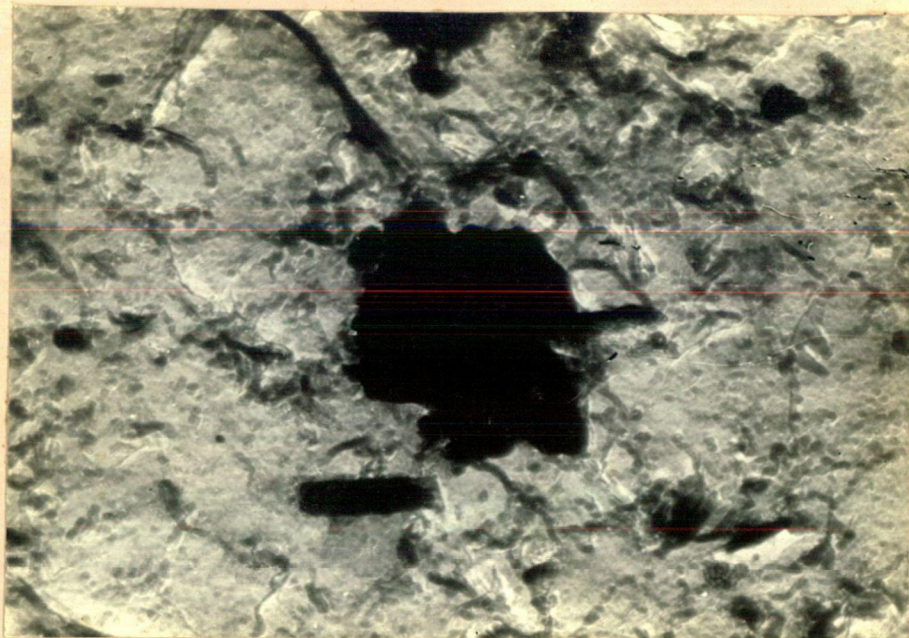


Air quenched - 1000 X

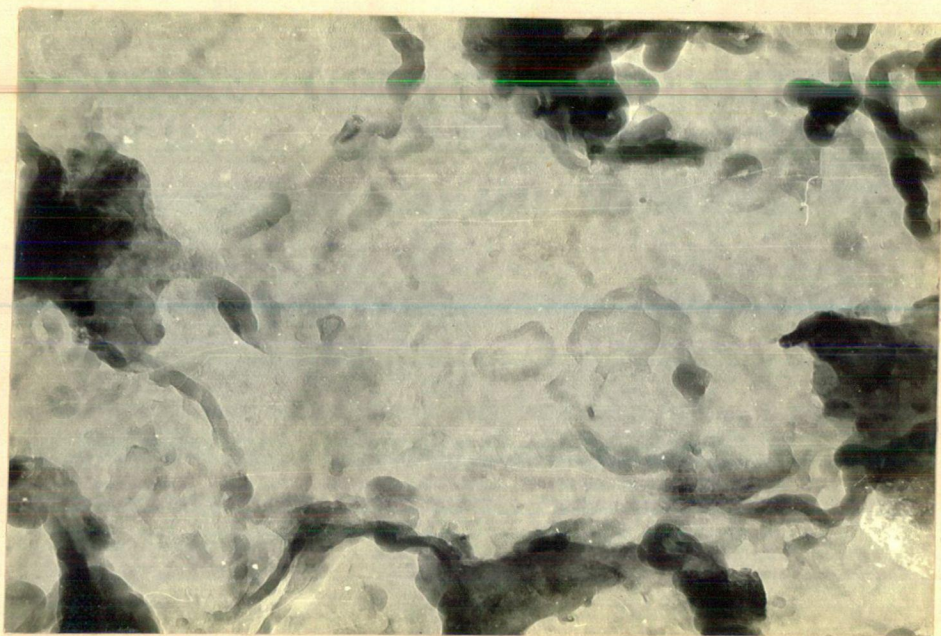


Tempered - 1000 X

Fig. 7-46 - A-5; Air Water and Oil quenched subsequent to FSG completion and furnace cooling upto 850°C. Tempered between 1 and 2 hrs. Etched 4% Nital.



Tempered -1/2 hour X 17,000.



Tempered - 9 hours X 35,000.

Fig. 7.47 - Replica-Electron micrographs.
A-5, Oil quenched subsequent to FSG
completion and furnace cooling at 850°C.
Tempered at 600°C 4%. Nital etch.

yield fully martensitic structures in 15 mm dia. specimens on oil-quenching. It can be seen from these photo-micrographs that the martensitic network is not broken on tempering in case of water-quenched martensitic structures, except that the size of ferrite plates is reduced drastically on tempering. While in case of oil-quenched and tempered structures, the martensitic network is almost completely broken. Air-quenched and tempered microstructures invariably show fine pearlite in the base matrix in all the cases.

7.4.2.4 Replica Studies:

Fig. 7-47 shows the sub-structural details of A-5 specimens, oil quenched and tempered for short as well as for long durations. These electron-micrographs can be seen with reference to the optical micrographs shown in Fig. 7-46. Sub-structure in Fig. 7-47(a) shows the martensitic base-matrix with primary and secondary graphite nodules, while Fig. 7-47(b) shows the structure of the same specimen after 9 hours of tempering at 600°C . It can be seen that the base-matrix becomes relatively free from carbon after 9 hours of tempering at 600°C , and that the secondary nodules have diffused to the larger primary nodules, making the structure almost free from tiny secondary nodules, or it may be that several tiny secondary graphite nodules have diffused together to form larger nodules.

7.4.3 Discussion of Results

Depending upon the TTT characteristics of un-alloyed and alloyed pearlitic malleable compositions, a variety of microstructures shall be obtained on following different cooling rates from the austenitic temperature range. A typical TTT curve of unalloyed pearlitic malleable iron is shown in Fig. 3-2. It is clear from the results of present work that the increasing amounts of copper addition shift the TTT curve to the right compared to the unalloyed compositions. This has been shown in the microstructures of as-quenched specimens in different media viz. water, oil and air in case of unalloyed as well as alloyed compositions (Figs. 7-41 to 7-46). Only those compositions, which were alloyed with more than 1.0 wt % copper, yielded martensitic structure on oil quenching, while the unalloyed compositions or the alloys with less than 1.0 wt.% copper did not yield a martensitic structure on oil quenching. Thus, only fine pearlitic structures were produced on oil quenching in case of unalloyed compositions and the alloys, that contained less than 1.0 wt.% copper. This may be attributed to the fact that the manganese content of all these compositions was lying between 0.4 and 0.65 wt.% (medium level). Normally, the unalloyed compositions, that are intended to be made in pearlitic grades, are alloyed with 1.0-1.2 wt.% Mn in order to have better hardenability (111, 127-129, 133, 134, 141). In the present investigation, however, Mn was maintained at medium level, so that the influence of copper on hardenability-

and mechanical properties could be comparatively pre-dominant. It can be seen from Figs. 7-44 to 7-46 that copper contents beyond 1.1 wt.%, yield a fully hardened structure in 15 mm diameter rods on oil quenching. This effect is most predominant in alloys containing 2.0 wt.% copper contents (A-4 and A-5 alloys, Fig. 7-45 and 7-46).

Water-quenched structures, though fully martensitic in all the cases, are of little significance from practical view-point mainly because of the quench cracks, that will be expected to develop in actual geometries. Air-quenched structures were fine pearlitic, as expected, except that the degree of fineness of pearlite varied with the extent of alloying.

Figures 7-41 to 7-46 also show the corresponding tempered structures, drawn for nearly 2 hours at 600°C, such that a tempered hardness of nearly 300 HV₃₀ is obtained. Only expected microstructures are obtained on tempering in each case. It may be stated here that the intention in the present work was not to carry out the tempering to spheroidisation stage, since it was aimed to retain the hardness in the range of 300±5 HV₃₀ in all the cases, obviously because high strength would be associated with this hardness range.

Data summarised in Tables 7-9 to 7-13 and plotted in Figs. 7-23 to 7-38 show the tempering characteristics of unalloyed as well as copper alloyed pearlitic malleable

irons. The basic differences in the tempering characteristics of unalloyed and copper alloyed compositions have been brought out in Figs. 7-35 to 7-38. It is the age hardening characteristic of Fe-Cu system (Fig. 5-1), to which mainly, these differences may be attributed. The hardness is held at higher levels in copper alloyed compositions for the same temperature and duration of tempering, compared to the unalloyed composition, basically because of the precipitation-hardening characteristics of Fe-Cu system. Also, the drop in hardness between 2 and 6 hours of tempering at draw temperatures less than 600°C , is practically negligible in case of copper alloyed compositions, meaning that the hardness is virtually held constant between 2 and 6 hours of tempering in such cases. While, this is not the case with unalloyed compositions, since hardness continues to drop under similar tempering conditions stated above. It can be seen from Figs. 7-35 to 7-38 that the range of drop in hardness between 2 and 6 hours ^{of} tempering at 600°C is narrow in case of copper alloyed compositions compared to the unalloyed one. But this gap widens at 680°C even in case of copper alloyed compositions.

On quenching from 850°C , subsequent to FSG completion and furnace cooling upto this temperature, copper is held in super-saturation. As this structure is tempered at 600°C , there is an initial drop in hardness due to the decomposition of martensitic network, after which, the drop in hardness

is partly counter-balanced by simultaneous precipitation of copper from the base-matrix. The result is that the steep drop in hardness on tempering is partly checked, and if the tempering temperatures are 600°C or less, the hardness may be virtually held constant between 2 and 6 hours of tempering at these temperatures. But, if the tempering temperatures are higher than 600°C , the drop in hardness may continue to increase as tempering proceeds, since coarsening of copper precipitates may occur at higher temperatures like 680°C , for example. Therefore, such higher temperatures may not be favoured in practice for tempering of copper-alloyed compositions. Similar phenomenon was observed in S.G. irons, alloyed with copper, by S.Gupta et al. (152,153). Results of ~~the present work are also in agreement with the observations~~ of Mishra, Sharma and Anantharaman⁽¹⁶⁹⁾ on the tempering characteristics of copper bearing Ni-Cr steels. Also, it is already established that the precipitation hardening characteristics of Fe-Cu system can be usefully utilised in strengthening the base-matrix of either ferritic or pearlitic malleable irons (Section 5.2.2.7).

Advantage was taken of these typical tempering characteristics of copper bearing pearlitic malleable irons in the present study, in order to retain a hardness of nearly $300 \pm 5 \text{ HV}_{30}$ in the tempered tensile-test specimens, after ~2 hours of tempering at 600°C . However, an average tempered hardness of $300 \pm 5 \text{ HV}_{30}$ was aimed in all un-alloyed and copper alloyed tensile specimens.

It is significant that the best mechanical properties were obtained between 1.1 and 1.2 wt% copper contents of base iron (Fig.7-39 and 7-40) in all the cases of air, water and oil quenched tensile specimens. It may be stated here that the same alloy content (1.1/1.2 wt % Cu) was found optimum in the present work with respect to the FSG and percent shortening in FSG characteristics of copper bearing white irons. Also, the amount of copper partitioning to the eutectic cementite was found to be maximum at the same copper content of base white iron.

Results of the present work show that almost similar properties develop in air as well as in oil-quenched specimens. It is because, by and large, almost similar microstructures develop in tempered specimens of air and oil quenched cases, except when the copper content exceeds 1.25 wt% and approaches 2.0 wt%. As stated earlier, oil quenched structures in 15 mm dia rounds containing 2.0 wt% Cu shall be martensitic and shall, therefore, yield intermediate structures of martensitic hardening on tempering. Tempering was not carried to the stage of spheroidisation in the present work, since it was aimed to produce only high strength pearlitic malleable irons in the UTS range of 84 to 85 kgs/mm² with reasonable percentage elongation. The percentage elongation obtained at 1.12 wt% Cu content (A-1 series, Fig.7-39 and 7-40) was nearly 6.0% corresponding to a UTS value of 83 kgs/mm² in air-quenched and tempered state. Similar percentage elongation was found in

unalloyed composition too, but it was corresponding to a lower UTS value of 73.6 kgs/mm² in air-quenched and tempered state (Table 7-14). These results are in agreement with the findings of previous workers like P.B. Burgess⁽⁹⁰⁾, B.Thyberg⁽¹²⁸⁾ and Heine et al.⁽⁸⁹⁾. Higher percentage elongation found at higher UTS value in case of copper alloyed compositions has been attributed by most workers to the fact that Cu reduces the size of temper carbon nodules and partly renders them spherical in shape.

Best mechanical properties found at about 1.1/1.2 wt% copper content in the present work are also in full agreement with the findings of earlier workers like P.B.Burgess⁽⁹⁰⁾ and B.Thyberg⁽¹²⁸⁾.

'Interrupted annealing' or what is known as 'continuous pearlitic malleable heat-treatment process'⁽¹¹¹⁾, was considered the most suitable technique for the manufacture of high-duty pearlitic malleable iron castings. This technique was used in the present work since another important aim of the present work was to reduce the total processing period, and this technique was considered most suitable for the purpose because it does not involve any re-resolutionising period and therefore, some processing time is cut-down. However, strict controls on temperature, furnace atmosphere, quality of quench oils etc. are imperative for obtaining proper results by this technique.⁽¹¹¹⁾

7.4.4 Conclusions:

1. Drop in hardness of copper alloyed compositions between 2 and 6 hours of tempering at 600°C is almost negligible compared to the one obtained in case of un-alloyed compositions. This was mainly because of the precipitation of copper from the base-matrix, as tempering proceeds. Thus, the drop in hardness due to tempering is partly counter-balanced by simultaneous precipitation of copper from the base-matrix in case of copper alloyed compositions.

2. Copper alloyed compositions yield higher hardness values compared to unalloyed compositions for similar tempering temperatures and durations.

3. Almost similar mechanical properties were obtained in oil as well as air-quenched cases, since the ^{Mn} content in most alloys was of medium level.

4. Best mechanical properties were found between 1.1 and 1.2 wt % copper content of base-alloys.

5. Copper bearing compositions yield higher percentage elongation at high strength levels compared to un-alloyed compositions.

6. 'Interrupted annealing' process is considered most suitable for speedy manufacture of high duty pearlitic malleable irons.

7. Both the oil and air-quenched varieties of Cu alloyed pearlitic malleable iron were found to possess superior mechanical properties compared to the minimum strength requirements of 120-90-02 grade of S.G. Iron.

CHAPTER VIII

SUMMARY OF RESULTS:

1. Graphite is an integral part of cast white iron structures.
2. Formation of graphite nuclei is initiated during liquid to solid transformation. Their growth occurs partly due to their coagulation through diffusion near the eutectic temperature and partly due to partial decomposition of eutectic cementite in the temperature range of approximately 1140°C and 920°C on further cooling.
3. Presence of such tiny graphite particles (less than $5/6$ microns in size) at eutectic cementite/Austenite interface was not considered deleterious for the final mechanical properties.
4. Only those structures may be termed "Mottled", which develop very large irregular clusters of graphite of size not less than 100 to 200 μ (microns) so that these spots may be clearly visible to the naked eye. Such graphite formations are highly deleterious for the final mechanical properties.
5. Micro-hardness of eutectic cementite is not appreciably influenced by the increasing amounts of silicon or copper in the base melt or by a change in the section thickness of cast-white iron.
6. On getting thermally activated during pretreatments, relatively smaller graphite nodules would diffuse into

the larger nodules, causing their further growth. Many sub-microscopic graphite particles thus grow to the microscopic sizes. Therefore, a large number of optical sized graphite nodules appear on pre-treatment.

7. No "incubation period" is, therefore, required for the nucleation of graphite particles during either the pre-treatment or the first stage of graphitisation. Fundamentally, "incubation period" can not be defined in terms of microscopic sizes.
8. Graphitisers like Si and Cu cause a considerable increase in the number of nodules formed during pre-treatments. Maximum number of nodules were found at 1.4 wt % Si in unalloyed series and at 1.2 wt % Cu in copper bearing compositions.
9. Maximum percentage shortening in FSG period was obtained at ~1.4 wt % Si in unalloyed series, while this maxima was found at ~1.2 wt % Cu in copper bearing alloy (having constant 0.8/0.9 wt % Si) due to any pre-treatment. Only pre-baking treatment was considered suitable for industrial practice. Nearly 57% shortening in FSG period was obtained due to pre-baking at ~1.4 wt % Si content in unalloyed series. This value was found to be nearly 70% in case of copper bearing alloys at ~1.2 wt % Cu content. These results are valid for 10 mm. thick sections only.
10. Maximum amount of copper partitions to the eutectic

ementite phase at 1.2 wt % copper content, after which no further amount of copper partitions to the cementite phase. Increasing amounts of copper partition to the austenite phase as the average copper content of base alloy increases.

11. Copper content of either austenite or cementite phase of any alloy does not change with the progress of graphitisation at 920°C. Also, no appreciable segregation of copper was found in eutectic cementite phase of any alloy.
12. "Interrupted Annealing process" or what is known as the "Continuous pearlitic malleable heat treatment process" was found most suitable for making pearlitic malleable iron, considering both the mechanical properties of pearlitic malleable iron as well as the duration of processing.
13. Optimum mechanical properties were found in both oil as well as in air quenched and drawn conditions. Best mechanical properties were found again at ~1.1/1.2 wt % copper content of base alloy. Mechanical properties at this copper content were nearly 15% superior than the unalloyed compositions (B-1 series, 1.6% Si + 0.02% Bi) at the same average hardness of 300 ± 5 HV₃₀. Both these varieties were found to possess superior mechanical properties compared to 120-90-02 grade of S.G. irons.

14. Precipitation hardening characteristics of Fe-Cu system can be usefully utilised during the normal course of tempering process for strengthening the base-matrix. This phenomenon results in superior mechanical properties of copper alloyed compositions.
15. Copper was found to improve the yield strength and percentage elongation of pearlitic malleable irons.
16. 1.1/1.2 wt % copper content yeilds optimum results with regard to its effect on the graphitisation characteristics as well as on the mechanical properties of pearlitic malleable irons.

CHAPTER 9

SUGGESTIONS FOR FURTHER STUDIES:

1. Precise determinations of TTT and hardenability curves of alloys containing varying quantities of copper contents should be carried out. Such studies would be greatly useful for actual plant practice. This data could be ~~made~~ available in the form of monograms for ready use.
2. Influence of graphitisers and carbide stabilisers on the thermodynamic stability of eutectic cementite in the temperature range of 1145°C to 900°C should be determined. This might explain the behaviour of eutectic cementite during freezing. Also, this data would explain the kinetics of decomposition of eutectic cementite in these temperature ranges.
3. Influence of graphitisers and carbide stabilisers on the structure of eutectic Cementite should be determined. This might explain the present observations that the micro hardness of eutectic cementite does not change appreciably with progressive additions of either Si or Cu to the base-melt. These studies may have a bearing on the thermodynamic stability of eutectic cementite, stated in point 2 above.

REFERENCES

1. S.A. Saltykov Metallurgica, 14, No. 8, 10 (1939)
H. Brucher. Trans. No. 951.
2. K. Futakawa J. Japan Inst. Metals, 21, No. 6, 382,
(June 1957).
3. R.A. Sidorenko, Phy. Metals Metallog, 14, No. 2, 131, (1962).
F.A. Sidorenko and
A.S. Kosnarev
4. G. Sandoz AFS Trans., 70, 352 (1962).
5. J. Burke Acta Met., 7, No. 4, 268, (1959).
6. J. Burke JISI, 443, (apr. 1960).
7. H.A. Schwartz JISI, 138, 205 (1938).
8. B.F. Brown and AFS Trans. 59, 181, (1951).
M.F. Hawkes
9. H. Kitagawa and Trans., Japan Inst., 2, No. 2, 130 (1961).
N. Shibata
10. J. Burke and JISI, 176, 147 (1954).
W.S. Owen
11. D.S. Gill and Foundry, 60 (Aug. 1959).
O.S. Epplesheimer
12. B. Walker and JISI, 200, 1037 (1962).
V. Kondic.
13. A.S. Appleton JISI, 194, 160 (1960).
14. A. Hultgren and JISI, 176, 351 (1954).
G. Ostberg
15. J. Burke Foundry Trade Journal, 112, 323, 389-
392 (March 29, 1962).
16. R.J. Light AFS Trans., 79, 465 (1971).
17. W.S. Owen and JISI, 182, 38 (1956).
J. Wilcock
18. T. Ellis, JISI, 201, 582 (1963).
I.M. Davidson and
C. Bodsworth

19. (a) W.S. Owen JISI, 167, 117 (1951).
(b) J.G. Humphrays and W.S. Owen JISI, 198, 38, (1961).
20. J. Burke Acta Met., 7, 268, (1959).
21. C.E. Birchenall and H.W. Mead J. Metals, 8, 1004, (1956).
22. J. Burke JISI, 194, 443, (1960).
23. K. Pearce JISI, 200, 28, (1962).
24. K. Pearce Foundry Trade Journal, 112, 193, (Feb. 15, 1962).
25. H.A. Schwartz, J.D. Hedbery and R. Eriksen AFS-Trans., 58, 578, (1950).
26. R.W. Heine and K.M. Htun. AFS Trans., 74, 65-69, (1966).
27. G. Sandoz, B.F. Brown and W.A. Pennigton Modern Castings, 39, 93, (Jan. 1961)
Also, AFS Trans., 69, 41, (1961).
28. G. Sandoz "Recent Research in Cast Iron". Ed. H. Merchant, Gordon and Breach, New York, 509, (1968).
29. S.V. Bhide and S. Banerjee Cast Metals Research Journal, 11, 4, (March 1975).
30. A. Berman and V. Kondic JISI, 176, 385, (1954).
31. J.H. Hickley and A.G. Quarrel JISI, 178, 337, (1954).
32. Richard Schneidewind AFS Trans., 55, 252 (1948).
D.J. Reese and A. Tang.
33. J. Burke and N. Swindells "Recent Research on Cast Iron". Ed. H. Merchant, Gordon and Breach, New York, 449, (1968).
34. E.A. Vasiliev Russian Castings Production, No. 7, 310-311, (July 1971).
E.I. Bader and V.A. Ekasanev

35. J. Burke JISI, 208, 951, (Oct. 1970).
36. J. Burke JISI, 196, 42, (1960).
37. H. Morrough and
W.J. William JISI, 176, 375, (1954).
38. (a) C.R. Loper Jr.
and R.W. Heine AFS-Trans., 68, 312; 327, (1960).
- (b) C.R. Loper and
R.W. Heine AFS-Trans., 69, 583, (1961).
39. R.W. Heine,
C.D. Nelson and
S.Pal et al AFS-Trans., 70, 941, (1962).
40. A. Hulgren and
Y. Lindbloom JISI, 176, 365, (1954).
41. A. Taub Foundry, 862, 82, (Oct. 1958).
42. R.W. Heine and
C.R. Loper Jr. AFS Trans., 69, 583, (1961).
43. F.D. Hutchinson, —
J.W. Vorberger and
C.R. Ferra AFS Trans., 79, 479, (1971).
44. P.B. Burgess and
R.G. Trimberger AFS Trans., 78, 169, (1970).
45. S. Banerjee and
C.R. Loper Jr. AFS Trans., 74, 759, (1966).
46. J.E. Rehder and
J.E. Wilson AFS Trans., 66, 387, (1958).
47. James F. Ellis and
C.K. Donoho AFS Trans., 66, 203, (1958).
48. L.R. Jenkins AFS Trans., 66, 166, (1958).
49. E.H. Belter and
R.W. Heine AFS Trans., 65, 134, (1957).
50. H.A. Schwartz AFS Trans., 50, 1, (1942).
51. George Sandoz NRL report-5268, U.S. Naval Research
Laboratory (1959).

52. C.R. Loper Jr.,
R.W. Heine and
J. Waring AFS Trans., 68, 328-336, (1960).
53. Y. Surendra,
H.Moh.Roshan and
V. Panchanathan "Industrial Metallurgy".Proceedings
of Inter. Symp. Bangalore, 9-13 May,
p-167, (1972).
54. M.C. Mittal,
K.V. Prabhakar and
M.R. Sheshadri "Industrial Metallurgy" Proc. Int.
Symp. Bangalore, 9-13 May, p-252, (1972).
55. K.R.Kinsman and
H.I. Aaronson Metallurgical Transactions, 8, No.4,
959, April (1973).
56. E.I.Bader
E.A. Vasilev et al. Russian Cast.Prod.--No.3, 116-117
March (1971).
57. H.Kowalka Giesserei, 59, p.498-506, Aug.10(1972).
58. George Sandoz Modern Castings, 44, 13, Jan.(1962).
59. C.T. Moore BCIRA Journal, 385-405, May(1961).
60. C.T. Moore BCIRA Journal, P.683-690, Nov.(1962).
61. C.T. Moore and
L.W.L. Smith BCIRA Journal, 10, 73, (1962).
62. G. Sandoz AIME Trans., 215, 1052, (1959).
63. M.A. Krishtal Metallurgy and Metal working, No.4,
24, (1955).
64. Y.Surendra,
H.Moh Roshan and
V.Panchnathan Trans. IIM., 26, No.3, 73, (June 1973).
65. A.K. Chakraborty and
P.P. Das Trans. IIM., 36, Sept.6(1972).
66. K.R. Kannan,
K.V. Prabhakar,
M.R. Sheshadri and
A. Ramchandran. IFJ, 18, No.1, 1, (June 1972).
67. J.G. Pearce Iron and Steel, 37, 99, March, (1964).
68. M.R. Krishnadev
and I.Le May JISI, 458, May (1970).
69. J.Carroll Prod. Engg. Journal, 10, 3-13, March(1970).

70. J. Polleg The British Foundryman., 436, Oct. (1964).
71. Albert de Sy Foundry, 92, No. 2, 43-47, (1964).
72. K. Bromag Foundry Trade Journal, 123, 845, (Dec. 7, 1967).
73. Albert de Sy AFS Trans., 67, 321, (1959).
74. N. Carter and Foundry Trade Journal, 121, No. 2605, R. Banton 607, Nov. 10, (1966).
75. J.G. Pearce and Foundry Trade Journal, 118, No .2517, 257, K. Bromag March 4, (1965).
76. R.W. Heine, Foundry Trade Journal, 112, No. 2353, T.W. Mueller and 482, April 19, (1962). J.W. Widmeyer
77. C.T. Moore and Foundry Trade Journal, 170, Feb. 8 (1962). L.W.L. Smith
78. D.A. Robins Foundry Trade Journal, 111, No. 2346, 635, Nov. 23, (1961).
79. J.C. Prytherck and Foundry Trade Journal, 110, No. 2306, G.N.J. Gilbert 197, Feb. 16, (1961).
80. Y. Kawano, 40th International Foundry Congress, N. Moyama and Moscow, (1973). K. Kurai
81. W. Westerholt, AFS Cast Metal Research Journal, 2, W. Thurry and No. 2, 78, June (1973). R. Hummer
82. T.D. Hutchinson, AFS Trans., 81, 403, (1973). C.R. Ferra and H. Ramsone
83. M.J. Lalich and AFS Trans., 81, 217, (1973). C.R. Loper Jr.
84. M.J. Lalich, AFS Trans., 80, 401, (1972). C.R. Loper Jr., R.W. Heine and P.C. Rosenthal
85. R.F. Amrhein and AFS Trans., 80, 269, (1972). R.W. Heine

86. T.C. Rooney,
C.C. Wang,
P.C. Rosenthal,
C.R. Loper and
R.W. Heine AFS Trans., 79, 189, (1971).
87. J.F. Sulliran,
P.C. Rosenthal,
C.R. Loper Jr. and
R.W. Heine AFS Trans., 79, 537, (1971).
88. T. Levin,
P.C. Rosenthal,
C.R. Loper Jr. and
R.W. Heine AFS Trans., 79, 493, (1971).
89. M. Reis,
P.C. Rosenthal,
C.R. Loper Jr.,
R.W. Heine AFS Trans., 79, 565, (1971).
90. P.B. Burgess AFS Trans., 71, 477, (1963).
91. "Some effects of Bi in Malleable Iron!"
AFS Malleable div. Heat Treat.
Committee (6-D), AFS Trans., 71, 749, (1963).
92. G. Sandoz AFS Trans., 70, 218, (1962).
93. R.W. Heine,
T.W. Mueller AFS Trans., 69, 221, (1961).
94. R.W. Heine and
T.W. Mueller AFS Trans., 69, 511, (1961).
95. C.R. Loper Jr. and
R.W. Heine AFS Trans., 67, 380, (1959).
96. W.G. Scholz,
D.V. Doane and
G.A. Timmons AFS Trans., 63, 251, (1955).
97. R.C. Schnay,
J.E. Wilson and
J.E. Rehder AFS Trans., 63, 457, (1955).
98. J.V. Dawson Modern Castings, 113-120, June, (1969).
99. J. Pelleg Modern Castings, 45, No. 2, 25, (Feb. 1964).

100. "Some effect of Bi in Malleable Irons"
AFS Malleable div. Heat Treat.
Committee (6D), Modern Castings, 45,
749, Jan. (1964).
101. T.R. Baruch,
A.J. Stone and
W.H. Lownie Jr. Modern Castings, 45, 699, Jan. (1964).
102. J.B. Lang and
D.A. Robins Modern Castings, 43, 275, (June 1963).
103. C.R. Loper and
R.W. Heine Modern Castings, 46, 495, (Sept. 1964).
104. R.D. Schellay Modern Castings, 52, No4, 70, Oct. (1967).
105. E.A. Lange and
R.W. Heine AFS Trans., 60, 169, (1952).
106. E.A. Lange and
R.W. Heine AFS Trans., 61, 107, (1953).
107. C.E. Kempka and
R.W. Heine AFS Trans., 62, 53-69, (1954).
-
108. C.E. Kempka and
R.W. Heine AFS Trans., 63, 19, (1955).
109. A.H. Zrimsek,
E.H. Belter and
R.W. Heine AFS Trans., 64, 72, (1956).
110. H.H. Johnson and
W.K. Bock AFS Trans., 65, 450, (1957).
111. P.B. Burgess AFS Trans., 74, 156, (1966).
112. J.de.Menezes
Vasconcelos, and
P.B. Burgess AFS Trans., 79, 459, (1971).
113. "Suggested rating chart for nodular
irons" Foundry Trade Journal, 117,
526, Oct. 22, (1964).
114. G.N.J. Gilbert Foundry Trade Journal, 116, 35,
Jan. 9, (1964).
115. J.W. Goth Foundry, 92, No.5, 66-71, (1964).

116. S.R. Sahay, J. Ramesam and R.V. Tamhankar Trans., IIM, 26, No.3,5, (June 1973).
117. Floyd Brown American/Foundryman, 25, No.2,50, (Feb. 1954).
118. W. Mitter and P. Koss Zeitschrift Fur Metallkunde, 62, 482-487, (June 1971).
119. T. Ohide and G. Ohira IMONO, 44, 539-545, July (1972).
120. G. Angelov and L. Chadjikrastev Giessereitechnik, 18, 300-301, Sept. (1972).
121. A.S. Meshcheryakov et al. Russian Castings Production, No.6, 262, June (1971).
122. S. Banerjee IFJ, 20, No, 7,1, July (1974).
123. " Malleable, modified malleable and S.G. Iron produced from a single Malleable base melt, Foundry Trade Journal, March 15, 329, (1962).
124. J.V. Dawson Foundry, 60-62, Feb. (1971).
125. R.H. Greenlee AFS Trans., 66, 268, (1958).
126. G.N.J. Gilbert Foundry Trade Journal, 121, No.2002, 507, Oct. 20 (1966).
127. R.W. Heine AFS Trans., 66, 12, (1958).
128. B. Thyberg Foundry Trade Journal, 103, 213, (1957).
129. P.W. Green AFS Trans., 66, 387, (1958).
130. R.F. Marande Modern Castings, 53, No.5,77, (May 1968).
131. G.E. Kempka AFS Trans., 63, 675, (1955).
132. R.W. Heine AFS Trans., 64, 91, (1956).
133. "Comparison of liquid and Air-quenched pearlitic malleable irons Part II" AFS Committee 6E, AFS-Trans., 65, 304, (1957).
134. R. Opitz Foundry Trade Journal-p. 449, April 12, 1962 and p. 485, April 19 (1962).

135. U.K. Bhattacharya IFJ, 13, No.8-9, 1, Jan-Feb.(1968)
and IFJ,13, No.10-11, 1March-April(1968).
136. G.N.J. Gilbert. Research report No.381, BCIRA,
April, (1954).
137. T.R. Brown Foundry Trade Journal, 112, No.2357,
159, Feb. 8, (1962).
138. D.R. Miller Foundry 97, 140, Sept.(1969).
139. W.D. Huskonen Foundry, 97, No. 1, 46-48, (1969).
140. R. Cech and Foundry, 97, No. 1, 49-51, (1969).
R. Light
141. U.K. Bhattacharya 33rd International Foundry Congress-
New Delhi, p.19, Dec.(1966).
142. A.P. Alexander AFS Trans., 81, 115, (1973).
143. P.S. Cowen Foundry, 99, No.9, 60, Sept.(1971),
Pt.I and 99, No.10, 78-81, Oct.(1971)
Pt. II.
- ~~144. G.J. Cox~~ Foundry Trade Journal, 117, 273,
Sept. 3, (1964).
145. R. Lavoux Handley Foundry Trade Journal, 116, No.2475,
and T.I. Jones 595, May 14(1964).
146. G.J. Cox Foundry Trade Journal, 121, No. 2593,
209, Aug. 18, (1966).
147. J. Bradshaw Foundry Trade Journal, 125, No.2691,
July 4, (1968).
148. C. Vishnevsky and Modern Castings, 43, No.6, 290,
J.F. Wallace June (1963).
149. C.R. Isleib and AFS Trans., 65, 75, (1958).
R.E. Savage
150. C.K. Donoho Modern Castings, 46, No.4, p.608, (1964).
151. S.N. Anantnarayan Trans., IIM, 12, 83-91, March (1959).
152. A.K. Chakrabarti The British Foundryman, 68, pt.1, 1,
and P.P. Dass Jan.(1975).
153. S. Gupta, Indian Journal of Technology, 12,
A.K. Chakrabarti 50-56, Feb. (1974).
and P.P. Das

154. E.I. Bader Russian Castings Production, No.12, 515, Dec.(1974).
155. Gabriel Joly AFS Trans., 56, 66, (1948).
156. J.E.Rehder AFS Trans., 56, 138, (1949).
157. Richard Schneid- AFS Trans., 56, 410, (1949).
ewind and
D.J. Reese
158. H.A.Schwartz and AFS Trans., 56, 458, (1949).
W.K.Bock
159. P.B. Burgess AFS Trans., 77, 172, (1969).
160. E.M.Stein, K.R. AFS Trans., 78, 435, (1970).
Grube and A.R.Elsea
161. C.R.Loper Jr., Modern Castings, 46, 520, (1964).
N.Takizawa
162. C.H.Lorig and 'Copper as an alloying element in
R.R.Adams Steel and Cast Iron', McGraw Hill (1948).
- ~~163. R.W.Heine AFS Trans., 58, 277, (1950).~~
164. A.L. Boegehold Metal Progress, 73, Oct., (1956).
165. P.B. Burgess and AFS Trans., 75, 453, (1967).
A.Hernandez
166. 'Malleable Iron Casting', Oxford, IBH
Publishing Co., New Delhi. p.366,120.
167. Z.Paley and AFS Trans., 83, 35, (1975).
W.M.Williams
168. F.W.Jacobs and AFS Trans., 83, 263, (1975).
F.L. Preston
169. K.B.Mishra, R.S. IIM Trans., 28, 64, (1975).
Sharma and T.R.
Anantharaman
170. Katsuya Ono, Hiromu Tanimura, Koretaka
Kodama, Karchiro Sato- International
Foundry Congress, New Delhi 23-1,
Dec.(1966).
171. R.W.Heine, C.R. 'Principles of Metal Casting', McGraw
Loper and P.C. Hill and Kogakusha, 614, 642, (1967).
Rosenthal

172. B.J. Vyas, B.Bowonder and P.K.Rohatgi AFS International Cast Metals Research Journal, 1, No.1, 35, March (1976).
173. L.A. Newmeier, B.A.Betts et al, AFS International Cast Metals Journal, 1,No.1,17, March(1976).
174. M.Remondino, F.Pilastro et al AFS International Cast Metals Journal, 1,no.1,39, March (1976).
175. J.H. Sale AFS Trans., 83,107, (1975).
176. M.C. Ashton, R.K. Buhr, J.G. Magny and K.G. Davis AFS Trans., 83, 51, (1975).
177. N.K. Dutta and N.N. Engels AFS Trans., 83,121, (1975).
178. R.S. Lee AFS Trans., 83,153, (1975).
179. S. Yamamoto et al. AFS Trans., 83,217, (1975).
180. R.K. Nanstad, F.J. Worzala and C.R. Loper Jr. AFS Trans., 83,245, (1975).
181. D.R. Askeland and S.S. Gupta AFS Trans., 83,313, (1975).
182. G. Bylund, H.Bark, B.Fredrikson and T. Thoren AFS Trans., 83,385, (1975).
183. P.K. Basutkar, C.S. Park, R.E.Muller and C.R. Loper AFS Trans., 81,180, (1973).
184. R.S. Lee AFS Trans., 81, 105, (1973).
185. E. Compomanes and R. Goller AFS Trans., 81, 428, (1973).
186. P.D. Reuschen, N.L. Church and Paul D. Merica AFS Trans., 81,309, (1973).
187. N.L. Church and Paul D. Merica. AFS Trans., 81,301, (1973).
188. R.W. Heine AFS Trans., 81,462, (1973).

189. R.K. Buhr AFS Trans., 79, 247, (1971).
190. P.K. Basutkar, AFS Trans., 79, 169, (1971).
C.R. Loper Jr.
191. P.K. Basutkar and AFS Trans., 79, 176, (1971).
C.R. Loper Jr.
192. E.F. Runtz Jr., AFS Trans., 79, 141, (1971).
J.F. Janowak,
A.K. Hochstein and
C.A. Wargel
193. E. Compomanes AFS Trans., 79, 57, (1971).
194. N.L. Church AFS Trans., 79, 371, (1971).
195. R.S. Lee AFS Trans., 433, (1971).
196. A. Lazaridis, AFS Trans., 79, 351, (1971).
F.J. Worzaola,
C.R. Loper Jr. and
R.W. Heine
197. Takeomi Okumoto, AFS Trans., 79, 473, (1971).
~~Kyuji Hasegawa and~~
Minoru Tanikawa
198. J.F. Janowak and AFS Trans., 79, 594, (1971).
C.R. Loper
199. C.A. Jones, AFS Trans., 79, 547, (1971).
J.C. Fisher and
C.E. Bates
200. F.E. Kusch AFS Trans., 79, 69, (1971).
201. R.W. Heine and AFS Trans., 79, 399, (1971).
C.R. Loper
202. G.Fr. Hillner and AFS Trans., 83, 167, (1975).
K.H. Kleeman
203. G.S. Murthy, Trans., IIM., 25, No .2, (June 1972).
P.C. Angelo and
R.V. Tamhankar
204. M.C. Ashton AFS Cast Metals Research Journal,
8, 71 (1972).
205. L.S. Darken and "Physical Chemistry of Metals",
R.W. Gurry McGraw-Hill Book Co., Inc., 363, (1953).

APPENDIX

Four hypothetical compositions were considered in which, the total carbon was kept fixed at 6.0 wt %, while the copper content was varied as 0.5%, 1.0%, 2.0% and 3.0%, balance in each case being iron. This composition would very approximately correspond to that of cementite (Fe_3C), with varying percentages of copper.

Correction calculation procedures outlined in section 6.6.2 were used in these four individual cases in order to determine K_i (Mass concentration of copper found by the probe analyser) values from presumed and known C_i (Mass concentration of copper in the sample) values.

Case I

Composition	-	Fe	-	93.0
		Cu		1.0
		C		6.0
		Total		100.0

(i) Absorption Correction(A): for Cu, K_α radiations only.

Philibert absorption correction:

$$A = \frac{f(\chi_M(\text{sample}))}{f(\chi_{\text{standard}})} = \frac{f(\chi_M)}{f(\chi_{100\text{Cu}})} \text{ for Cu, } K_\alpha \text{ radiations only.}$$

for Cu in Cu-Fe-C system, Philibert Equation:

$$f(\chi_{100\text{Cu}}) = \frac{1}{\left(1 + \frac{\chi_{\text{Cu}}}{\sigma}\right) \left(1 + \frac{\chi_{\text{Cu}}}{\sigma} \cdot \frac{h}{1+h}\right)}$$

$$\chi_{Cu} = \mu_{Cu-Cu} \cdot \text{Cosec } \theta$$

where,

$$\begin{aligned} \theta &= \text{take off angle} \\ &= 52.7 \times 1.984 \\ &= 104.556 \end{aligned}$$

$$h_{\text{std.}} = \frac{1.2 A_i}{Z^2} \quad \left[\begin{array}{l} A = \text{Atomic weight of standard.} \\ Z = \text{Atomic No. of standard.} \end{array} \right]$$

$$= \frac{1.2 \times 635}{29^2} = 0.090$$

σ = Lenard coefficient

$$= \frac{4.5 \times 10^5}{(V - V_i)^{1.65}}$$

where,

V = Excitation voltage or
(Electron Beam voltage)

V_i = Critical excitation voltage.

hence,

$$V_{Cu} = 9 \text{ KV.}$$

and $V = 25 \text{ KV.}$

hence,

$$\begin{aligned} \sigma &= \frac{4.5 \times 10^5}{(25 - 9)^{1.65}} \\ &= 4600 \end{aligned}$$

hence,

$$f(\chi_{100-Cu}) = \frac{1}{\left(1 + \frac{104.556}{4600}\right) \left(1 + \frac{104.556}{4600} \times \frac{0.090}{1+0.090}\right)}$$

$$= 0.977$$

similarly,

$$f(\chi_M) = \frac{1}{\left(1 + \frac{\chi_M}{\sigma}\right) \left(1 + \frac{\chi_M}{\sigma} \cdot \frac{h_M}{1+h_M}\right)}$$

$$\begin{aligned} \chi_M &= \text{Cosec } \theta (0.01x\mu_{\text{Cu-Cu}} + 0.06x\mu_{\text{C-Cu}} + 0.93\mu_{\text{Fe-Cu}}) \\ &= 1.984(0.01x52.7 + 0.06x4.24 + 0.93x317) \\ &= 586.452. \end{aligned}$$

and,
$$h_M = \frac{1.2}{0.01x\frac{29^2}{63.5} + 0.06x\frac{6^2}{12} + 0.93x\frac{26^2}{55.83}}$$

$$= 0.10368$$

hence,

$$f(\chi_M) = \frac{1}{(1 + \frac{586.452}{4600})(1 + \frac{586.452}{4600} \times \frac{0.10368}{1+10368})}$$

$$= 0.877$$

hence,

Absorption correction (A) factor

$$\begin{aligned} &= \frac{f(\chi_M)}{f(\chi_{100-\text{Cu}})} \\ &= \frac{0.877}{0.977} \\ &= 0.897 \end{aligned}$$

(ii) Atomic Number Correction factor(Z)

Duncumbs and Reed expression:

$$\begin{aligned} Z &= \frac{R_M \cdot \bar{S}_i}{R_i \cdot \bar{S}_M} \\ &= \frac{R_{\text{sample}}}{R_{\text{std.}}} \times \frac{\bar{S}_{\text{std.}}}{\bar{S}_{\text{sample}}} \end{aligned}$$

where,

- R = Back scattering coefficient.
- \bar{S} = Mean electron stopping power.

since $U_i = \frac{V}{V_i}$

$$\frac{1}{U_{Fe}} = \frac{V_{Fe}}{25} = \frac{7.1}{25}$$

$$\frac{1}{U_{Cu}} = \frac{V_{Cu}}{25} = \frac{9}{25}$$

$$\frac{1}{U_c} = \frac{V_c}{25} = \frac{0.28}{25} = 0.011.$$

V_{Fe} , V_{Cu} and V_c given in Table.

Also,

R_{Cu}	=	0.862	from the table $\frac{1}{U}$ VS atomic No. (Z).
R_c	=	0.975	
R_{Fe}	=	0.859	

and,

$$\begin{aligned} R_M &= \sum C_i R_i \\ &= 0.01xR_{Cu} + 0.06xR_c + 0.93xR_{Fe}. \\ &= 0.01x0.862 + 0.06x0.975 + 0.93x0.859. \\ &= 0.864 \end{aligned}$$

Since, $\bar{S}_i = \frac{1}{\left(\frac{V+V_i}{2}\right)} \cdot \frac{Z_i}{A_i} \cdot \ln \frac{1.17(V+V_i)/2}{J_i}$

Hence,

$$\begin{aligned} \bar{S}_{Cu} &= \frac{1}{17} \cdot \frac{29}{63.5} \ln \frac{1.17(25+9)/2}{377} \\ &= \frac{1.342}{17} = 0.07894. \end{aligned}$$

J = Mean ionisation potential given in table J vs Z.

$$\begin{aligned}\bar{S}_{Fe} &= \frac{1}{16.05} \cdot \frac{26}{55.85} \ln \frac{1.17(25+7.1)/2}{332} \\ &= \frac{1.335}{16.05}\end{aligned}$$

$$\begin{aligned}\bar{S}_c &= \frac{1}{12.64} \times \frac{6}{12} \ln \frac{1.17(25+0.28)/2}{146} \\ &= \frac{1.144}{12.64}\end{aligned}$$

hence,

$$\begin{aligned}\bar{S}_M &= 0.01 \times \bar{S}_{Cu} + 0.06 \times \bar{S}_c + 0.93 \times \bar{S}_{Fe} \\ &= 0.01 \times \frac{1.342}{17} + 0.06 \times \frac{1.144}{12.64} + 0.93 \times \frac{1.335}{16.05} \\ &= 0.08356\end{aligned}$$

hence,

$$\begin{aligned}Z &= \frac{R_M}{R_{Cu}} \times \frac{\bar{S}_{Cu}}{\bar{S}_M} \\ &= \frac{0.864}{0.862} \times \frac{0.07894}{0.08356} \\ &= 0.94686\end{aligned}$$

(iii) Fluorescence correction factor (F):

Since Cu is the element having highest atomic number in the alloy, there will be no fluorescence correction factor for Cu in Cu-Fe-C system.

Net Correction:

Hence, using the final expression for net correction:

$$\begin{aligned}K_i &= C_i \cdot Z \cdot A \cdot F \\ &= 0.01 \times 0.94686 \times 0.897 \times 1 \\ &= 0.0084933.\end{aligned}$$

Case II.

Composition - Fe - 93.5

Cu - 0.5

C - 6.0

Total 100.0

(i) Absorption correction factor (A):

$$\begin{aligned} \chi_M &= \text{Cosec } \theta (0.005 \mu_{\text{Cu-Cu}} + 0.06 \mu_{\text{C-Cu}} + 0.935 \mu_{\text{Fe-Cu}}) \\ &= 1.984 (0.005 \times 52.7 + 0.06 \times 4.24 + 0.935 \times 317) \\ &= 589.5799 \end{aligned}$$

and

$$\begin{aligned} h_{(M)} &= \frac{1.2}{0.005 \times \frac{29^2}{63.5} + 0.06 \times \frac{6^2}{12} + 0.935 \times \frac{26^2}{55.83}} \\ &= \frac{1.2}{11.56737} \\ &= 0.10374 \end{aligned}$$

hence,

$$\begin{aligned} f(\chi_M) &= \frac{1}{(1 + \frac{589.5799}{4600}) (1 + \frac{589.5799 \times 0.10374}{4600 \times 1 + 0.10374})} \\ &= 0.87585 \end{aligned}$$

hence,

absorption correction factor (A)

$$\begin{aligned} &= \frac{f(\chi_M)}{f(\chi_{100-\text{Cu}})} \\ &= \frac{0.87585}{0.977} \\ &= 0.89646 \end{aligned}$$

(ii) Atomic Number Correction Factor(Z):

$$\begin{aligned}
 R_M &= \sum C_i R_i \\
 &= 0.005xR_{Cu} + 0.06xR_C + 0.935xR_{Fe} \\
 &= 0.005x0.862 + 0.06x0.975 + 0.935x0.859 \\
 &= 0.86597.
 \end{aligned}$$

hence,

$$\begin{aligned}
 \bar{S}_M &= 0.005x\bar{S}_{Cu} + 0.06x\bar{S}_C + 0.935x\bar{S}_{Fe} \\
 &= 0.005x\frac{1.342}{17} + 0.06x\frac{1.144}{12.64} + 0.935x\frac{1.335}{16.05} \\
 &= 0.08359
 \end{aligned}$$

hence,

$$\begin{aligned}
 Z &= \frac{R_M}{R_{Cu}} \times \frac{\bar{S}_{Cu}}{\bar{S}_M} \\
 &= \frac{0.86597}{0.862} \times \frac{0.07894}{0.08359} \\
 &= 0.94867.
 \end{aligned}$$

(iii) Fluorescence Correction Factor(F)

$$F = 1$$

hence, net correction:

$$\begin{aligned}
 K_i &= C_i \cdot Z \cdot A \cdot F \\
 &= 0.005x0.94867x0.89646x1 \\
 &= 0.00425
 \end{aligned}$$

<u>Case III</u>	Composition - Fe -	92.0
	Cu -	2.0
	C -	6.0
	<u>Total =</u>	<u>100.0</u>

(i) Absorption Correction factor (A)for copper K_{α} radiations only in Cu-Fe-C system.

$$f(\chi_M) = \frac{1}{\left(1 + \frac{\chi_M}{c}\right) \left(1 + \frac{\chi_M}{\sigma} \cdot \frac{h_M}{1+h_M}\right)}$$

$$\begin{aligned} \chi_M &= \text{Cosec}\theta (0.02\mu_{\text{Cu-Cu}} + 0.06\mu_{\text{C-Cu}} + 0.92\mu_{\text{Fe-Cu}}) \\ &= 1.984(0.02 \times 52.7 + 0.06 \times 4.24 + 0.92 \times 317) \\ &= 581.209 \end{aligned}$$

$$\begin{aligned} h_{(M)} &= \frac{1.2}{0.02 \times \frac{2c^2}{63.5} + 0.06 \times \frac{6^2}{12} + 0.92 \times \frac{26^2}{55.83}} \\ &= 0.10358 \end{aligned}$$

$$\begin{aligned} \text{Hence, } f(\chi_M) &= \frac{1}{\left(1 + \frac{581.209}{4600}\right) \left(1 + \frac{581.209}{4600} \times \frac{0.10358}{1+0.10358}\right)} \\ &= 0.87730 \end{aligned}$$

Hence, absorption correction factor (A)

$$\begin{aligned} &= \frac{f(\chi_M)}{f(\chi_{100-\text{Cu}})} \\ &= \frac{0.87730}{0.977} \\ &= 0.89795. \end{aligned}$$

(ii) Atomic Number Correction factor (Z)

$$\begin{aligned}
 R_M &= \sum C_i R_i \\
 &= 0.02 \times R_{Cu} + 0.06 \times R_C + 0.92 \times R_{Fe} \\
 &= 0.02 \times 0.862 + 0.06 \times 0.975 + 0.92 \times 0.859 \\
 &= 0.86602
 \end{aligned}$$

$$\begin{aligned}
 \text{Hence, } \bar{S}_M &= 0.02 \times \bar{S}_{Cu} + 0.06 \times \bar{S}_C + 0.92 \times \bar{S}_{Fe} \\
 &= 0.02 \times \frac{1.342}{17} + 0.06 \times \frac{1.144}{12.64} + 0.92 \times \frac{1.335}{16.05} \\
 &= 0.08352
 \end{aligned}$$

$$\begin{aligned}
 \text{Hence, } Z &= \frac{R_M}{R_{Cu}} \times \frac{\bar{S}_{Cu}}{\bar{S}_M} \\
 &= \frac{0.86602}{0.862} \times \frac{0.07894}{0.08352} \\
 &= 0.94947
 \end{aligned}$$

(iii) Fluorescence Correction factor (F) = 1.Hence, Net Correction

$$\begin{aligned}
 K_i &= C_i \cdot Z \cdot A \cdot F \\
 &= 0.02 \times Z \times A \times 1 \\
 &= 0.02 \times 0.94947 \times 0.89795 \times 1 \\
 &= 0.01705
 \end{aligned}$$

Case IV

Composition - Fe = 91.0

Cu = 3.0

C = 6.0

Total = 100.0(i) Absorption Correction Factor (A)for Cu K_α radiations only in Cu-Fe-C system

$$\mu_M = \text{Cosec} \theta (0.03 \times \mu_{Cu-Cu} + 0.06 \times \mu_{C-Cu} + 0.91 \times \mu_{Fe-Cu})$$

$$= 1.984(0.03 \times 52.7 + 0.06 \times 4.24 + 0.91 \times 317)$$

$$= 575.96591$$

$$h_{(M)} = \frac{1.2}{0.03 \times \frac{29^2}{63.5} + 0.06 \times \frac{6^2}{12} + 0.91 \times \frac{26^2}{55.83}} = 0.10348$$

$$\text{Hence, } f(X_M) = \frac{1}{\left(1 + \frac{575.96591}{4600}\right) \left(1 + \frac{575.96591}{4600}\right) \times \frac{0.10348}{1+0.10348}}$$

$$= 0.89910$$

(ii) Atomic Number Correction factor (Z)

$$R_M = \sum C_i R_i$$

$$= 0.03 \times R_{Cu} + 0.06 \times R_C + 0.91 \times R_{Fe}$$

$$= 0.03 \times 0.862 + 0.06 \times 0.975 + 0.91 \times 0.859$$

$$= 0.86605$$

Hence,

$$\bar{S}_M = 0.03 \times \bar{S}_{Cu} + 0.06 \times \bar{S}_C + 0.91 \times \bar{S}_{Fe}$$

$$= 0.03 \times \frac{1.342}{17} + 0.06 \times \frac{1.144}{12.64} + 0.91 \times \frac{1.335}{16.05}$$

$$= 0.08348$$

Hence,

$$Z = \frac{R_M}{R_{Cu}} \times \frac{\bar{S}_{Cu}}{\bar{S}_M}$$

$$= \frac{0.86605}{0.862} \times \frac{0.07894}{0.08348}$$

$$= 0.95004$$

(iii) Fluorescence Correction Factor (F) = 1

Hence, Net Correction.

$$K_i = C_i \cdot Z \cdot A \cdot F.$$

$$= 0.03 \times Z \times A \times 1.$$

$$= 0.03 \times 0.95004 \times 0.89910 \times 1$$

$$= 0.02562$$

Summary of Results

Hypothetical Composition Wt%.	C_i	K_i
Fe- 93.5, Cu-0.5, C-6.0	0.005	0.00425
Fe- 93.0, Cu-1.0, C-6.0	0.01	0.0084933
Fe- 92.0, Cu-2.0, C-6.0	0.02	0.01705
Fe- 91.0, Cu-3.0, C-6.0	0.03	0.02562

Note- Calibration curve plotted between K_i and C_i values is shown in Fig.7-17.

